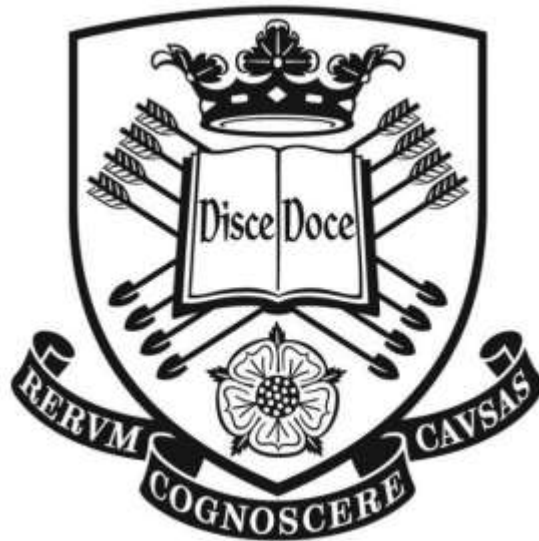# Energy Evaluation and Optimal Design of Semi-transparent Photovoltaic Façade for Office Buildings in Central China

Shen Xu

A thesis submitted to University of Sheffield in partial fulfilment of the requirements for the degree of Doctor of Philosophy

School of Architecture

University of Sheffield

May 2014

Abstract

In recent years, interest in building integrated photovoltaic (BIPV) has increased considerably. This thesis aims to evaluate the energy performance of semi-transparent photovoltaic façade for office buildings in central China and to propose optimal design based on the evaluation.

In this study, an experimental room was set up in Wuhan, which is typical city of central China in climate. Then, the calculation models for energy evaluation of PV façades are developed and validated based on field experiments. The architectural models were developed with a series of generic office rooms. Finally, the architectural models and validated models were incorporated into the simulations with Energy Plus for energy evaluation of semi-transparent PV façade.

Energy evaluations based on the PV generated electricity were performed in four cities of China. The results show that with the varieties of cities and building orientations, building forms, and materials and arrangements of PV modules, there was a distinct difference in annual power generation of PV façades.

Energy evaluations based on the overall energy consumption were performed for two types of the PV façades in Wuhan. The impacts of the properties of PV glazing and the architecture factors on the overall energy of semi-transparent PV façades was addressed. For example, in large window-to-wall ratio (WWR) office rooms, mono-crystalline semi-transparent PV of high PV coverage ratio (PVR) could be energy efficient. Therefore, use of optimal PVR and WWR based on the combination of room depth and orientation can achieve overall energy consumption saving.

In addition, the suitability of optimal PVR/WWR strategies for PV façades in different architectural conditions was investigated with the consideration of Chinese Design Standard for Energy Efficiency of Public Buildings. The mono-crystalline semi-transparent PV could only achieve a better overall energy performance in the cases of small WWR and small depth room meanwhile amorphous-silicon fail to achieve a better overall energy performance in all cases.

Acknowledgements

List of Abbreviations

AC	Air conditioning
AM	Air mass
BAPV	Building attached photovoltaic
BIPV	Building integrated photovoltaic
CSWD	Chinese Standard Weather Data
DC	Direct current
EVA	Ethylene-vinyl acetate copolymer
HC	Heating and cooling
NOCT	Normal operating cell temperature
PV	Photovoltaic
PVR	PV coverage ratio
STC	Standard test conditions
TRY	Test Reference Year
TMY	Typical Meteorological Year
WWR	Window-to-wall ratio

List of Important Symbols

Symbols	Description
P_d	DC electrical power of PV generation (W)
E_{PV}	DC electrical energy of PV generation (kWh/m^2)
A	aperture surface area of PV cell (m^2)
t	time (hour)
G	solar irradiance (W/m^2)
G_h	horizontal total irradiance (W/m^2)
G_b	horizontal beam irradiance (W/m^2)
G_d	horizontal diffuse irradiance (W/m^2)
G_i	total irradiance on inclined surface (W/m^2)
$G_{b,i}$	beam irradiance on inclined surface (W/m^2)
$G_{r,i}$	reflected irradiance on inclined surface (W/m^2)
$G_{d,i}$	diffuse irradiance on inclined surface (W/m^2)
G_o	hourly extraterrestrial irradiation on a horizontal surface
R_b	ratio of beam irradiance on inclined surface to horizontal beam irradiance (dimensionless)
α_s	solar elevation (rad)
β	inclination angle of the surface (rad)
γ_i	azimuth angle of the inclined surface (rad)
γ_s	azimuth angle of the sun (rad)
δ	declination of the sun (rad)
θ_i	angle of incidence on the surface (rad)
θ_z	solar zenith angle (rad)
φ	local latitude (rad)
ω	hour angle (rad)
n	day (d)
A_I	anisotropy index in the Hay model (dimensionless)
f	modulating function in the Reindl model (dimensionless)
I_{sc}	solar constant (W/m^2)
ρ	average ground reflectance (dimensionless)

η	PV cell/module conversion efficiency (dimensionless)
η_0	PV cell/module conversion efficiency under STC (dimensionless)
$\eta(T_c)$	PV cell/module conversion efficiency under T_c (dimensionless)
β_C	temperature coefficient（K^{-1}）
T	temperature (K)
T_c	PV cell/module operating temperature (K)
T_a	ambient temperature (K)
NOCT	Normal operating cell temperature (℃)
E	annual overall energy consumption of the building room with the semi-transparent PV façades (kWh/m^2)
P	instant power of the PV panel (W/m^2)
α_i	solar absorptance of layer i (dimensionless)
T_i	temperature of boundary i (dimensionless)
T_{out}	outdoor temperature (K)
T_{in}	indoor temperature (K)
$h_{out,c}$	convective heat transfer coefficients for the outside surface (dimensionless)
$h_{in,c}$	convective heat transfer coefficients for the inside surface (dimensionless)
h_{out}	outside heat transfer coefficient (dimensionless)
h_{in}	inside heat transfer coefficient (dimensionless)
ξ	emissivity of the front glass (dimensionless)
σ	Stefan–Boltzmann constant
τ	total solar transmittance of semi-transparent PV (dimensionless)
τ_i	solar transmittance of layer i (dimensionless)
λ_i	the heat conductivity of layer i (W/mK)
λ_{sc}	heat conductivity of the solar cell layer (W/mK)

λ_{EVA} heat conductivity of EVA layer (W/mK)

d_i thickness of layer i (m)

N   inward-flowing fraction of the absorbed radiation

α solar absorptance (dimensionless)

τ' visible transmittance of the semi-transparent PV glazing (dimensionless)

τ'_i visible transmittance of layer i (dimensionless)

U   U-factor, overall heat transfer coefficient (W/m^{2}K)

SHGC   solar heat gain coefficient (dimensionless)

SC   Shading coefficient (dimensionless)

Table of Contents

List of Tables

List of Figures

Chapter 1 Introduction

1.1. Research background

Global awareness of energy use and its environmental implications has been raised in the recent report by the Inter-governmental Panel on Climate Change (IPCC) (Solomon et al., 2007). Because economic expansion requires energy consumption, rapid economic growth is accompanied by rapidly increasing energy consumption in China since the policy of "Reforming and Opening" was adopted by the Chinese government in 1978 (Zhang, 1995). In general, industry, transportation and buildings are the three primary sectors of energy demand. According to the International Energy Agency, commercial and residential buildings account for 30.9% of the total end-use energy consumption in China (Birol, 2010). With further development of the economy and improvements in the living standards of people, the proportion of buildings in the total energy consumption will continue to increase; buildings are estimated to account for 35% of the total energy consumption in China by 2020 (Yao et al., 2005). The only way to alleviate the ever-growing building energy demand in China is to implement a building energy efficiency policy and to promote advanced technologies and proper building design strategies for energy efficient buildings (Xie et al., 2011；Hong, 2009).

Photovoltaic (PV) has been regarded as one of the best ways to harness the renewable energy for buildings (Parida et al., 2011). Solar power is converted to direct current electricity by PV materials, such as monocrystalline silicon, polycrystalline silicon, amorphous-siliconcadmium telluride, and copper indium gallium. (Petter Jelle et al., 2012). The crystalline silicon PV and the amorphous-silicon PV are commonly used in the market. The advantage of the crystalline silicon cell is that the practical efficiency is high, and the disadvantage is the large amount of energy consumed in production and the high cost, while the advantage and disadvantage of amorphous-silicon is the opposite to those of crystalline silicon. (Goetzberger and Hebing, 2000). Building integrated photovoltaic (BIPV) are photovoltaic materials that are used to replace conventional building materials in parts of the building envelopes, such as the roofs, skylights or façades. Due to the Chinese government's incentive policies, the application of solar PV modules has developed rapidly, and a significant number of

BIPV demonstration buildings have been built since 2009 (Xie et al., 2011). In particular, BIPV technology is becoming widely used in parts of the façades of modern buildings (Roberts and Guariento, 2009 ; Weller et al., 2010 ; Zhang et al., 2012 ; Taleb and Pitts, 2009). Office buildings are particularly suitable for BIPV technology, as office buildings consume energy primarily in daytime, which is when the PV system collects and converts solar energy into electricity; thus, the effort and cost associated with energy storage can be avoided (Lam et al., 2003). Such PV façades are being used increasingly in the designs of office buildings in China (Peng et al., 2011). Accordingly, the development of an optimal PV façade design for architects, constructers, and installers is becoming increasingly urgent.

The results of extensive studies on the evaluation of the power generation of BIPV modules indicated that the solar irradiance and PV module temperature should be considered as the most important factors because they affect both the electrical efficiency and the output of the BIPV system. Moreover, the energy evaluation of semi-transparent PV on an office façade should be regarded in view of the overall energy rather than only the electricity produced by the PV system. Semi-transparent PV modules not only generate electricity but also introduce daylight, which can reduce artificial lighting energy consumption during the daytime (Li et al., 2009). Conversely, semi-transparent PV modules reduce the heat gain in a building by blocking the incoming solar radiation due to absorption in the PV cells (Fung and Yang, 2008), which increases heating demand indoors in winter but reduces the cooling demand in summer. The researchers suggested that the properties of PV material and the different combinations of architectural factors have a profound impact on the overall energy consumption of semi-transparent PV façade buildings, particularly through their effects on PV electricity generation, lighting, heating and cooling.

Moreover, the climate is the key factor for building energy evaluation as well as the overall energy-saving effects of semi-transparent PV systems. In Brazil, the use of a semi-transparent PV window has been shown to save up to 43% of the energy consumption (Leite Didoné and Wanger, 2013). In addition, 55% energy savings were achieved in Japan (compared to a single-glazed window) with a solar cell transmittance of 40% and window-to-wall ratio (WWR) of 50% (Miyazaki et

al., 2005), and energy savings in the range of 16.7–41.3% were achieved in Singapore for a WWR range of 70–100% (Ng et al., 2013). Other previous studies (Lu and Law, 2013; Olivieri et al., 2014) have also demonstrated the importance of considering climatic conditions in the investigation of semi-transparent PV window applications.

In brief, it is an urgent task to promote the optimal design and usage of PV applications, especially BIPV systems, in China. Studies of semi-transparent PV façades must be further performed in terms of the overall energy performance under the local conditions of central China. Related calculation methods and models must be developed to allow for a wider range of studies of semi-transparent PV façades under different architectural conditions and different PV coverage ratio (PVR). Such work would provide a solid foundation for the further development of research and applications of semi-transparent PV façades in China.

1.2. Research aim and objectives`

The general aim of this research is **to evaluate the energy performance of semi-transparent photovoltaic façade for office buildings in central China and to propose optimal design based on the evaluation**.

The major research objectives include the following:

(1) **To establish an experimental room with semi-transparent PV façade under the real climate conditions and to develop the experimental methodology of the measurement and calibration for collecting effective data.** *(Chapter 3)*

(2) **To estimate the annual power generation of the PV façades in the representative cities of China.** *(Chapter 4)*

(3) **To evaluate the overall energy performance of two type of semi-transparent PV façades for office buildings in Wuhan, China.** *(Chapter 5-Chapter 7)*

(4) **To develop an optimizing design approach for semi-transparent PV façade by the use of optimal PVR/WWR.** *(Chapter 5-Chapter 7)*

(5) **To investigate the suitability of optimal PVR/WWR strategies in different architectural conditions.** *(Chapter 8)*

1.3. Methodologies and approaches
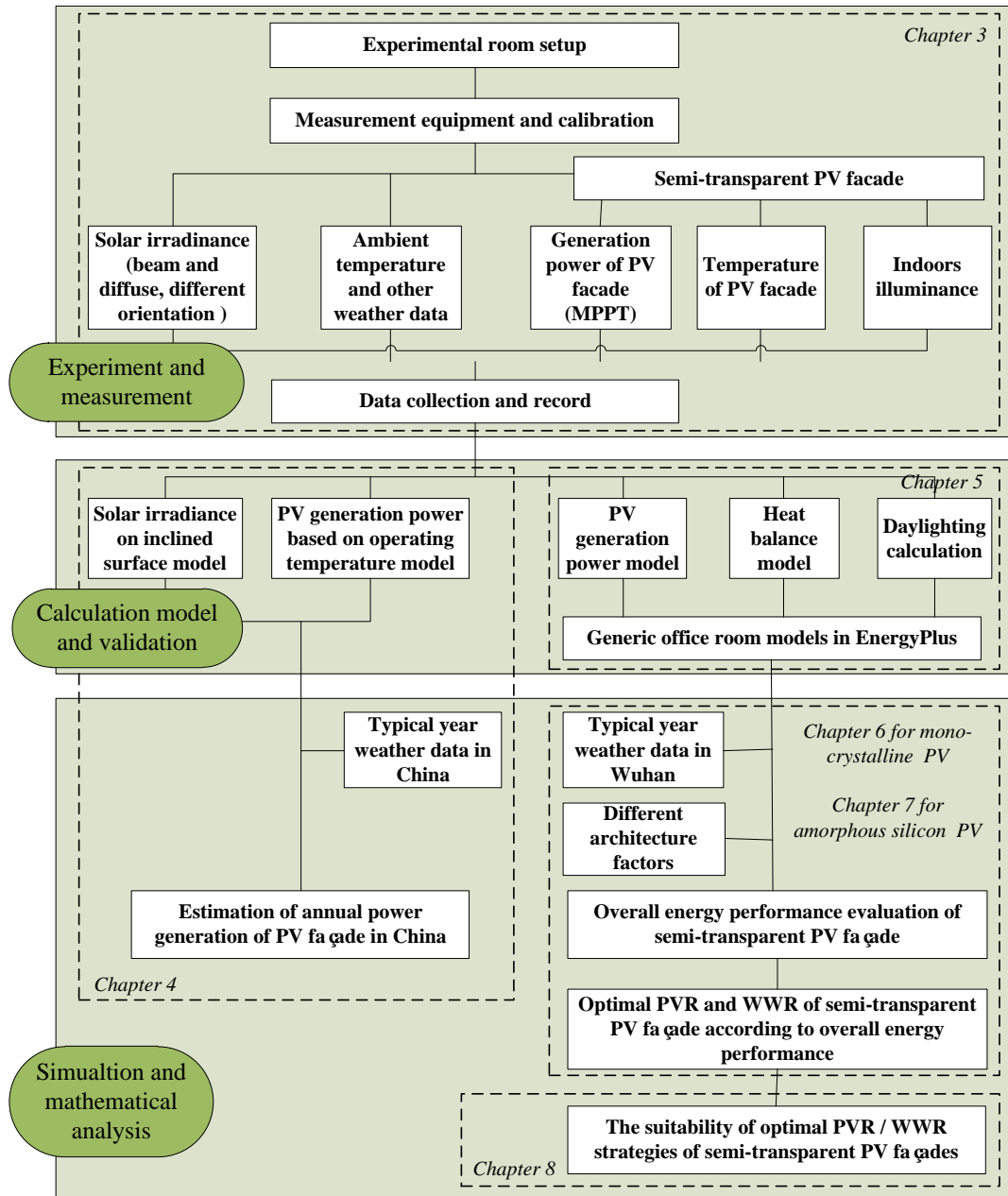
Figure 1.1 Methodologies structure

This study is a comprehensive research program involving the methodologies of experiment and field measurements, calculation models development and validation, simulation and mathematical analysis. Field measurements are performed in the first stage to investigate the electrical, thermal, optical characteristics of different semi-transparent PV glazings. At the same time, calculation models and methods are constructed to predict the energy performance

of these glazing under the prevailing weather conditions. These models are validated against the measured data to confirm the accuracy. Subsequently, the validated PV models and typical office buildings models are incorporated into the building simulation program to evaluate the overall energy consumption. Finally, the results of evaluation are used to define the optimal design for this region. Figure 1.1 shows the methodologies structure.

(1) Experiment and field measurement

The goal of the experimental study performed in this work is to achieve more accurate data regarding the properties of semi-transparent PV glazings. The experimental room containing two inner and separate chambers was set up on the roof of a building in Wuhan. The building component such as PV glazing could be fixed on the south vertical façade of the experiment room. The methodology of measurement and calibration was developed to achieve vital data of the environmental parameters and the parameters related to PV façades. A board range of data including temperature, solar irradiance, illuminance and PV generation power was measured and recorded systemically in a long period for more than one year. In addition, the PV façades parameters achieved from the field experiment in this study were compared with the previous literature of other researchers.

(2) Calculation models development and validation

Firstly, the measured data were applied to develop calculation models of determining the solar irradiance on inclined surface and PV generation power based on operating temperature. Both of the validated models are indispensable to estimate the annual power generation of PV façades.

Secondly, the measured data were applied to develop PV power generation model, thermal model and daylighting calculation method for both mono-crystalline and amorphous-silicon semi-transparent PV façades.

Thirdly, architectural models were developed to provide a series of generic office rooms for overall energy evaluation of semi-transparent PV façades. The

generic office rooms were set to allow control of three variables, the room depth, WWR and orientation, and were fixed on other necessary settings including building envelop materials, running schedule of people and equipment etc.

(3) Simulation and mathematical analysis

With validated calculation models and typical year weather data, the annual power generation of PV façade were calculated in several representative cities of China. The mathematical analysis were carried out on the effects of location and orientation, effects of building forms, effects of PV material and PV arrangements.

With the calculation methods, architectural models and typical year weather data, the overall energy consumption evaluations were carried out in the research for two semi-transparent PV façades in Wuhan, a representative city of central China in climate. In addition, the suitability of optimal PVR / WWR strategies for PV façades under different architectural conditions was investigated with the consideration of Chinese Design Standard for Energy Efficiency of Public Buildings.

1.4. Organisation of the thesis

This thesis consists of nine chapters. A brief description of each chapter is outlined as follows.

Chapter 1 is an introductory chapter that describes the background information related to the research topic, and outlines the content of this thesis. The research aim and the objectives of this research are introduced in this chapter. The investigation methodologies and approaches are also presented.

Chapter 2 reviews the past work in the existing literature relevant to the current research. The important discoveries and conclusions by previous studies have been acknowledged and considered thoroughly. In addition, the research gaps are identified in this chapter.

Chapter 3 presents the experimental study of semi-transparent PV façades on the rooftop of the building in Wuhan, China. The set-up of experimental room, with semi-transparent PV façades, the data measurements and data quality control

methods, is described. The general measured results in the different weather conditions are presented using graphical approaches.

Chapter 4 presents the climate, solar irradiance and their relevance of power generation of PV façade. The calculation methods of solar irradiance on inclined surface and PV generation power based on operating temperature are explained and are validated with recorded data from the experimental room. Employed with the validated calculation methods and the typical year weather data of CSWD, the parametric studies are carried out on estimation of the annual power generation of PV façades in China.

Chapter 5 presents the calculation models and methods developed for both mono-crystalline silicon PV façades and amorphous-silicon semi-transparent PV façades, which includes the PV power generation model, the heat balance model and the daylighting calculation method. The measured data obtained from the field experiments are presented to compare with the simulated results as validation in this chapter.

Chapter 6 presents the evaluation of the energy performance of mono-crystalline semi-transparent PV façades. A discussion of the parametric analysis of the overall energy performance and a comparison analysis between mono-crystalline semi-transparent PV glazings and traditional glazings is conducted. The optimal strategy by PVR for mono-crystalline semi-transparent PV façades and its impact is proposed and discussed in this chapter.

Chapter 7 presents the evaluation of the energy performance of amorphous-silicon semi-transparent PV façades. A discussion of the parametric analysis of the overall energy performance and a comparison analysis between amorphous-silicon semi-transparent PV glazings and traditional glazings is conducted. The optimal strategy by WWR for amorphous-silicon semi-transparent PV façades and its impact is proposed and discussed in this chapter.

Chapter 8 presents other implications of semi-transparent PV façades in office buildings. The effects of other architectural factors on overall energy performance when semi-transparent PV façades are used are discussed. The suitability of the optimal PVR/WWR strategies in different architectural conditions is investigated.

Environmental performance of the semi-transparent PV façades based on the carbon reduction by the amount of CO_2 and polluted emission including SO_2, NO and carbonaceous dust are presented in this chapter.

Chapter 9 summaries the main contribution of this thesis, states its limitations, and provides the suggestions for further investigation.

Chapter 2 Literature review

In Chapter 1, research objectives and methodologies have been identified and discussed. To further support the research ideas, the profound literature review is essential. In this chapter, contributed studies and knowledge related to the research objectives and methodology were reviewed in terms of four categories: photovoltaic technology and its development in China (Section 2.1), building façades and overall building energy performance (Section 2.2), semi-transparent PV façades and its impact on building energy performance (Section 2.3), tools and computation software (Section 2.4). Important discoveries and conclusions by these previous studies have been acknowledged and considered as an important basis for the formation of this study.

2.1. Photovoltaic technology and its development in China

2.1.1. Solar photovoltaic technology

Photovoltaic technology is known as a method to generate electrical power by solar cells, converting energy from solar energy to a flow of electrons. The continuous flow of electrons produces electrical power and is the basis of all types of PV applications (Gevorkian, 2007).

The most commonly used materials for photovoltaic devices include mono-crystalline silicon (Wawer et al., 2011; Sastry et al., 2010; Huld et al., 2011), poly-crystalline silicon (Becker et al., 2013), amorphous-silicon (Gracin et al., 2013; Rozario et al., 2014), cadmium telluride, and copper indium gallium. (Gevorkian, 2007). Each material exhibits different practical efficiency and prime cost. (Table 2.1) (Goetzberger and Hebing, 2000). The advantage of the crystalline silicon cell is that the practical efficiency is high, and the disadvantage is the large amount of energy consumed in production and the high cost, while the advantage and disadvantage of amorphous-silicon is the opposite to those of crystalline silicon.

The amount of electrical power generated by a solar PV device is continuously changing with the changes of the environmental factors (Alonso-Abella et al., 2014). Therefore, the use of Maximum Power Point Tracking (MPPT) techniques are required to maintain each cell the PV array's operating point at its MPP. Many MPPT techniques have been proposed in the literature, e.g., the Perturb and

Observe (P&O) methods (Hua and Shen,1998), the Constant Voltage (CV) method (Yu et al., 2004), the Incremental Conductance (IC) methods (Hussein et al.,1995), the Artificial Neural Network method (Sun et al., 2002), the Fuzzy Logic method (Kotta et al., 2006). These techniques vary in many aspects, including simplicity, convergence speed, hardware implementation, sensors required, cost, range of effectiveness and the need for parameterisation. The P&O, CV and IC techniques are the most widely used. Considering the different types of solar insolation and solar irradiance variations, the three MPPT techniques are compared by using the Matlab tool Simulink (Li et al., 2007). The P&O method is adopted in many BIPV projects for its advantage of highly efficient tracking results and economic feasibility. These studies have been reviewed to ensure the accuracy of the measurements of PV power generation in field studies, which is further discussed in chapter 3.

Table 2.1 PV material and efficiency

Cells material	Module efficiency	Area need for 1KWp	Costs	Efficiency impacted by temperature	Sensitivity with solar direct radiation
Mono-crystalline silicon	12%~15%	7 m2~9m2	High	Great	High
Poly-crystalline silicon	11%~14%	7.5 m2~10 m2			
Amorpho-silicon	6%~8%	14 m2~20 m2			
CIS material	8%~12%	9 m2~11 m2	Low	Small	Low
CdTe material	7%~10%	12 m2~17 m2			

2.1.2. Development of photovoltaic applications in China

The development of solar photovoltaic has become a very interesting and attracting topic in China in recent years. The demand and industry of solar

photovoltaic technology grows in a rapid speed after 2006. To demonstrate such development, the annual production and installation of photovoltaic modules are presented in Table 2.2 (Li and Wang, 2007 ; Chen, 2012 ; OFweek Research, 2012 ; Xu, 2012). Both the installation and production exhibited rapid growth; however, compared to the amount of production, the domestic installation in China is significantly lagging. China has great advantages in terms of field-tested, adequate, and relatively low priced PV products. These advantages provide great opportunities for the development of solar PV applications, including building integrated photovoltaic systems, in the future.

Table 2.2 Annual installation and production of photovoltaic in China

Unit: MWp	Year							
	2004	2005	2006	2007	2008	2009	2010	2011
Installation	10	8	10	20	40	160	500	2200
Production	50	200	400	1088	2600	4011	10500	21000

Meanwhile, in recent years, to address China's enormous energy consumption needs, the Chinese government mandated the implementation of all types of sustainable energy resources. Solar energy is one important part of this plan. Just in two years from 2012 to 2013, nine solar PV related policies that support the development of solar photovoltaic projects were released, as presented in Table 2.3 (NDRC, 2011 ; NDRC, 2013 ; NEA, 2012a ; NEA, 2013). These massive government-supported policies promote the development of solar photovoltaic technology in many aspects of research and development, including the solar PV manufacturing industry, distributed solar power implementation, BIPV projects, grid connection of solar PV projects, etc.

With the advantages from both the market and government supports, increasing numbers of solar PV projects are emerging in China. Table 2.4 presents the PV projects supported by the program known as the Golden Sun Demonstration Program, which was initiated by the Ministry of Science and Technology (MOST) and the National Energy Administration (NEA) (Xu et al., 2011 ; Lv, 2012).

Increasing numbers of projects are being approved and supported by this program, and they serve as the demonstration projects to further promote the development of solar PV power usage in China.

Table 2.3 Government-supported policies of PV released from 2012 to 2013

Issuing time	Issuing agency	Document title
January 2012	State Council	Five Year Plan for Renewable Energy Development
July 2012	NEA	12th Five Year Plan for Solar Energy Development
September 2012	NEA	Notice on Application for Scaling Up Demonstration Zones for Distributed Solar Power
September 2012	NEA	Notice on Application for Scaling Up Demonstration Zones for Distributed Solar Power
November 2012	State Grid	Opinions on Providing Good Services to the Grid Connection of Distributed PV Power Generation (Provisional)
July 2013	State Council	Opinions on Promoting the Healthy Development of Photovoltaic Industry
August 2013	NDRC	Notice on Promoting the Healthy Development of Solar PV Industry through Price Leverage
August 2013	NEA	Notice on the Construction of Scaling Up Demonstration Zones for Distributed Solar Power
August 2013	NDRC	Provisional Management Measures for Distributed Power

Note：NEA: National Energy Administration

NDRC: National Development and Reform Commission

Table 2.4 PV projects supported by the Golden Sun Demonstration Program

Phase	Year	Approved projects	Approved capacity (MW)
Ⅰ	2009	98	201
Ⅱ	2010	50	272
Ⅲ	2011	140	690
Ⅳ	2012	167	1709
Total		455	2872

Table 2.5 Breakdown of the cumulative PV installations in 2010

Category	Amount (MWp)	Change (compared to 2009)	Share (%)	Change (compared to 2009)
Rural electrification	75	+29%	9.4	- 9.9%
Communication and industry	42	+5	5.3	- 8.0%
PV products	40	+0%	5.0	+ 0%
BIPV/BAPV	256	+250%	32.0	+7.6%
Large scale PV stations	387	+335%	48.4	+19.2%
Total	800	+167%	100	0%

　　Among all of the solar PV projects in China, BIPV and BAPV (building attached photovoltaic) projects comprise a large fraction of them (Li and Wang, 2007; Chen, 2012; OFweek Research, 2012; Xu, 2012). Table 2.5 presents the breakdown of the cumulative PV installations in 2010, with BIPV and BAPV comprising 32% of the total installations. More than 256 MWp of solar PV capacity were installed in one year, which increased by 250% compared to that in 2009. The market share of BIPV/BAPV increased from 24.4% to 32.0%, indicating the rapid development of PV usage in buildings. Table 2.6 presents the BIPV projects supported by the Golden Sun Demonstration Program. The increase in

BIPV projects in the program also increased significantly. However, most of these BIPV/BAPV projects are installed with PV panels on the roof area. The implementations of PV façades in buildings are still at the very beginning stage, with few implementations in practice. The need for research and development of PV façades in China is urgent, especially because of the significant demand for BIPV and the lack of relevant field experiments and research studies.

Table 2.6 BIPV projects supported by the Golden Sun Demonstration Program

Phase	Year	Approved projects	Approved capacity (MW)
Ⅰ	2009	111	91
Ⅱ	2010	99	90.2
Ⅲ	2011	106	120
Ⅳ	2012	_	250
Total		_	551.2

2.2. Building façades and overall building energy performance

The PV façade, as one type of building façade, has an impact on energy performance that shares some similarities with the other types of buildings façades. The studies of the impact of façades (windows and walls) on building energy performance have been widely performed in the past decades, and a review of these studies is an important basis for the research of the impact of PV façades on building energy performance.

2.2.1. Impacts of different factors of façades on energy consumption

The configurations and layouts of façades have a profound impact on the energy performance. The WWR (window-to-wall ratio) has been identified as one of the most important factors among all of the façade configurations. S. Saridar (Saridar and Elkadi, 2002) performed a research study in which several buildings in Eastern Mediterranean are examined to discover the impact of WWR of façade on energy consumption. Table 2.7 presents the WWR of three building façades of

architectures built in different periods of time. The differences between the cases are obvious in terms of energy performance by the different WWR.

Table 2.7 WWR and annual lighting electricity consumption of several types of buildings

Date of construction	WWR			Annual electricity consumption (Kwh/m^2)
	South Wall	North Wall	East/West Wall	
1978	0.72	0.87	0.63	3.26
1982	0.25	0.25	0.08	30.52
1994	0.58	0.58	0.58	7.63
1997	1	0	0.44	20.37

Furthermore, other factors, such as building orientation, climate, glazing type, and fixed exterior shading, are also identified in terms of the relationship between the façades and the building energy performance, such as annual energy use and peak cooling loads, and these factors have been thoroughly analysed in a number of studies conducted over the past several decades. The impact of the selection of design strategies, including glazing type and fixed exterior shading, on energy use and peak loads is assessed through a series of parametric studies in the book Window Systems for High-Performance Buildings (Carmody et al., 2004). The effect of the façade on energy use is also a consistent thread in the book ClimateSkin (Hausladen et al., 2008) and is a major element in the book, PlusMinus 20°/40° Latitude (Hindrichs and Daniels, 2007). The premise of the latter book is that most of the global population lives in the region from 20° north to 40° south latitude, and therefore, this is a region on which design teams and manufacturers should focus attention for building performance. A majority of sources on this topic stress the potential of the building envelope in reducing energy use through the use of daylighting, solar heat gain control strategies, natural ventilation, and integration with HVAC and lighting systems.

To date, a number of studies (Jaber and Ajib, 2011; Serra et al., 2010; Jin and Overend, 2014; Ghadimi et al., 2013; Goia et al., 2014; Infield et al., 2006; Han et

al., 2013; Infield et al., 2006; Charron and Athienitis, 2006) have been conducted on energy saving buildings using climate-sensitive windows and façade technologies, including double façade skin, advanced shading and PV façades. A study (Jaber and Ajib, 2011) investigated different effects of the U-value, SHGC (solar heat gain coefficient), orientation, and size of the windows on the annual heating and cooling energy demand. Three different climate zones with four glazings: single glazed, double glazed L, double glazed H and triple glazed. The study indicated that 20-24% of the energy use can be saved by a well-optimised glazed window according to different climates of Amman, Aqaba and Berlin.

From all of the above-mentioned studies, the two most important aspects identified among the different branches of these studies are daylighting performance and thermal performance (heating and cooling). These aspects are particularly important in office buildings because they are mainly operating during the daytime. The daylight and thermal demand is largely affected by building façades.

2.2.2. Daylighting performance

Daylighting provides the visual and pleasant indoor environment for people in office rooms as a natural lighting source. The colour rendering index of daylighting is the best in all lighting sources and thus it is a high quality source of light. Daylighting is achieved by the light passing through building façades (window glazing or any semi-transparent material).

In Hong Kong, Li and Lam (Li et al., 2010) measured the illuminance on façades and investigated the energy savings from the use of daylighting for different façades (windows). A study of the effect of building envelope on the daylighting efficiency in an office building was performed by Boyano (Boyano et al., 2013), the results led to the conclusion that lighting plays a significant role in energy use. Different reports suggested that reducing the WWR can lead to a better energy performance, but simultaneously reduces the daylighting efficiency (Poirazis et al., 2008; Motuziene et al., 2010; Susorova et al., 2013). Motuziene and Joudis (Motuziene et al., 2010) analysed the office buildings in Lithuania and suggested that with 20–40% of the optimal WWR, the energy performance

remained the best. However, such low WWR would have problems meeting the daylighting requirements.

2.2.3. Thermal performance: U-value and SHGC

In terms of the thermal performance of building glazing façades, a large amount of studies in the past decades have identified the following as the two most important and significant values: U-value and SHGC.

The U-value can be referred to as an 'overall heat transfer coefficient' that measures how well parts of a building transfer heat, i.e., the higher is the U value, the worse is the thermal performance of the building envelope. A low U value usually indicates high levels of insulation. The U-value is useful because it is a way of predicting the composite behaviour of an entire building element rather than relying on the properties of individual materials (Brennan, 2014). In addition, U-values are important because they form the basis of any energy or carbon reduction standard. In practice, nearly every external building element must comply with thermal standards that are expressed as a maximum U-value. Knowledge of the U-values at an early stage in the design process avoids subsequent expensive re-working in a project. The U-value allows the designer to test the feasibility of their project at an early stage to ensure it is appropriate for the purpose and will comply with the regulatory frameworks.

The SHGC is the fraction of incident solar radiation admitted through a window, both directly transmitted and absorbed and subsequently released inward. SHGC is expressed as a number between 0 and 1. The lower a window's solar heat gain coefficient, the less solar heat it transmits. The nationally recognised rating method by the National Fenestration Rating Council (NFRC) is for the whole window, including the effects of the frame. Alternately, the centre-of-glass SHGC is sometimes referenced, which describes the effect of the glazing alone. Whole window SHGC is lower than glass-only SHGC, and the value of whole window SHGC is generally below 0.8 (RIBA, 2014).

2.3. Semi-transparent PV façades and its impact on building energy performance

In recent years, it appears that interest in energy conservation and renewable energy application in buildings has greatly increased, as evidenced by building integrated photovoltaic (BIPV) technology becoming widely used as part of the façade in modern buildings (Roberts and Guariento, 2009; Weller et al., 2010). Semi-transparent solar PV façades, different from conventional solar PV modules, have PV cells incorporated into glazing materials (Lim et al., 2013). In addition to generating electricity, semi-transparent PV façades allow daylighting and reduce heat gain in buildings due to the blocking of some of the solar radiation by the PV cells; such semi-transparent PV façades are anticipated to be widely used as façades in office buildings.

Semi-transparent PV is beneficial to energy savings in buildings because it not only generates electricity but also introduces daylight, which can reduce the artificial lighting energy consumption(Li et al., 2009). In addition, semi-transparent PV reduces the heat gain by blocking the solar radiation with the PV cells, which will increase the heating demand of the inner space in winter but reduce cooling demand in summer (Lu and Law, 2013). These impacts above are contradictory in terms of overall energy conservation, and studies suggest that the answer lies in the balance of the penetration of daylight and the solar heat gain.

Semi-transparent PV façades can be achieved by different PV materials. Mono-crystalline silicon and amorphous-silicon are the two most commonly used materials for semi-transparent PV glazings. These two PV technologies are different in many ways, including PV electricity generation efficiency, thermal characteristics, transparency and the integration in glazings. As a result, their impacts on energy performance are also different.

2.3.1. Mono-crystalline silicon semi-transparent PV

For mono-crystalline semi-transparent PV glazing, the mono-crystalline solar cells on the laminate are spaced so that the partial light filters through the PV module and illuminates the indoor space (Figure 2.1). Light effects from these panels lead to an ever changing pattern of shading in the building itself. The indoor rooms remain shaded, yet not constrained. Adding layers of glass to the base unit of a semi-transparent PV glass module can offer thermal insulation (Roberts and

Guariento, 2009). For mono-crystalline semi-transparent PV glazing, the PVR (PV coverage ratio) largely controls the transparency of the PV glazing and is thus a very important parameter.

Figure 2.1 Image of mono-crystalline semi-transparent PV glazing

The PVR determines the solar transmittance of mono-crystalline semi-transparent PV façades and appears to be an important factor in terms of window and façade design of BIPV because it controls the amount of solar radiation through the building envelope, which has an impact on the energy consumption of the lighting, cooling and heating systems (Vartiainen, 2010; Miyazaki, 2005; Yun et al., 2007; Nalanie Mithraratne, 2014; Jiang et al., 2008). Vartiainen (Vartiainen, 2001) found that the façade layout of different proportions of PV cells and window glazing area will have a significant impact on the overall benefits on lighting energy savings. Miyazaki (Miyazaki, 2005) found that energy consumption was minimised with the solar cell transmittance of 40% and a window-to-wall ratio (WWR) of 50%. Yun et al. (Yun et al., 2007) explored the overall energy performance of limited combinations of the window ratio and room depth in a ventilated photovoltaic façade. The above-mentioned studies and other related studies (Nalanie Mithraratne, 2014; Jiang et al., 2008) indicate that an optimal PVR exists and should be investigated thoroughly as an important part of

the design approach in terms of maximising the benefit of the use of a PV system on the overall energy performance.

Different climate environments would result in different overall energy savings due to the optimisation of the PVR used on PV façades. In Brazil, semi-transparent windows save as much as 43% of the energy consumption (Yun et al., 2007), while in Japan, 55% of the overall energy is saved using a solar cell transmittance of 40% compared to a normal glazing façade (Wong et al., 2008). In Singapore, energy savings of 16.7% to 41.3% can be achieved using mono-crystalline semi-transparent PV façades (Leite Didoné and Wagner, 2013). Other studies (Ng et al., 2013; Lu and Law, 2013) also suggest that it is important to consider the impact of the urban and climate environment on the design of mono-crystalline semi-transparent PV façades.

2.3.2. Amorphous-silicon semi-transparent PV

Different from mono-crystalline semi-transparent PV glazings because the layer of the amorphous-silicon PV cell is so thin or is laser grooved to enable light to pass through, filtered light is transmitted through thin-film amorphous-silicon semi-transparent PV glazings instead of the shadowed light of the mono-crystalline semi-transparent PV glazings. Semi-transparent thin-film PV modules are especially appropriate for use as PV façades (Figure 2.2).

Figure 2.2 Image of amorphous-silicon semi-transparent PV glazing

Studies of amorphous-crystalline semi-transparent PV glazings are relatively limited. Evelise Leite Didoné (Leite Didoné and Wagner, 2013) investigated the potential of energy saving and electricity generation of semi-transparent PV glazings (amorphous-silicon included) of office buildings in Brazil. The study indicated that it is possible to reduce the energy consumption for artificial lighting and AC and furthermore to generate energy using amorphous-silicon semi-transparent photovoltaic panels in windows. The study also provided a comparison between semi-transparent PV glazing and Low-E glazing, which proved that Low-E glazing has a better energy performance. Poh Khai Ng (Ng et al., 2013) performed an energy analysis of semi-transparent PV glazings (several amorphous-silicon models included) in Singapore. The study revealed the potential to use amorphous-silicon semi-transparent PV glazings for all orientations in tropical countries including Singapore. This study specifically indicated that optimising the WWR with different design strategies is necessary to achieve the highest electricity benefit for semi-transparent PV glazings (amorphous-silicon included). In terms of field experimental research, L. Olivieri (Olivieri et al., 2014) investigated four amorphous semi-transparent PV modules of different transmittances in Madrid. The study found that the solar protection and insulating properties of amorphous-silicon semi-transparent PV modules are lower than those achieved by a reference glazing, whose characteristics are in accordance with the Spanish Technical Building Code. The electricity conversion efficiency is found to be minimally affected by the transmittance of amorphous semi-transparent PV glazings.

2.4. Tools and computational software

2.4.1. Assistant tools and software for the optimal design of a PV system

A large number of assistant tools and software have been developed in recent years to provide the necessary information for designers and engineers in designing and simulating PV systems. These tools can be categorised into four types (Norton et al., 2011):

Table 2.8 Tools and their features for the optimal design of PV systems

PV f-Chart	For design and analysis PV systems. Predicts monthly performance of PV system with array efficiency calculated by cell temperature. Provides long period performance by weather data.
PVWATTS	Simulates PV electricity generation of grid-connected PV system with internet access (USA only)
PVSYST	Simulation based on database of meteorological and inbuilt geographical. Using 3D CAD facility for visualisation. Losses are considered such as wiring losses, temperature losses, reflection losses etc. Capable of modelling grid-connected system of different inverters and load profiles with measured data.
PVSOL	Used for optimization and design of PV systems. Provides a database of a large PV and inverter manufacturers. Defined component specifications by users are accepted. Capable of different PV surface inclinations and orientations. Performs
SOLCEL-II	Predict PV electricity generation by hourly values such as normal radiation, air temperature, inplane insolation and wind speed etc. Simulates hourly performance of PV system by employing MPPT, voltage regulator and temperature co-efficiency etc.
TRNSYS	Provides PV system simulation as sequential modular program. Individual components (empirical or analytical) can be adopted to perform different simulation needed.
PVFORM	Designed for standalone and grid-connected applications with inputs such as insolation, air temperature, wind speed etc. MPPT is also considered in this program with partial load efficiency.

(1) Pre-feasibility tools: These tools are used for determining the suitability of BIPV systems for particular projects. In these tools, BIPV applications are examined through PV electricity generation and the life cycle cost.

(2) Sizing tools: These tools are used for optimising the size of different parts of a BIPV system. The determination is based on the purpose and life cycle cost of the analysed system.

(3) Simulation tools: These tools are used for simulating the detailed behaviours and performance of a PV system in a given situation. Information is provided regarding the financial and environmental features of the analysed PV system.

(4) Open-architecture research tools: These tools are used for adding new components or modifying existing components into main programs.

To further illustrate the tools and computational software that are most commonly used for the optimal design of a PV system, several tools and their features are described in Table 2.8 (Klein and Beckman, 1993; Marion and Anderberg, 2000; Mermoud, 1995; Hoover, 1980; Klein et al., 1979; Menicucci and Fernandez, 1989).

2.4.2. Computation simulation tools for energy performance simulations

The energy requirements of a building depend not only on the individual performance of the envelope components (walls, windows and roofs) and HVAC and lighting systems but also on their overall performance as an integrated system within the unique building. For a large commercial building, the complex and dynamic interactions occurring in the building with its environment and its systems and plants must be modelled and simulated for analysis. The modelling technique available to architects, engineers and building managers concerned with energy conservation is simulation of the building energy use. Energy simulation is a valuable tool for architects and engineers to evaluate building energy consumption before the building is built. Alternative designs or materials can immediately be evaluated to determine how much they affect the annual energy consumption. Through parametric analyses, professionals can extend their design concepts to

incorporate new technologies and innovations, thus creating opportunities for increased energy savings.

Over the decades, a large number of energy simulation programs have been developed. Some of the more popular simulation packages and their information are listed below (Hong et al., 2000).

Table 2.9 Building simulation software packages

Program	Developer organizations	Website
DOE-2	Lawrence Berkeley Laboratory, USA	(http://eande.lbl.gov/BTP/simulations/DOE2.html)
BLAST	University of Illinois, USA	
ESP	University of Strathclyde, UK	http://www.strath.ac.uk/Departments/ESRU/ESP-r.htm)
TRNSYS	University of Wisconsin, USA	(http://sel.me.wisc.edu/trnsys/
DEST	Tsinghua University, P.R. China	http://www.dest.com.cn/
EnergyPlus	Department of Energy, USA	http://apps1.eere.energy.gov/buildings/energyplus/

Among all of the tools above, EnergyPlus is the one used most often in recent years. EnergyPlus is a popular building energy simulation program that builds on the strengths of BLAST and DOE-2. EnergyPlus was written in Fortran 90 with a structured, modular code that is easy to maintain, update, and extend. The EnergyPlus source code is open for inspection and is understandable, which enables developers around the world to develop new modules algorithmic or interfaces in EnergyPlus.

Modelling the performance of a building with EnergyPlus enables building professionals to optimise the building design to use less energy and water. Each version of EnergyPlus is tested extensively before release. EnergyPlus models heating, cooling, lighting, ventilation, other energy flows, and water use. EnergyPlus includes many innovative simulation capabilities: time-steps less than an hour, modular systems and plant integrated with heat balance-based zone simulation, multi-zone air flow, thermal comfort, water use, natural ventilation, and photovoltaic systems (Crawley et al., 2001). In terms of the EnergyPlus structure, it has three basic components: simulation manager, a heat and mass balance simulation module, and a building systems simulation module. The simulation manager controls the entire simulation process. The heat balance calculations are based on IBLAST, a research version of BLAST with integrated HVAC systems and building loads simulation. Many studies (Tabares-Velasco et al., 2012; Andolsun et al., 2011; Rempel et al., 2013; Mateus et al., 2014) have validated many aspects of the EnergyPlus simulation capabilities, including thermal calculation, daylighting simulations, and ventilation simulation, with measured data. The validations provided in the mentioned studies and references have shown that Energy Plus is relatively reliable in general conditions. In terms of particular studies of BIPV((Leite Didoné and Wagner, 2013; Ng et al., 2013; Miyazaki et al., 2005; Wong et al.,2008), Energy Plus has also been used widely as it provides an excellent access to architecture modelling tools like SketchUP, which is very useful for architects to create the needed architecture models for simulations. The use of Energy Plus in BIPV studies seems to indicate the reliability of its results. However, in a given simulation condition, different settings of the boundary conditions could lead to a slightly varied result and such limitation should be carefully considered, which however could be solved by carried out more validation tests of the results under the exact boundary conditions of the needed simulation conditions.However, no simulation tool, not even EnergyPlus, exists that provides the calculation models for semi-transparent PV glazings. Special modification based on existing tools is required for simulation of the overall energy performance of semi-transparent PV glazings.

2.5. Conclusions

In this chapter, contributed studies and knowledge were reviewed in terms of four categories. Important discoveries and conclusions by previous studies were acknowledged and considered thoroughly, which enabled several conclusions to be made:

(1) BIPV is in great demand and has a promising future in China, with the significant advantages of the production market and government policy.

(2) Building façades have been recognised to have multiple significant impacts on the overall energy performance, including daylighting and heating and cooling electricity consumption. Parameters such as WWR, Room depth, U-value, and SHGC significantly impact the overall energy performance. Many studies have been performed to develop strategies to optimise the parameters to achieving a better energy performance.

(3) Studies of the two main types of semi-transparent PV glazings primarily focus on the impact of transmittance/PVR/WWR on energy performance. Different strategies related to optimal transmittance have been made to achieve a better energy performance.

(4) There are varied computational tools specifically designed for the installation of PV systems on building roofs. In terms of computational simulation tools, EnergyPlus is capable of simulating overall energy performance and is acknowledged as reliable and is often applied in academic studies.

However, few studies to date have attempted a comprehensive determination of the optimal PVR/WWR for semi-transparent PV technology using different combinations of architectural factors, such as room depth, WWR and orientation. Accordingly, no general trends have been defined regarding variations in optimal PVR. Such knowledge will play a crucial role in future optimal design approaches for semi-transparent PV façades; as a result, improvements in the understanding of the variation in PVR are urgently required. In particular, previous studies providing accurate assessments of the overall energy performance of semi-transparent PV façades in China are extremely limited, and few relevant experiments have been

conducted under the climatic conditions similar to those in central China. Studies conducted under real climatic conditions are necessary because several studies investigating semi-transparent PV in different climate zones have produced different results.

Chapter 3 Experimental room set-up and field measurement

The determination of performance for semi-transparent PV façade requires the tests are conducted in the outdoor environment. The experimental room allow the semi-transparent PV glazing to be tested in realistic, but controlled, conditions. This is important for achieving the electrical, thermal and optical characteristics of the PV glazings.

The aim of this chapter is to demonstrate the experimental study involved a series of field measurements using an experimental room with the semi-transparent PV façades in realistic climate conditions of Wuhan, China. In Section 3.1, the experimental rooms for studying building components used by previous researchers are reviewed, and the knowledge and experience gained from such experimental rooms are introduced. Next, the experimental methodology in our research is presented in Section 3.2 and Section 3.3, with the descriptions of layout of the experimental room, the parameters of the PV modules used in the test, and the measurement equipment and arrangements. Finally, the general field measurement results are presented in Section 3.4.

3.1. The motivation of experimental room set-up

3.1.1. Review of previous experimental room

To provide high-quality test environments for evaluating the energy performance of building components under realistic climate conditions, some experimental rooms were constructed by previous researchers over the past decades. During the testing of a broad range of building components, the experimental procedures and measurement techniques have been developed and improved gradually. The two important cases of experimental rooms are described and the successful methodologies on the use of these experimental rooms are summarised in subsequent paragraphs.

(1) MoWiTT for thermal performance of windows

Klems (1984) constructed and calibrated an experimental room called MoWiTT (Mobile Window Thermal Test) at Lawrence Berkeley Laboratory in the U.S. The U-value and G-value of the building components, the two characteristic parameters of the thermal and solar-optical transmittance, were determined using careful measurements under realistic field conditions in MoWiTT (Klems, 1988a;

Klems and Keller, 1987). Consisting of dual, guarded, room-sized calorimeters in a mobile structure, the MoWiTT is capable of simultaneously exposing two fenestration samples, each experiencing a room-like interior environment, to ambient outdoor weather conditions and of measuring the net heat flow through each fenestration with good accuracy.
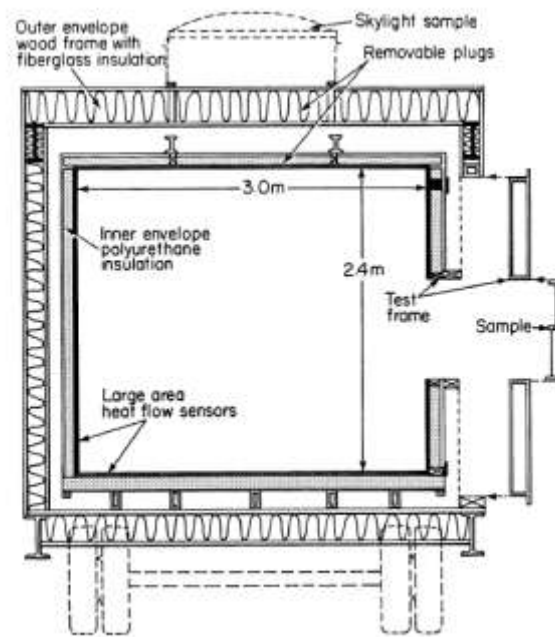
Figure 3.1 Section of MoWiTT
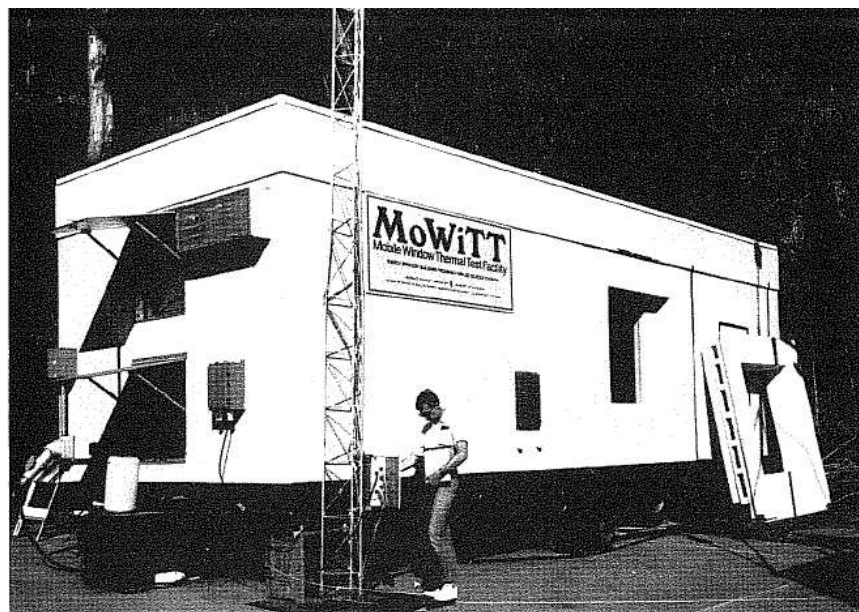
Figure 3.2 Image of MoWiTT

MoWiTT was also applied to the validation work of a glazing simulation package, WINDOW. The experimental results from MoWiTT and the simulation results from WINDOW exhibited good agreement in the studies of Klems (Klems, 1988a; Klems, 1988b).

(2) PASLINK test cell

Funded by the European Commission research projects, the PASLINK test cells that can provide high-quality test environments were established to quantify the performance of a passive solar building. All types of building components, including advanced glazed components, window components, synergy façade, air supply window, conservatory, shading elements, ventilated roof, hybrid PV ventilated façades, façade heating system and solar collectors, had been tested in the experiment room of PASLINK (Strachan and Vandaele, 2008).

Many European laboratories, such as the Belgian Building Research Institute at Limelette, Belgium, the Building Research Establishment in East Kilbride, Scotland, the Fraunhofer Institute, Germany and Pilkington in Lathom, England established experimental rooms.

One example of the PASLINK test cell was constructed in Porto, Portugal, to investigate the energy performance of the SOLVENT window under local climate conditions. The test cell was equipped with a so-called pseudo-adiabatic shell (PAS), which limits the heat loss through the floor, roof and walls to a very low and precisely quantifiable value. A large amount of environmental parameters were recorded systematically, which included global and diffuse solar radiation, outdoor air temperature, relative humidity, wind speed and direction. The PASLINK test cell is equipped with instrumentation to measure parameters related to the SOLVENT window, including glazing temperature at each glazing surface, air temperature in the open air channel, velocity of the air at the centre of the air gap, and air temperature at various points inside the test cell. The tests were performed in both summer and winter. Each configuration of the SOLVENT window was monitored for at least one week, with each week including at least two days with a clear sky. During the monitoring period, the test room temperature was maintained at 23.5 ±0.5 ℃ by a heating and cooling system (Lea and Maldonado, 2008).

With the data collected in the experiment room, the models of the SOLVENT window were developed to evaluate the energy savings in the applications of innovative building components to realistic buildings.

Figure 3.3 Image of the PASLINK test cell for the SOLVENT window

(3) Summary of the experimental room

Although the construction and development of an experimental room is expensive and time-consuming, such work has its unique advantages. The experimental room provides an evaluation of the visual appearance and the detection of building details, such as thermal bridges. The availability of an experimental room established in different climate zones allows the performance of building components to be verified under local climate conditions.

From the construction and development of an experimental room by previous researchers, the general methodology of the experimental procedures and analysis techniques are summarised as follows: (Strachan, 2008)

First, the suitable size of the building component is designed to fit in the experimental room.

Second, field experiments record the relevant data for the evaluation of the building component.

Third，key parameters and indicators of building components acquired from the experiments are used to develop simulation models.

Fourth, careful validation is performed to confirm the accuracy of the calculation models with the measurement results.

Finally, the validated models of building components are incorporated into simulation programs to investigate full-scale building energy performance in the climate of interest.

3.1.2. General considerations on experimental room and measurement

In this study, to evaluate the performance of semi-transparent PV façades in actual Wuhan weather conditions, an experimental room was installed on the roof of a 5-storey building in Wuhan (29°58'N, 113°53'E). The field measurement data were collected to develop and validate the mathematical models of semi-transparent PV façades, which are presented in the later chapter. For the above purpose, general considerations on the experimental room and the measurements performed are listed below.

(1) The experimental room should be located in a location free from shading in Wuhan.

(2) The PV glazing should be fixed on the south façade of the experimental room.

(3) There should be two equivalent units in the experimental room so that the performance of two PV glazings on the façade can be recorded for a comparative study.

(4) To investigate the energy performance of the two units with PV façades, each unit should be designed as a separate chamber.

(5) The experiment should be conducted for a long period, i.e., greater than 12 months, and the field-measured data should be systematically recorded in a proper interval time.

(6) To acquire the essential parameters pertaining to the electrical, thermal and optical characteristics of the PV glazings, data from field measurements should include temperature, illuminance, PV generating electricity and solar radiance, among other parameters.

(7) The requisite methods should be taken to guarantee the necessary precision and accuracy in the measurements.

The details regarding the experimental room set-up and the field measurements are described below.

3.2. Experimental room set-up

3.2.1. Layout of the experimental room

An experimental room containing two inner and separate chambers to determine the PV glazing performance for two glazings simultaneously was set up on a flat roof of the building in the campus of Huazhong University of Science and Technology. There are no nearby buildings and trees in the south of the experimental room; therefore, the tests were not influenced by shading. The experimental room had a length, width, and height of 4.65 m, 3.4 m, and 3.6 m, respectively, and was constructed using mineral wool board with a thickness of 12 mm as the thermal insulation of the walls. The experimental room contained two inner chambers sharing a guarded room, each of which included a window that was 1.1 m long and 1.3 m high on the southern vertical façade. The windows were designed as a changeable system by which different types of glazing components could be fixed on the window. The plan, section and photo of the experimental room are shown in Figure 3.4 to Figure 3.6. A detailed description of the experimental room is presented in Table 3.1.

The author of the thesis is the prime investigator of the experimental study. The author designed the layout of experimental room, set the experimental schedule and organized all kinds of tasks in the experiment. The workers from

Wuhan Lingyun Building Decorative Engineering Company Ltd. built up the experimental room. Some students of Huazhong university of Science and Technology installed the glazing on the facade and collected the measured data during the experimental period.
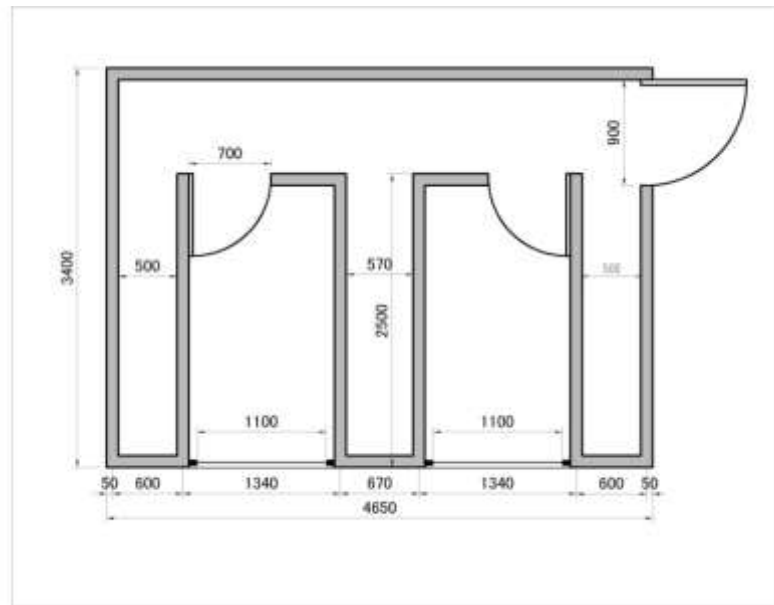
(a)
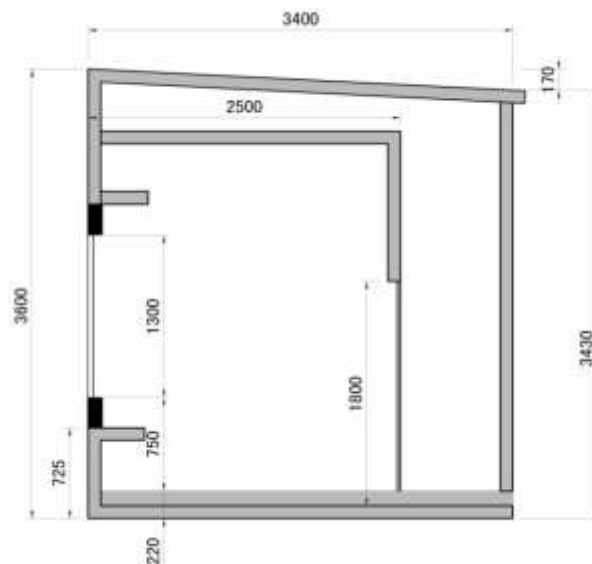
(b)

Figure 3.4 Layout of the experimental room

(a) Plan, (b) Section

Figure 3.5 Image of the experimental room

Table 3.1 Descriptions of the experimental room

Dimensions of the experimental room	4.65m×3.4m×3.6m (length×depth×height(from front))
Dimensions of the inner room	1.34m×2.4m×3.0m (length×depth×height)
Dimension of the window	1.1m×1.3m (length×height)
Window area	1.43m^2
Wall material	Mineral wool board (thermal insulating material) thickness: 12mm
Construction structure	Steel
Special design	Break the heat bridge
Inner room temperature control	"GREE" air-conditioning, power: 1.25W
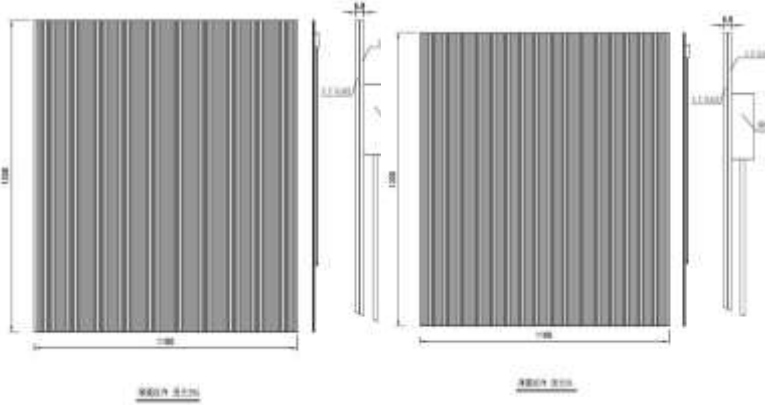
3.2.2. Properties of the PV glazings

Four types of PV glazing modules were studied in the test. They are fixed on the window one-by-one for different test groups for their performance comparison against each other. The properties of the PV glazing modules, which were provided by the respective manufacturer company, are listed below. Three of the PV glazings are semi-transparent, and the fourth PV glazing is opaque. To ensure the airtightness between the PV glazing and the widow frame, every time when the PV glass got replaced, a cover plate together with full-length rubber seals on each edge is used, by which it is considered as airtight state. Both the Two inner chambers are preceded with the same method to ensure the same identity of the two rooms.

Table 3.2 Descriptions of the four PV glazings considered in the study

PV glazing code	PV-1	PV-2
PV glazing type	Monocrystalline semi-transparent PV	
Dimensions	1.1m×1.3m(length×height)	
Layers of the glazing (external to internal)	6mm super white tempered glass (low iron tempered glass)-EVA- monocrystalline solar cells-EVA-6mm semi-tempered glass	
Dimensions of the solar cells	Number: 6×6 (series×parallel) Size: 156mm×156mm	Number: 6×6 (series×parallel) Size: 125mm×125mm
Solar cell area	0.8761m^2	0.5625 m^2
Solar cell ratio of the PV glazing	61.3%	39.3%
Reference output power	140W	95W
Operating voltage	18.45V	18.74V
Operating	7.588A	5.069A

current		
Open circuit voltage	21.23V	21.97V
Short circuit current	8.793A	5.765A
Picture		
Effective transmittance (visible light)	35%	60%
Manufacturer	CSG Holding Co., Ltd. (China)	
Weight	44.5kg	
Total thickness	12mm	

PV glazing code	PV-3	PV-4
PV glazing type	Amorphous-silicon semi-transparent PV	Amorphous-silicon opaque PV
Dimensions	1.1m×1.3m(length×height)	
Layers of the glazing (external to internal)	6 mm super white tempered glass (low iron tempered glass)-EVA- Amorphous -silicon thin film-EVA-6 mm semi-tempered glass	6 mm super white tempered glass (low iron tempered glass)-EVA- Amorphous-silicon thin film-EVA-6 mm opaque glass
Dimensions of the solar cells	1.1m×1.3m(length×height)	

Soar cell area	/	
Solar cell ratio of PV glazing	/	
Reference output power	75W	150W
Picture		
Effective transmittance (visible light)	20%	0%
Manufacturer	CSG Holding Co., Ltd. (China)	
Weight	44.5kg	
Total thickness	12mm	

3.3. Measurement equipment and arrangements

3.3.1. Measurement equipment

The field experiment was conducted 24 h a day from June 2012 to August 2013. The equipment included a thermocouple, luxmeter, pyranometer, and power recorder used to collect the series of data of temperature, illuminance, solar irradiance, and PV output power, respectively. All of the above data were acquired by a data logger with the interval of 1 minute all throughout the experimental period and were sent to the computer nearby for storage. General data describing the weather conditions were recorded at hourly intervals using the Davis Vantage Pro 2 weather station. All of the pieces of measurement equipment are listed in Table 3.3.

Table 3.3 Descriptions of measurement equipment

Device	Specification and Manufacturer	Measurements
Pyranometer	Jinzhou Sunshine，TBQ-2，China	Horizontal and vertical total solar irradiance
Luxmeter	TES，TES-1339R，Chinese Taiwan	Indoor and outdoor illuminance
Thermocouple	T type thermocouple, China	Glazing surface and air temperature
Power recorder	Agilent, 34972A, USA	PV output current and voltage
Data logger	Agilent, 34972A, USA	Data acquisition
Weather station	Davis, Vantage Pro 2，USA	Ambient temperature, barometric pressure, humidity, wind velocity- and direction.

3.3.2. Arrangements of the temperature measurement

A total of 12 T-type thermocouples were used to measure the temperature on both the inside surface and the outside surface of the PV glazing and the ambient temperature of the inner room, the guarded room and the outside of the experimental room. All of the thermocouples were connected to a Data Acquisition apparatus, Agilent 34972A, made in the USA. The simultaneous temperature data were captured once per minute and were sent to a computer through a network cable. These thermocouples were calibrated by placing them together with a standard mercury thermometer (with precision of 0.1 ℃) into a thermostatic water bath of temperature ranging from 0 ℃ to 100 ℃. Through this calibration, the accuracy of the thermocouples was improved to ±0.1 ℃, which meets the test requirements. The arrangement of the temperature measurement points is presented in Figure 3.6. To avoid the unnecessary solar heat gain from solar radiation on the

thermocouple of the outer surface, a small opaque aluminum foil is used to block the solar radiation and prevents it from heating up the thermocouple. Since the touch point of thermocouple is very small, it is considered that the opaque aluminium could effciently avoid the unnecessary solar heat for the thermocouple while it barely affects the heat transfer process and the temperature of the PV glass.
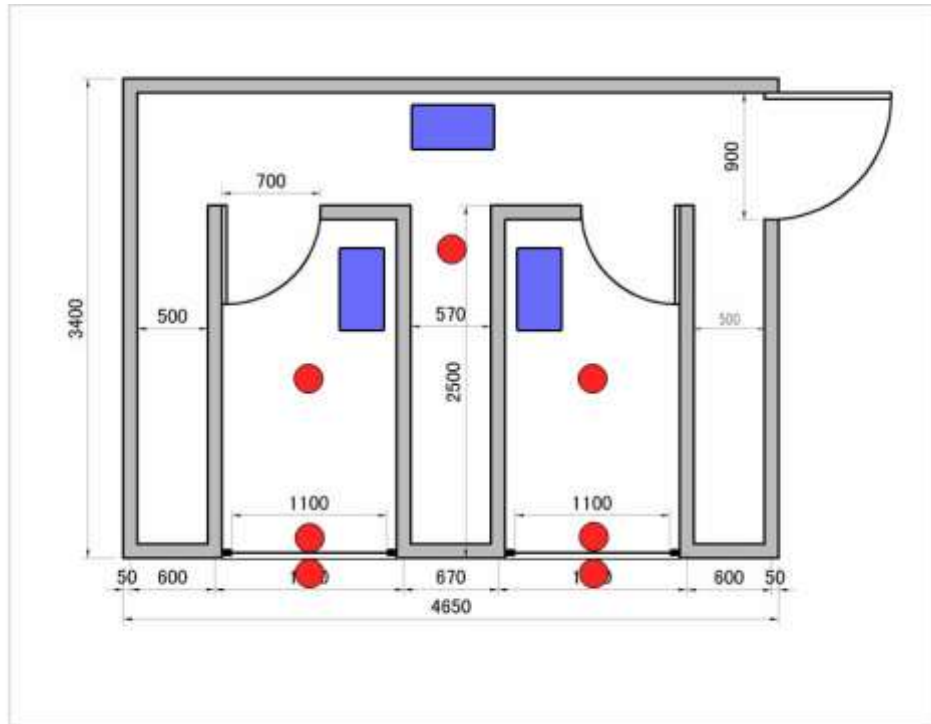
Figure 3.6 Arrangement of the temperature measurement points

3.3.3. Arrangements of the solar irradiance measurements
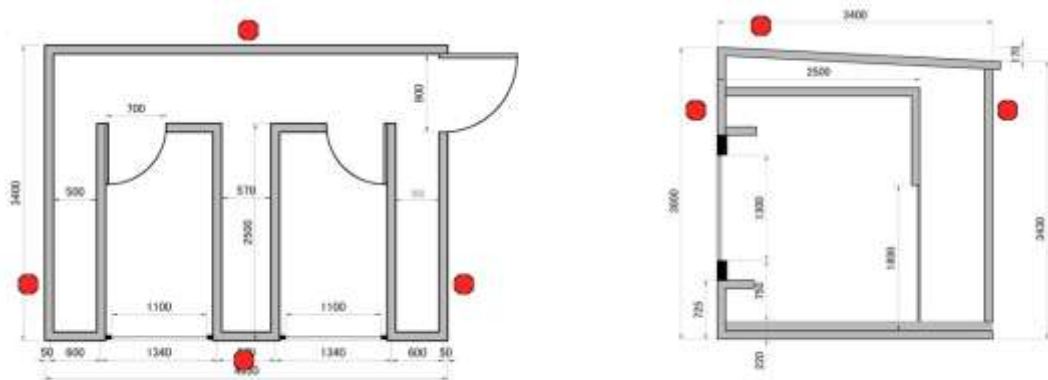
Figure 3.7 Arrangement of the solar irradiance measurement points

TBQ-2 pyranometers with an accuracy of ±5% manufactured by Jinzhou Sunshine, China, were installed on each of the east, south, west and north facing façades and were used to measure the global solar irradiance on the four vertical planes. Two pyranometers were installed on the flat roof of the experimental room as a group. One pyranometer was used to measure the global solar irradiance on horizontal plane, and the other pyranometer nearby, which was fitted with a shadow ring to block the direct sun, was used to measure the diffuse solar irradiance on the horizontal plane. The ring has a polar axis design requiring adjustment for solar declination every few days. The pyranometers were connected to the Agilent 34972A apparatus, and the exact solar irradiance data were calculated using the measured voltage sent from the pyranometers to the Agilent 34972A and the sensitivity of each pyranometer. The data were recorded at the interval of 1 minute and sent to the computer for storage-. The pyranometer device was calibrated by the manufacturer before performing the experiments, and the sensitivity of each pyranometer was labelled on the instrument. The arrangement of the solar irradiance measure points is presented in Figure 3.7, and an image of the group of pyranometers on the horizontal roof is shown in Figure 3.8. The specifications of the pyranometer are presented in Table 3.4.

Figure 3.8 Image of the group of pyranometers on the experimental room roof

Table 3.4 Specifications of the TBQ-2 pyranometer

Specification	TBQ-2
Sensitivity	7-14μV/(W/m-2)
Wavelength range	0.3-3.0μm
Accuracy of measurement	±5%
Measurement range	0-2000W/m-2
Response time	30 sec (99%)
Weight	2.5kg

3.3.4. Arrangements of the PV output power measurements

Because the maximum of the PV output power varies according to the solar irradiance, the maximum power point is changing constantly under real weather conditions. The maximum power, determined by the optimal voltage multiplied by the corresponding current, is the point determined by the MPPT. In this test, MPPT systems were used to track the maximum power point of PV panel through the control of the Perturb and Observe (P&O) algorithm, by which the MPPT system could attain high accuracy. The Agilent 34972A instrument collected the voltage and current of each PV glazing every minute throughout the test period.

3.3.5. Arrangements of the daylighting illuminance measurements
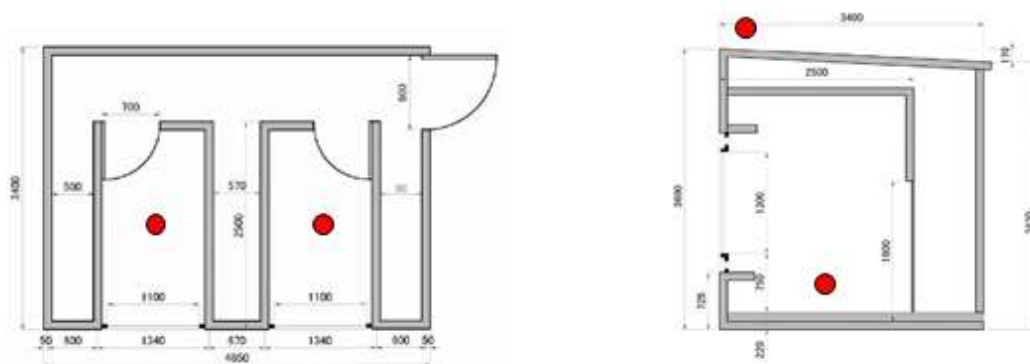
Figure 3.9 Arrangement of the illuminance measurement points

Table 3.5 Specifications of the TES-1339R luxmeter

Specification	TES-1339R
Measurement range	4 efficient digit reading(99.99lx, 999.9lx, 9999lx, 99990lx, 999900lx)
Accuracy of measurement	±3%
Temperature characteristic	±0.1%/℃
Sampling rate	5 times/sec
Weight	320g

Likewise, the arrangement of the illuminance measurement points is presented in Figure 3.9. The measurements of illuminance are obtained by luxmeters (TES-1339R) manufactured and calibrated by TES Electrical Electronic Corp., Taiwan, China. The two luxmeters were fixed in the centre of the inner chamber and at a height of 0.75 m, which is as high as a work desk in a general office, to record the indoor illuminance. Another luxmeter was installed in a glass box on the roof of the experimental room to determine the outdoor illuminance. The three luxmeters were connected to a computer directly through an RS232 cable. The artificial lighting sources were switched off during the daily tests, and the illuminance data by luxmeter were recorded once per minute. The inner wall and ceiling of the chamber were in the colour of creamy white and the floor was in the colour of grey, resembling a typical office environment. The specifications of the luxmeter are presented in Table 3.5.

3.3.6. Other arrangements

Figure 3.10 Image of the building orientation calibration process
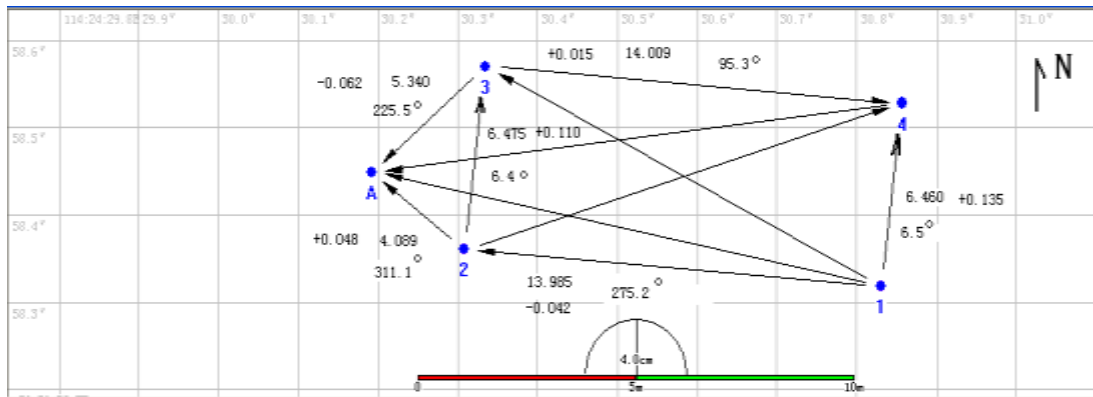
Figure 3.11 Orientations analysis by GIS devices

Using the GIS devices, the orientation of the y-axis of the building where the experimental room is located is $5°$ east of due north. Thus, we moved the orientation of the experimental room to $5°$ west of due north with respect to the y-axis of the building, making the orientation of experimental room due south. The processes in the calibration of the orientation of the building are shown in Figure 3.10 and Figure 3.11.

3.4. General measurements in the field experiments

The field experiment was conducted 24 h a day from June 2012 to October 2013. In the entire period, four types of PV glazings were individually installed on the southern façade of the experimental room. The general measurements in the field experiments are presented below. In a year of continuous experimental measurements, both mono-crystalline silicon PV glazing and the amorphous-silicon PV glazing were tested on the south wall with more than two-week period for each of the four seasons, including sunny and cloudy days.

3.4.1. Solar irradiance measurements

The total irradiance of the horizontal surface and the vertical surface of the eastern, southern, western and northern orientations were recorded every minute for the period of more than one year. In addition, the horizontal diffuse irradiance was also collected at the same time. The measurements of four sunny days of spring, summer, autumn and winter were selected to present the general tendency and characteristics of solar irradiance in different directions in Wuhan. As shown in Figure 3.12, the southern vertical total solar irradiance is as much as half of the horizontal total solar irradiance in 2013/4/17, a sunny day in spring, and is as much as one-third of the horizontal total solar irradiance in 2012/7/24, a sunny day in summer. However, the southern vertical total solar irradiance is slightly larger than the horizontal total solar irradiance in 2012/11/11, a sunny day in autumn, and that in 2013/1/13, a sunny day in winter. The maximum solar irradiance at noon reached approximately 300 W/m^2, 200 W/m^2, 700 W/m^2 and 600 W/m^2 on the sunny day in spring, summer, autumn and winter, respectively. These results implied that solar energy for the southern façade in autumn and winter should be studied for better utilisation.
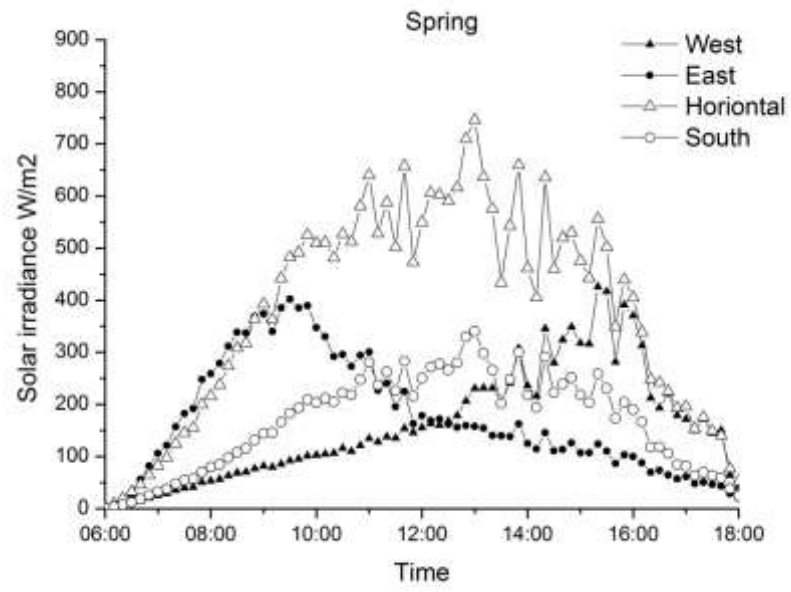
(a)
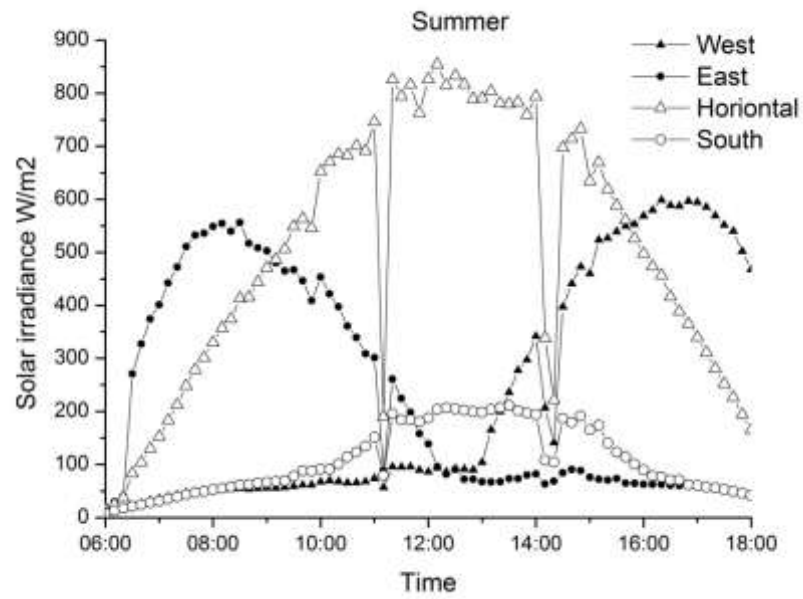
(b)
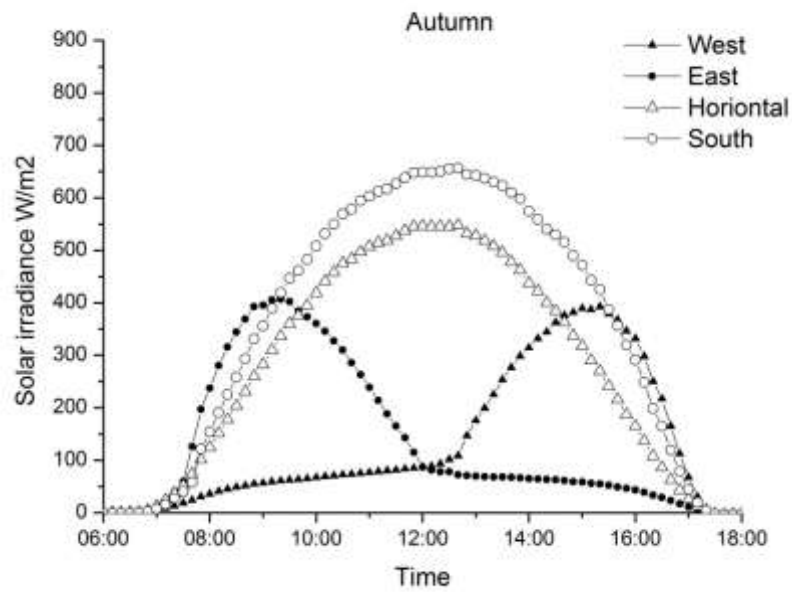
(c)
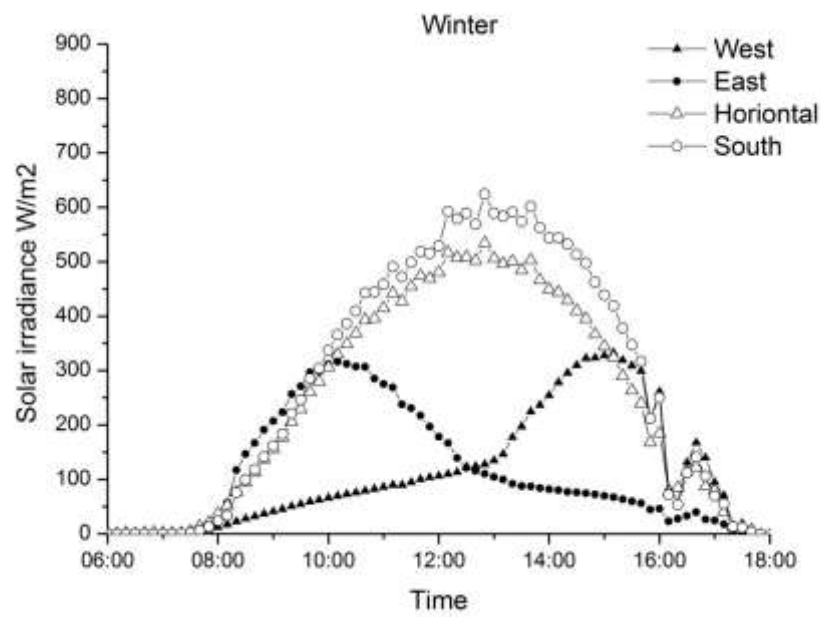
(d)

Figure 3.12 Measurement of total solar irradiance of various orientations

(a) data from 2013/4/17, a sunny day in spring; (b) data from 2012/7/24, a sunny day in summer; (c) data from 2012/11/11, a sunny day in autumn; (d) data from 2013/1/13, a sunny day in winter.

Sunny

(a)

Cloudy

(b)
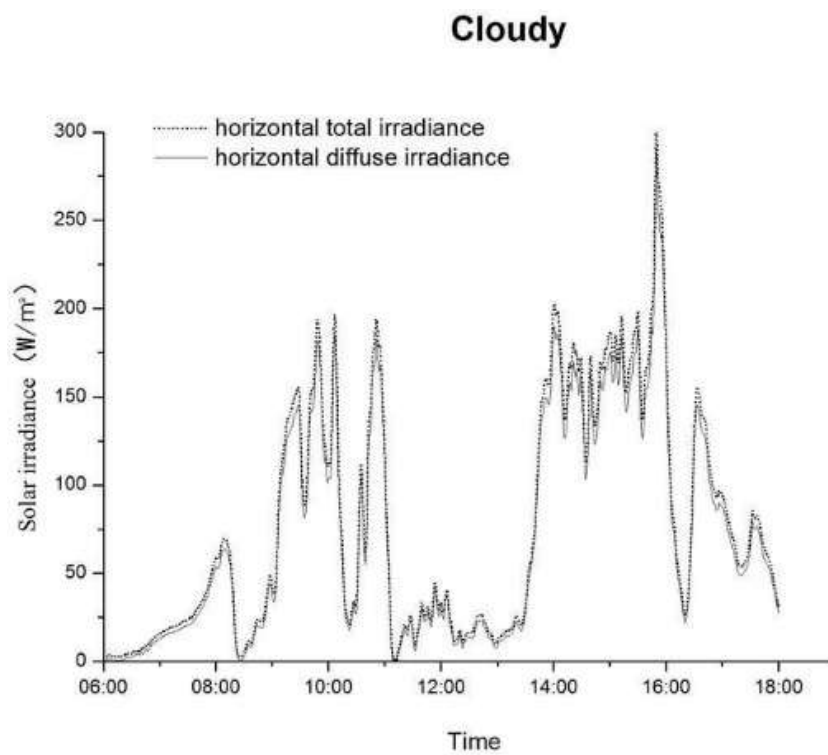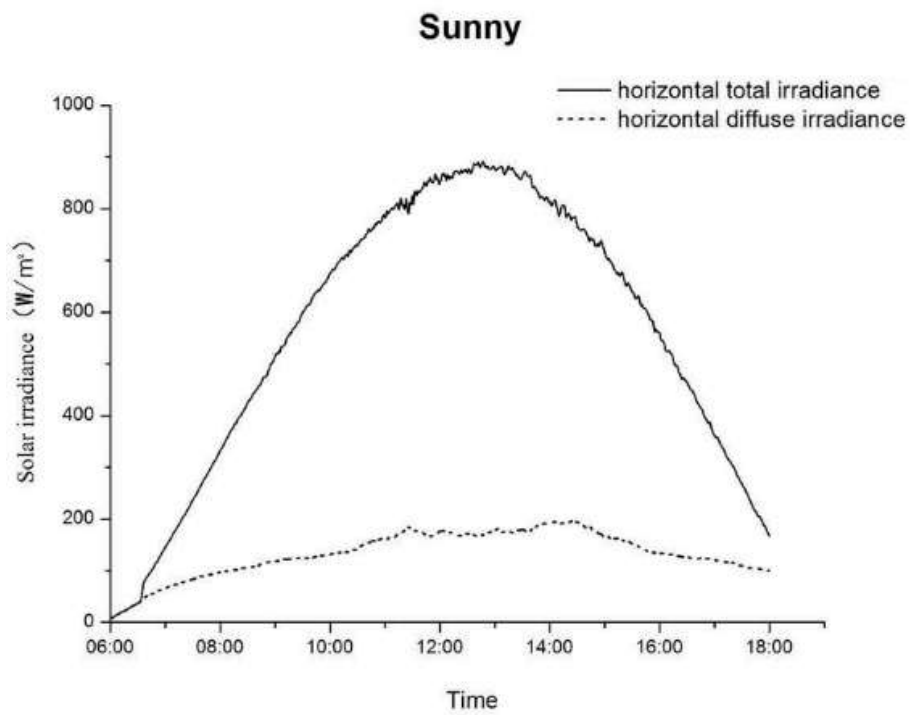
Figure 3.13 Measurements of solar horizontal total irradiance and diffuse irradiance

(a) data from 2013/8/7, a sunny day; (b) data from 2013/9/10, a cloudy day

The daily horizontal total solar radiance and the horizontal diffuse irradiance are plotted in Figure 3.13. On a sunny day, the diffuse solar irradiance accounted for a small part of the total solar irradiance. On a cloudy day, the diffuse solar irradiance was generally equal to the total solar irradiance. The measurements of the horizontal total solar radiance and the horizontal diffuse irradiance were applied to the validation studies in Section 4.3.3.

3.4.2. PV generation power and PV temperature measurements

Figure 3.14 shows the records from 2013/4/17, one day selected randomly in the experimental period, when the mono-crystalline semi-transparent PV glazing, denoted PV-2, and the amorphous-silicon semi-transparent PV glazing, denoted PV-3, were installed on the façades of both rooms for comparison. The daily solar irradiance on southern vertical façade and the generation power of both semi-transparent PV glazings are plotted in Figure 3.14 (a), which reveals the identical tendency of the three curves. Figure 3.14 (b) reveals that the PV generation power had a linear dependence with the solar irradiance on the PV module.

(a)
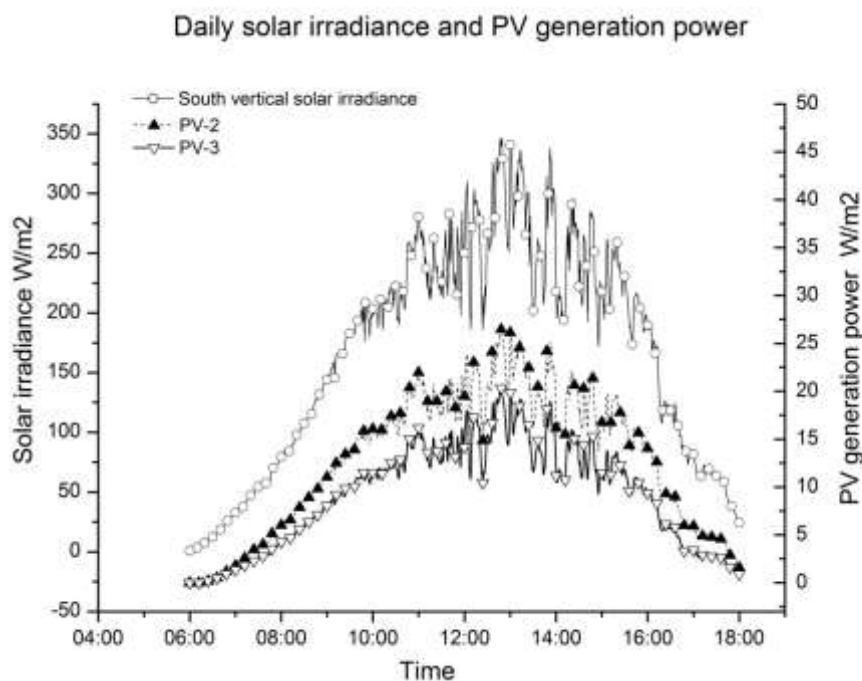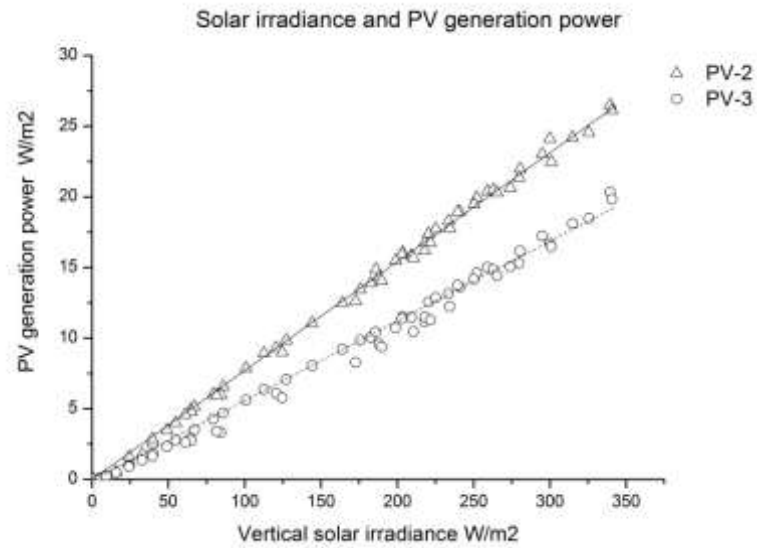
Figure 3.14 Measurements of solar irradiance and PV generation power

Figure 3.15 shows the measurement of the PV temperature and the calculation of the PV conversion efficiency from the measurement of the PV generation and solar irradiance. According to the measurement data, the equations that indicate the correlation of PV generation power and solar irradiance and the correlation of PV efficiency and PV temperature will be discussed in the Section 4.2.2. The data of figure 3.15 is from the measurements of August 4, 2012.

(a)

(b)
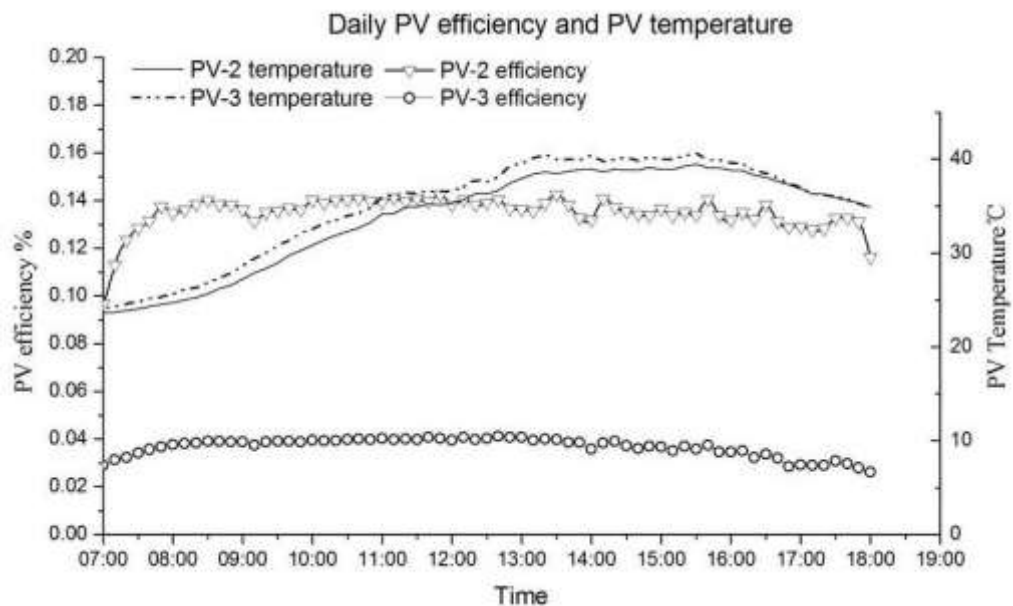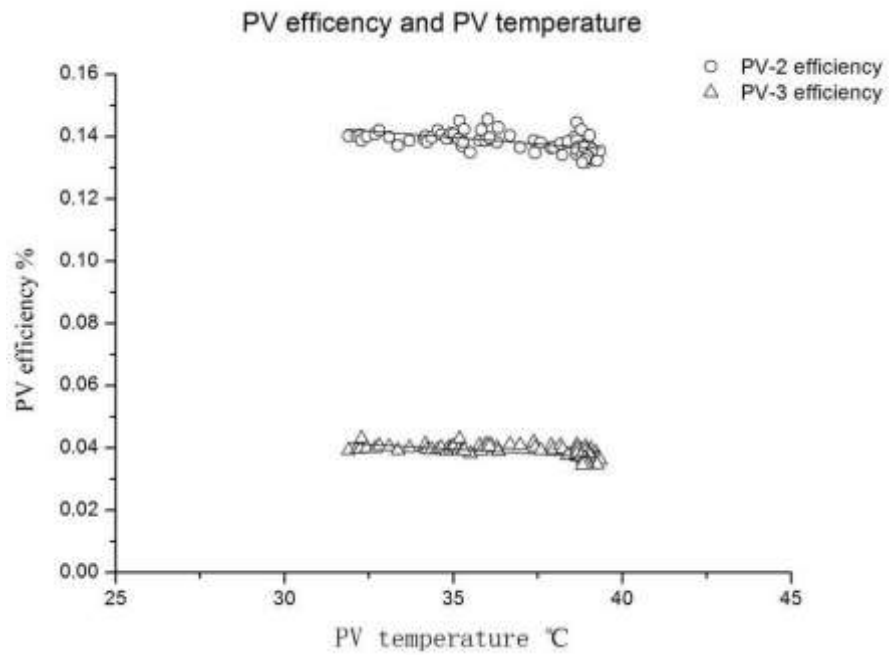
Figure 3.15 The PV efficiency and the PV temperature

Table 3.6 Parameters of four PV glazings

PV coding	Type of PV module	PV conversion efficiency (STC)	Temperature coefficient
PV-1	mono-crystalline semi-transparent PV modules (60% coverage of PV cells)	14.7%	0.69%
PV-2	mono-crystalline semi-transparent PV modules (40% coverage of PV cells)	14.0%	0.72%
PV-3	amorphous-silicon opaque PV modules	7.8%	0.23%
PV-4	amorphous-silicon semi-transparent PV modules	4.9%	0.21%

(PV electricity generation coefficient is calculated by the average value from the data recorded from eight random days (two from each season))

Four types of PV glazings were successively installed on the southern façade in the experimental period; based on these measurements, the parameters of the PV properties for the four types of PV glazing were calculated, as presented in Table 3.6. Temperature coefficients obtained by previous researcher were 0.59% for crystalline-silicon PV and 0.16% for amorphous-silicon PV (Wong et al., 2005). This parameters obtained from the field experiment in this study agree reasonably well with the results of previous research work.

3.4.3. Daylighting illuminance measurements

Daylighting can be introduced to an indoor room by using a semi-transparent PV façade. The illuminance on the horizontal surface of the indoor room with a mono-crystalline semi-transparent PV façade and the illuminance on the outdoor horizontal surface are plotted in Figure 3.16 (data from 2013/10/24). Figure 3.16 (a) shows the generally identical tendency for the outdoor and the indoor illuminance values；Each point on the figure represents both indoor (as Y-axis) and outdoor (as X-axis) luminance level. The linear dependence of the indoor illuminance and the outdoor illuminance can be observed in Figure 3.16 (b).
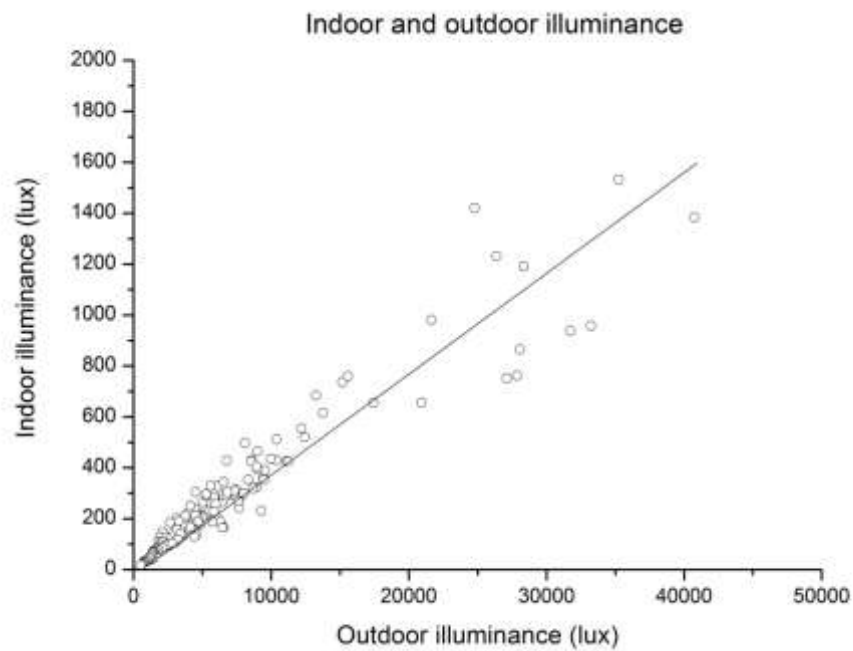
(a)
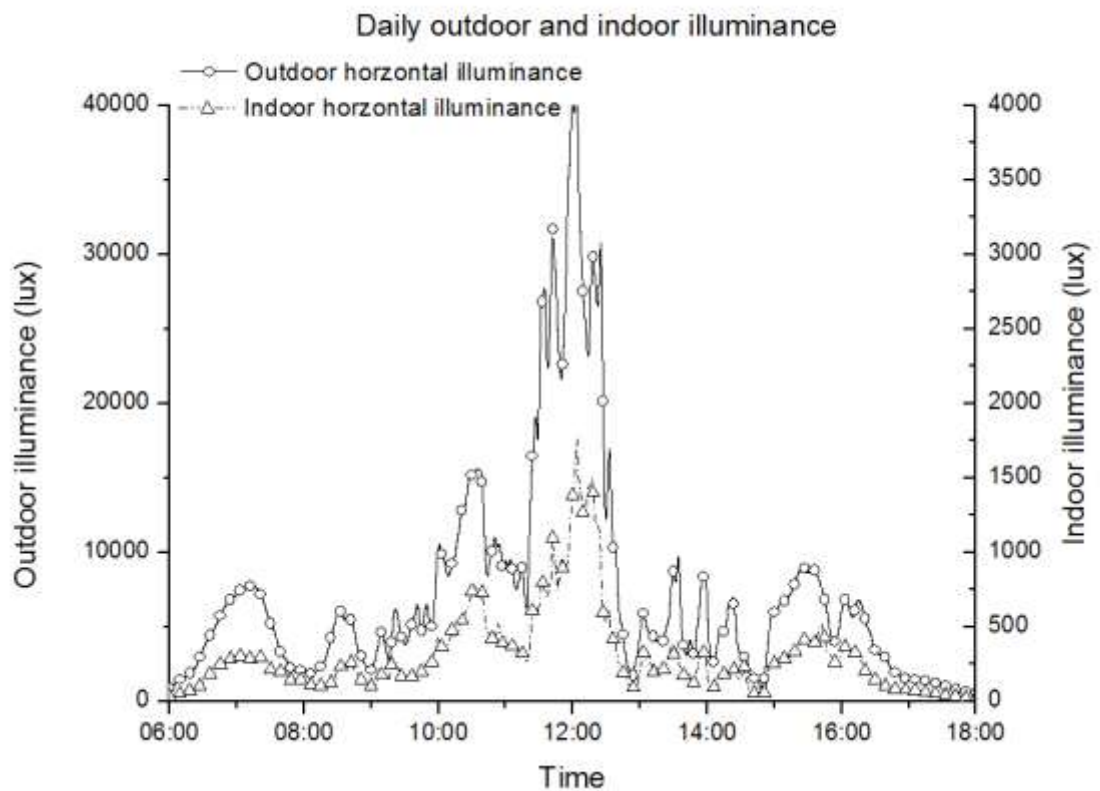
(b)

Figure 3.16 Measurements of daylighting illuminance

3.5. Conclusions

To evaluate the energy performance of PV façades in the realistic local climate, the experimental room with two inner and separate chambers was set up on the flat rooftop of a building in Wuhan. Several types of PV glazing were successively installed on the southern vertical façade of the experimental room for field measurements. In addition, the methodology of measurement and calibration was developed to achieve the vital data. The experiment room was equipped with instrumentations to record a broad range of data for over a year, including temperature, solar irradiance, illuminance and PV generation power. The collected data were used to validate the calculation models of PV façades in the Chapter 4 and Chapter 5.

With smart design, skillful construction, durable measurement and careful calibration in the experimental room, the systemically measured and recorded data of environmental parameters and the parameters that are related to PV façades was verified to be effective and valid. The PV façades parameters achieved from the field experiment in this study agree reasonably well with the results of previous works of other researchers. In addition, the establishment of the experimental room can be considered an achievement in this study because not only it provided high-quality data in the realistic local climate but also the experimental procedures and measurement techniques were developed and gained in the process.

Chapter 4 Climate, solar irradiance and estimation of annual power generation of PV façades in China

Building energy consumption, as well as the generated electrical energy of BIPV façades, is related to the climate and solar irradiance, which vary from location to location and from year to year. This chapter commences by discussing the climate and solar irradiance and their relevance to the power generation of PV façades, and then estimates the annual power generation of PV façade with validated models and typical year weather database in China.

In Section 4.1, the thermal climate zones and the solar climate zones in China are described. After the introduction of the Chinese Standard Weather Data (CSWD) that is the widely used for the typical year weather data in mainland China, the thermal climate and solar climate of Wuhan are presented using the CSWD. In Section 4.2, the calculation methods of solar irradiance on an inclined surface and PV generation power based on operating temperature are explained. The recorded data from the experimental room are used to validate the calculation methods. The measured results and calculated results exhibited a good agreement in the validation study. In Section 4.3, along with the validated calculation methods and the typical year weather data of the CSWD, parametric studies are performed on the estimation of the annual power generation of PV façades in China.

4.1. Climate and solar irradiance

4.1.1. Thermal climate zones and solar climate zones in China

Building design and energy use in the built environment are directly related to the local climate, and the specific electrical power yields via feasible application with PV façades are associated with the local solar resource. The thermal climate and solar climate in China are presented as follows.

China is a huge country, covering approximately 9.6 million square kilometres. Approximately 98% of the land area stretches between a latitude of 20◦N and 50◦N, from the subtropical zones in the south to the temperate zones (including warm-temperate and cool-temperate) in the north (Chao, 1986; Zhang and Lin, 1992). China also has a complex topography, ranging from mountainous regions to flat plains. Due to the large area and complex topography, the climate in China differs from region to region.

There are different ways to classify climate regions or zones in terms of the different purposes of the different criteria. For the consideration of building thermal design, five thermal climate zones, namely Severe Cold, Cold, Hot Summer and Cold Winter, Mild, Hot Summer and Warm Winter, are commonly used in China. The zoning criteria are mainly based on the average temperatures in the coldest and hottest months of the year. The numbers of days that the daily average temperature is below 5 ℃ or above 25 ℃ are counted as complementary indices for determining the zones. Figure 4.1 shows the geographical layout of the thermal climate zones of China (CSBTS and MCC, 1993).
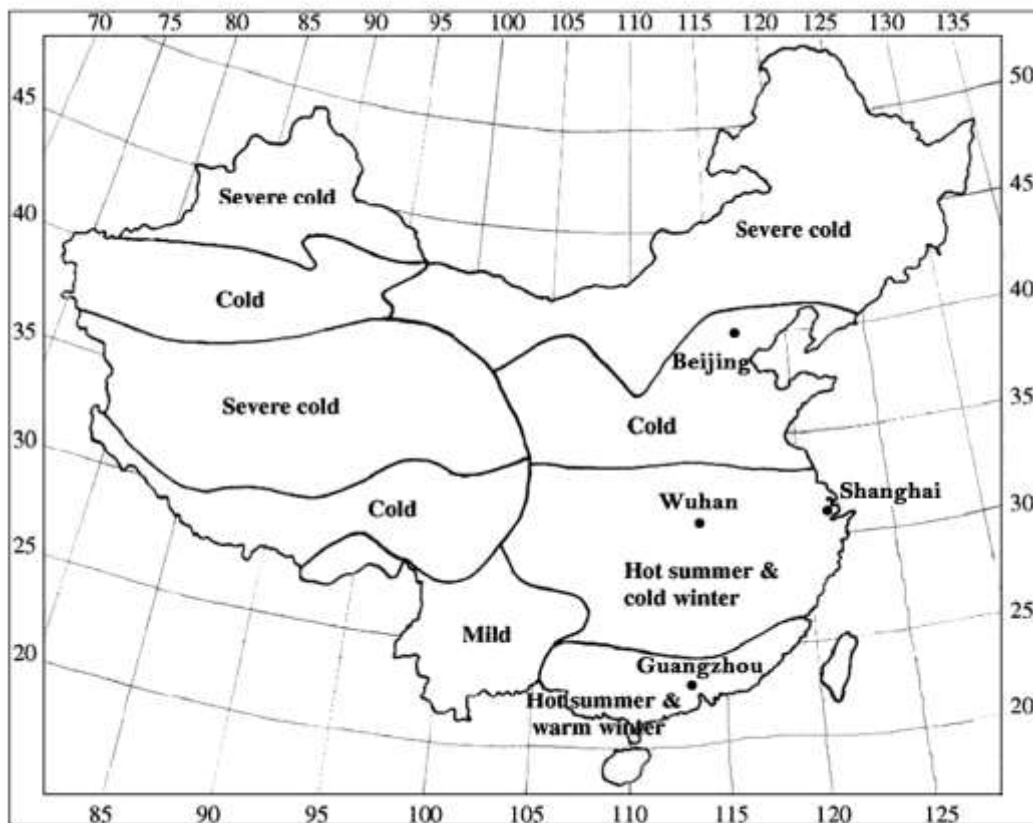
Figure 4.1 Thermal climate zones of China

At the same time, the solar energy resource exhibits a large amount of potential and unequal distribution in China. For the consideration of solar insolation, four solar climate zones are widely used in China: I rich area (over 6700 MJ/(m²a)), II moderate area (5400-6700 MJ/(m²a)), III utilisable area (4200-5400 MJ/(m²a)) and

IV poor area (less than 4200 MJ/(m^2a)). Figure 4-2 shows the geographical layout of the solar climate zones of China (Shen and Zeng, 2005).
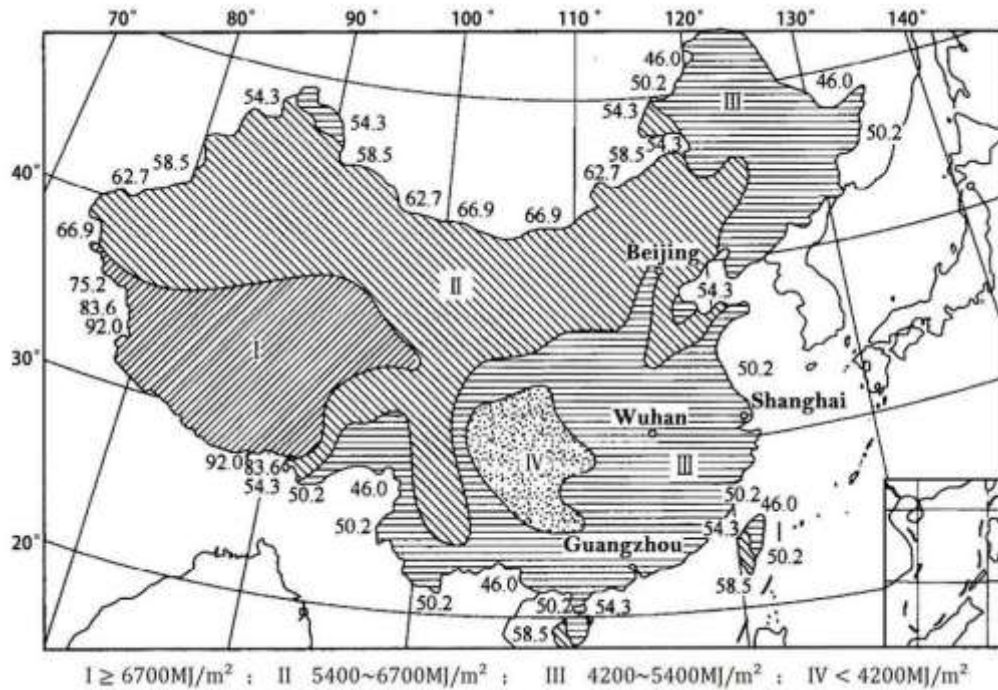
Figure 4.2 Solar climate zones of China

4.1.2. Typical year weather database in China

The hourly and daily weather parameters, including temperature, solar irradiance, wind direction and speed and humidity, vary from year to year; therefore, the weather database of a typical year is required to provide the data representative of the prevailing climatic conditions and weather patterns for the specific location (Smart and Ballinger, 1984). Serving as input for driving the calculation models within the simulation tools, the typical year weather database is necessary for the building energy simulations and analyses that are widely applied by engineers, architects, and researchers to determine the building energy efficiency and to optimise the building design. The typical year weather database is selected to be the data of a single year of 8760 hourly data selected from the multi-year datasets that satisfy the statistical tests (Yang et al., 2007).

There are different types of typical years that are involved with weather data sources, weather formats and methods. For example, the Test Reference Year

(TRY) is one of the earliest, which was established by the American Society of Heating, Refrigerating and Air-conditioning Engineers (ASHRAE) in 1976 (NCC, 1976). Later, the Typical Meteorological Year (TMY) was developed by Sandia National Laboratories in the United States (NCC, 1981).

The TMY is the accepted method for generating a typical year and is widely used by many countries and areas, including the U.S. (Hall et al., 1978), Canada (Siurna et al., 1984), and Greece (Pissimanis et al., 1988) In Hong Kong, China, a great amount of research studies have been performed to obtain typical weather year data using the two methods of TRY and TMY (Hui and Lam, 1992; Lam et al., 1992).

In mainland China, the Chinese Standard Weather Data (CSWD) is widely used for typical weather data; the CSWD were developed by Dr. Jiang Yi of the Department of Building Science and Technology at Tsinghua University and the China Meteorological Bureau (CMB et al, 2005). The CSWD consists of a set of 270 typical hourly data weather files that were used for simulating the energy use in buildings and calculating the renewable energy utilisation by researchers in China (Yu et al., 2009).

The Department of Energy (DOE) in the United States provided the weather data files that can be used in the EnergyPlus Energy Simulation Software (DOE, 2014). The weather data for China, which were derived from the source of CSWD, are available on the DOE website. The typical weather files that were used in Chapter 4 and Chapters 5-8 of this thesis were from a CD-ROM file in the CSWD book and from the DOE website, respectively. These two datasets are the same regarding the weather data source and different regarding the weather data format.

4.1.3. Thermal climate and solar climate in Wuhan

Wuhan was selected as the location where the energy performance of feasible BIPV is studied in this thesis; the general information and comparative analysis of the thermal climate and the solar climate in Wuhan are presented in this section.

Wuhan is located in the middle of China, with a latitude of 29°58′-31°22′N, a longitude of 113°41′-115°05′E and an area of 8,494 km². Wuhan is situated at the confluence of the Hanshui and Yangtze Rivers along the middle reaches of the

latter. The location of Wuhan, together with its subtropical monsoon climate, enables hot air to collect and become difficult to dissipate. Thus, Wuhan deserves its reputation as being one of the "Three Furnaces of China".

Figure 4.3 shows plots of the daily average, maximum and minimum ambient temperature in Wuhan from the weather files of the CSWD from January to December. Spring is quite short in Wuhan and begins in March, with the rapid rise of temperature, even to a maximum of above 20 ℃. Summer is very hot and humid, continuing for a long period from May to September. Midsummer starts in July. The maximum temperature during this time mostly stays at 37-39 ℃ during the day, yet the minimum is still high at night, generally at 28℃. Autumn starts after October, with temperature gradually declining and the air becoming dry. The average temperature is 20-25 ℃, but sometimes it can reach 30 ℃ or above in autumn. Autumn quickly transitions into winter, as long as there is cold air coming from the north, leading to a rapid decrease in the temperature. Winter begins at the end of December and runs through the next February, with an average temperature in the range of 1-3℃. When there is fine weather, the temperature can be as high as 7-8 °C; however, when there is a cold wave or sleet, the temperature is usually below the freezing point. Winter in Wuhan is very cold and, although the temperature is not as low as in some northern cities, the wind-chill from the river winds and the high humidity makes it feel colder, and temperatures can drop to -5 ℃.

(a)January　　　　　　　　(b)February
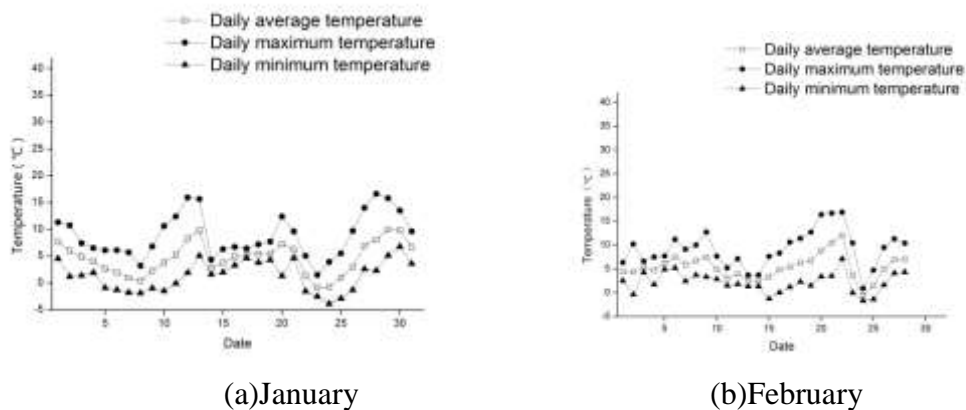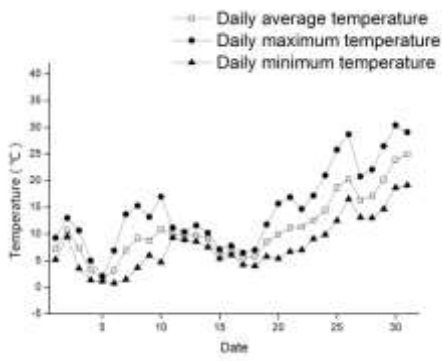
(c)March
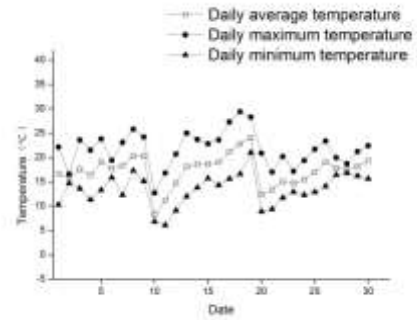
(d)April
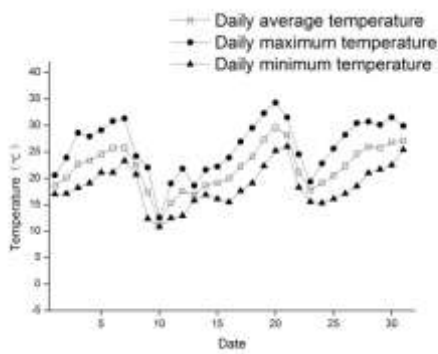
(e)May
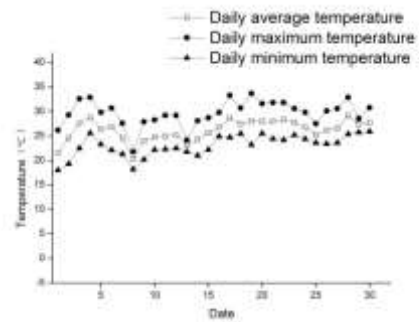
(f)June
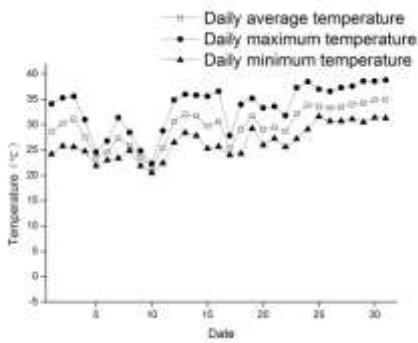
(g)July
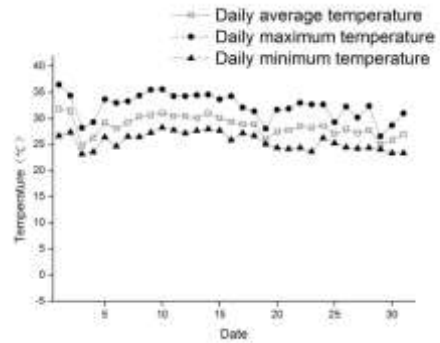
(h)August
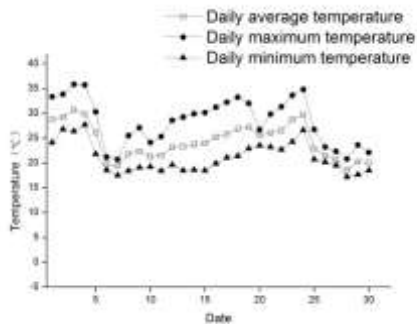
(i)September

(j)October
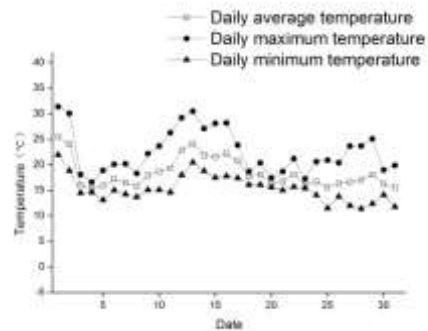
(k)November   (l)December
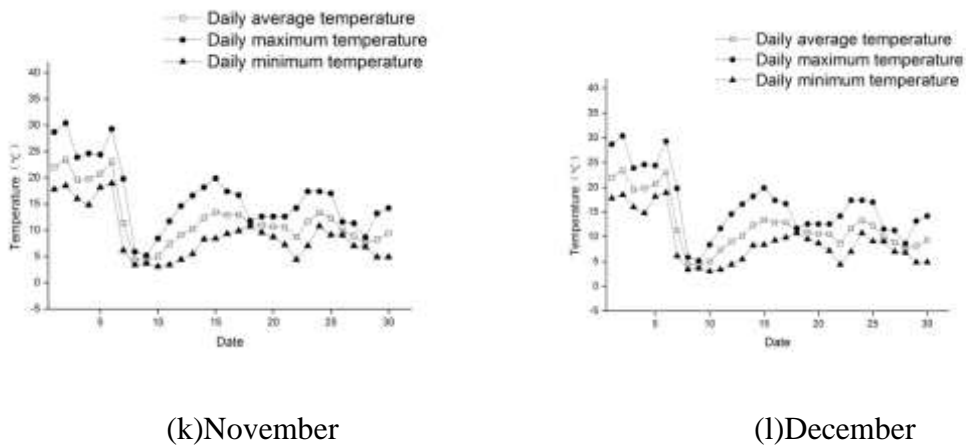
Figure 4.3 Daily average, maximum and minimum temperatures of Wuhan

Table 4.1 Latitudes of four Chinese cities

City	Wuhan	Shanghai	Beijing	Guangzhou
Latitude	30.39 °N	31.22 °N	39.92 °N	23.11 °N
Climate zone	Hot Summer and Cold Winter	Hot Summer and Cold Winter	Cold	Hot Summer and Warm Winter

Figure 4.4 shows the monthly average temperature of four Chinese cities, namely Wuhan, Shanghai, Beijing, Guangzhou, from January to December. The temperature curves of Wuhan and Shanghai are very close to each other because both of them are located in the same climate zone. The monthly average temperature of Wuhan in January is higher than that of Beijing by 10 °C and lower than Guangzhou by 10 °C. The monthly average temperature of Wuhan in July is the highest in the four cities, at 30 °C. From the this figure, **Wuhan can be regarded as the typical city for central China in climate**, where building design for energy efficiency and thermal comfort in buildings should be considered carefully regarding the Hot Summer and Cold Winter climate.
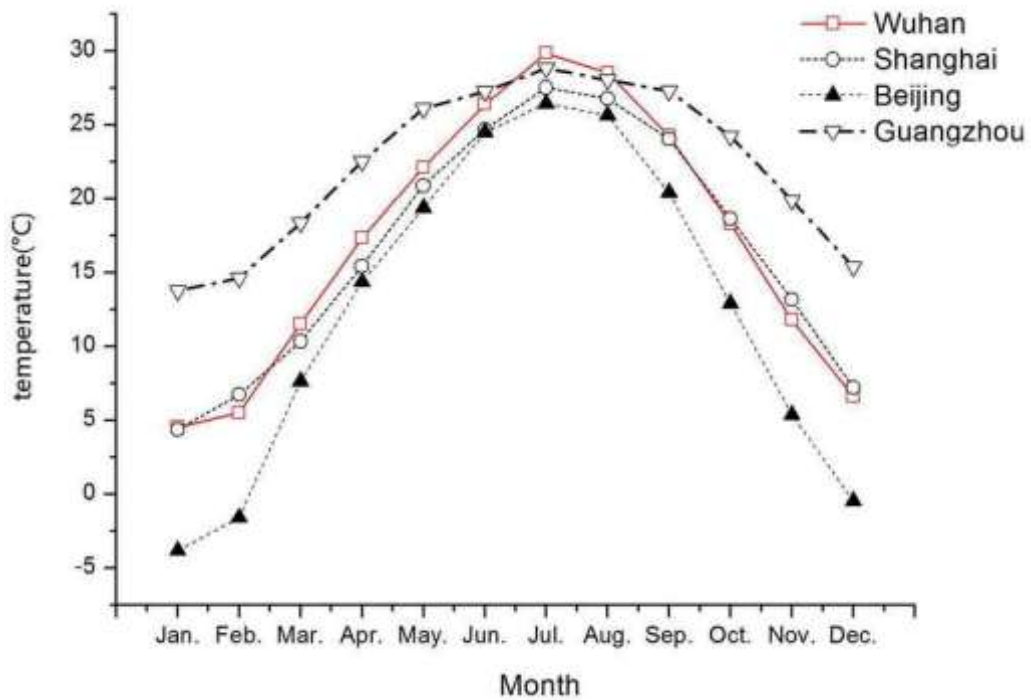
Figure 4.4 Monthly average temperatures of four Chinese cities

Five worldwide cities at latitudes similar to that of Wuhan were selected for comparison with the monthly average temperature. As shown in Figure 4.5, the maximum average temperature of Wuhan in summer is the highest one of the five cities. Compared with Kagoshima and Atlantic, the Wuhan minimum average temperature in winter is close to approximately 5 ℃, while the Wuhan maximum average temperature in summer is higher than those of Kagoshima and Atlantic by 5 ℃. For cities in the latitude of approximately 30 °N, where the winters are as cold as Wuhan, the summer is found to be no hotter than that in Wuhan. Compared with Cairo and Houston, the Wuhan maximum average temperature in summer is higher than those of Cairo and Houston by 2 ℃, while the Wuhan minimum average temperature in winter is lower than those of Cairo and Houston by 10 ℃ and 6 ℃, respectively. For cities in the latitude of approximately 30 °N, where the summer is not hotter than that in Wuhan, the winter is found to be much warmer than the winter in Wuhan. From this figure, the weather condition in Wuhan is found to be more extreme compared to other areas of the same latitude around the world.

Table 4.2 Longitude and latitude of five worldwide cities

City	Wuhan	Cairo	Kagoshima	Houston	Atlantic
Country	China	Egypt	Japan	U.S.	U.S.
latitude	30.39 N	30.04 N	31.59 N	29.76 N	33.74 N
longitude	144.3 E	31.23 E	130.55 E	95.36 W	84.38 W
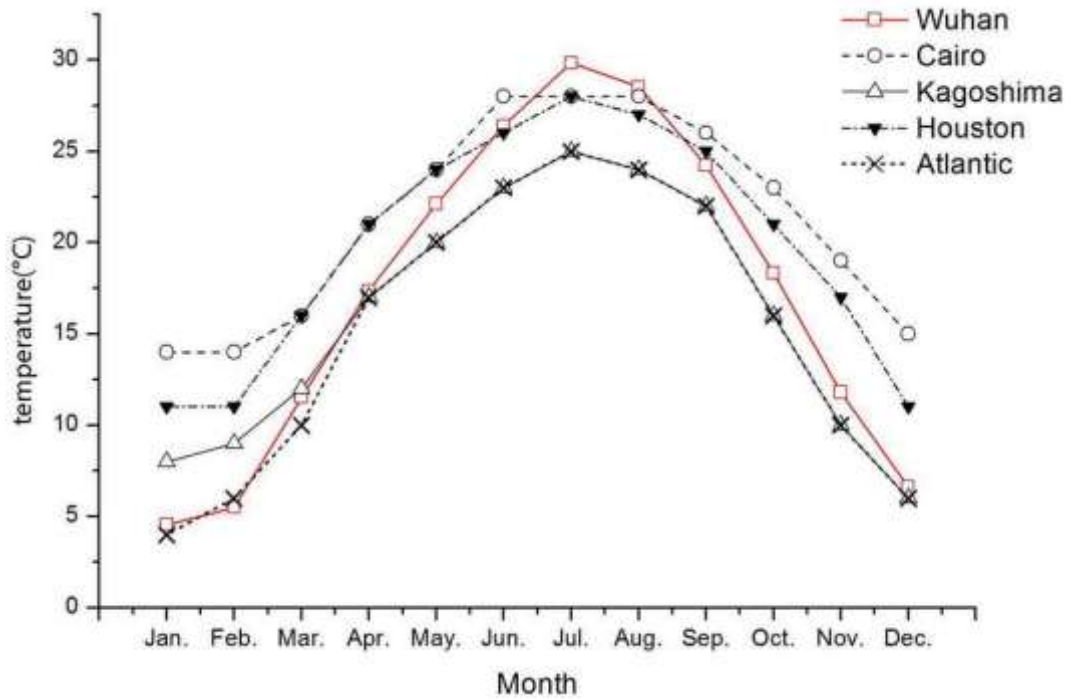
Figure 4.5 Monthly average temperatures of five worldwide cities

Figure 4.6 shows the column plots of the horizontal total solar irradiance, horizontal beam solar irradiance and horizontal diffuse solar irradiance in Wuhan from January to December, which was derived from the weather files of the CSWD. The total solar irradiance in July and August is the highest over the entire year, reaching 151 kWh/m^2 and 137 kWh/m^2, respectively, while those in January and December are the lowest, at only 56 kWh/m^2 and 61 kWh/m^2, respectively, The general tendency of the maximum in summer and minimum in winter also can be found in the solar beam irradiance and the solar diffuse irradiance. However, the solar beam irradiance is larger than the solar diffuse irradiance only in three months, specifically May, June and July.

Monthly solar irrdiance
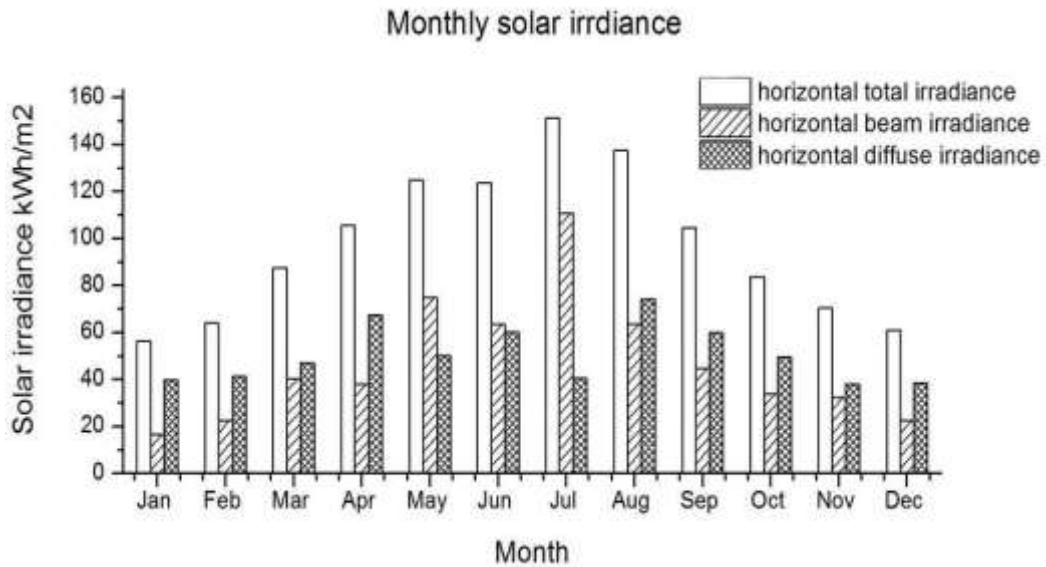
Figure 4.6 Monthly solar irradiance in Wuhan

4.2. Calculation methods for annual power generation of PV façades

According to the definition of the Photovoltaic Cell Conversion Efficiency, the power generation of PV can be written as equation (4.1)

$$P_d(t) = \eta AG \tag{4.1}$$

where P_d is the DC electrical power of PV generation, η is the PV cell conversion efficiency, A is the aperture surface area of the PV cell, and G is the solar irradiance.

In a certain time, the DC electrical energy E of PV generation can be calculated from equation (4.2).

$$E_{PV} = \int P_d(t)dt \tag{4.2}$$

where t is the time in hours.

From equations (4.1) and (4.2), it can be concluded that the actual PV cell conversion efficiency, η, and the actual solar irradiance, G, are indispensable to estimate the annual power generation of the PV façade. G is perpendicular to the surface in the equation 4.1. The calculation methods of both values are discussed in Section 4.2.1 and Section 4.2.2.

4.2.1. Solar irradiance on the inclined surface

Because they are installed on the building envelope as façades, the PV modules are located at different orientations and inclinations to harmonise with the building appearance. Because solar irradiance is unequally distributed on the building envelope of different orientations and inclinations, it is necessary to know the incident solar irradiance on an inclined surface to access the power generation of the PV façade. There is usually no available measurement for the surface of interest. Therefore, the irradiance on the inclined surface must be calculated from the horizontal global and diffuse irradiance values, which are readily available from the weather stations and the typical weather data.

In general, the total solar irradiance on the horizontal surface includes two parts: the beam irradiance and the diffuse irradiance. In mathematical form, it can be written as equation (4.3).

$$G_h = G_b + G_d \qquad\qquad (4.3)$$

where G_h, G_b and G_d are the horizontal total irradiance, horizontal beam irradiance and horizontal diffuse irradiance, respectively. The data of three irradiance values can be obtained from typical weather data.

The total solar irradiance on the inclined surface, G_i, includes three parts: the beam irradiance on the inclined surface ($G_{b,i}$), the diffuse irradiance on the inclined surface ($G_{d,i}$) and the reflected irradiance on the inclined surface ($G_{r,i}$). As shown in equation (4.4), the total irradiation on an incline surface is the sum of the three parts (Noorian et al., 2008).

$$G_i = G_{b,i} + G_{d,i} + G_{r,i} \qquad\qquad (4.4)$$

The three parts of the irradiance on an inclined surface can be individually calculated using the following equations.

First, the beam irradiance on an inclined surface is calculated based on solar geometry. The beam irradiance on the surface with inclination angle β, $G_{b,i}$, can be calculated using equation (4.5) (Posadillo and López Luque, 2009).

$$G_{b,i} = G_b \times R_b = G_b \frac{\cos\theta_i}{\sin\alpha_s} \qquad\qquad (4.5)$$

R_b is the geometric factor ($R_b \geq 0$), i.e., the ratio of beam irradiance on an inclined surface to the horizontal beam irradiance. θ_i is the angle of incidence on

the surface, and α_s is the solar elevation. According to the geometry relationship of the sun, the earth and the incline surface, α_s and θ_i can be calculated using equations (4.6) and (4.7).

$$\sin\alpha_s = \sin\varphi\sin\delta + \cos\varphi\cos\delta\cos\omega \tag{4.6}$$

$$\cos\theta_i = \sin\delta\sin\varphi\cos\beta - \sin\delta\cos\varphi\sin\beta\cos\gamma_i + \cos\delta\cos\varphi\cos\beta\cos\omega +$$
$$\cos\delta\sin\varphi\sin\beta\cos\gamma_i\cos\omega + \cos\delta\sin\beta\sin\gamma_i\sin\omega \tag{4.7}$$

where φ is the local latitude, which is 29°58′ N for Wuhan, β is the inclination angle of the surface, and ω is the hour angle, which represents the angle between the sun meridian and the local meridian (Iqbal, 1983).

$$\omega = 15^o \times (t - 12) \tag{4.8}$$

where t is the time in hours with the 24-hour time system, γ_i is the azimuthal angle of the inclined surface, which is the angle between the vertical plane that contains the normal to the wall and the vertical plane that runs north-south, and γ_s is the azimuthal angle of the sun. The azimuthal angle is measured from the south and is negative when the sun is to the east of south but positive when sun is to the west of south. The solar declination angle, which is denoted by δ, varies seasonally because of the tilt of the earth on its axis of rotation and the rotation of the earth around the sun. The declination is zero at the equinoxes (March 22 and September 22), positive during the northern hemisphere summer and negative during the northern hemisphere winter. The declination reaches a maximum of 23.45° on June 22 (summer solstice in the northern hemisphere) and a minimum of -23.45° on December 22 (winter solstice in the northern hemisphere). The declination angle can be calculated using equation (4.9)

$$\delta = 23.45^o \times \sin\left[360^o \times (284 + n)/365\right] \tag{4.9}$$

where n is the day of the year with January 1 as n=1.

Second, the reflected irradiance describes the reflected sunlight of non-atmospheric objects such as the ground. To calculate the reflected irradiance, both the beam and the diffuse radiation are usually assumed to isotropically reflect. The surface with inclination angle β from the horizontal has a view factor to the

ground of $(1-\cos\beta)/2$. Thus, the reflected irradiance on an inclined surface, $G_{r,i}$, can be calculated from equation (4.10) (Vartiainen, 2000).

$$G_{r,i} = (G_b + G_d)\rho(\frac{1-\cos\beta}{2})$$
(4.10)

where ρ is the average ground reflectance. In general, the reflectance is assumed to be 0.2 in the weather condition without snow.

Third, the diffuse irradiance on an inclined surface is difficult to accurately determine because of the different spatial distribution of the cloud. For entirely cloudy sky, the diffuse irradiance is isotropically distributed over the sky hemisphere. The diffuse irradiance $G_{d,i}$ can be calculated using equation (4.11) (Liu and Jordan, 1962).

$$G_{d,i} = G_d(\frac{1+\cos\beta}{2})$$
(4.11)

However, the theoretical overcast sky, which is appropriate for equation (4.11), does not always occur in practice. Many researchers introduced new mathematical models of diffuse irradiance on inclined surfaces. Hay proposed an anisotropy index A_I to weigh the circumsolar and isotropic irradiance components. The index A_I is defined in equation (4.12) (Hay and Davies, 1980).

$$A_I = G_b/G_o$$
(4.12)

where G_o is the hourly extraterrestrial solar irradiation on a horizontal surface. The calculation method of G_o is shown in equation (4.13) (Duffie and Beckman, 1980).

$$G_o = \frac{12 \times 3600}{\pi} I_{sc}(1+0.033\cos\frac{360n}{365})$$
$$\times[\cos\phi\cos\delta(\sin\omega_2 - \sin\omega_1) + \frac{2\pi(\omega_2 - \omega_1)}{360}\sin\phi\sin\delta]$$
(4.13)

where I_{sc} is the solar constant, whose suggested value is 1367 W/m^2 by the World Radiometric Center (WRC) (Li et al., 2011).

According to the Hay model (Hay, 1979), the diffuse irradiance on an inclined surface is calculated from equation (4.14).

$$G_{d,i} = G_d[(1-A_I)\frac{1+\cos\beta}{2} + A_I R_b]$$
(4.14)

Subsequently, Reindl et al. added a horizon brightening diffuse term to the Hay model. The magnitude of the horizon brightening is controlled by a modulating function f, which is defined in equation (4.15).

$$f = \sqrt{G_b/G}$$
(4.15)

By multiplying the modulating function f to the horizon brightening correction term $\sin^3(\beta/2)$, which is used in Temps and Coulson model (Temp and Coulson, 1977), the diffuse irradiance on an inclined surface in the Reindl model can be calculated from equation (4.16) (Reindl et al., 1990).

$$G_{d,i} = G_d[(1-A_I)(1+f\sin^3(\beta/2))\frac{1+\cos\beta}{2} + A_I R_b]$$
(4.16)

Because the relevant parameters can be achieved from typical weather files and the specification of the inclined surface, the solar irradiance on the PV façade can be approximately simulated. In particular, for the vertical building façade, the inclination angle of the surface is 90 °.

4.2.2. PV generation power based on the operating temperature

The correlations that express the PV cell/module conversion efficiency as a function of the PV operating temperature are well documented (Skoplaki and Palyvos, 2009). The PV conversion efficiency is calculated in the traditional linear expression as equation (4.17) (Evans, 1981).

$$\eta(T_c) = \eta_0 \left[1 - \beta_c(T_c - 25°C)\right]$$
(4.17)

where T_c is the PV cell/module operating temperature, $\eta(T_c)$ is the actual PV conversion efficiency on the operating temperature of T_c, β_c is the temperature coefficient, and η_0 is the PV conversion efficiency under Standard Test Conditions (STC) . According to the IEC 60904-1 norm (Geneva, 2006) the Standard Test Conditions (STC) are as follows: (IEC, 2006; IEC, 2007; IEC, 2008a ; IEC, 2008b)

- Irradiance: 1000 W/m2.

- Cell temperature: 25 ℃.

- Spectral distribution: AM 1.5 (according to IEC 60904-3) (Geneva, 2008).

- Normal incidence.

The PV conversion efficiency η_0 and the temperature coefficient β_c depend on the solar cell material. The efficiency of mono-crystalline silicon solar cells is approximately 14-18%, whereas that of poly-crystalline silicon is 13-16% (Sonnenenergie, 2005; Sonnenenergie, 2008). Both values can be achieved using on-site tests, where the PV cell/module power generations are measured at two different temperatures for a given solar radiance flux (Hart and Raghuraman, 1982).

According to equation (4.17), the PV operating temperature is the key parameter with important influence on the PV electrical efficiency and the PV system generated energy. In other words, the question of how to estimate the annual PV performance in conversion efficiency becomes the question of how to estimate the annual PV temperature. The PV actual temperature is clearly a function of weather variables such as ambient temperature, wind speed and solar irradiance. Nevertheless, the Nominal Operation Cell Temperature (NOCT) calculation method can be applied to simulate the annual PV temperature as equation (4.18).

$$T_c = T_a + (NOCT - 20)\frac{G}{800}$$

(4.18)

where T_c is the PV cell/module operating temperature, T_a is the ambient temperature, G is the solar irradiance on PV module in W/m^2, and $NOCT$ is the normal operating cell temperature in ℃.

Several international standards introduce the method to calculate the $NOCT$. While operating in a normal temperature environment (NTE), which is specified as follows, the PV module $NOCT$ is calculated using equation (4.19).

$$NOCT = (T_c - T_a)_{NTE} + 20°C$$

(4.19)

NTE means:

－ Irradiance: 800 W/m2,

－ Cell temperature: 20 ℃,

－ Average wind speed: 1 m/s,

－ Mounting: open rack, titled normally to the solar noon sun.

The reported *NOCT* are 46-50 °C for the PV module (Garcia and Balenzategui, 2004). The simulation of the PV module annual temperature and performance based on NOCT calculations was used by Spanish researchers with the Typical Meteorological Year of Madrid (Balenzategui, 1999).

Because of the hourly data of ambient temperature are available from typical weather files, and the solar irradiance on the PV module is obtained from the calculations in Section 4.2.1, the annual power generation of the PV façade can be estimated.

4.2.3. Validation on calculation methods

Validation works were performed to verify the calculation methods discussed in Section4.2.1 and Section 4.2.2 with measurement data in the experimental room, which was presented in the Chapter 3.
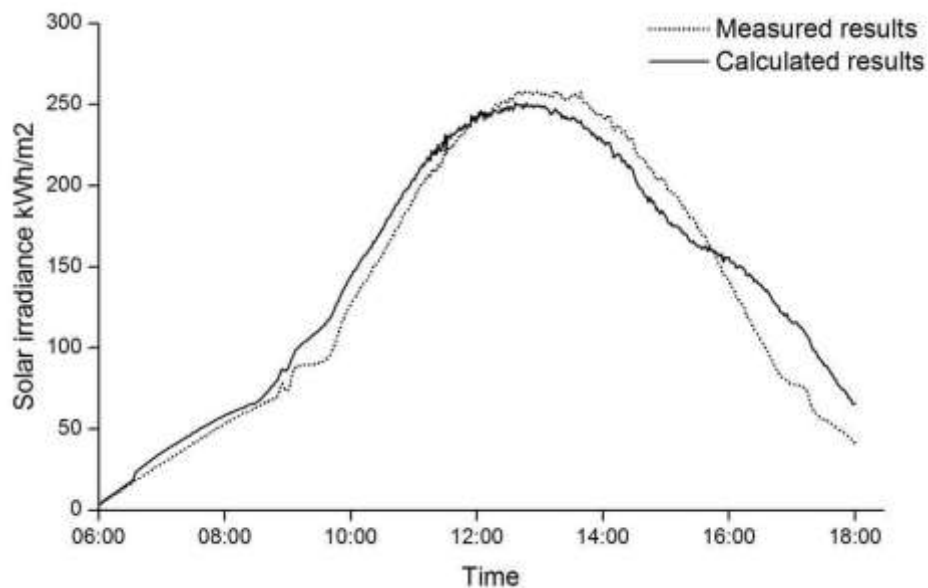
Figure 4.7 Validation of the solar irradiance calculation under sunny conditions

The total solar radiation, diffuse and direct solar radiation measured from field experiment are served as input values in equation 4.3- equation4.16, thus to calculate the solar radiation(vertical) on south wall. By doing so, the comparisons between the measurements and calculation results of the solar radiation on south wall are then available and shown in Figure 4.7 and Figure 4.8.

First, the calculation of solar irradiance on an inclined surface was validated. With the measured horizontal total solar irradiance and horizontal diffuse solar irradiance, the total solar irradiance on the vertical façade was calculated using equations 4.3 to 4.16 to match with the measured results in the field experiments. Figure 4.7 presents the validation of the solar irradiance calculation on the southern façade with sunny-day (7 August 2013) data, whereas Figure 4.8 presents a similar work with cloudy-day (10 September 2013) data. The average error between the calculated results and the measured results is 6.2% and 5.8% in Figures 5.7 and 5.8. The solar irradiance on a vertical façade of the other orientation was also validated, and the measurements and calculations are consistent.
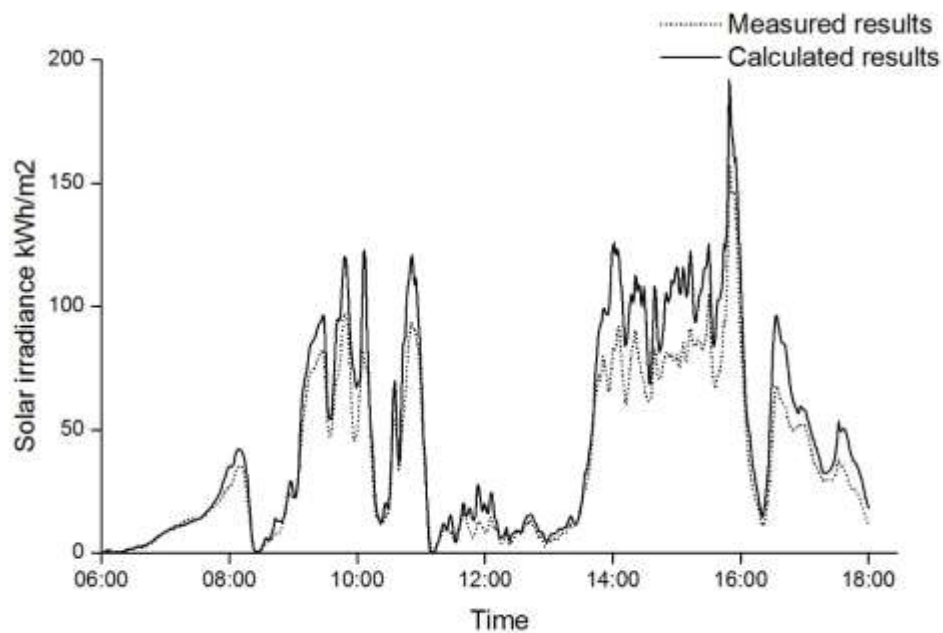
Figure 4.8 Validation of the solar irradiance calculation under cloudy conditions

The ambient temperature and temperature of south wall measured from field experiment are served as input values in equation 4.18- equation4.19, thus to calculate the temperature of PV glazing. By doing so, the comparison between the measurements and calculation results of the temperature of PV glazings is then available and shown in Figure 4.9. The solar radiation on the south wall measured from field experiment are served as input values in equation 4.1, inputted with η (efficiency) calculated by equation 4.17, thus to calculate the PV electricity generation. In the calculation, a standard efficiency of 14% (PV-2) is given by the

manufacturer. By doing so, the comparison between the measurements and calculation results of the PV electricity generation is then available and shown in Figure 4.10.

Second, the calculation of the PV generation power based on operating temperature was validated. The PV temperature was calculated using equation 4.18 with the measured ambient temperature and total solar irradiance on the PV façade. The calculated PV temperature and the measured PV temperature were plotted in Figure 4.9. Then, the PV generation power was calculated using equations 4.1 and 4.17 with the PV conversion efficiency according to the PV operating temperature. The calculated and the measured PV generation powers were plotted in Figure 4.10. The calculated and the measured results are consistent in Figures 4.9 and 4.10. The data of figure 4.9 and 4.10 were from the measurements of April 17, 2013. Beside the data that were collected in April 17, 2013 and presented in the figures, all valid data in the experiment period also verify the aforementioned equations.
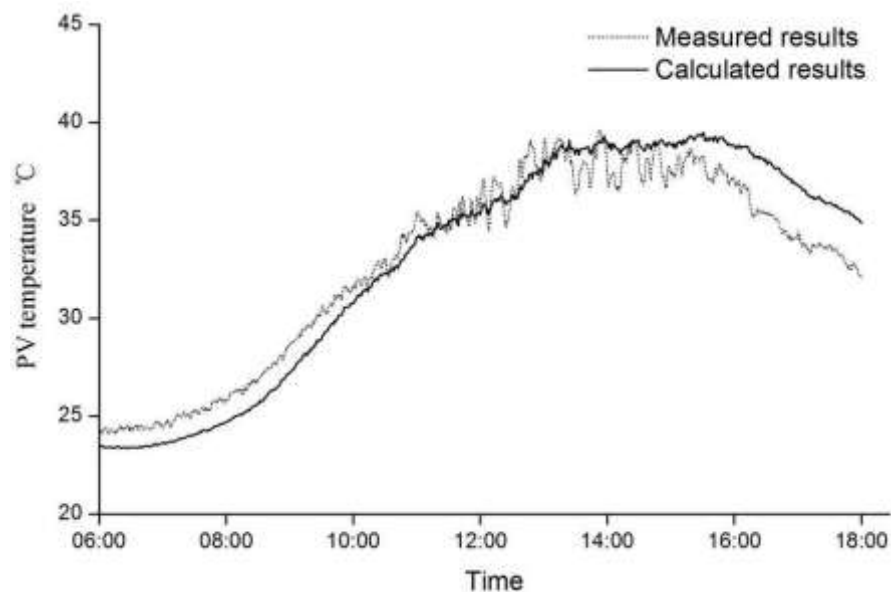
Figure 4.9 Validation of the calculation method of the PV operating temperature
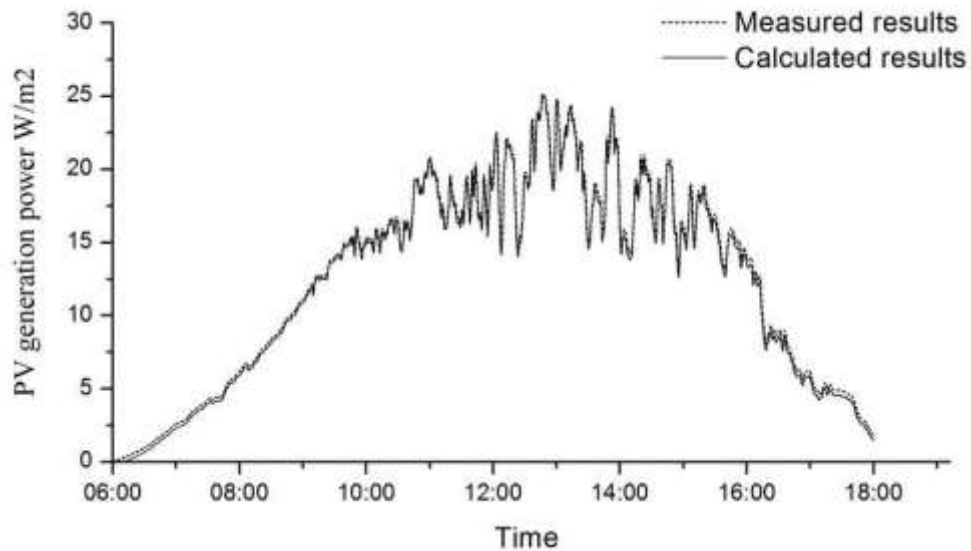
Figure 4.10 Validation of the calculation method of the PV generation power based on the PV operating temperature

4.3. Parametric studies on the annual power generation of the PV façades in China

With the validated calculation models and the solar radiation and ambient temperature data provided by the typical yearly weather data, the annual power generation of the PV façade can be estimated. In this section, the parametric studies were performed on the PV output energy in several representative cities in China and different integrations of the PV façades. The results of the parametric studies can provide a reference for the optimal design of the PV façades.

4.3.1. Effects on the location and orientation

The annual power generation of the PV façades was simulated in four Chinese cities: Beijing, Shanghai, Wuhan and Guangzhou, which are the representative cities in North China, East China, Central China and South China, respectively. PV modules should be installed on the façades of different orientations in these four cities.
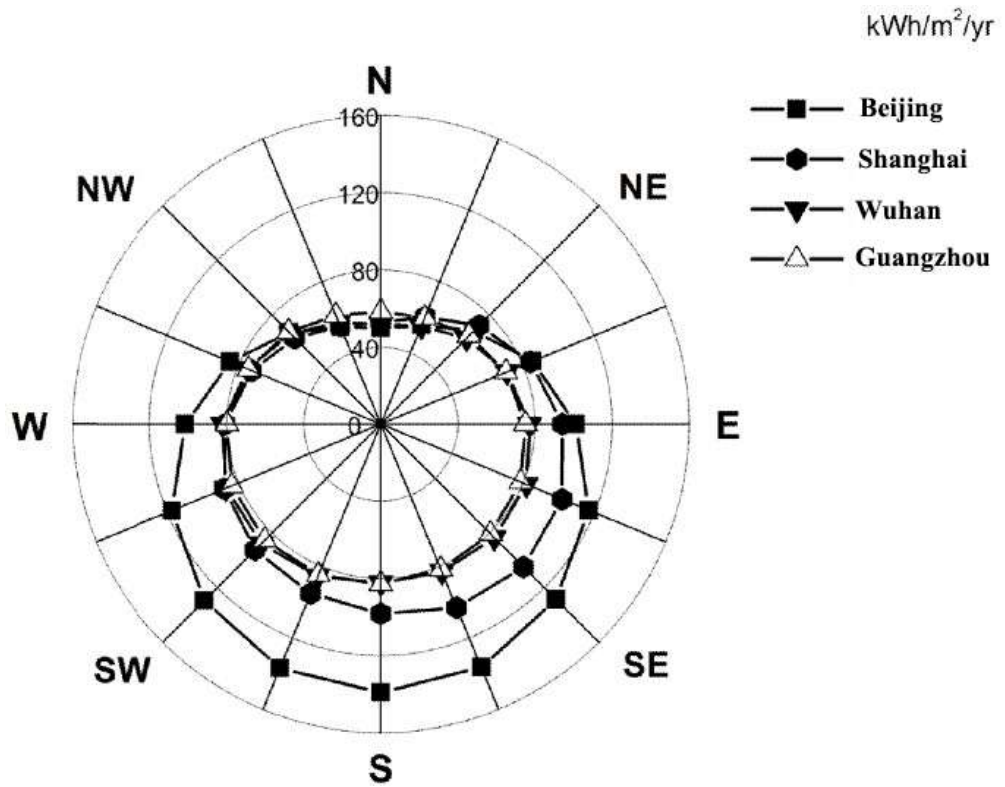
Figure 4.11 Annual power generation of the PV façades of every orientation in four cities of China
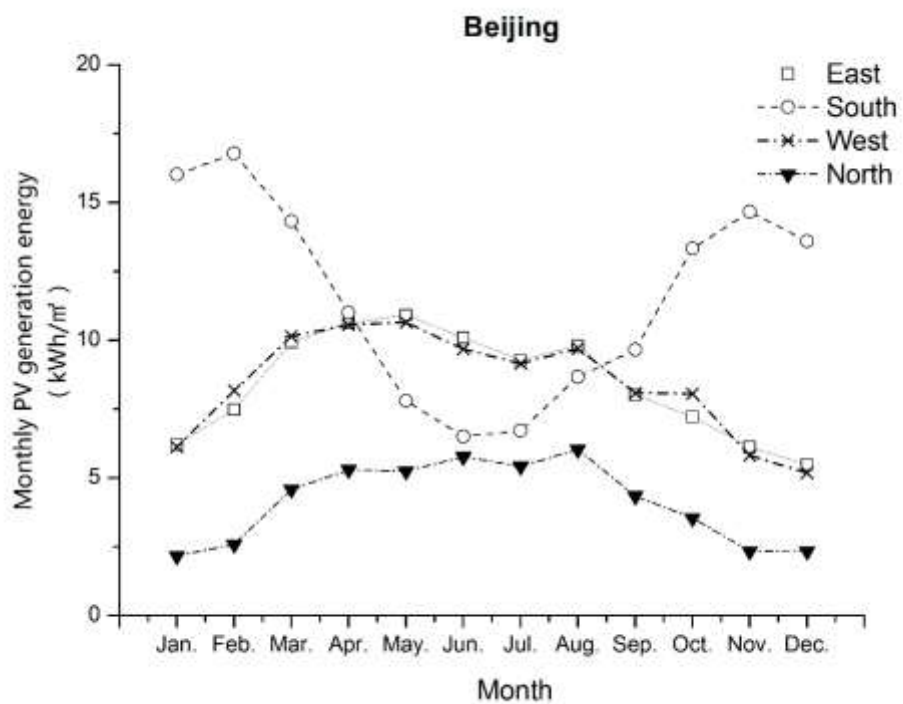
(a)
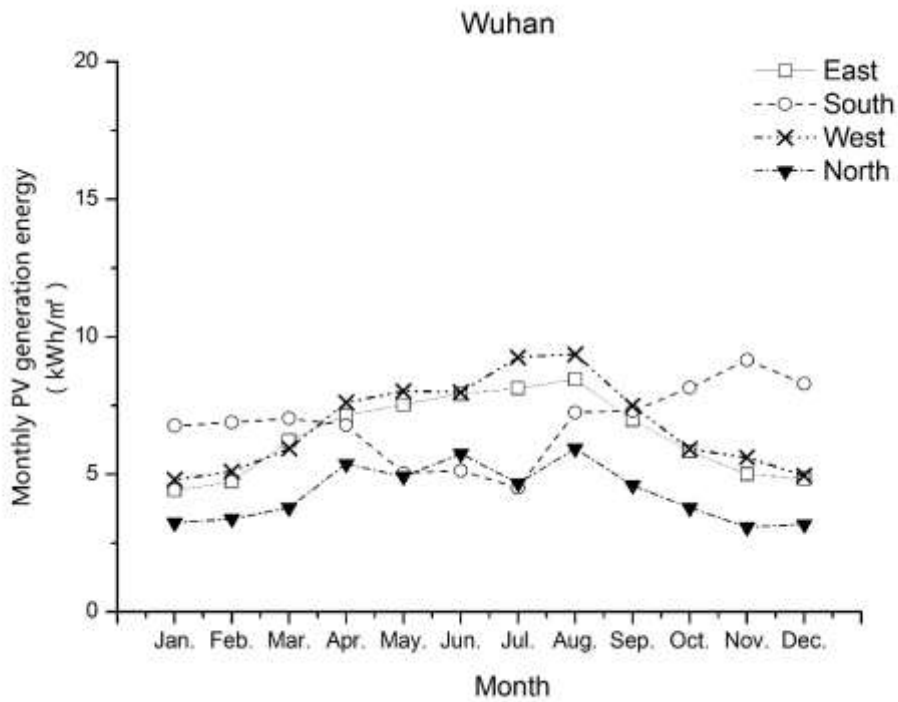
(b)

Figure 4.12 Monthly power generation of the PV façades in Beijing and Wuhan

Suppose that a mono-crystalline PV module (conversion efficiency is 14% at STC) with the area of one square meter was installed on the vertical façade of different orientations in Beijing, Shanghai, Wuhan and Guangzhou. The annual power generation of the PV façades was calculated and plotted in Figure 4.11. As shown in this figure, the orientation of maximum PV output energy was south, whereas the orientation of minimum PV output energy was north for all four cities. The annual power generation of the southern PV façade reached 139.1 kWh/m^2, 98.2 kWh/m^2, 82.3 kWh/m^2 and 82.9 kWh/m^2 in Beijing, Shanghai, Wuhan and Guangzhou, respectively. Beijing was significantly better than the other three cities. In terms of the north PV façade, the annual power generation was 49.7k Wh/m^2, 52.8 kWh/m^2, 51.7 kWh/m^2 and 58.2 kWh/m^2. Beijing has the highest value, whereas Guangzhou has the lowest value, but the overall value is not notably different. In general, the gap between the most favourable orientation (south) and the most unfavourable direction (north) in Beijing is relatively large, and the difference of the photovoltaic power generation in Wuhan and Guangzhou is relatively small.

The monthly power generation of the PV façades in Beijing and Wuhan was illustrated in Figure 4.12. There are similar characters for both cities. The monthly PV power generations of the east façade and west façade are notably close but are greatly different from the result of the north and south. For the southern PV façade, the maximum PV energy is in winter, and the minimum PV energy is in summer. On the contrary, the minimum PV energy is in winter for the eastern, western and northern façades. The dissimilar character for Beijing and Wuhan is that the difference in PV energy in different orientations is great in Beijing and relatively small in Wuhan.

4.3.2. Effects on the building form

PV modules are installed on the building façades, and the architectural form affects the orientation of the PV modules; thus, the PV power generation in the entire building is associated with the form of architecture. The three most typical building forms (rectangular, rhombus and circular) are selected for the parametric study. The mono-crystalline PV (conversion efficiency is 14% at STC) is arranged on the building façades with 3.6 m in storey height and 30 m in horizontal length. Form 1 is a rectangular plane building with PV modules covering the south façades; form 2 is a rhombus plane building with PV modules covering the southeast and southwest façades; form 3 is a circular building with PV modules covering the south semi-circular façades. The building forms were presented in Figure 4.13 (a).

The annual power generations of the PV façades in the three building forms were shown as columns in Figure 4.13 (b). The gap in PV energy of the three building forms was slightly high in Beijing and relatively small in the other cities.

| Form 1 | Form 2 | Form 3 |
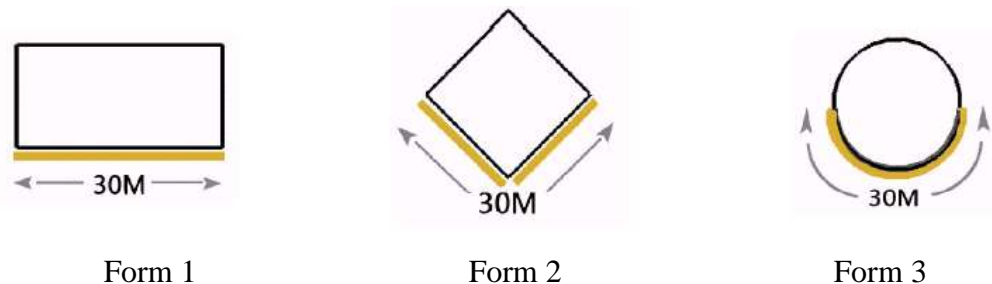
(a)
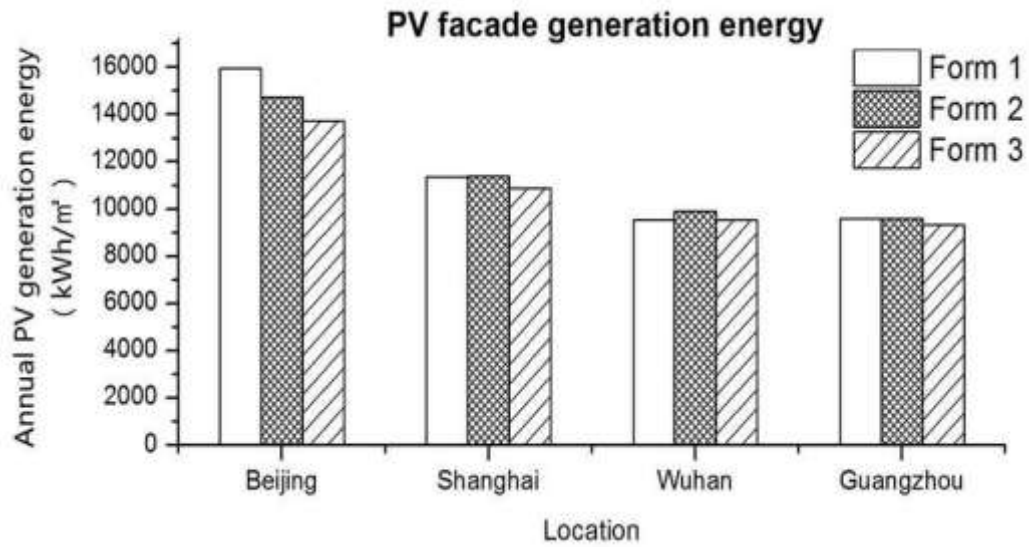
(b)

Figure 4.13 Annual power generation of the PV façades in three building

forms

4.3.3. Effects on the PV material and PV module arrangements

Although the form and site of the buildings may be identical, the PV façades power generation varies according to the PV material and PV arrangement. Parametric studies were performed with the assumption that the south façade (3.6 m in storey height and 30 m in horizontal length) of a rectangular-form building in Beijing were covered with PV modules in four arrangements.

Supposed the conversion efficiency are 14% for mono-crystalline PV, 7.8% for amorphous-silicon opaque PV and 4.9% for amorphous-silicon semi-transparent PV, which could be regarded identically from the measurements. Arrangement 1 is composed of a 0.9-meter-high solid wall and a 2.7-meter-high curtain wall. Mono-crystalline opaque PVs (conversion efficiency is considered to be 14%) were installed on the solid wall, and mono-crystalline semi-transparent PVs (photovoltaic coverage ratio is 50%) were used on the curtain wall. Arrangement 2 is composed of two 0.9-meter solid walls and one 1.8-meter-high curtain wall. Mono-crystalline opaque PVs were installed on the solid wall, and transparent low-E glazing was used on the curtain wall. Arrangement 3 is composed of one 0.9-meter solid wall and one 1.8-meter-high curtain wall. Amorphous-silicon

opaque PVs (conversion efficiency is considered to be 7.8%) were plugged on the solid wall, and the amorphous-silicon semi-transparent PVs (conversion efficiency is considered to be 4.9%) were used by the curtain wall. Arrangement 4 is composed of two 0.6 m long PV shading with an angle of inclination of $60°$. The mono-crystalline opaque PVs are integrated to the shading. The four arrangements were illustrated in Figure 4.14.

Figure 4.15 shows the column graphics of the annual power generation in the four PV arrangements. The annual total PV generation energy is sorted in descending order as Arrangement 1, Arrangement 2, Arrangement 4 and Arrangement 3. The annual PV generation energy per square meter area in descending order is as Arrangement 4, Arrangement 2, Arrangement 1 and Arrangement 3. Using amorphous-silicon PV modules with the lower electrical efficiency, arrangement 3 has the lowest total power generation and power generation per square meter. Although the total generation energy of Arrangement 4 is not so high, but it has the highest generation energy per square meter among all four arrangements. The generation energy per square meter of arrangement 4 is 1.5 times that of arrangement 2 and 2.5 times that of arrangement 1. This result implies that in terms of the PV generation energy, the arrangement with the inclined PV shading has an obvious advantage on the vertical arrangement of solid wall in Beijing.
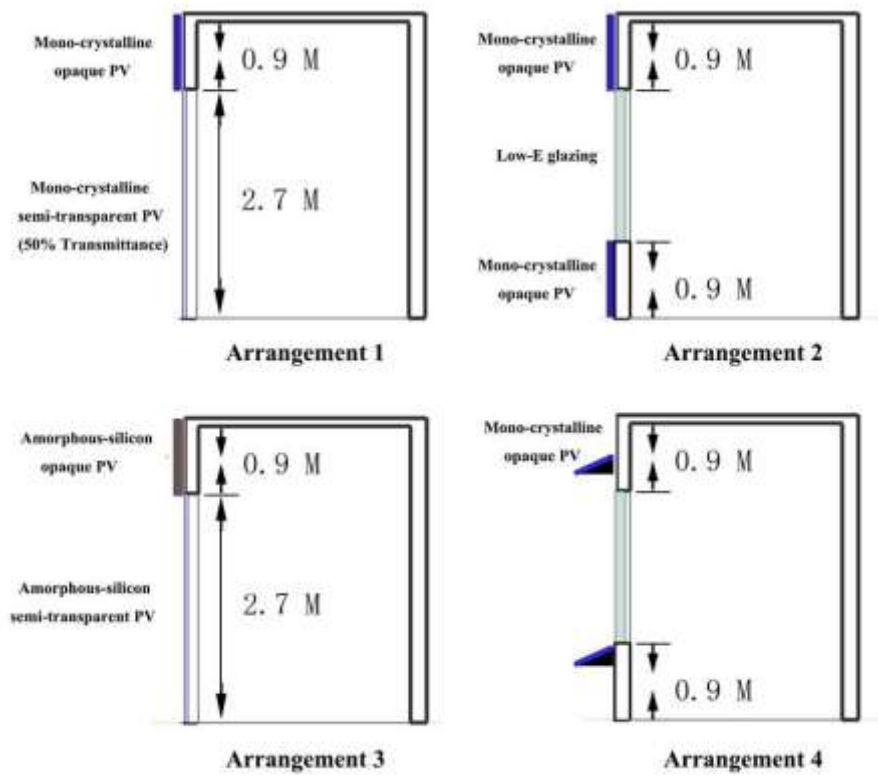
Figure 4.14 Illustration of four arrangements for the PV façades
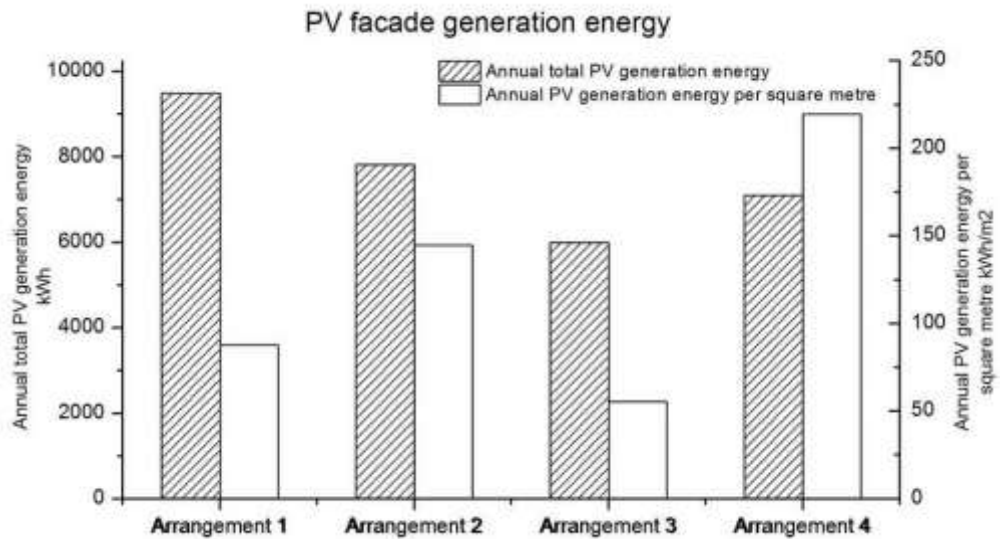
Figure 4.15 Annual power generation of the PV façades in four arrangements

4.4. Conclusions

The calculation models of solar irradiance on an inclined surface and PV generation power based on the operating temperature are developed and validated with the measured data. The good agreements between measured results and calculated results demonstrate that the calculation models can predict annual power generation of PV façades with good accuracy. In addition, the developed and validated calculation method in this chapter can be used as an easy-to-use tool in the pre-design of BIPV.

With the validated calculation methods and the typical yearly weather data of CSWD, the annual power generation of PV façades in China is calculated in parametric studies. The results show that with various cities, building orientations, building forms, materials and arrangements of PV modules, there is a distinct difference in the electrical output energy of PV façades. PV façades have maximum electrical generation in the south and minimum in the north. However, although the gap between the most favourable orientation (south) and the most unfavourable direction (north) in Beijing is relatively large, the difference of the photovoltaic power generation in Wuhan and Guangzhou is relatively small. In addition, the difference of PV electrical energy generated in rectangular, rhombus and circular building forms was slightly higher in Beijing and relatively small in the other cities. The parametric study results can serve as reference for architects, engineers and installers in the BIPV project in China.

Chapter 5 Calculation methods and architectural models for energy evaluation of semi-transparent PV façades

In previous Chapter 4, calculation methods for PV generation of semi-transparent PV glazing is presented. However, to further investigate the energy performance of semi-transparent PV façade integrated in building, complete calculation methods of PV generation, thermal and daylighting are required and presented in Section 5.2. In addition, architectural models are also required to serve as architectural conditions and presented in Section 5.3. Models of baseline buildings are necessary as they provide references to evaluate how much energy is saved by semi-transparent PV façades in office buildings and is presented in Section 5.4. This chapter would provide a solid foundation for further simulation investigations in this study for semi-transparent PV façade.

5.1. Introduction

In Chapter 4, a calculation method for the PV generation of semi-transparent PV glazing is presented. However, to further investigate the energy performance of semi-transparent PV façades that are integrated in buildings, complete calculation methods of PV generation, thermal and daylighting are required. In addition, architectural models are also required to serve as architectural conditions. Thus, this chapter presents the calculation methods and architectural models for the energy evaluation for both mono-crystalline and amorphous-silicon semi-transparent PV façades.

To evaluate the total energy of semi-transparent PV, relevant calculation models and methods are necessary to predict different thermal and optical characteristics of PV façades under different environmental and architectural conditions. These characteristics involve the PV electricity generation output, temperature behaviours of PV glazing, heat transfer process of PV glazing and daylighting-related process of PV glazing. Based on these characteristics, the overall energy consumption is calculated for further analysis. In this chapter, the calculation models and methods for simulations are developed for both mono-crystalline silicon PV and amorphous-silicon semi-transparent PV, which includes PV power generation model, thermal model and daylighting calculation method. Relevant studies (Ciulla et al., 2014; Hoang et al., 2014; Torres Lobera and Valkealahti, 2013; Ishaque et al., 2011; Mei et al., 2003; Kamthania and

Tiwari, 2014; Yun et al., 2007) have been reviewed to ensure the comprehensiveness and practicability of the models and methods. Field experiments were performed to obtain measured data to compare with the simulated results for validation.

The semi-transparency of PV façades makes them more involved with the building environment and the performance of building energy consumption (Leite Didoné and Wagner, 2013 ; Lu and Law, 2013 ; Olivieri et al., 2014 ; Wong et al., 2008). Thus, PV façades and architectural factors are more related to each other than the usual PV applications on roofs. In this case, architectural models are developed as an important part to investigate the energy performance of semi-transparent PV glazing that is used as office façades, which includes parameters of WWR, room depth, orientation and other necessary settings of the building envelop materials, running schedule of people and equipment, etc. Models of two baseline buildings without PV applications are also introduced in this chapter, which serve as comparison cases with semi-transparent façades.

To serve and represent the general climate condition in Central China, Wuhan is chosen as the typical city, which has been thoroughly discussed in Chapter 4. Chinese Standard Weather Data (CSWD) is used for the typical year weather data in simulations. In terms of validations for calculation methods, real climate data recorded by field experiments is used and rewritten into the CSWD format to serve as the climate conditions to provide the comparisons between the measurement data and calculation results.

5.2. Calculation methods of semi-transparent PV glazing

Calculation models and methods of semi-transparent PV glazing are developed for detailed simulation of the overall energy performance of PV façades. The PV power generation model for different PVR glazings is developed to predict the electricity generation under different conditions of solar radiation and glazing temperature. A thermal model is developed for different PVR glazings to predict the temperature on the PV layer and provide the necessary properties to incorporate into Energy Plus to perform computation simulations (Energy Plus does not

provide a calculation model for semi-transparent PV glazings). In the daylighting calculation method, lighting control is introduced to maximise the benefit of natural daylight, which is affected by different PVR PV glazings. Studies have discussed the calculation models and methods for PV-glazing, and some (Wong et al., 2008 ; Jiang et al., 2008) focused on the semi-transparent PV glazing. However, few studies have carefully considered the effect of different PVR; thus, there is a lack of development of calculation models and methods for different semi-transparent PVR.

5.2.1. PV power generation model

The PV power generation efficiency is affected by the temperature of solar cells: the PV efficiency decreases with increasing temperature (Ye et al., 2013). Moreover, a PV panel with high PVR absorbs more solar radiation and achieves a higher temperature than a panel with low PVR; this produces inconsistent results in terms of PV power generation efficiency even under identical climatic conditions (Jiang et al., 2008). To address this issue, a temperature coefficient power generation (Skoplaki and Palyvos, 2009) must be included.

$$P = G\, \eta_{\mathrm{O}}[1 - \beta_{\mathrm{C}}(T_{\mathrm{c}} - 25^{\circ}\!\mathrm{C})] \tag{5.1}$$

where P is the instant power of the PV panel, G is the solar radiation on the PV plane (W/m^2), η_{o} is the PV efficiency under standard conditions (0.14 for mono-crystalline PV and 0.049 for amorphous-silicon PV given by manufacturer), β_{C} is the temperature coefficient, and T_{c} is the solar cell temperature ($^{\circ}\!\mathrm{C}$), which is affected by PVR. In this model, the solar cell temperature T_{c} is unknown and must be provided using heat balance models (as described in Section 5.2.2). In the present study, the temperature coefficient β_{C} was determined to be -0.72%/$^{\circ}\!\mathrm{C}$ based on field experiments.

The results that were obtained using the power generation model were compared with the measurements that were obtained during field experiments. A model of same settings of sizes and materials of the experiment room is built with SketchUp (Figure 5.1) and then transferred into Energy Plus to provide the simulation condition for validation of simulated results. The weather data is recorded by experiment room and rewritten into CSWD format and used to provide

the same weather condition for validation. Such a model is used for the validation results (Figure 5.2, Figure 5.3, Figure 5.6 and Figure 5.7).
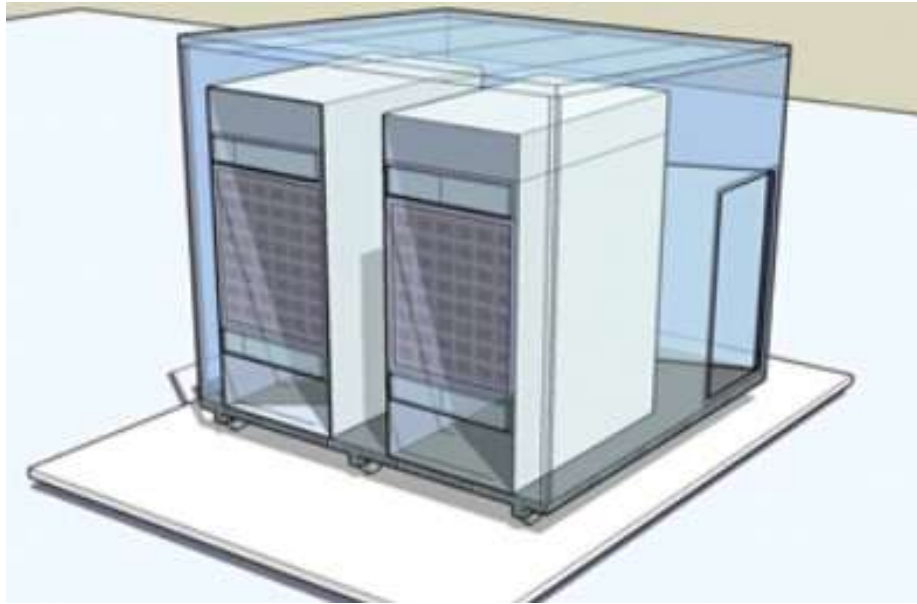
Figure 5.1 Computation models for energy plus to compared with field experiment room

To perform a validation for calculated results of PV electricity output power by PV power generation model, G is provided by Energy Plus, calculated with the rewritten CSWD in real weather data measured by field experiments; Tc is calculated by the thermal model in 5.2.2, η_o and β_C is given fixed value discussed in paragraph above previously. By doing so, the calculated results of PV electricity output power is given with equation 5.1. Such calculated results are then used to compare with experiments results.

It was demonstrated that the power generation model can predict the PV electricity output with satisfactory accuracy. For example, Figure 5.2 compares the measured and calculated PV electricity output results for a semi-transparent PV panel with PVR of 40% using the climate data of August 1 2013, and the results are clearly indicates good agreement, with an average deviation of 7.5%. Other comparisons in all four seasons were also made; the results show good agreement, with less than 9.2% deviation in all cases. Figure 5.3 shows the PV electricity output results of the amorphous-silicon semi-transparent PV glazing with the

climate date of June 3rd 2013. Both comparisons indicate that the power generation model can predict the PV electricity output with a satisfactory accuracy.
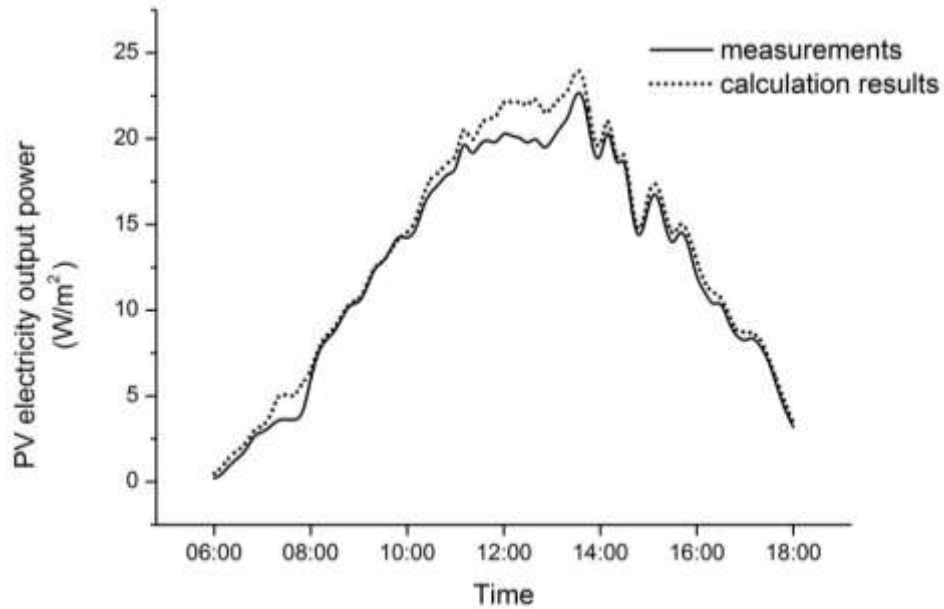
Figure 5.2 Validation of the power generation of the mono-crystalline semi-transparent PV
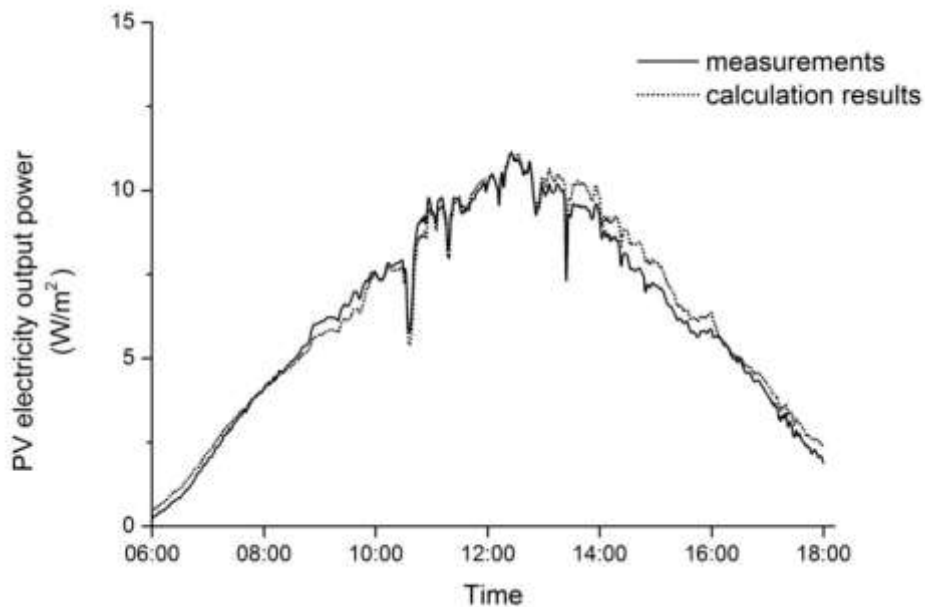
Figure 5.3 Validation of the power generation of the amorphous-silicon semi-transparent PV

5.2.2. Thermal calculation model

The temperature of the solar cell layers of semi-transparent PV panels must be calculated using a thermal model. The thermal calculation model would provide the temperature T_c in equation 5.1, which is changing by time and thus affects the PV power generation, which makes it a critical part of the calculation of PV yield and its efficiency. With the temperature T_c in equation 5.1, the accumulations of PV electricity generation is calculated by a time step of 30 minutes. In terms of the relation between the thermal calculation model and the Energy Plus, the thermal calculation model would also provide the necessary properties of the investigated glazings for Energy Plus including U-value, SHGC and visible transmittance, by which the process of thermal calculation is carried out by Energy Plus.

For mono-crystalline silicon, the single-glazing semi-transparent PV glass consists of multiple layers of materials, including internal and external layers of clear glass (each is 6 mm thick) with a central layer of EVA (ethylene-vinyl acetate copolymer) that contains a silicon cell of different PVR. In the adopted thermal model, the semi-transparent PV glass is divided into 3 layers with 4 boundaries as illustrated in figure 5.4. The properties of each layer are provided by the manufacturer and presented in Table 5.1.

Table 5.1 Properties of individual layers of the mono-crystalline semi-transparent PV

layer	thickness (mm)	thermal conductivity (W/mK)	absorptance	transmittance	reflectance
glass	6	0.760	0.108	0.810	0.082
EVA	1.8	0.116	0.060	0.900	0.040
silicon cell	0.3	168.0	0.970	0	0.030
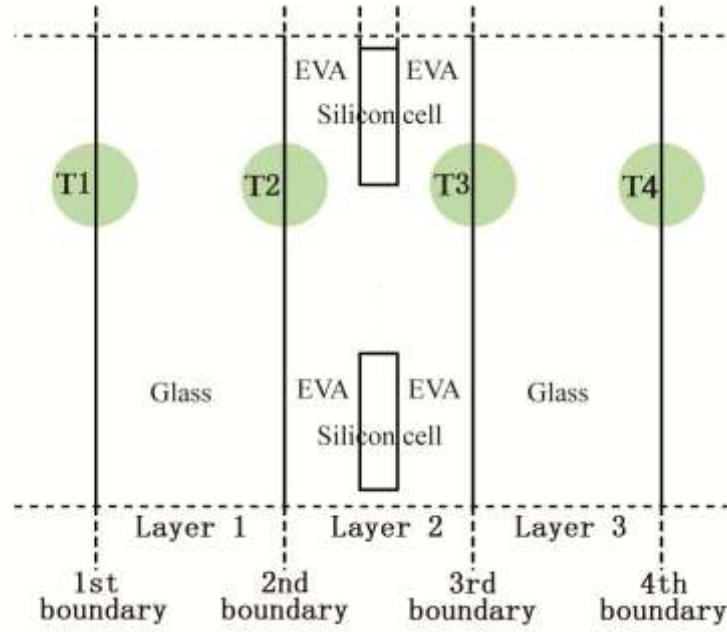
Figure 5.4 Schematic illustration of the mono-crystalline semi-transparent PV

The temperature of each boundary was calculated based on heat balance equations. The temperature of the solar cell layer T_c was assumed to be the average of T_2 and T_3 because the difference between these two values was negligible in the context of the model outcome. The heat storage in the single glazing was not considered, and the heat transfer was assumed to be in quasi-steady state. Thus, the heat balance equations for the first, second, third, and fourth boundaries were established in equations (5.2), (5.3), (5.4), and (5.5), respectively.

$$G\alpha_1 = (T_1 - T_{out})h_{out,c} + \xi\sigma\left[(T_1 + 273.15)^4 - (T_{out} + 273.15)^4\right] + \frac{\lambda_1}{d_1}(T_1 - T_2) \tag{5.2}$$

$$G\tau_1\left[(1 - PVR)\alpha_{EVA} + PVR\alpha_{sc}\right] + \frac{\lambda_1}{d_1}(T_1 - T_2) = \frac{\lambda_2}{d_2}(T_2 - T_3) + P \tag{5.3}$$

$$G\tau_1(1 - PVR)\tau_{EVA}\alpha_3 + \frac{\lambda_2}{d_2}(T_2 - T_3) = \frac{\lambda_3}{d_3}(T_3 - T_4) \tag{5.4}$$

$$\frac{\lambda_3}{d_3}(T_3 - T_4) = h_{in,c}(T_4 - T_{in}) + \xi\sigma\left[(T_4 + 273.15)^4 - (T_{in} + 273.15)^4\right] \tag{5.5}$$

where G is the solar radiation on the PV plane (W/m^2), α_i is the solar absorbance of layer i, and T_i is the temperature of boundary i. In addition, T_{out} and T_{in} are the outdoor and indoor temperatures, respectively; $h_{out,c}$ and $h_{in,c}$ are the convective heat transfer coefficients for the outside and inside surfaces of the semi-transparent PV panel, respectively; ξ is the emissivity of the front glass; σ is the Stefan–Boltzmann constant (W/m^{2}K^4); τ_i is the solar transmittance of layer i; PVR is the solar cell coverage ratio; λ_i is the heat conductivity of layer i (W/mK); λ_{sc} and λ_{EVA} are the heat conductivity of the solar cell and EVA, respectively (W/mK); P is the PV power generation (W/m^2); and d_i is the thickness of layer i (m). The external and internal surface convection heat transfer coefficients were set to 16 W/m^{2}K and 3.6 W/m^{2}K, respectively, based on the obtained data from the standard entitled "Calculation specification for thermal performance of windows, doors and glass curtain-walls" (JGJ/T 151-2008) (MHUDC, 2008).

For amorphous-silicon semi-transparent PV glazing, it consists of inside and outside layers of 6-mm clear glass and an amorphous-silicon layer in the middle. Similar to mono-crystalline semi-transparent PV, the amorphous-silicon semi-transparent PV glass is divided into three layers with four boundaries, and its schematic illustration is shown in Figure 5.5. The properties of each layer is provided by the manufacturer and shown in Table 5.2. The temperature of each boundary is calculated through heat balance. The temperature of the solar cell layer T_c is assumed to be the average value of T_2 and T_3. Thus, the heat balance equations for the first, second, third, and fourth boundaries were established as in equations (5.6), (5.7), (5.8), and (5.9), respectively.

$$G\alpha_1 = \left(T_1 - T_{out}\right)h_{out,c} + \xi\sigma\left[(T_1 + 273.15)^4 - (T_{out} + 273.15)^4\right] + \frac{\lambda_1}{d_1}(T_1 - T_2)$$

(5.6)

$$G\tau_1\alpha_2 + \frac{\lambda_1}{d_1}(T_1 - T_2) = \frac{\lambda_2}{d_2}(T_2 - T_3) + P$$

(5.7)

$$G\tau_1\tau_2\alpha_3 + \frac{\lambda_2}{d_2}(T_2 - T_3) = \frac{\lambda_3}{d_3}(T_3 - T_4)$$

(5-8)

$$\frac{\lambda_3}{d_3}\left(T_3 - T_4\right) = h_{in,c}\left(T_4 - T_{in}\right) + \xi\sigma\left[\left(T_4 + 273.15\right)^4 - \left(T_{in} + 273.15\right)^4\right]$$

(5.9)

Table 5.2 Properties of each individual layer of the amorphous-silicon semi-transparent PV

Layers	Thickness	Thermal conductivity （W/mK）	Absorptance	Transmission	Reflectance
Glass	6mm	0.760	0.108	0.810	0.082
amorphous-Silicon	1.5mm	0.25	0.770	0.200	0.030
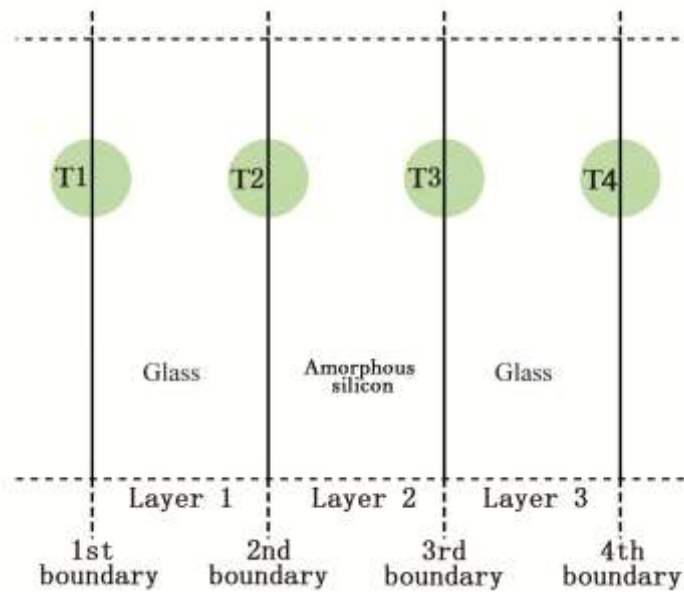
Figure 5.5 Schematic illustration of the amorphous-silicon semi-transparent PV

By using there rewritten CSWD weather data provided by field experiments T1, T2, T3, T4 are calculated with equation 5.2-5.5 and equation 5.6-5.9 for both type of PV glazing. Such calculated results are then used to compare with experiments results.
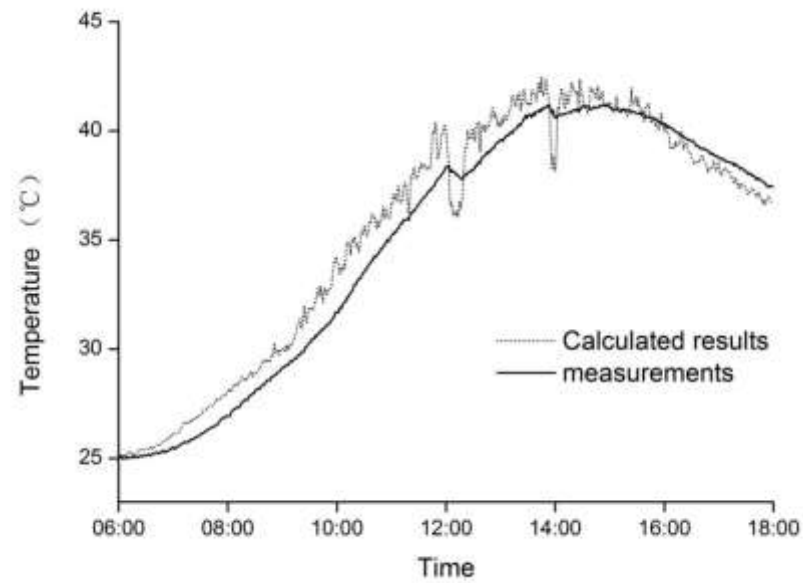
Figure 5.6 Comparison of the measured and the calculated inside-surface
temperatures for the mono-crystalline semi-transparent PV glazing
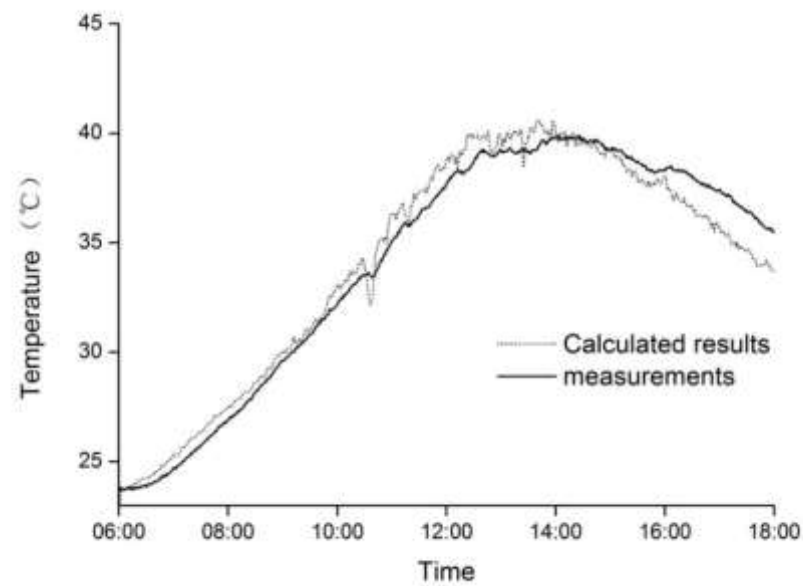
Figure 5.7 Comparison of measured and the calculated inside-surface temperatures
for the amorphous-silicon semi-transparent PV glazing

The results that were calculated from the thermal model were compared with the measurements collected during the field experiments. Figure 5.6 illustrates the variations in the inside-surface temperature of an semi-transparent PV panel with PVR of 40% throughout the course of a day (March 1 2013). Figure 5.7 shows the inside-surface temperature of the amorphous-silicon PV throughout the course of a day (June 3 2013). Both temperatures clearly demonstrate that the calculated results are consistent with the measurements.

To calculate the heat and solar radiation transfer, which affects the heating and cooling loads of the indoor space, it is necessary to obtain the U-factors and solar heat gain coefficient (SHGC) for different PVR glazings (MHUDC, 2008). These values are incorporated into Energy Plus to obtain the heat gain and loss data and the heating and cooling demand in certain architectural conditions. These calculation properties and methods can be used for both mono-crystalline and amorphous-silicon semi-transparent PVs with a small change accordingly.

SHGC can be calculated according to equation (5.10):

$$SHGC = \tau + N\alpha \qquad (5.10)$$

where τ is the total solar transmittance of semi-transparent PV, τ_i the solar transmittance of layer i, N is the inward-flowing fraction of the absorbed radiation, and α is the total solar absorbance of semi-transparent photovoltaics with different PVR and can be obtained from WINDOW 6.3 using the properties in Table 1. Furthermore, τ and N can be defined as shown in equations (5.11), (5.12) and (5.13). In terms of these two types of PV glazing, amorphous-silicon semi-transparent does not have a wide variation of solar transmittance, where τ_3 is the solar transmittance of the amorphous-silicon layer. This property is different from mono-crystalline PV layer, where the solar transmittance is controlled by the PVR and glazing that it contains.

For mono-crystalline semi-transparent PV:

$$\tau = \tau_1 \tau_2 \tau_3 (1 - PVR) \qquad (5.11)$$

For amorphous-silicon semi-transparent PV:

$$\tau = \tau_1 \tau_2 \tau_3 \tag{5.12}$$

$$N = \frac{h_{in}}{h_{in} + h_{out}} \tag{5.13}$$

where h_{out} and h_{in} are the outside and inside heat transfer coefficients, respectively, for the surfaces of semi-transparent PV panels. Similarly, the U-factors can be calculated for different PVR using equation (5.14).

$$U = \frac{1}{\dfrac{1}{h_{out}} + \dfrac{d_1}{\lambda_1} + \dfrac{d_2}{\lambda_2} + \dfrac{d_3}{\lambda_3} + \dfrac{1}{h_{in}}} \tag{5.14}$$

In the present study, the outside- and inside-surface heat transfer coefficients were set to 20.2 W/m^{2}K and 8.3 W/m^{2}K, respectively, based on the obtained data from the standard entitled "Calculation specification for thermal performance of windows, doors and glass curtain-walls" (JGJ/T 151-2008) (MHUDC, 2008).

After the calculation of SHGC and U-factor, the heating and cooling loads were simulated in Energy Plus.

5.2.3. Daylighting calculation method

According to the Standard for Lighting Design of Buildings for China (GB50034-2004) (CABR, 2008), the indoor illuminance should reach 300 Lux in a general office room. To simulate this code and the energy saving by daylight, daylight detection and lighting control for simulation is introduced using Energy Plus. When the daylight illuminance level is below 300 Lux, artificial lighting will achieve the required illuminance level with extra electricity consumption. According to the code, lighting settings in this study are assumed as fluorescent lights to represent the current usage of artificial lighting system in office building. However, in the future, the use of a more energy-efficient lighting setting like LED could have a major impact on the results, which is not included in this study. To

obtain the daylighting simulation outcome in Energy Plus, visible transmittance is required and given as equations (5.15) and (5.16).

For mono-crystalline semi-transparent PV:

$$\tau' = \tau_1' \tau_2' \cdots \tau_n' (1 - \alpha_{PVR}) \tag{5-15}$$

For amorphous-silicon semi-transparent PV:

$$\tau' = \tau_1' \tau_2' \cdots \tau_n' \tag{5-16}$$

where τ' is the total visible transmittance of the semi-transparent PV glazing, τ'_i is the visible transmittance of layer i. τ' is incorporated into Energy Plus for daylight simulation. Thus, the daylight illuminance is calculated and recorded using daylight sensors in Energy Plus, and the lighting energy consumption is simulated and calculated (Wong et al., 2008).

5.3. Architectural models

Architectural models are a crucial part of the investigation of the energy performance of semi-transparent PV. To develop these models, information was obtained by conducting a survey of 60 office building cases in the Wuhan area. Two typical types of office buildings were identified in the survey: buildings with core tubes and slab-type buildings. The division of large rooms into separate smaller rooms was common in both types of office buildings; in fact, most of the investigated cases exhibited such division. Thus, these separate rooms were incorporated into the described models and used to represent the generic office rooms in the present study, as shown in Figure 5.8.

These generic office rooms were set to allow control of three main variables: (1) room depth, as shown in Figure 5.9(a), (2) WWR, as shown as Figure 5.9 (b), and (3) orientation. By adopting various combinations of these variables, different PVR could be examined under different architectural conditions, as shown in Figure 5.9 (c). The room depth was varied from 4 m to 13 m at intervals of 1 m; this range can be considered representative of common office room sizes in the Wuhan area. The WWR was restricted to the range of 0.2−0.7 based on the

guidelines in the Design Standard for Energy Efficiency of Public Buildings, which was proposed by the Ministry of Housing and Urban–Rural Development of the PRC(CAB, 2004), which forbids office buildings with a WWR above 0.7 in the hot summer/cold winter climate zone. The PVR was varied from 10% to 80% at intervals of 5%. PVR below 10% will make PV applications uneconomical; conversely, PVR above 80% will block the entire window area, which makes it difficult for daylight to enter the room and for occupants to see outside. The adopted PVR interval of 5% should make different effects of PVR distinguishable while maintaining a sufficiently practical simulation parametric analysis.
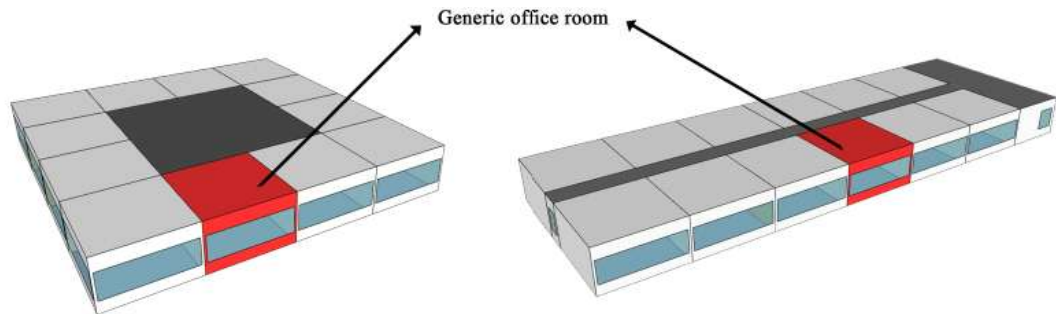
Figure 5.8 Illustrations of the generic office rooms
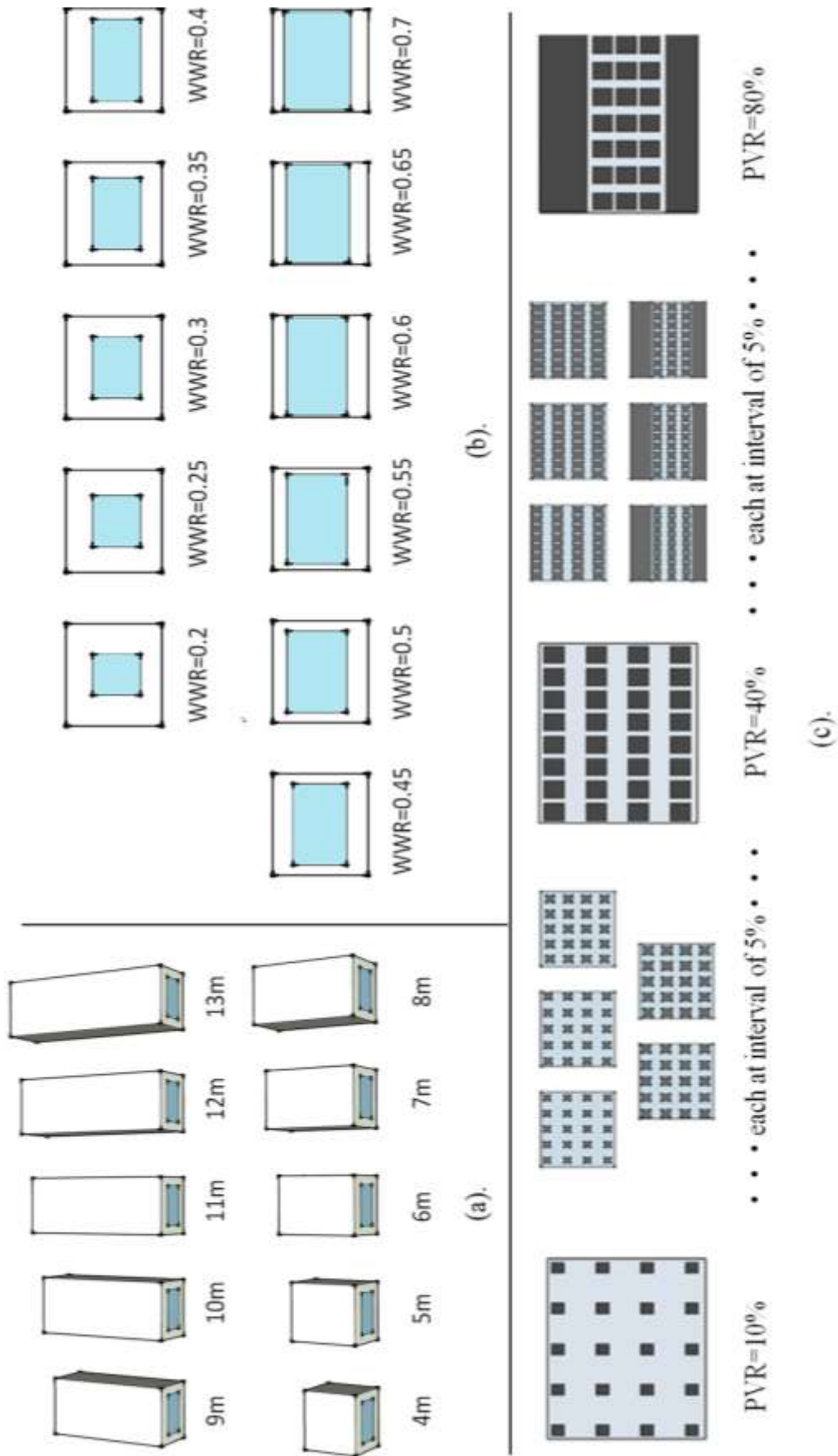
Figure 5.9 Illustrations of the variations in (a) room depth, (b) WWR, and (c) PVR

Table 5.3 Thermal and optical properties of the building envelope layers

Layers	Thickness (mm)	Thermal conductivity （W/mK）	Density (kg/m3)	Specific heat (J/kg K)
Exterior wall				
Brick	200	0.89	1920	790
insulation board	40	0.03	50	1210
Surface finish*2	20	0.16	800	1100
Interior wall				
Brick	100	0.89	1920	790
Surface finish*2	20	0.16	800	1100
Ceiling/floor				
Standard wood board	8	0.12	540	1210
Cast concrete	120	1.60	2200	860
Surface finish	20	0.16	800	1100

Table 5.4 Hourly schedules of office rooms

	Time				
	0:00-7：00	7:00-8:00	8:00-17:00	17:00-19:00	19:00-24:00
Cooling system （℃）	37	28	26	26	37
Heating system （℃）	12	18	20	20	12
Lighting, equipment operation schedules(fraction of full occupant)	0	0.5	0.95	0.3	0

Other simulation-required features are fixed assumptions based on the Design Standard for Energy Efficiency of Public Buildings (CABR, 2008) as follows:

- A rectangular office room at an intermediate floor level that is 5 m wide and 4 m high.

- The thermal properties of the exterior wall, interior wall, ceiling and floor are shown in Table 5.3.

- A single window area with no sunblind as the semi-transparent PV model will serve as the shading device.

- Room lights are set equally in the room with a design value of 11 W/m^2. A daylight control sensor is located in the geometric centre of the room at the height of 0.75 m to represent the average luminance level, which is the alternative method for multiple sensors to simplify the calculation process. Daylight control will initiate artificial lighting when the indoor illuminance level is below 300 Lux.

- The cooling and heating temperature set-point schedule of air conditioning is shown in Table 5.4 with a COP of 4.5. The ventilation system is set at 1.5 air changes/h.

- The office occupant is set at 0.25 person/m^2 with the electricity consumption of equipment at 20 W/ m^2.

Lighting and office equipment operation schedules are set according to the office occupant condition in Table 5.4.

5.4.   Models of baseline buildings for comparison

Models of baseline buildings are necessary because they provide the references to evaluate how much energy is saved using semi-transparent PV façades in office buildings. Because PV glazing of different PVR has various effects on the overall energy performance, baseline buildings can serve as a "ruler" and help us to further understand the benefit from optimal PVR in certain architectural conditions. With the energy saved using semi-transparent PV façades, the economic evaluation including the PBT (payback time) analysis is also available, based on which the

suitability of optimal PVR/WWR of semi-transparent PV façades is further discussed in Chapter 8.

In China, there is no official academic general reference of baseline building models for building energy studies to serve as comparison cases. However, certain architectural codes and regulations provide us with requirements of energy-efficient buildings. According to the Chinese Design Standard for Energy Efficiency of Public Buildings (GB-50189-2005) (CABR, 2008), the standard of "energy-efficient building" is provided, which can save approximately 50% energy compared to traditional public buildings that are built in the 80s and 90s. Because there are is other available option for reference cases in China, two types of baseline buildings are developed based on the requirements of the Chinese Design Standard for Energy Efficiency of Public Buildings (GB-50189-2005). The two types of baseline buildings are described as follows:

● Baseline building A

General and traditional office buildings that are built in the 80s and 90s. In GB-50189-2005, these buildings are defined as consuming two times more energy than energy-efficient buildings.

● Baseline building B

Energy-efficient office buildings that satisfy the minimum requirements of GB-50189-2005.

GB-50189-2005 provides the requirements of different aspects for different climate zones and conditions of energy-efficient buildings. However, not every requirement is necessary in the Hot-Summer Cold-Winter climate zone and suitable for the comparison cases in this study. We defined three main aspects of requirements as the basis to develop the baseline buildings: (1) envelope properties, (2) operation setting, and (3) operation schedule.

The first aspect is building envelope properties, which affect the heat transfer process of a building. Table 5.5 shows the requirements that are defined for the envelope properties of energy-efficient office buildings based on GB 50189-2005, which is specifically for the Hot-Summer Cold-Winter climate zone. Because the

architectural models in this study are assumed in the intermediate floor, the inner ceiling, inner wall, exterior wall and window are included as such.

Table 5.5 Requirements for the envelope properties of energy-efficient office buildings

Envelope		Thermal conductivity (W/m^{2}K)	
Roof		≤0.7	
Exterior wall		≤1.0	
Exterior window		U-value (W/m^{2}K)	Shading coefficient(SC) (East、South、West)
One side window (including transparent façade)	WWR≤0.2	≤4.7	/
	0.2<WWR≤0.3	≤3.5	≤0.55
	0.3<WWR≤0.4	≤3.0	≤0.50
	0.4<WWR≤0.5	≤2.8	≤0.45
	0.5<WWR≤0.7	≤2.5	≤0.40

Note: only applicable for Hot Summer Cold Winter climate zone

SHGC can be calculated by SC.

SHGC = SC/1.15

The operation setting is given as: room lights were assigned a design value of 11 W/m^2 in all instances; COP (coefficient of performance) of air conditioner was set to 4.5, and the ventilation system was set to ensure 1.5 air changes/h; office occupancy was set to 0.25 people/m^2, and the electricity consumption of the equipment was assumed to be 20 W/m^2. Most settings are coherent to the settings of architectural models for the semi-transparent energy evaluation in 5.3. The operation schedule is shown in Figure 5.3.

Other necessary setups for the models of baseline buildings were provided and discussed in Section 5.3. The main difference between the architectural models for the semi-transparent energy evaluation and the baseline buildings are the properties

of the building envelope (façades). Thus, the energy performance and characteristics of the semi-transparent envelopes can be better revealed.

5.5. Conclusions

In this chapter, calculation models and methods including PV power generation model, thermal model and daylighting calculation method are established and validated by field experiments. The results obtained using the power generation model was compared with measurements obtained during field experiments. It was demonstrated that the power generation model could predict PV electricity output with satisfactory accuracy. Thermal model that is developed for both crystalline silicon and amorphous-silicon PV of different PVR as the temperature of the solar cell layers of semi-transparent PV panels need be calculated using this models. The results calculated from the thermal model were compared with the measurements collected during field experiments, which demonstrates clearly that the calculated results agree well with the measurements. In such cases, it is believed these calculation models and methods can be used for further study of overall energy performance of semi-transparent PV façades with satisfactory accuracy.

Architectural models are developed based on the survey of 60 cases of office buildings in the Wuhan area. Generic office rooms are developed with variation of WWR, room depth, orientation. Based on the solid survey in a large area in Wuhan, it is believed the architectural models are proper and can be used for further study of overall energy performance of semi-transparent PV façades.

Two kinds of baseline buildings (A and B) are developed to help us to further understand the benefit from optimal PVR in certain architectural conditions, which is also based on the requirements of Chinese Design Standard for Energy Efficiency of Public Buildings. These standards have been largely used and proved by a lot real projects in China and it is believed they could serve well in objective comparison study for semi-transparent PV façades.

Chapter 6 Evaluation on energy performance of office buildings with mono-crystalline semi-transparent PV façades

With the calculation methods and architectural models presented in Chapter 5, energy (electricity) consumption of lighting, heating and cooling is calculated, based on which, this chapter presents a discussion of energy evaluation of mono-crystalline semi-transparent with a parametric analysis (Section 6.2). An optimizing design approach for mono-crystalline semi-transparent PV façade by optimal PVR is explored (Section 6.3). In addition, energy saving of mono-crystalline semi-transparent PV compared to three traditional glazings is investigated and presented in Section 6.4.

Throughout the evaluation (Chapter 6 Chapter 7 and Chapter 8), the main calculation and model assumptions are made and presented in Chapter 5. However, to further concentrate on the impact of semi-transparent glazing, several more assumptions are necessary and made as following with certain possible limitations :

1. The construction of the façades is simplified without detailed consideration of air leakage, heat bridge and other possible impacts from façades components. In a real situation, especially in a poorly built and maintained building, this could lead to a significant impact on energy performance.

2. All the energy units relevant to the overall energy consumption are unified by electricity unit (kWh), or (kWh/m^2). The impact of better usage of passive applications without the use of electricity in buildings could have an impact on the results. However, with the same configurations (which are also represent the most common cases of office buildings in Central China) for the study cases, the results still give a fair and consistent outcome and conclusions of how different semi-transparent PV façadess impact on general office building cases.

3. The indoor shading methods of curtain or other shading devices are assumed not existed as semi-transparent provides a certain level of shading. However, if indoor shading is used in some particular circumstances, these shading devices could lead to significant impact on energy performance.

4. The operation schedule of the building is a fixed assumption with same daily routines, in which people behave equally by the fractions of percentage of different activities. However, in a real case people could behave differently, for example, if there's a party planned on weekend, the activity could lead a significant change to the energy consumption.

5. Semi-transparent PV façades with single glazing were thoroughly studied. However, other types of glazing such as double-glazing PV were not included in this study. Double glazing is currently commonly used in buildings, and the potential of semi-transparent PV double-glazing façades is notably promising because they provide better thermal performance than single glazing. The advantage of PV glazing could be even more prominent in Semi-transparent double glazing PV façades.

6.1. Introduction

Evaluation on energy performance of PV façades should be carried out in terms of the overall energy peroformance. PV façades affect the overall energy of a building in many ways. First, with a higher PV coverage ratio, less daylight is available indoors, which increases the daytime demand for artificial-lighting energy. This result is particularly crucial in office buildings that primarily operate in the daytime. The PVR also affects the indoor heat gain from solar radiation, which affects the indoor heating and cooling demands. Additionally, different PV coverage ratios have different electricity outputs from PV generation. Hence, the overall energy assessment is required for the optimal design of PV façades. The overall energy performance can be evaluated using the overall energy consumption as:

Overall energy consumption = Lighting energy consumption + cooling and heating energy consumption – PV electricity generation.

The energy consumption of equipment and other systems in a building are not included in this assessment because they do not have an obvious relation to PV façades in terms of the overall energy performance. The evaluation of the energy performance of office buildings with mono-crystalline semi-transparent PV façades

includes three main assessments: (1) PV electricity generation, (2) artificial-lighting electricity consumption, and (3) heating and cooling electricity consumption.

The PVR significantly affects the overall energy consumption of the buildings, including PV generation, lighting, cooling, and heating. In a study of Bing Jiang and Jie Ji, the effect of the PVR on the thermal and electrical performance of a photovoltaic-Trombe wall showed that a larger PV coverage ratio reduced the thermal performance (Lukač and Žalik, 2013). Another study (Jiang et al., 2008) found that a certain PVR consumed the lowest energy consumption under specific architectural conditions. In another study (Wong et al., 2008), different solar cell transmittances had various effects on the overall energy performance of different window-to-wall ratio cases, and lighting control was an important element in maximising the benefit of a semi-transparent PV façade. Different ventilated PV façades in a range of PVR were evaluated to determine their effects on the overall energy performance to obtain the optimal design (Miyazaki et al., 2005). These studies suggest that identifying the optimal PVR for PV façades can help reducing the overall energy consumption. In the early design stages of PV façades, the effect on the overall energy consumption should be considered.

Different climate environments result in different overall energy savings because of the optimised PVR on PV façades. In Brazil, semi-transparent windows save as much as 43% of energy consumption (Yun et al., 2007); whereas in Japan, 55% overall energy is saved using a solar cell transmittance of 40% compared to a single glazing façade (Wong et al., 2008). In Singapore, energy is saved by 16.7-41.3% (Leite Didoné and Wagner, 2013). Other studies (Ng et al., 2013; Lu and Law, 2013) also suggest that it is important to consider the effect of the urban and climate environment on the design of semi-transparent PV façades.

This chapter discusses the energy evaluation of mono-crystalline semi-transparent with a parametric analysis. The validated calculation models and methods in Chapter 5 were incorporated into the previously defined architectural model to investigate the effects of different PVR on the energy performance using Energy Plus. The overall energy performance, which includes PV electricity

generation, lighting, heating and cooling electricity consumption, was examined under different architectural conditions. Different combinations of room depth and WWR were carefully examined for a southern orientation, whereas the PVR was varied from 10% to 80% at 5% intervals. The criterion of electricity consumption per floor area (kWh/m^2) was used to account for the differences in floor area for different values of room depth, which provided normalised results. All figures are evaluated using an annual value or average annual value (if it is not specifically mentioned) to see the entire picture of overall energy consumption of all four seasons.

6.2. Parametric analyses of the overall energy performance of mono-crystalline semi-transparent PV façades

6.2.1. Effects on the PV electricity generation

Solar cells convert solar energy into electricity and typically operate with a specific conversion efficiency, which is primarily affected by the material characteristics and operating temperature of the cells. Compared to transparent glass, mono-crystalline silicon solar cells typically have higher solar absorbance. Thus, the amount of gained solar heat can be increased by adopting a denser solar cell array and a higher PVR. Accordingly, this principle should also increase the temperature and reduce the conversion efficiency of the solar cells. In the present study, the temperature and conversion efficiency of solar cells were investigated throughout March 1 2013 (Figure 6.1), which was a steady sunny day with little cloud coverage to minimise the effect of incident climates. The temperature of the solar cell significantly increased significantly (more than 18°C) in the morning and reached the highest value at noon; then, it slowly decreased in the afternoon but maintained a relatively high temperature compared to that in the morning. Meanwhile, the PV electricity conversion efficiency decreased in the morning and reached its lowest point at noon with a deviation of approximately 0.02. The conversion efficiency began to increase in the afternoon but remained relatively lower than that in the morning. The results demonstrate that the conversion efficiency decreases with increasing temperature and vice versa.

With different PVR, for example, when it is at noon, the temperature for the 80% PVR case was 7 ℃ higher than that for the 10% PVR case; this temperature difference corresponded to a 0.007 decrease in conversion efficiency, which is 5.5% lower than the 10% PVR case. The results demonstrate the importance of considering PVR in PV electricity generation. This discovery indicates that with the increase of PVR in PV faҫades, the marginal returns of the PV electricity yield is diminished. The increase in PVR does not proportionally increase the PV electricity yield. This marginal effect becomes more significant with high solar radiation conditions; for example, at noon when solar radiation reaches its peak value, the deviation of the PV conversion efficiency of different PVR also appears most significant.

In conclusion, the analysis of the PV electricity conversion efficiency indicates two important facts: (1) temperature significantly affects the conversion efficiency; (2) the marginal returns of electricity yield are diminished by the increase in temperature because of a higher PVR.
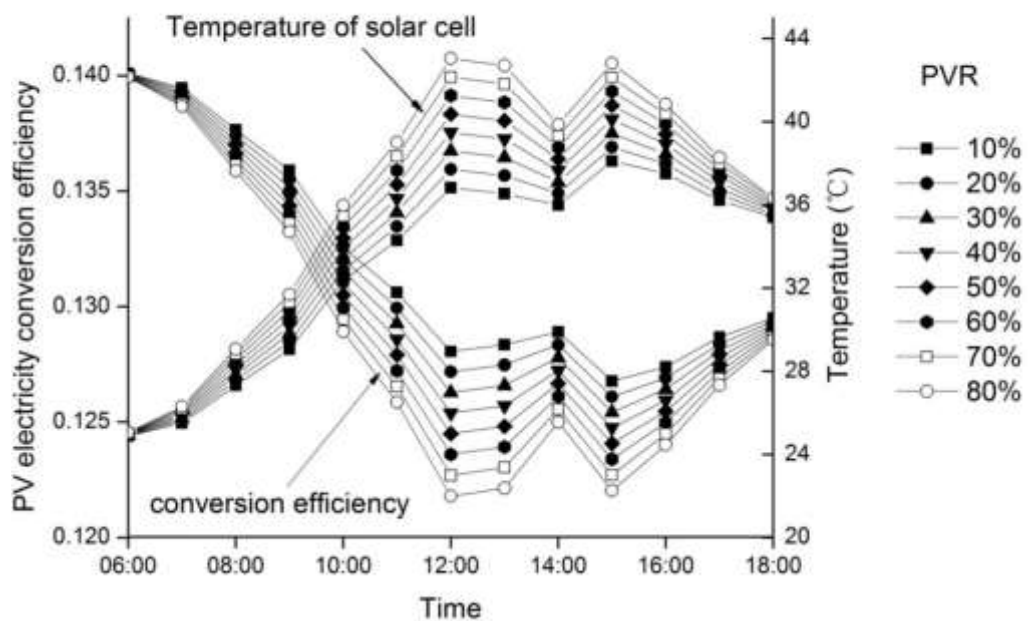
Figure 6.1 Solar cell temperature and its conversion efficiency

in different PVR cases

6.2.2. Effects on the daylight and the lighting electricity consumption

The amount of daylight that is blocked by solar cells can considerably vary in response to differences in PVR among semi-transparent PV panels, which can have a vital effect on the indoor illuminance. If the indoor illuminance decreases below a given threshold, artificial lighting is required to achieve a comfortable lighting environment, and electricity must be consumed to achieve this result. However, the room depth and WWR may also affect the performance of semi-transparent PV panels at different PVR. Thus, it is important to understand the relationship between PVR and the indoor illuminance for different combinations of room depth and WWR.

For larger room depth (i.e., deeper rooms), it is more difficult for daylight to reach deep inside the room. Thus, even for identical PVR, daylight illuminance tends to vary depending on the room depth conditions. Figure 6.2 illustrates the indoor daylight illuminance for different PVR under various room depth conditions for a fixed WWR of 0.35. The results show that the indoor illuminance rapidly decreases with increasing PVR, with more pronounced decreases at smaller values of room depth. The illuminance decreases from 2000 lx to less than 600 when PVR increases from 10% to 80% in a 4 m deep room. In a 13 m deep room, the illuminance decreases from 230 lx to less than 50 lx. In such a room with less than 50 lx illuminance level, artificial lighting must be on full operation to maintain a comfortable lighting environment indoor. In general, shorter rooms (i.e., smaller room depth) experience much higher daylight illuminance than deep rooms (i.e., with larger room depth). Moreover, indoor illuminance remains below 400 lux for all cases where the room depth exceeds 9 m. These results demonstrate that the effects of PVR on daylight illuminance strongly depend on the room depth.
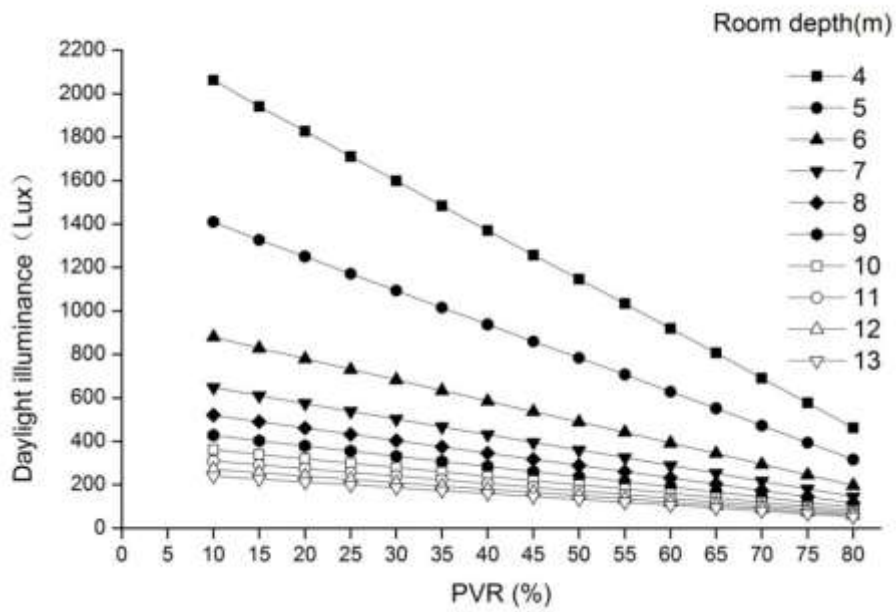
Figure 6.2 Indoor daylight illuminance of different PVR

in different room depth cases

With artificial-lighting compensation, Figure 6.3 shows the lighting electricity consumption of different PVR in different room depth cases. It is obvious that the artificial-lighting electricity consumption increases when daylight illuminance decreases because of higher PVR. However, this result does not occur with a linear dependence. For small-room-depth cases, the lighting electricity consumption increases much faster when PVR exceeds 50%; for larger-room-depth cases, the increase is closer to a linear dependence. For example, in a 4 m deep room, the lighting energy consumption increases from 17 kWh/m^2 to 18 kWh/m^2 with only notably limited increase when PV increases from 10% to 80%; however, in a 13 m deep room, the lighting energy consumption increases from 21 kWh/m^2 to 32 kWh/m^2 with more than 11kWh/m^2 increase. However, because of the advantage of higher indoor illuminance, small-room-depth cases consume less lighting electricity of at most 15 kWh/m^2.
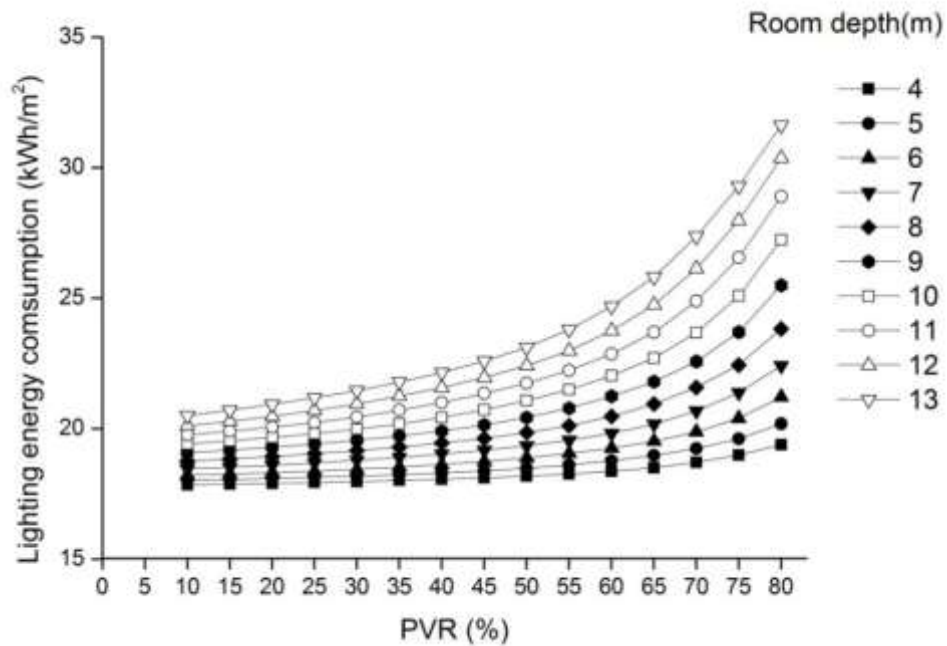
Figure 6.3 Lighting electricity consumption of different PVR

in different room depth cases

We previously discussed the effect of different PVR in different room depth cases. The effects of different PVR in different WWR cases are discussed as follows.

Compared to a small WWR case, a large WWR case allows more daylight to reach inside the room and has a bigger window area to install mono-crystalline semi-transparent PV, which leads to better illuminance indoor and reduce the artificial-lighting demand. Figure 6.4 shows the average indoor daylight illuminance of different PVR in different WWR cases at a fix room depth of 6 m. Similar to the depth cases, illuminance decreases when PVR increases. In a 0.2 WWR room, the illuminance decreases from 1100 lx to less than 300 lx when PVR increases from 10% to 80%. In a 0.7 WWR room, the illuminance decreases from 300 lx to less than 50 lx. However, the difference among different WWR cases is much smaller compared to the different room depth cases. This result indicates that the WWR less significantly affects the daylight illuminance than the room depth, which is also true for lighting energy consumption as Figure 6.5 shows. The lighting electricity consumption increases with the increase in PVR. However, the

difference is smaller among the WWR cases with electricity savings of at most 9 kWh/m^2.
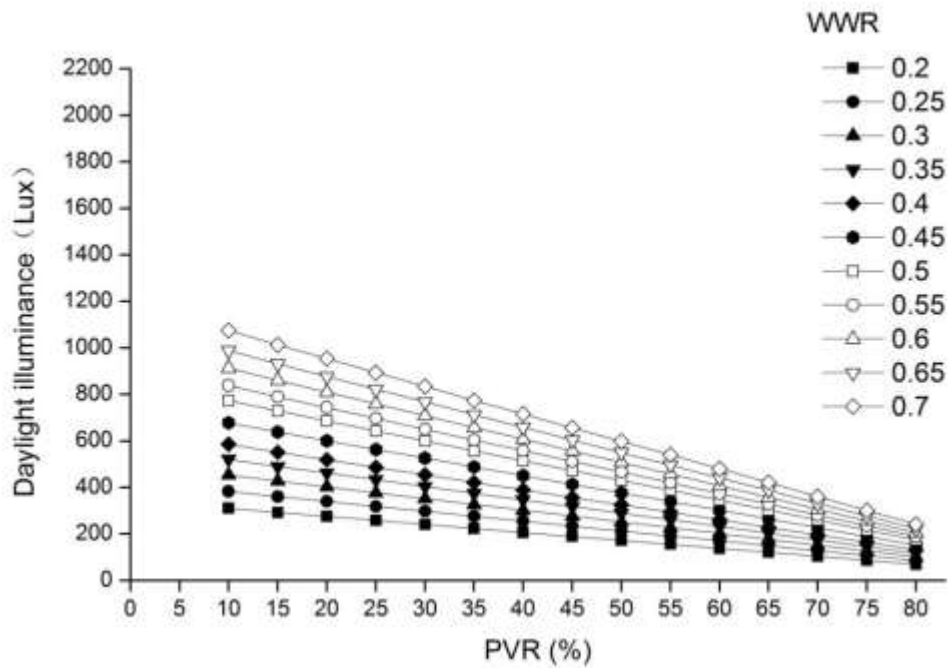
Figure 6.4 Indoor daylight illuminance of different PVR in different WWR cases
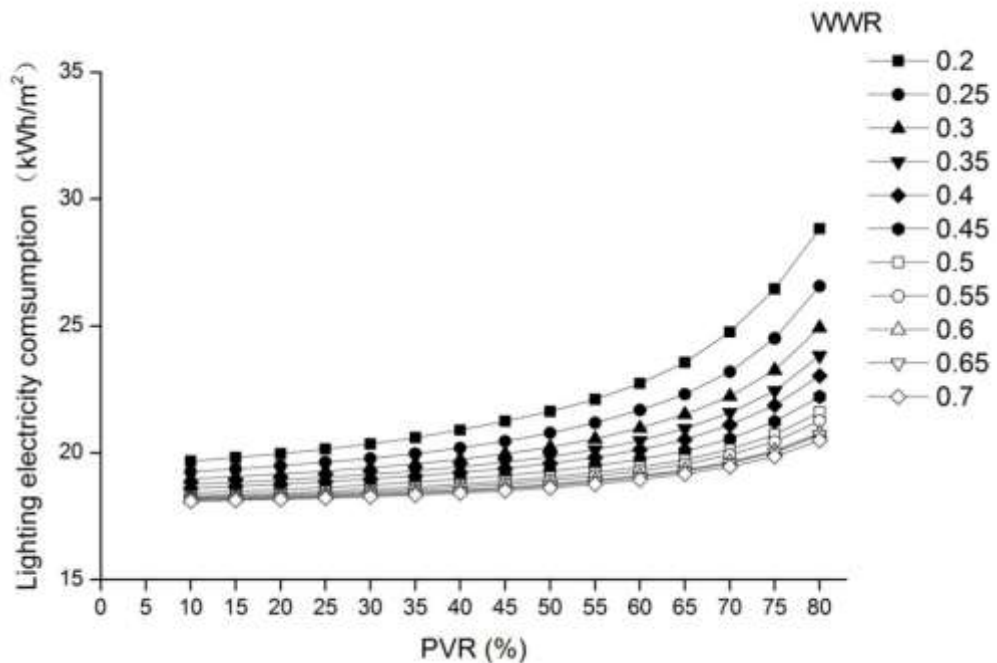
Figure 6.5 Lighting electricity consumption of different PVR in different WWR cases

To further understand the effect of mono-crystalline semi-transparent PV on the lighting energy performance, the artificial-lighting energy consumption is deducted with the PV generation yield as shown in Figures 6.6 and 6.7. By doing so, we can observe the overall benefit of semi-transparent PV as PV façades in terms of the lighting performance.
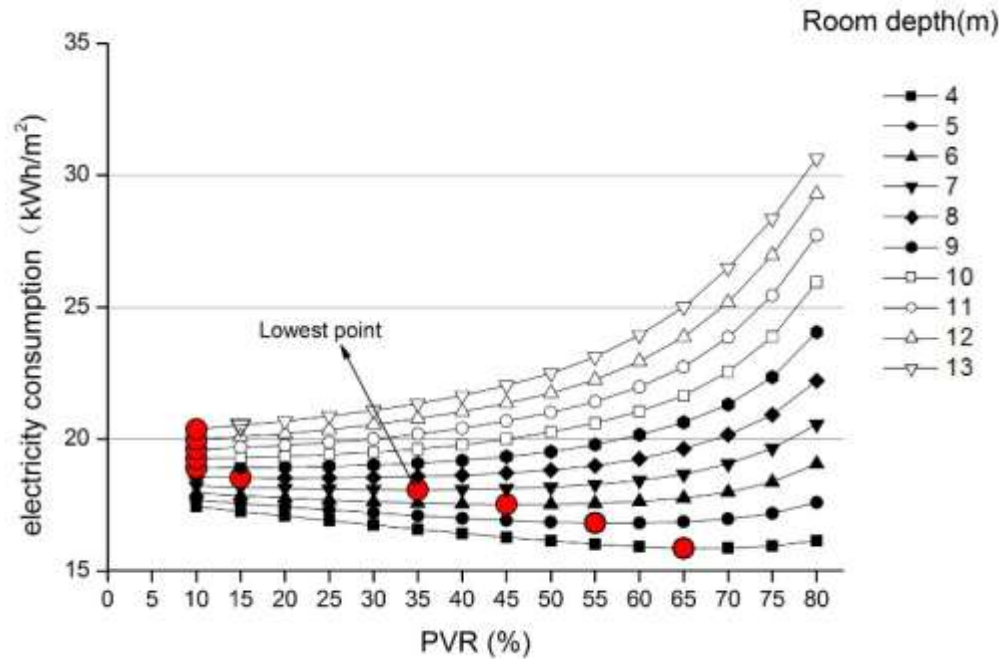
Figure 6.6 Deducted lighting electricity consumption with PV electricity yield deduction in different room depth cases

Figure 6.6 shows the lighting electricity consumption that was deducted with the PV electricity yield deduction in different room depth cases. The lowest point (red point) represents the lowest lighting electricity consumption after deducting the PV yield from the artificial-lighting energy consumption. In relatively deep-room cases (9-13 m), the lowest point remains at the lowest PVR of 10%, which indicates that the mono-crystalline semi-transparent PV façades do not positively affect the lighting energy performance in deep-room cases. However, in short rooms (4-8 m), as the room depth decreases, the lowest points tend to shift to higher PVR cases, which indicates that the PV façades positively affect the lighting energy performance, and this positive effect reaches its peak at high PVR when the

room depth decreases. For example, in a 5 m deep room, the lighting energy consumption with the deducted PV yield is minimum (16.81 kWh/m^2) when PVR is 55%, and the lowest value (15.8 kWh/m^2) is achieved at 65% PVR for a 4 m deep room.
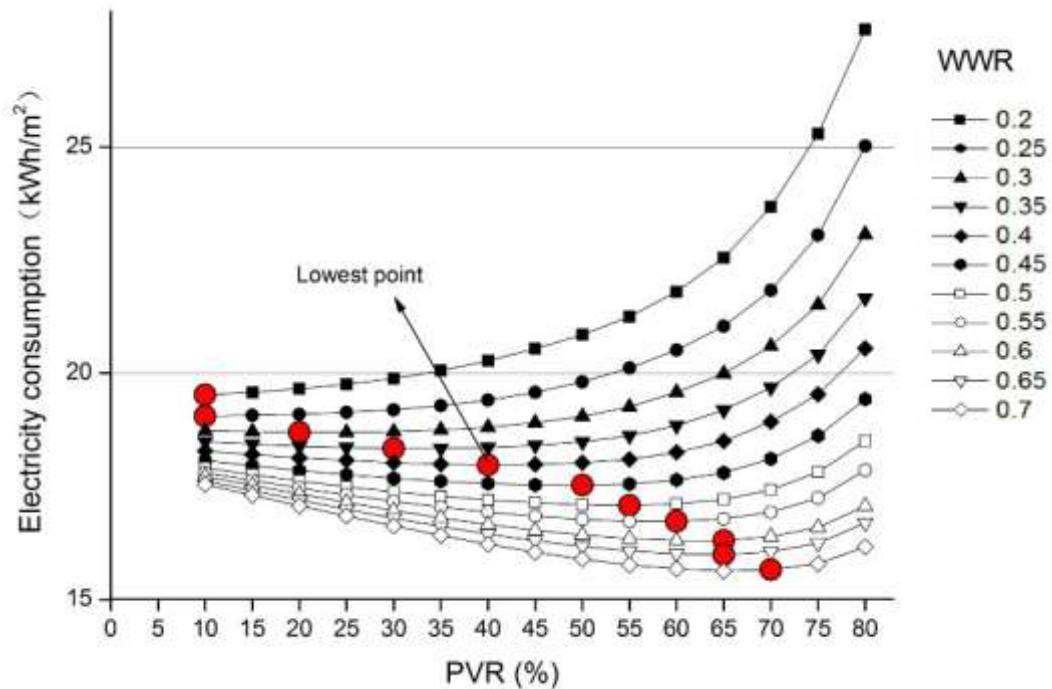
Figure 6.7 Deducted lighting electricity consumption with PV electricity yield deduction in different WWR cases

Figure 6.7 shows the deducted lighting electricity consumption with PV electricity yield deduction in different WWR cases. Again, the lowest point (red point) represents the lowest lighting electricity consumption after deducting the PV yield from the artificial-lighting energy consumption. In relatively small WWR cases (0.2-0.25), similar to the room depth cases in Figure 6.6, the lowest point remains at the lowest PVR, which indicates that the mono-crystalline semi-transparent PV façades do not positively affect the lighting energy performance when the window area are small (small WWR). However, in mid- and large-window room cases (WWR: 0.3-0.7), when the WWR increases, the lowest points tend to shift to higher PVR cases. Thus, PV façades positively affect the

lighting energy performance at higher PVR when the WWR increases. For example, in a room of 0.5 WWR, the lighting energy consumption with deducted PV yield is minimum (17.08 kWh/m^2) when the PVR is 55%, and the lowest value (16.3 kWh/m^2) is achieved for a room of 0.6 WWR when the PVR is 60%.

The analysis with deducted lighting electricity consumption with PV electricity yield implies that mono-crystalline semi-transparent PV façades are more suitable and provide better lighting energy performance in relatively short rooms or relatively large-window rooms. This discovery shows the importance of a proper PVR when mono-crystalline semi-transparent PV façades are used for better lighting energy performance.

6.2.3. Effects on the heating and cooling electricity consumption

Before we analyse the effects of heating and cooling electricity consumption, the factor of climate conditions should be discussed because the heating and cooling demand is strongly related to climate conditions.

In Wuhan, central China, which is in a typical hot-summer cold-winter climate zone, the amount of heat gain through window glass in summer is larger than that of heat loss in winter considering the use of air conditioning control system. Figure 6.8 shows the monthly heat gain and heat loss through clear window glass (WWR=0.35) of a typical room in Wuhan area. In summer, the heat gain reaches its peak of over 150 kWh in this simulated room in August, which is larger than the heat loss in winter with a peak value of less than 80 kWh. In the entire year, the total amount of heat gain is also lager than that of heat loss, which indicates that in Wuhan, saving energy from reducing the cooling loads is more effective than reducing the heating loads in terms of saving the total heating and cooling electricity consumption. Office buildings are more easily affected by solar radiation because they mainly function during daytime. Different amounts of solar radiation through mono-crystalline semi-transparent PV of different PVR can affect the heating and cooling loads. In winter, more solar radiation can reduce the heating demand, but it increases the cooling demand in summer.
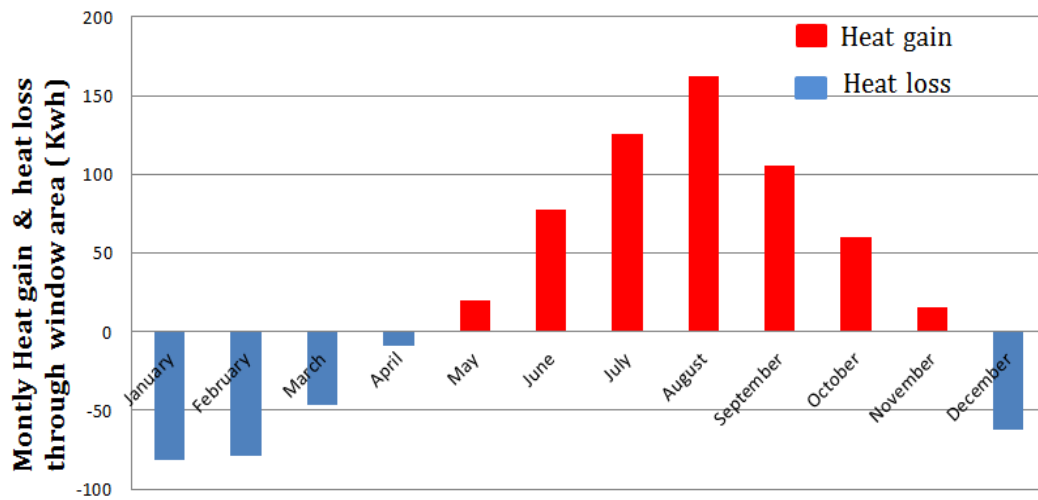
Figure 6.8 Monthly heat gain and heat loss through clear window glass (WWR=0.35) in the Wuhan

Heating and cooling loads of office buildings are more easily affected by solar irradiance because office buildings typically function primarily during daytime. Varying the amount of solar irradiance that enters a building by installing mono-crystalline semi-transparent PV panels with different PVR can affect the heating and cooling loads. Increasing the influx of solar irradiance can reduce the heating demand in winter; however, it also increases the cooling demand in summer.

A computation simulation is performed to investigate the effect of PVR on the annual heat gain and heat loss through mono-crystalline semi-transparent PV glazing in a generic room (WWR=0.2). As Figure 6.9 shows, the heat gain through PV façades significantly changes with a changing PVR; however, the heat loss remains constant for all PVR cases. With the increase in PVR (more solar radiation was blocked by mono-crystalline), the heat gain by solar radiation is largely reduced and significantly decreases the heat gain. The heat gain through PV glazing decreases from more than 1900 kWh to less than 400 kWh when PVR increases from 10% to 80%, which indicates that 78% of heat gain through glazing is reduced by increasing the PVR. However, the heat loss slightly increases with the increase in PVR. The amount of heat loss through a 10% PVR PV glazing is

513 kWh, and that number slowly increases to 550 kWh when the PVR increases to 80%.
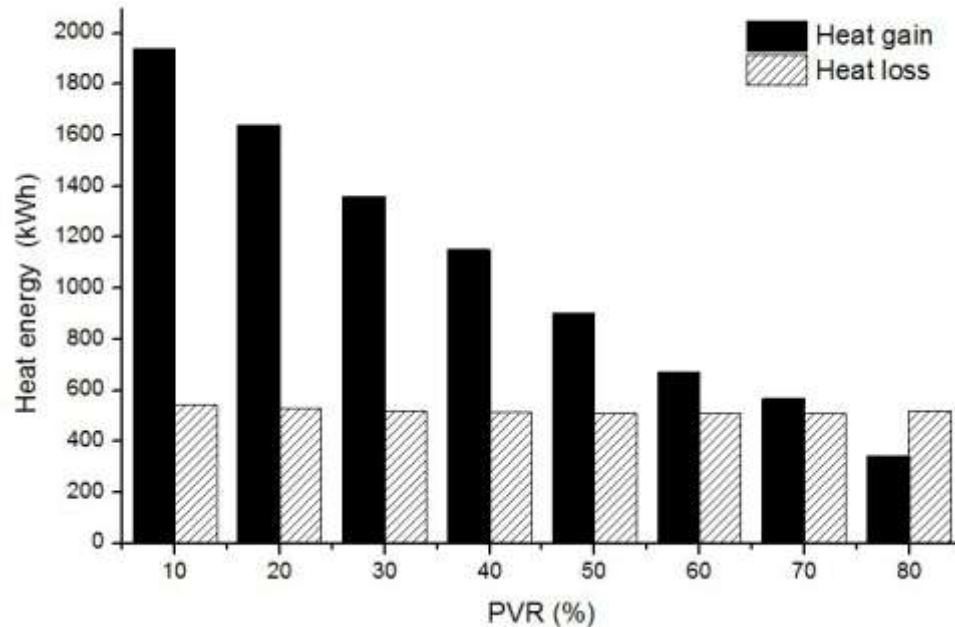
Figure 6.9 Heat gain and heat loss through mono-crystalline semi-transparent PV glazing in a 4m-depth room (WWR=0.2)

A combined value of heat gain (heat gain minus heat loss) and heat loss is shown in Figure 6.10 to investigate the heat balance through mono-crystalline semi-transparent PV glazing of different PVR. The total heat balance state is "gaining heat" when the PVR is 10-70%. This result indicates that the indoor environment obtains too much heat from solar radiation and the outside environment. Thus, the indoor cooling demand increases and costs more energy if we want to maintain a comfortable temperature indoor. In this case, how to reduce the cooling demand is the main issue in terms of saving energy consumption. When the PVR increases as Figure 6.9 shows, the heat gain and heat loss tend to balance when the PVR is approximately 70%. After the PVR surpasses 70%, the heat balance state turns into "losing heat". In general, this analysis indicates that a high PVR is beneficial to reduce the heating demand and the AC electricity consumption.
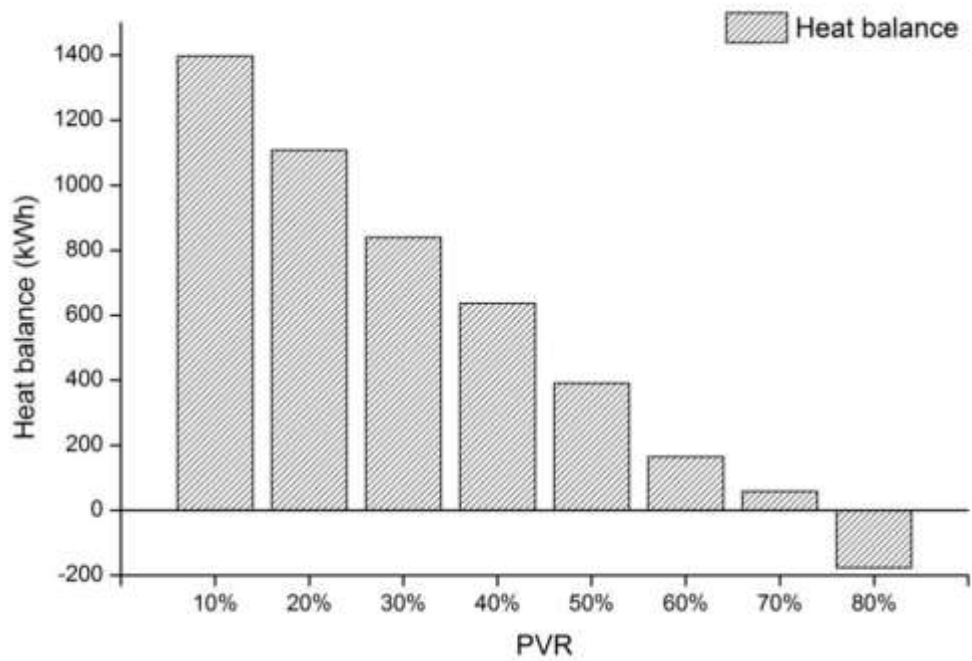
Figure 6.10 Combined value of heat gain and heat loss (heat gain minus heat loss)
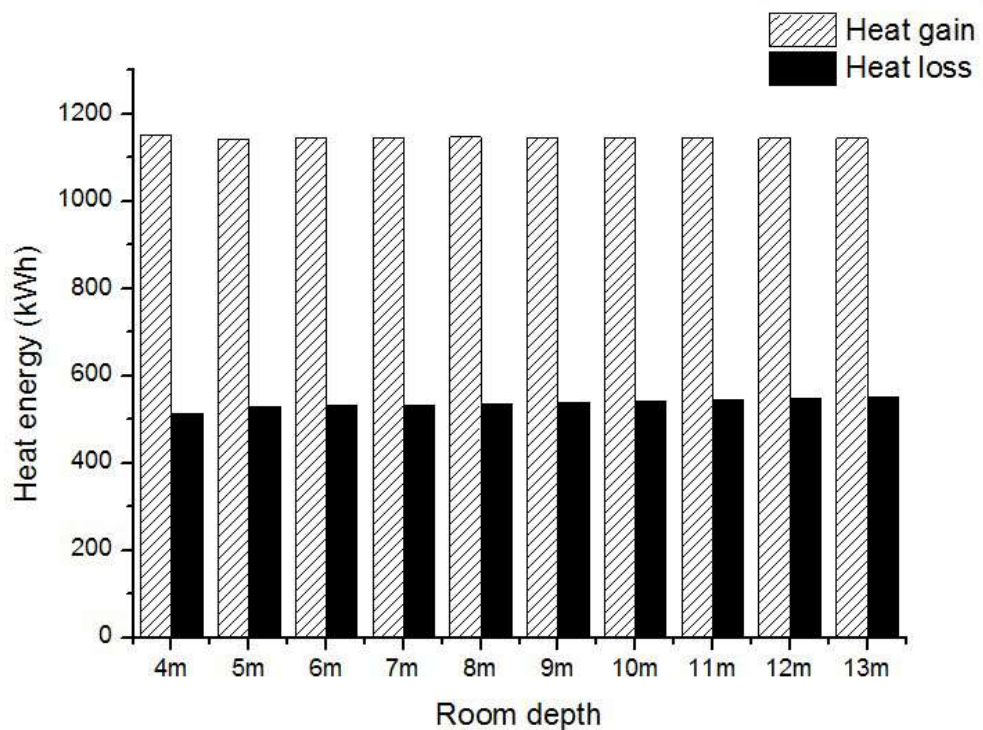
Figure 6.11 Heat gain and heat loss through mono-crystalline semi-transparent PV

glazing with a fixed PVR of 40% (WWR=0.2)

To investigate the effect of the room depth, the heat gain and heat loss through mono-crystalline semi-transparent PV glazing of different room depths are simulated. In this simulation, the PVR is set at a fixed value of 40% (WWR=0.2). The results are shown in Figure 6.11, and we observe that both heat gain and heat loss changes notably little with the increase in room depth.

The analysis of heat balance through PV glazing indicates that a high PVR can reduce the cooling demand because it reduces the heat gain. However, further analysis of the heating and cooling energy of generic rooms remains necessary as a final result of how the PV façades of different PVR affect the cooling and heating demand and the electricity consumption.
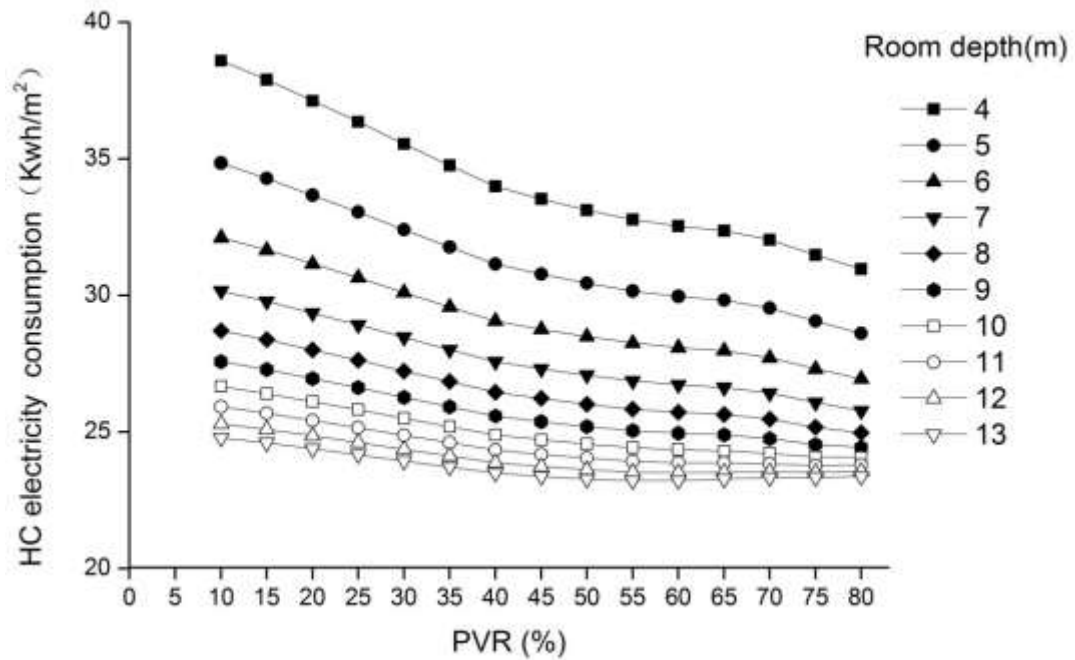
Figure 6.12 Heating and cooling electricity consumption of different PVR in different room depth cases at a fixed WWR of 0.35

Figure 6.12 illustrates the heating and cooling electricity consumption for different PVR for several room depth cases with a fixed WWR of 0.35. The heating and cooling electricity consumption first decreases with increasing PVR, although the rate of decrease decreases when the PVR exceeds 50%. The cases with higher PVR appear to perform better in terms of heating and cooling energy savings based

on the annual data. This result can be primarily attributed to the climatic conditions in central China, where the cooling load in summer is typically greater than the heating load in winter. However, the benefits of high PVR become less pronounced when the room depth increases: the shortest room has the highest heating and cooling electricity consumption, although the variations in consumption with changes in room depth become less pronounced when the room depth exceeds 9 m. These results highlight the importance of considering the PVR, particularly in cases with small room depths.
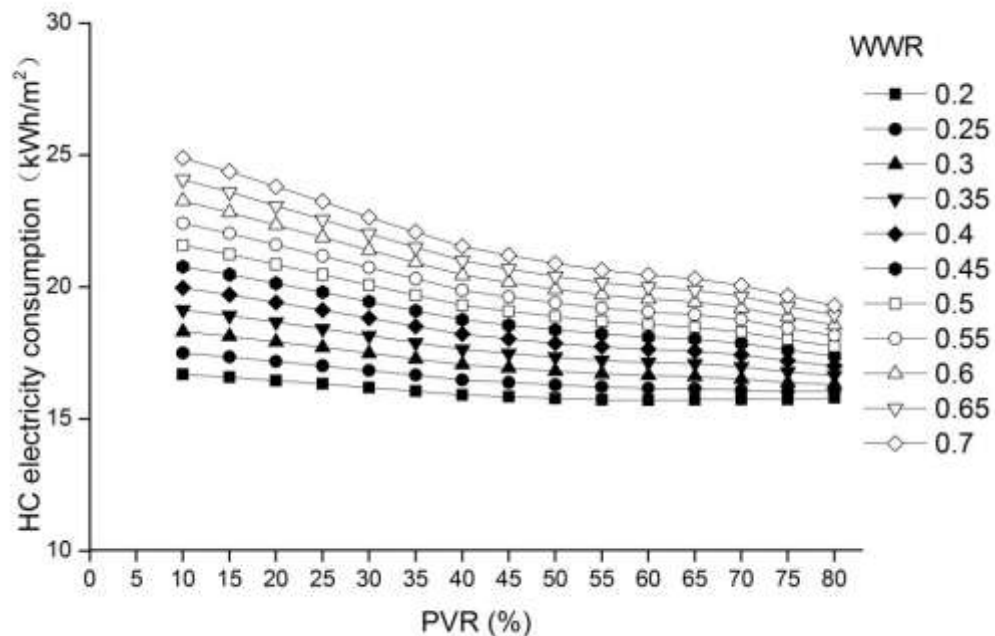
Figure 6.13 Heating and cooling electricity consumption of different PVR in different WWR cases

Figure 6.13 illustrates the heating and cooling electricity consumption for different PVR in cases with different WWR. For the cases with variable room depths, the heating and cooling electricity consumption first decreases with increasing PVR, and the rate of decrease decreases when the PVR exceeds 60%. Cases with small WWR typically perform better in terms of heating and cooling

energy saving, and the effects of varying PVR are typically less pronounced for small WWR. However, the effects of the WWR increase even among cases, which indicates that the heating and cooling electricity consumption continues to increase with increasing WWR with no signs of decreasing or stabilising.

To further understand the effect of mono-crystalline semi-transparent PV on the lighting energy performance, the heating and cooling electricity consumption is deducted using the PV generation yield and shown in Figures 6.14 and 6.15. By doing so, we can observe the overall benefit of semi-transparent PV as PV façades in terms of the heating and cooling energy performance.

The main difference from the cases without considering the PV generation benefit (Figure 6.11) is that the heating and cooling electricity consumption of the generic rooms decrease (saving more energy) at a bigger value when the PVR increases, as Figures 6.14 and 6.15 show.
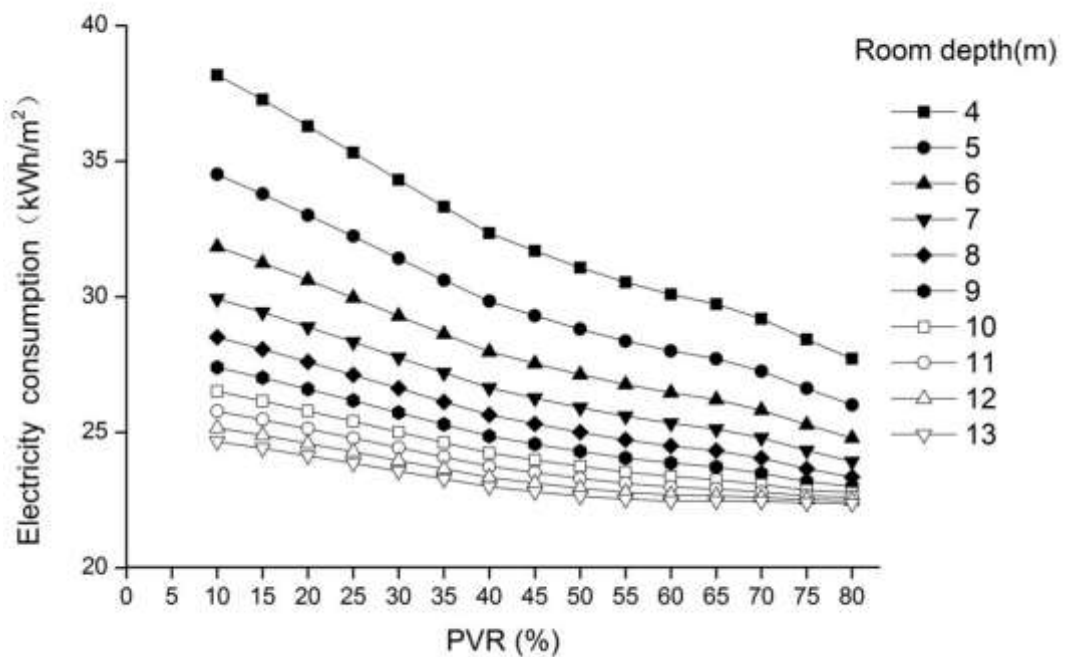
Figure 6.14 Deducted heating and cooling electricity consumption with the PV electricity yield deduction in different room depth cases

For example, in Figure 6.14 (different room depth cases), with the PV electricity yield, in a 4 m deep room, the heating and cooling electricity consumption decreases from 38.2 kWh/m^2 (at 10% PVR) to 27.7 kWh/m^2(at 80% PVR) with 11.5 kWh/m^2 electricity saved. Without the PV electricity yield, the heating and cooling electricity consumption decreases from 38.6 kWh/m^2 to 30.9 kWh/m^2 with 7.3 kWh/m^2 electricity saved (Figure 6.12). This result indicates that a high PVR reduce heating and cooling electricity consumption. However, this positive effect becomes less significant in deep rooms. The electricity saving is 11.5 kWh/m^2 for a 4 m deep room, and that number is 2.3 kWh/m^2 for a 13 m deep room. Again, these results highlight the importance of considering the PVR, particularly in cases with small room depths.
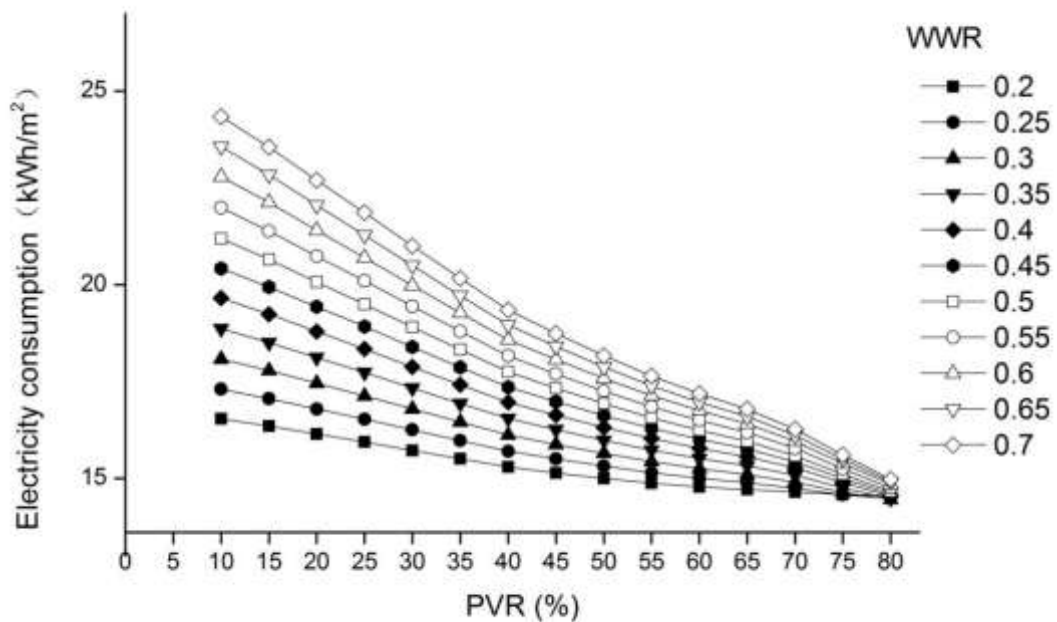
Figure 6.15 Deducted heating and cooling consumption with a PV electricity yield deduction in different WWR cases

In Figure 6.15 (different WWR cases), with the PV electricity yield, the heating and cooling electricity consumption rapidly decreases compared to that shown in Figure 6.13. For example, in a 0.7 WWR room, the heating and cooling

electricity consumption decreases from 24.3 kWh/m^2 (at 10% PVR) to 14.9 kWh/m^2 (at 80% PVR) with 9.4 kWh/m^2 electricity saved. Without the PV electricity yield, that consumption decreases from 24.9 kWh/m^2 to 19.3 kWh/m^2 with only 5.6 kWh/m^2 electricity saved (Figure 6.12). With higher PVR, the benefit from PV façades on saving the cooling and heating electricity consumption is more profound in all WWR cases. However, this positive effect becomes less significant in small WWR rooms (small window), where the electricity saving is 9.4 kWh/m^2 for a 0.7 WWR room and only 1.9 kWh/m^2 for a 0.2 WWR room.

6.2.4. Effects on the overall energy consumption

Based on the previously presented analysis, it can be concluded that increasing PVR under the climatic conditions in central China typically decreases the PV electricity conversion efficiency and the heating and cooling electricity consumption but increases the lighting electricity consumption. However, the effects of the room depth and the WWR on these relationships are pronounced, which demonstrates that these factors must be carefully considered when designing mono-crystalline semi-transparent PV technology for buildings. Therefore, it is necessary to evaluate the overall energy consumption considering all of these factors to determine an optimal PVR. With the electricity benefit of PV power generation, the overall electricity consumption is provided as follows.

Overall energy consumption = Lighting energy consumption + cooling and heating energy consumption – PV electricity generation.

Figures 6.16 (a) and (b) illustrate the overall energy consumption for cases with large WWR (0.6) for two different room depths (6 m and 12 m, respectively). These two figures can present the results in a large-window architectural situation. In such cases, the solar radiation and daylight are strong, which leads to an interesting "competition" between the decrease of lighting electricity consumption and the increase of heating and cooling electricity consumption. The key lies in whether the increase or decrease has a bigger effect on the overall energy consumption. In addition, because a larger window area indicates the larger area to install PV, the PV electricity generation is also more significant in such cases.

For a short room (6 m deep, Figure 16 (a)), the decrease in artificial-lighting energy is more significant than the increase in the heating and cooling electricity consumption. A PVR of 80% achieves the lowest overall electricity consumption, which saves 18.9% energy compared to the case with a PVR of 10%. This result can be primarily attributed to the influence of heating and cooling electricity consumption: high PVR can reduce the enormous cooling demands for short rooms. Conversely, for a room depth of 12 m, the greatest electricity savings are achieved for a PVR of 50%. This result can be primarily attributed to the decreases in lighting electricity consumption during daytime because of the smaller PVR; these savings overwhelm the effects of the heating and cooling electricity consumption.

Figures 6.17 (a) and (b) illustrate the overall energy consumption for cases with small WWR (0.3) for two different room depths (6 m and 12 m, respectively). These two figures can present the results in a small-window architectural situation, which has a relatively smaller total solar radiation and daylight than the large window cases in Figure 16. In addition, electricity generation is typically notably small compared to the lighting and heating electricity consumption because of the limited available area to install semi-transparent PV panels because the window area is small. In this case, with small PV electricity generation, it becomes less significant for semi-transparent PV applications. However, the influence of the PVR remains pronounced, particularly its effects on daylight and the heating and cooling demand. For the 6 m room, a PVR of 60% achieves the lowest electricity consumption, with electricity savings of 6.8% compared to a PVR of 10%. Conversely, in the 12 m room, a PVR of 20% achieves the lowest electricity consumption, with electricity savings of 17.3% compared to a PVR of 80%.
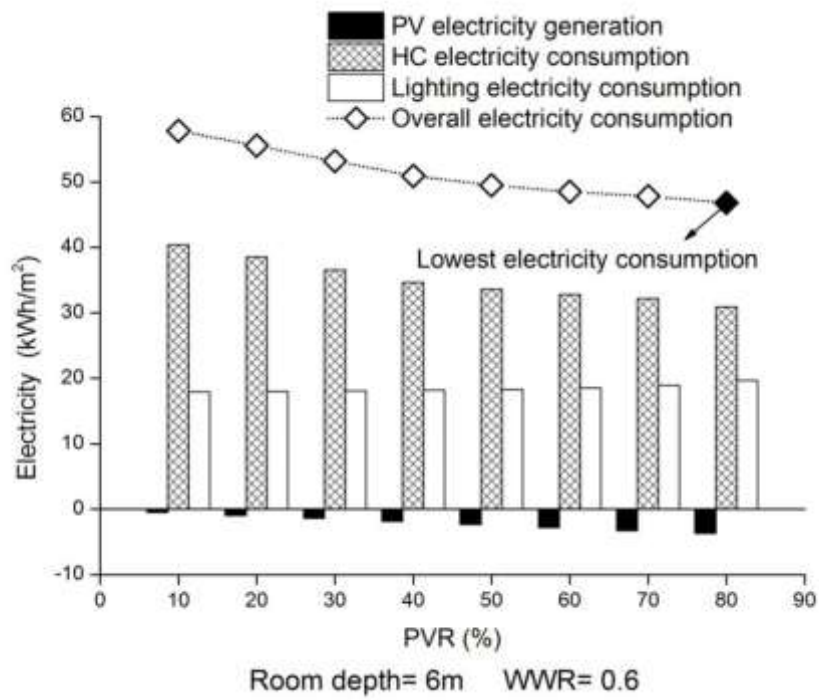
(a)
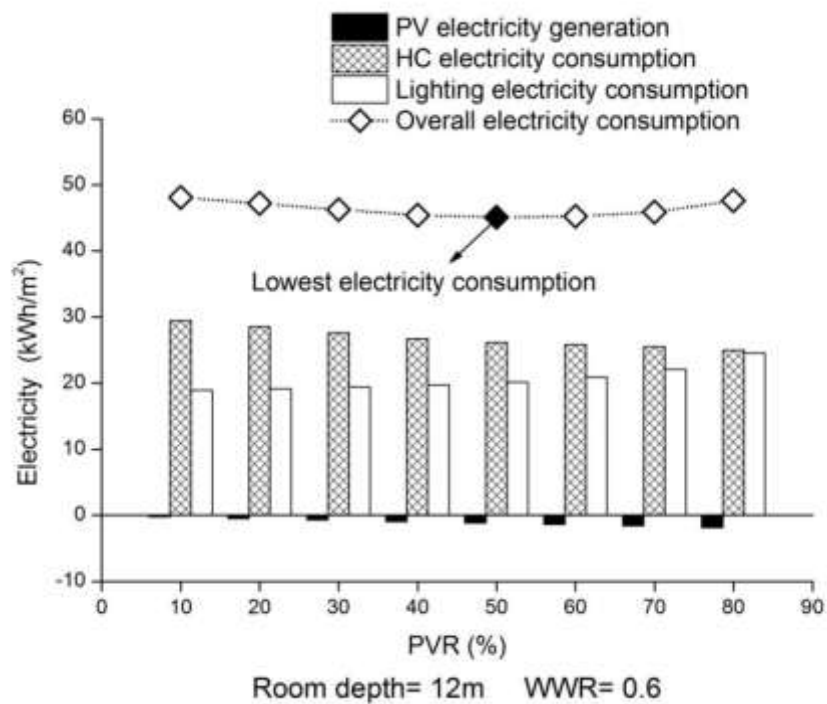
(b)

Figure 6.16 Overall energy consumption of large WWR rooms in two cases of

room depth (a) 6 m and (b) 12 m
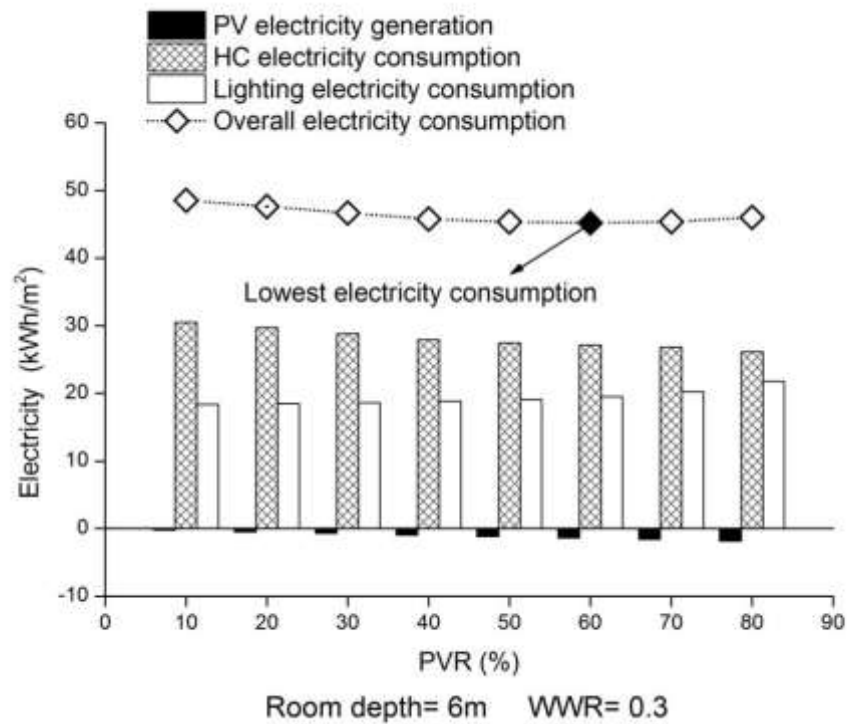
(a).
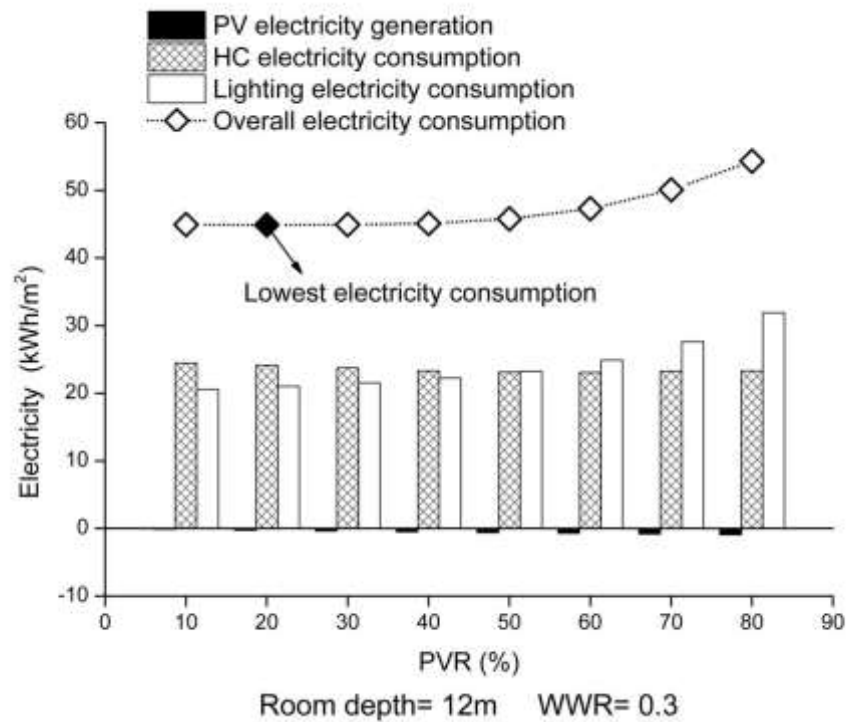
(b)

Figure 6.17 Overall energy consumption of small WWR rooms in two cases of
room depth (a) 6 m and (b) 12 m

6.3. Optimal PVR according to the overall energy performance

Based on the previous parametric analysis, it is clear that an optimal PVR (i.e., that which achieves the lowest overall electricity consumption) can be obtained based on a particular combination of WWR, room depth, and orientation. Thus, the optimal PVR should be selected by comparing the overall energy consumption results for all PVR cases under different architectural conditions (i.e., WWR, room depth, and orientation). The southern orientation is typically affected more extensively by solar energy than the other orientations; accordingly, it is often the preferred orientation to install photovoltaic applications. Variations in WWR and room depth can lead to considerable variations in the optimal PVR (Table 6.1).

Table 6.1 Optimal PVR in different combinations of room depth and WWR in the southern orientation

	Optimal PVR (%)									
WWR	**Room depth（m）**									
	4	5	6	7	8	9	10	11	12	13
0.2	75	55	50	40	35	20	10	10	10	10
0.25	80	60	55	50	40	40	30	10	10	10
0.3	80	75	60	55	50	40	40	30	20	10
0.35	80	80	75	55	55	45	40	40	35	30
0.4	80	80	75	60	55	50	45	40	40	40
0.45	80	80	80	75	60	55	50	45	40	40
0.5	80	80	80	75	70	60	55	50	45	40
0.55	80	80	80	80	75	60	55	55	50	45
0.6	80	80	80	80	75	75	60	55	55	50
0.65	80	80	80	80	75	75	60	60	55	50
0.7	80	80	80	80	80	75	75	60	55	55

From Table 6.1, two main trends of the optimal PVR can be concluded as follows.

(1) Optimal PVR tends to be lower in deep rooms and higher in short rooms.

(2) Optimal PVR tends to be lower in small WWR (small-window) rooms than large WWR (big-window) rooms.

Table 6.2 Electricity saving using optimal PVR compared to most disadvantaged PVR

Electricity Saving (%)											
WWR	**Room depth（m）**										Average
	4	5	6	7	8	9	10	11	12	13	
0.2	7	5	6	10	14	17	20	21	22	23	15
0.25	10	7	5	7	10	14	16	18	20	21	13
0.3	13	10	7	5	7	11	13	16	17	19	12
0.35	16	12	9	7	5	8	11	13	15	17	11
0.4	18	14	11	8	7	6	8	11	13	15	11
0.45	23	18	14	11	9	7	6	9	12	14	12
0.5	23	19	15	12	10	8	7	6	8	10	12
0.55	25	21	17	14	11	9	8	6	7	9	13
0.6	26	23	19	16	13	10	9	7	6	7	14
0.65	28	24	21	17	14	12	10	8	7	6	15
0.7	30	26	22	19	16	13	11	10	8	7	16
Average	20	16	13	12	11	10	11	11	12	13	13

The differences in the overall electricity consumption between the most and least favourable PVR were calculated and are shown in Table 6.2. In particular, electricity savings for different combinations of room depth and WWR were calculated as percentages. The electricity savings ranged from 5% to 30%, with an

average saving of 13% for the optimal PVR. Moreover, the optimal PVR was particularly important in short rooms with large WWR, where electricity savings of over 20% were achieved. From Table 6.2, two conclusions can be made.

(1) The differences in the overall electricity consumption of different PVR are more significant in deep rooms with small WWR.

(2) The differences in the overall electricity consumption of different PVR are more significant in short rooms with large WWR.

The variations in optimal PVR were also investigated. The optimal PVR decreased with increasing room depth (i.e., from 4 m to 13 m). This result can be primarily attributed to the fact that the electricity demand during daytime increases faster than the compensation of savings in heating and cooling. This result also explains why rooms with greater depths typically have smaller optimal PVR. Furthermore, the optimal PVR increases when the WWR increases from 0.2 to 0.7 primarily because the achieved electricity savings by adopting a larger WWR (combined with the greater PV electricity generation and lower cooling load) result in higher optimal PVR.

Table 6.3 Optimal PVR of different combinations of orientation and room depth

| Orientation | Optimal PVR (%) | | | | | | | | | |
| | Room depth（m） | | | | | | | | | |
	4	5	6	7	8	9	10	11	12	13
E	75	60	50	45	35	25	20	20	20	15
SE	75	60	50	45	40	35	30	30	25	20
S	80	80	75	55	55	45	40	40	35	30
SW	80	80	75	65	55	50	50	45	40	35
W	80	80	80	75	65	55	55	50	45	40

To demonstrate the effects of different orientations on the optimal PVR, different combinations of orientation and room depth (WWR) were investigated with a fixed WWR of 0.35 (8 m). The orientation was varied among east, southeast, south, southwest, and west (Table 6.3 and Table 6.4). The northern orientation was not included in this investigation because it is particularly unfavourable for PV applications. The results demonstrate that the optimal PVR is highest in the west orientation. Under the prevalent climatic conditions in central China, the cooling demands in the summer typically exceed the heating demands in the winter. Thus, in the summer, a high PVR can reduce the cooling load that is associated with the accumulated heat indoors during the daytime.

Table 6.4 Optimal PVR of different combinations of orientation and WWR（fixed room depth of 8m）

Orientation	Optimal PVR (%)										
	WWR										
	0.2	0.25	0.3	0.35	0.4	0.45	0.5	0.6	0.6	0.65	0.7
E	25	40	40	45	50	60	60	60	70	70	70
SE	25	40	40	45	50	60	60	65	70	70	75
S	35	40	50	55	55	60	70	75	75	75	80
SW	35	50	50	60	65	65	70	75	75	75	80
W	35	50	50	60	65	65	70	75	75	75	80

6.4. Energy saving of mono-crystalline semi-transparent PV glazing compared to three traditional glazings

In this section, the energy performance of the mono-crystalline semi-transparent PV façade layouts of each optimal PVR is compared with three traditional glazings: (1) single glazing, (2) Low-E double glazing and (3) normal double glazing. This comparison is a further evaluation of how the mono-crystalline semi-transparent PV competes with the traditional and commonly used glazings that are currently in China in terms of energy saving.

Figure 6.18 shows the sections of three traditional glazings: 3-mm single glazing (Figure 6.18(b)), 6 mm Low-E double glazing with a 12-mm air gap (Figure 6.18(c)) and 6-mm double glazing with a 12-mm air gap (Figure 6.18(d)). Figure 6.18 (a) shows the mono-crystalline semi-transparent PV, of which the layer consistency and calculation models were discussed and presented in Chapter 5. Single glazing, which is common in buildings built before 1990, is still produced and used in buildings today, but its usage has rapidly declined in recent years because of inferior energy performance. With the increase in the energy price and economic booming in China, more energy-efficient glazings are more commonly used in new developments. Double glazing is the most commonly used glazing in China today and has a much better performance than single glazing; additionally, the cost is affordable for most building developments. Low-E double glazing is currently the best glazing in the market in China. In terms of energy performance, the Low-E layer in the glazing can reduce the heat gain from the outside environment by reducing the long-wave radiation penetration. However, Low-E double glazing is much more expensive than normal double glazing and single glazing.

To perform such comparisons, calculation models for the three traditional glazings are required and are provided by Energy Plus. The properties (Table 6.5) of these glazings are also required, which are provided by the Chinese Calculation Specification for Thermal Performance of Windows, Doors and Glass Curtain-Walls (JGJ/T 151-2008). The properties are incorporated into Energy Plus to perform the computation simulations.

Table 6.5 Properties of three traditional glazings

Glazings	U-value (W/m^{2}K)	SHGC	Visible transmitance
Single glazing	5.8	0.870	0.87
Low-E double glazing	1.9	0.446	0.72
Double glazing	2.8	0.767	0.71
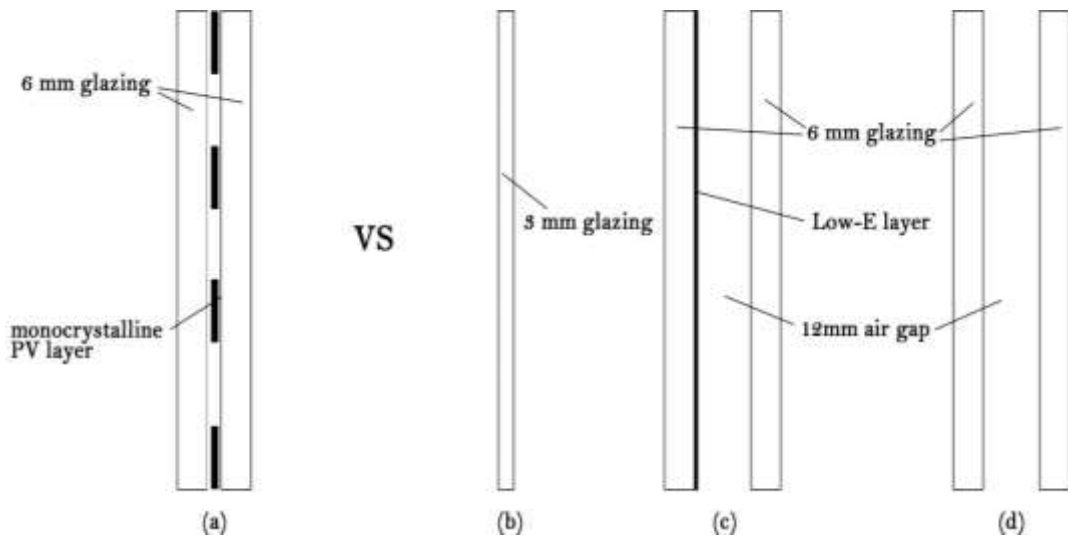
Figure 6.18 Mono-crystalline PV glazing and three traditional glazings

(a) Mono-crystalline PV glazing, (b) 3 mm single glazing, (c) 6 mm Low-E double glazing with a 12 mm air gap and (d) 6 mm double glazing with a 12 mm air gap

Two types of architectural models are used in this section and are illustrated in Figure 6.19. The first type is generic rooms with relatively small windows at a WWR of 0.3. The other type is generic rooms with larger windows at a WWR of 0.6. The 0.3 WWR model represents most traditional office buildings in China that were built before 2000. The large WWR model represents the emerging A-class office buildings with full glazing façades. The architectural-model details are discussed and provided in Section 5.3.
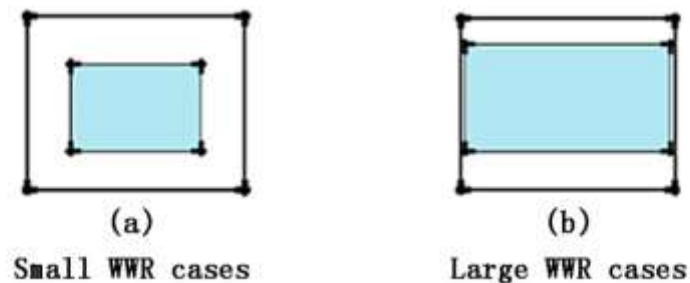
Figure 6.19 Illustration of small WWR cases and large WWR cases

The mono-crystalline semi-transparent PV and other three traditional glazings are first compared in the small WWR case and subsequently in the large WWR case to investigate the performance of lighting, heating and cooling energy. The PV electricity generation of the PV glazing is automatically included in all comparisons. The results are presented in annual values with different room depths.

6.4.1 Energy savings in small WWR cases
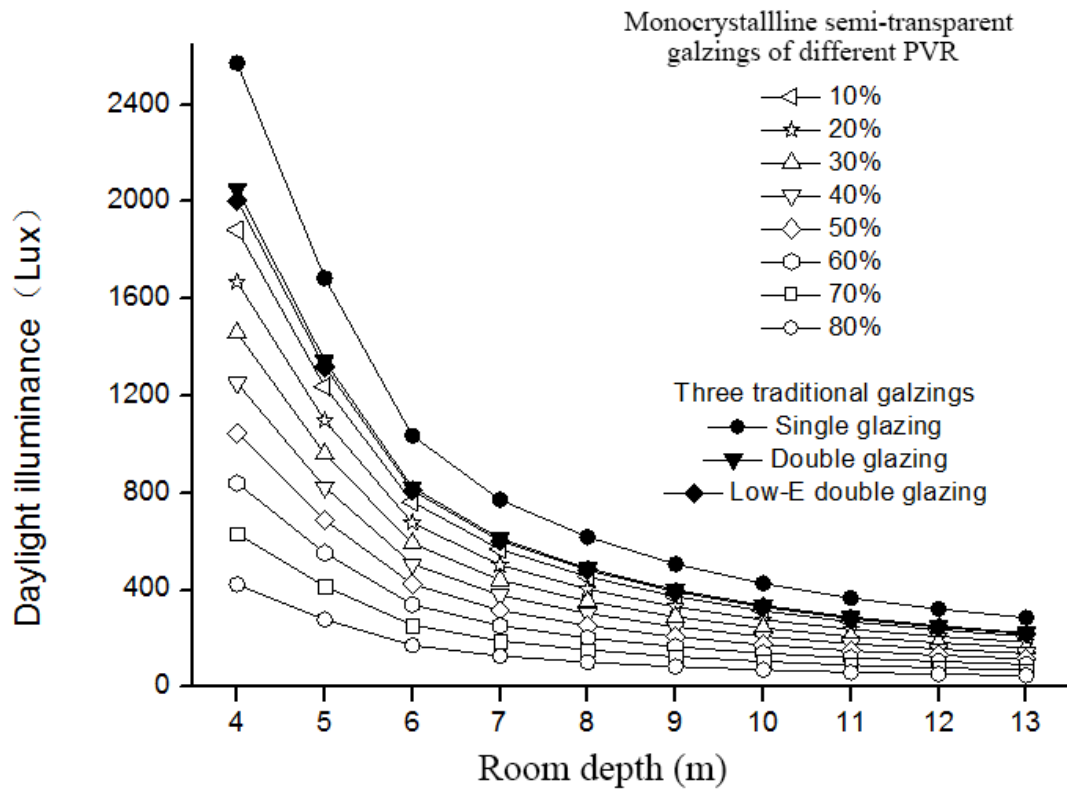
Figure 6.20 Daylight illuminance of different glazings at WWR of 0.3

Figure 6.20 shows the daylight illuminance of different glazings for the 0.3 WWR cases. The single glazing has the highest illuminance among all glazings, and all mono-crystalline semi-transparent PV glazings are inferior to the three traditional glazings. The 80% PVR mono-crystalline semi-transparent PV has the worst daylight level. However, generally, the illuminance level of the mono-crystalline semi-transparent PV glazing under 30% PVR is only 25% less than that of the Low-E double glazing and is also notably close to that of double glazing. It should be noticed that as long as the illuminance is above 300 Lux, the indoor lighting environment is comfortable, and an artificial lighting system is not

necessary. In such case, although the PV glazing has a much lower illuminance than the traditional glazings, the difference of artificial-lighting energy consumption between the two types of glazing is less significant than the daylight illuminance level. In other words, the effect of such difference on the artificial-lighting electricity consumption is not as obvious as the daylight illuminance performance.
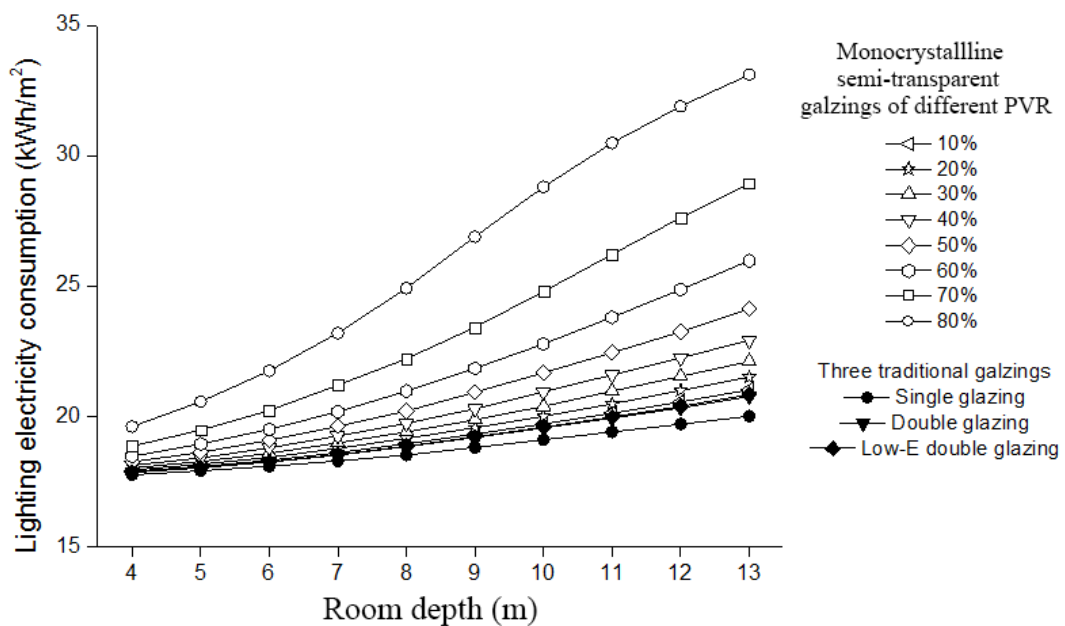
Figure 6.21 Lighting electricity consumption of different glazings at WWR of 0.3

Figure 6.21 shows the lighting electricity consumption of different glazings at 0.3 WWR. Because the traditional glazings have better daylight illuminance levels, they relatively achieve lower artificial-lighting electricity consumption. However, the difference varies in different room depth cases. In short rooms, the difference of artificial-lighting electricity consumption is relatively small between the mono-crystalline semi-transparent PV and the traditional glazings. This difference increases in deep rooms. For example, an 80% PVR PV glazing is 2.2 kWh/m^2 higher than the Low-E double glazing in a 4-m-deep room; however, in a 13-m-deep room, that number is above 13 kWh/m^2. This result indicates that the

effect of PV façades on the lighting electricity consumption is more profound in deep rooms.

However, when the PVR is below 50%, the difference between the mono-crystalline semi-transparent PV and traditional glazings is smaller than that when the PVR is above 50%. For example, compared to Low-E double glazing, a 40% PVR PV glazing leads to only approximately 20% more electricity consumption; this number is over 50% for a 80% PVR PV glazing.
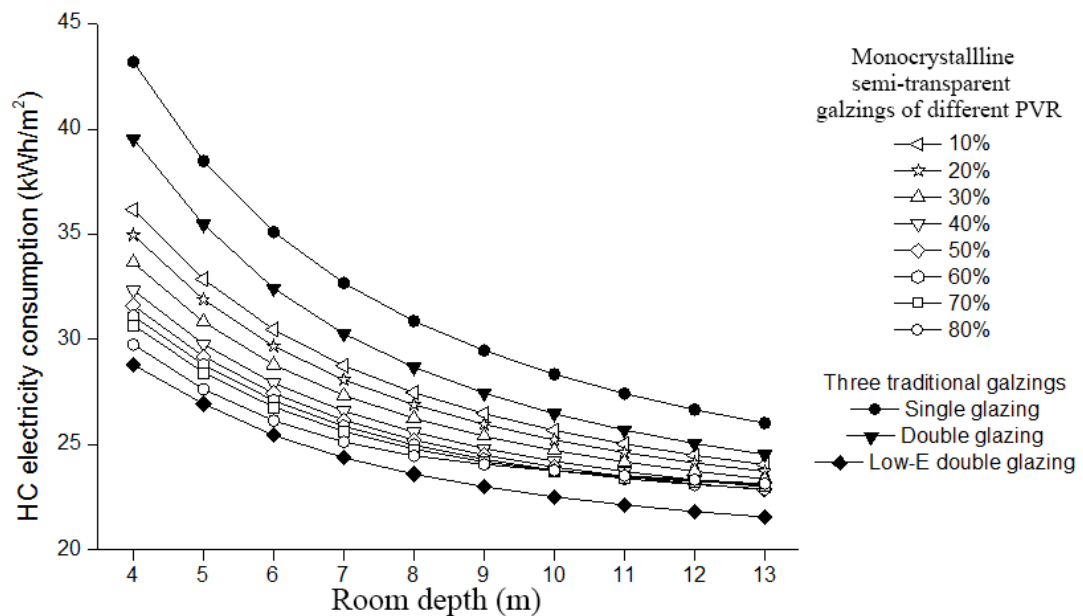
Figure 6.22 Heating and cooling electricity consumption of different glazings at WWR of 0.3

Figure 6.22 shows the heating and cooling electricity consumption of different glazings at 0.3 WWR. The Low-E double glazing has the lowest electricity consumption, and the mono-crystalline of different PVR has the second lowest electricity consumption. The single glazing has the highest electricity consumption among all types. The mono-crystalline semi-transparent glazing of 80% PVR can save more than 30% heating and cooling electricity compared to single glazing and 25% compared to double glazing. Compared to the best performing glazing (Low-E double glazing), PV glazings with at least 50% PVR maintains a small difference (less than 10%). This result shows the great potential of mono-crystalline semi-transparent PV in saving heating and cooling energy

because it performs better than the most commonly used glazing (double glazing) mainly because of the solar radiation blocking by PV cells in the summer, which saves the cooling demands indoor. This outcome again confirms the conclusion from Section 6.2.3, which is that saving the cooling energy consumption is more efficient and profound than saving the heating energy consumption in Hot-Summer Cold-Winter zones such as the Wuhan area.
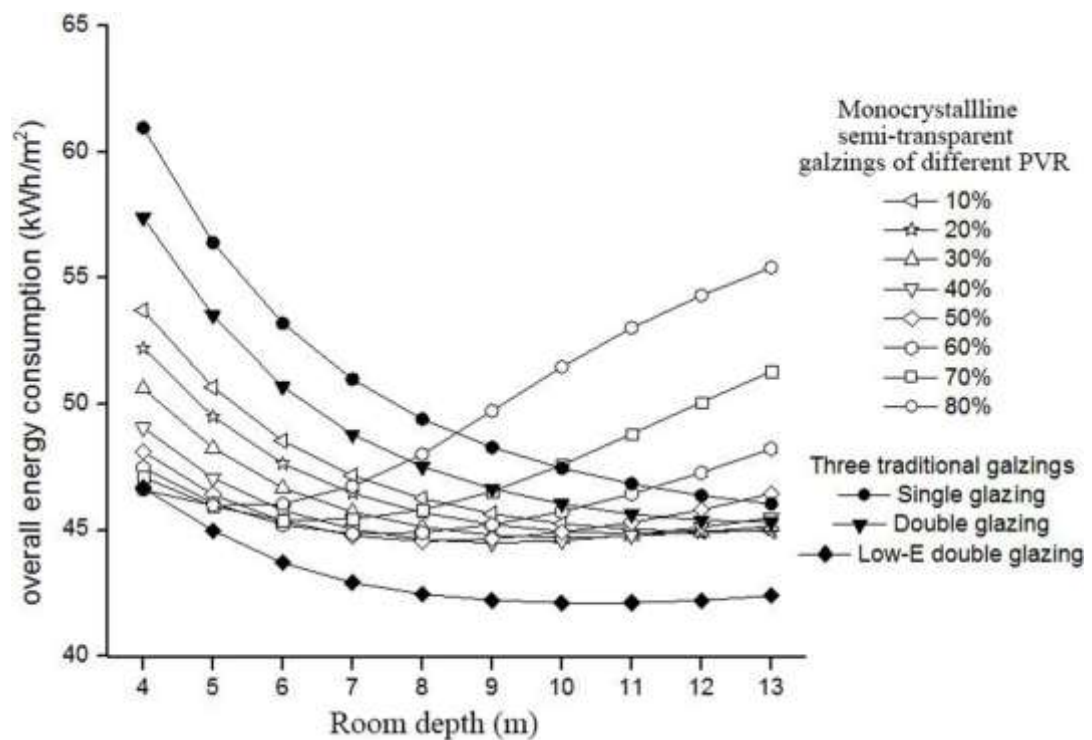
Figure 6.23 Overall energy consumption of different glazings at WWR of 0.3

Figure 6.23 shows the overall energy consumption of different glazings at 0.3 WWR. In small room depths cases below 8 m, the Low-E double glazing has the best energy performance, and the mono-crystalline semi-transparent PV of different PVR has the second best performance, whereas single glazing and double glazing have the worst energy performance. However, in large room depth cases above 8 m, the overall energy consumption of the mono-crystalline semi-transparent PV glazing of 50%-80% PVR is higher than single glazing and double glazing mainly because the increase in lighting electricity consumption is caused by high PVR.

By comparing the overall energy performance of different glazings in the above small WWR (small-window) cases, we conclude that:

(1) Low PVR (below 50%) mono-crystalline semi-transparent PV glazing has a better overall energy performance than single glazing and double glazing in all room depth cases.

(2) High PVR (above 50%) mono-crystalline semi-transparent PV glazing has a better overall energy performance than single glazing and double glazing in short rooms; however, in deep-room cases, it is worse than all traditional glazings.

(3) The overall energy performance of mono-crystalline semi-transparent PV glazings is worse than that of Low-E double glazing in all cases, particularly in deep rooms.

6.4.2   Energy savings in large WWR cases
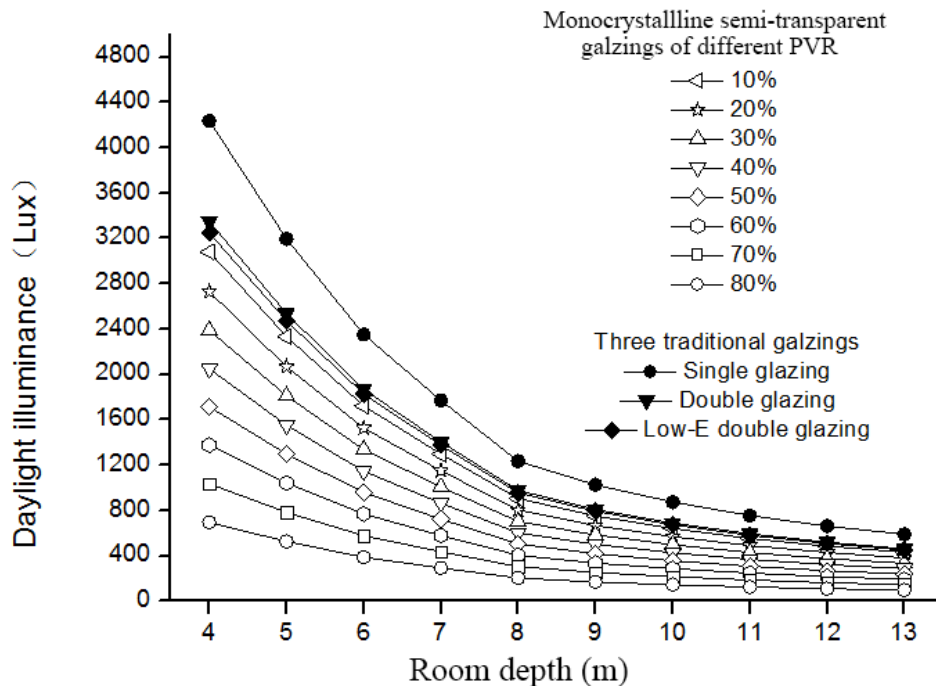
Figure 6.24 Daylight illuminance of different glazings at WWR of 0.6

Figure 6.24 shows the daylight illuminance of different glazings at 0.6 WWR. Similar to the small room depth cases, single glazing has the highest illuminance among all glazing types, followed by double glazing and Low-E double glazing. Mono-crystalline semi-transparent PV has the worst daylight illuminance level among the three traditional glazings. Figure 6.24 shows the lighting electricity consumption of different glazings at 0.6 WWR. Because the traditional glazings have better daylight illuminance, they also have lower lighting electricity consumption than the mono-crystalline semi-transparent PV glazing. The difference between PV glazings and traditional glazings increases from less than 5% to 30% when the room depth increases from 4 m to 13 m. In addition, when the PVR is over 60%, the lighting electricity consumption significantly increases compared to that of the low PVR glazing.
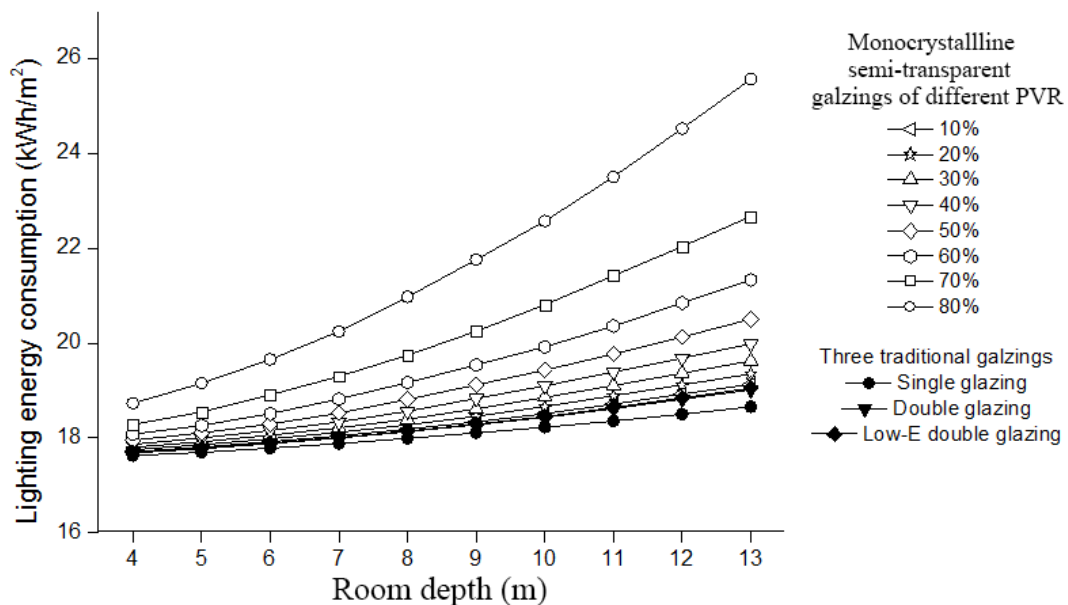
Figure 6.25 Lighting electricity consumption of different glazings at WWR of 0.6

Figure 6.26 shows the heating and cooling electricity consumption of different glazings at 0.6 WWR. Compared to the small WWR cases in Section 6.4.1, the difference in heating and cooling electricity consumption becomes more significant among mono-crystalline semi-transparent PV and single glazing and double

glazing. The 80% PVR PV glazing has identically good energy performance with the Low-E double glazing.
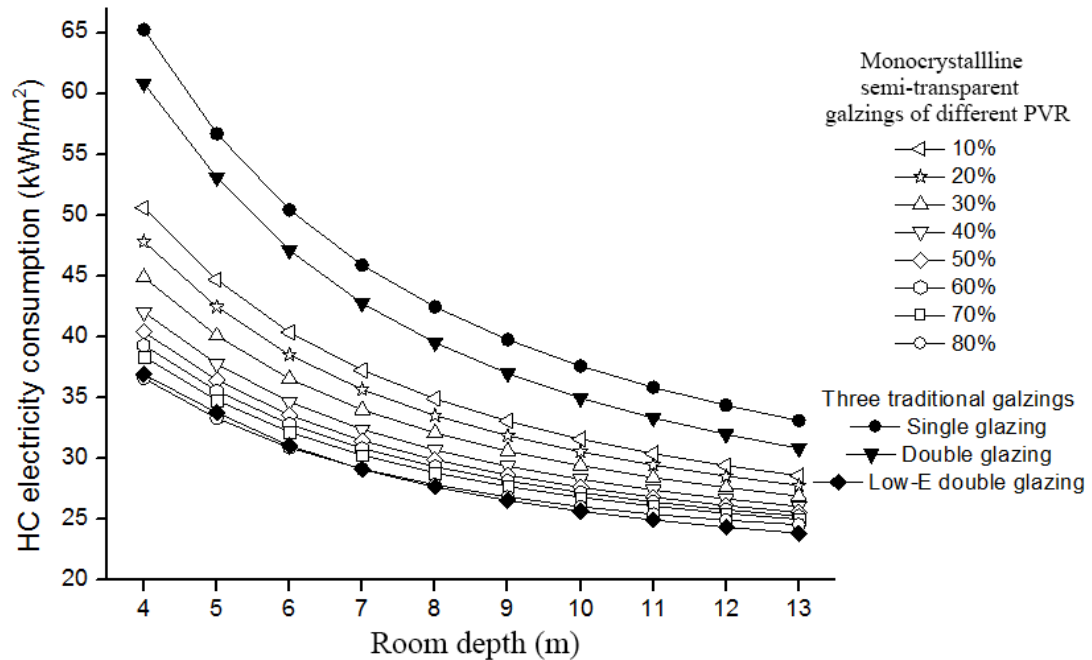
Figure 6.26 Heating and cooling electricity consumption of different glazings at WWR of 0.6

Figure 6.27 shows the overall energy consumption of different glazings at 0.6 WWR. The mono-crystalline semi-transparent PVs of 50%-80% PVR have the best energy performance among all glazings when the room depth is below 8 m. In addition, in all room depth cases, the energy performance of the PV glazing remains much better than single glazing and double glazing.

These discoveries indicate that in rooms with large windows, mono-crystalline semi-transparent PV glazing of high PVR has the most efficient energy performance, which is even better than Low-E double glazing in certain conditions. This result is particularly important because the office buildings are developing towards large-windows design in China. Nevertheless, its problem of high-energy consumption must be addressed, and mono-crystalline semi-transparent PV façade provides a promising option.
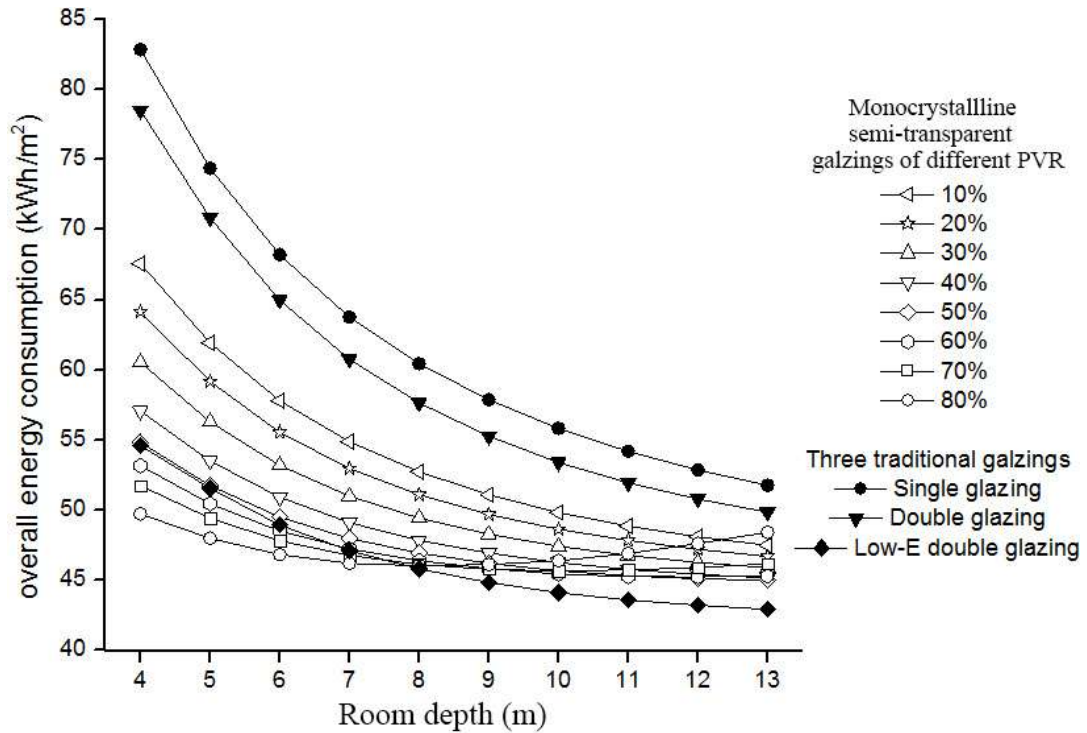
Figure 6.27 Overall energy consumption of different glazings at WWR of 0.6

By comparing the overall energy performance of different glazings in these large WWR (large-window) cases, we conclude that:

(1) Mono-crystalline semi-transparent PV glazing has a better overall energy performance than single glazing and double glazing in all room depth cases.

(2) High PVR (above 60%) mono-crystalline semi-transparent PV glazing has a better overall energy performance than all traditional glazings in rooms that are less than 8 m deep.

(3) In rooms with large windows, high PVR mono-crystalline semi-transparent PV glazing has the most efficient energy performance.

6.5. Conclusions

This chapter discuses the energy evaluation of mono-crystalline semi-transparent PV glazing on overall energy performance. The mono-crystalline semi-transparent PV and traditional glazings were compared. Optimal PVR is

investigated in different combinations of room depth, WWR and orientations. The main discoveries are listed as following.

In the parametric analysis of the overall energy performance, the PV electricity generation and the electricity consumption of lighting, heating and cooling are analysed, with the following discoveries:

(1) Temperature significantly affects the conversion efficiency. When the PVR increases, the PV electricity conversion efficiency decreases.

(2) When the PVR increases, the indoor daylight illuminance linearly decreases, and the electricity consumption increases. The room depth has a greater effect on the daylight performance than the WWR. In terms of lighting energy saving, mono-crystalline semi-transparent PV façades are more suitable and can provide better lighting energy performance in relatively short rooms, or in relatively larger-window rooms.

(3) Under the climatic conditions of central China, increasing the PVR appears to decrease the heating and cooling electricity consumption.

(4) An optimal PVR can be obtained with a particular combination of WWR, room depth, and orientation. When the overall energy performance is considered, adopting the optimal PVR can result in electricity savings of up to 30% (average savings: 13%) compared to the least favourable PVR. This result demonstrates the importance of selecting optimal PVR based on the architectural conditions.

(5) The rooms with small room depth have relatively smaller optimal PVR than rooms with lager room depth. Large WWR rooms have relatively larger optimal PVR than small WWR rooms. This result indicates that high PVR PV façades are more suitable for deep rooms with larger window and small PVR PV façades are more suitable for short rooms with small window.

In the comparison analysis between the three traditional glazings (single glazing, double glazing and Low-E double glazing) and the mono-crystalline semi-transparent PV glazing, the PV glazing generally has a better energy

performance than single glazing and double-glazing, particularly in large WWR cases:

(1) In small WWR rooms, low PVR (below 50%) mono-crystalline semi-transparent PV glazing has a better over energy performance than single glazing and double glazing in all room depth cases. In small WWR rooms, high PVR (above 50%) mono-crystalline semi-transparent PV glazing has a better overall energy performance than single glazing and double glazing in short rooms; however, in deep-room cases, it is worse than all traditional glazings.

(2) In small WWR rooms, the mono-crystalline semi-transparent PV glazing has a worse overall energy performance than Low-E double glazing in all cases, particularly in deep rooms.

(3) In large WWR rooms, high PVR mono-crystalline semi-transparent PV glazing has the best efficient energy performance, which is even better than Low-E double glazing in certain conditions. This result is particularly important because the office buildings are developing toward large window design in China.

Chapter 7 Evaluation on energy performance of office buildings with amorphous-silicon semi-transparent PV façades

In Chapter 6, the overall energy performance of mono-crystalline semi-transparent PV glazing has been examined. Amorphous-silicon semi-transparent PV glazing is examined in Chapter 7 using similar methods. With the calculation methods and architectural models presented in Chapter 5, the energy (electricity) consumption of lighting, heating and cooling., is calculated. Section 7.2 discusses the energy evaluation for amorphous-silicon semi-transparent using a parametric analysis. An optimizing design approach for amorphous-silicon semi-transparent PV façade by optimal WWR is explored in Section 7.3. In addition, energy saving of amorphous-silicon semi-transparent PV compared to three traditional glazings is investigated and presented in Section 7.4.

7.1. Introduction

In terms of the two types of PV glazing, amorphous-silicon semi-transparent does not have a wide variation of solar transmittance, which is different from mono-crystalline semi-transparent PV, where the solar transmittance is controlled using the PVR. On the contrary, the solar transmittance for amorphous-silicon PV glazing is usually higher than 70% with limited changes. In this case, a fixed solar transmittance value is used in this chapter for the amorphous-silicon semi-transparent PV in all studied cases. This solar transmittance is obtained from the observation value of the amorphous-silicon glazing that we use in the field experiments. Other necessary properties for the simulation analysis were discussed and provided in Chapter 5.

This chapter discusses the parametric analysis on the energy performance of amorphous-silicon semi-transparent PV façades in office buildings. The validated calculation models and methods for amorphous-silicon semi-transparent PV were discussed in Chapter 5 and incorporated into the architectural models and Energy Plus to investigate the effects of the amorphous-silicon PV in different WWR cases. The overall energy performance, which includes the PV electricity generation, lighting, heating and cooling electricity consumption, was examined under different architectural conditions. Different combinations of room depth and WWR were carefully examined for the southern orientation. The criterion of electricity consumption per floor area (kWh/m^2) was used to account for the differences in floor area for different room depth to provide normalised results. All

figures are evaluated using an annual value or average annual value (if it is not specifically mentioned) to see the entire picture of the overall energy consumption of four seasons.

7.2. Parametric analyses of the overall energy performance of amorphous-silicon semi-transparent PV façades

7.2.1. Effects on the PV electricity generation
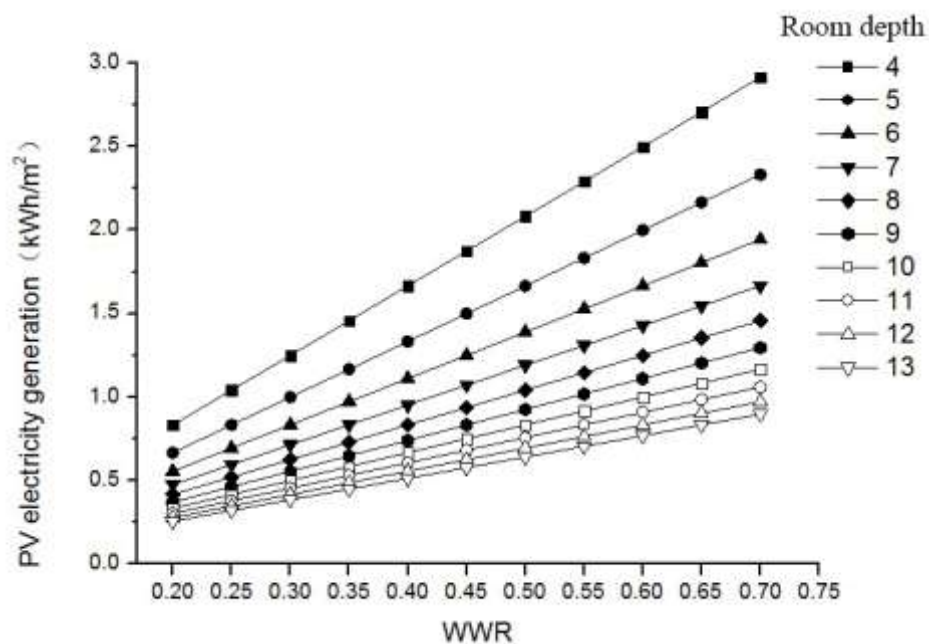
Figure 7.1 PV power generation of different WWR in different room depth cases

With the calculation method in Chapter 5, the PV generation conversion efficiency of amorphous-silicon semi-transparent PV is simulated and investigated throughout March 1 2013. Because the solar transmittance of the amorphous-silicon PV layer is fixed, the results show that there is no tangible relation between the WWR and the PV conversion efficiency. The conversion efficiency remains at 4.9% for all cases in that result. With a larger WWR, there is more window area for PV façades; thus, the PV electricity generation output increases when the WWR increases. Because there is no tangible relation between the WWR and the PV conversion efficiency, the PV electricity generation output linearly increases with the increase in WWR as Figure 7.1 shows. In addition, it

should be noticed that the amorphous-silicon semi-transparent PV (approximately 14%) has a much lower PV conversion efficiency than the mono-crystalline PV (approximately 4.9%). In these cases, the total amount of PV electricity output is also less significant.

7.2.2. Effects on the daylight and the lighting energy consumption
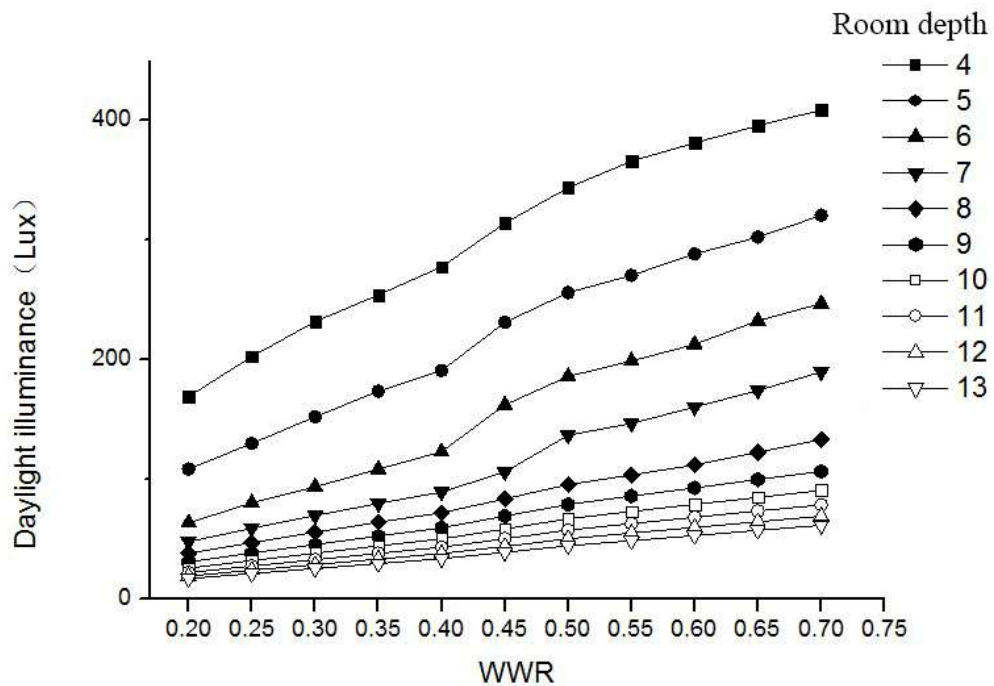
Figure 7.2 Indoor daylight illuminance of different WWR in different room depth cases

Figure 7.2 shows the indoor daylight illuminance of different WWR in different room depth cases. For a 4m deep room, illuminance increases 140% when the WWR increases from 0.2 to 0.7; this incensement for a 13m deep room is 260%.. However, most cases remain below 300 lux, which indicates the requirement of artificial-lighting compensation. When the room depth is above 8 m, the average daylight illuminance decreases below 100 lux and even 50 lux in many cases. In this situation, daylight becomes insignificant and meaningless. Artificial lighting must be provided to maintain a comfortable lighting environment (above 300 lx) indoor for office function. Moreover, when the room depth is above 8 m, the difference among different WWR becomes less significant. Compared to

the mono-crystalline semi-transparent PV glazing in Section 6.2.2, amorphous-silicon PV glazing is obviously inferior, and its predictable outcome is bad performance in lighting energy consumption mainly because the amorphous-silicon layer in the PV glazing has a low visible and solar transmittance value.
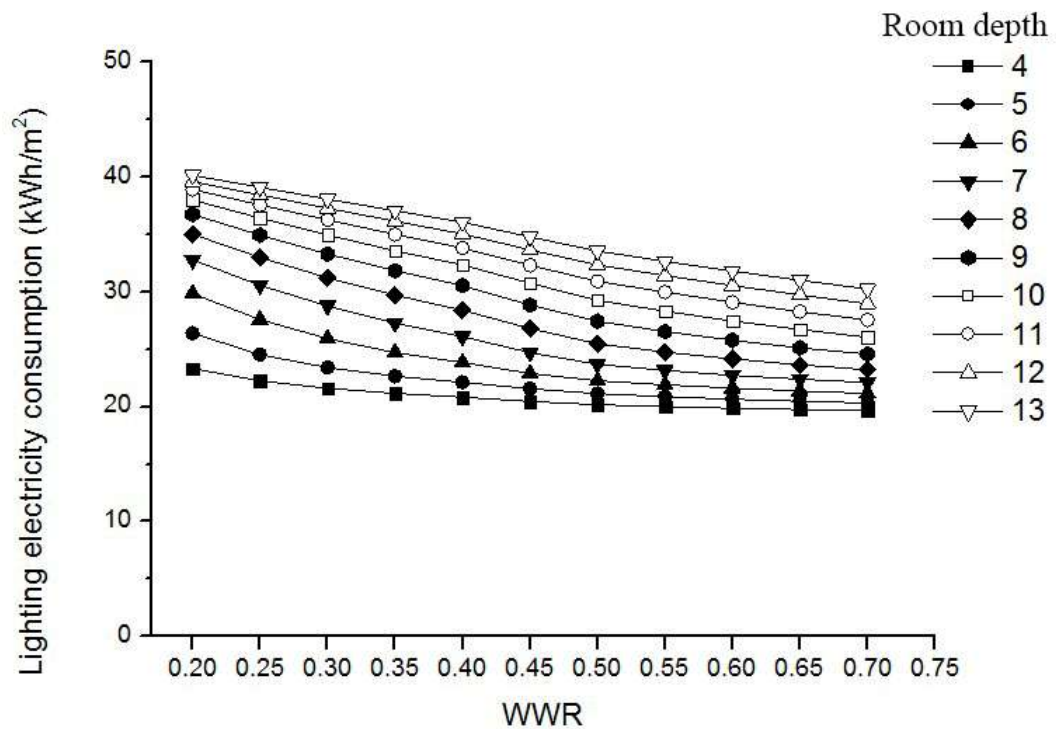
Figure 7.3 Lighting energy consumption of different WWR in different room depth cases

Figure 7.3 shows the lighting electricity consumption of different WWR in different room depth cases. The electricity consumption of different cases is within 20-40 kWh/m^2. As we predicted, this artificial-lighting electricity consumption is relatively higher than that of mono-crystalline semi-transparent PV glazing. Meanwhile, compared to the daylight illuminance, the difference in lighting electricity consumption is less significant. For a 4m deep room, lighting electricity consumption decreases 15% when the WWR increases from 0.2 to 0.7; this decreasement for a 13m deep room is 33%.. For short-room cases with room depth below 7 m, the lighting energy consumption remains almost constant after WWR exceeds 0.5.

7.2.3. Effects on the heating and cooling electricity consumption
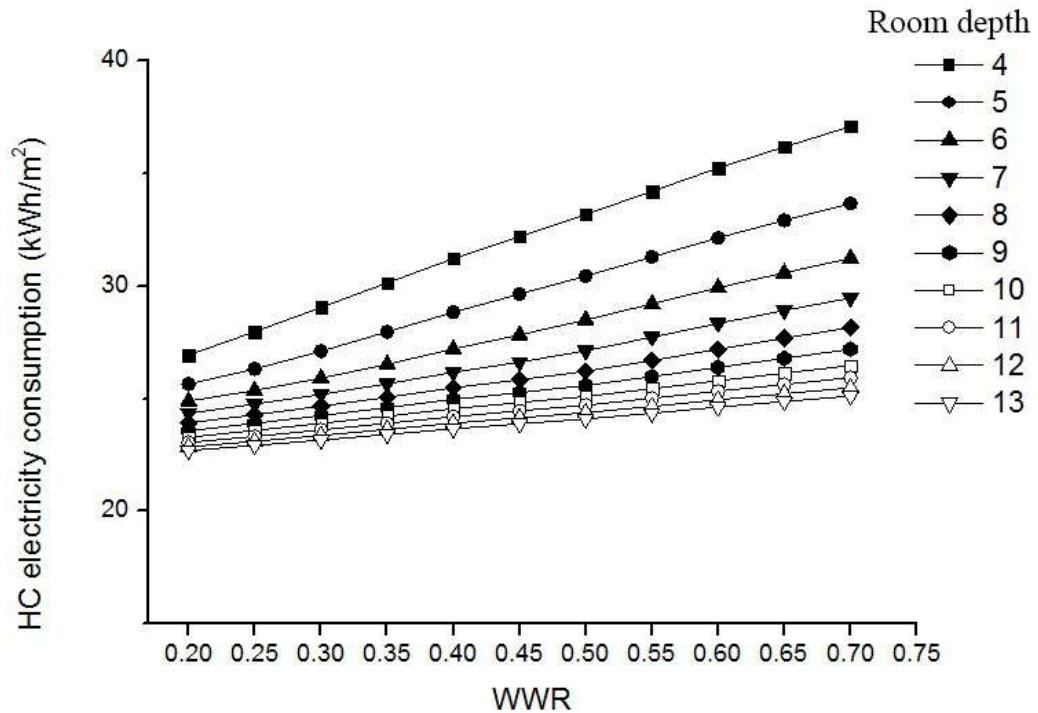
Figure 7.4 Heating and cooling electricity consumption of different WWR in different room depth cases

With a low solar transmittance, it could be predicted that the heat gain by solar radiation through amorphous-silicon semi-transparent PV is significantly reduced. This result is beneficial in the summer because it can reduce the cooling demand, however it also increases the heating demand in the winter because of the loss of solar radiation. As previously discussed in Section 6.2.3, in central China, which is a typical hot-summer cold-winter climate zone, the amount of heat gain through the window glass in the summer is larger than the amount of heat loss of solar radiation in the winter. This result indicates that saving the cooling energy will benefit more in terms of the overall energy performance. Figure 7.4 shows the heating and cooling electricity consumption of amorphous-silicon semi-transparent PV in different WWR and room depth cases. The electricity consumption of different cases is within 22-37 kWh/m^2 and increases when the WWR increases, which is lower than that of mono-crystalline PV (Figure 6.11). This outcome is consistent

with the prediction. Similar to the lighting energy consumption, the difference in heating and cooling electricity consumption among different WWR is less significant in large room depth cases. In addition, in large room depth cases, the heating and cooling energy increases more slowly when the WWR increases.

It can be concluded that amorphous-silicon semi-transparent PV glazing is beneficial in terms of saving the overall heating and cooling energy. It consumes relative less heating and cooling electricity than mono-crystalline semi-transparent PV glazing.

7.2.4. Effects on the overall energy consumption

Based on the above analysis, it can be concluded that amorphous-silicon semi-transparent PV decreases the heating and cooling electricity consumption but increases the artificial-lighting electricity consumption. Amorphous-silicon semi-transparent PV also has relatively lower PV electricity generation output than mono-crystalline semi-transparent PV glazing. However, the effects of the room depth and WWR on these relationships are pronounced, which demonstrates that these factors must be carefully considered when designing amorphous-silicon semi-transparent PV façades for buildings. Therefore, it is necessary to evaluate the overall energy consumption considering these factors (which were discussed in 6.2.4) to determine an optimal WWR.

Figure 7.5 shows the overall energy consumption of different WWR in different room depth cases. The overall energy consumption is mostly within 50 kWh/m^2 to 60 kWh/m^2 for all cases. For large room depth (>8 m) rooms, the overall energy consumption decreases when the WWR increases. The lowest overall energy consumption is observed with a WWR of 0.7. However, for small room depth (<8 m) rooms, when the WWR increases, the overall energy consumption decreases at first and subsequently increases after the WWR exceeds a certain value. This result indicates the existence of an optimal WWR in terms of the overall energy consumption.
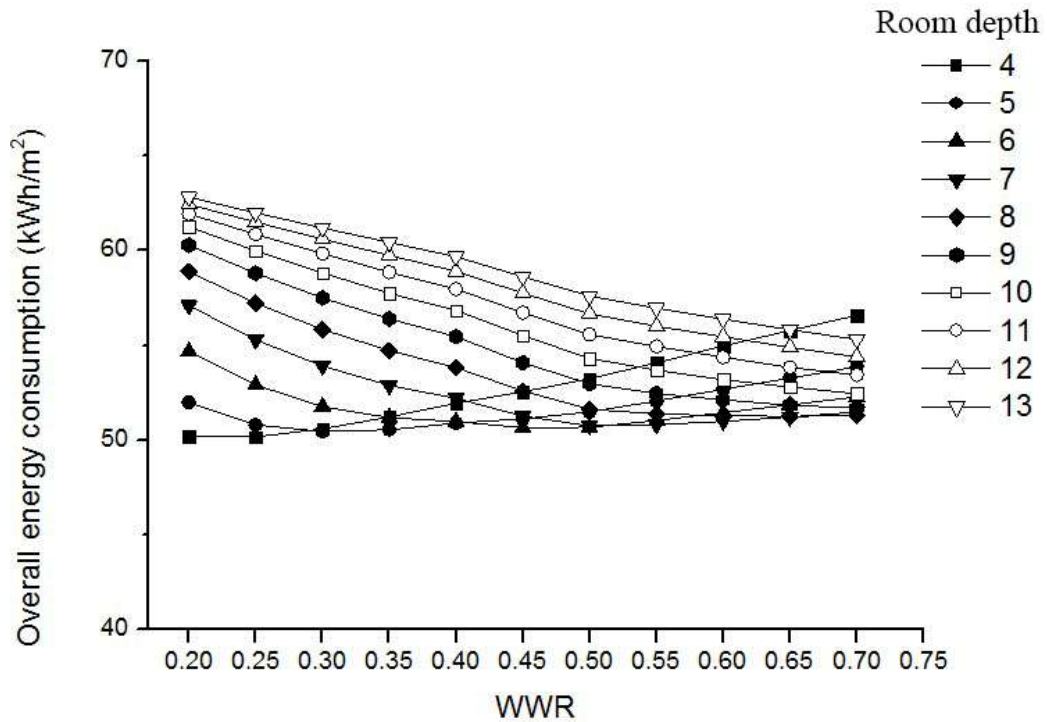
Figure 7.5 Overall energy consumption of different WWR in different room depth

cases

To further explain the details of the overall energy consumption, Figure 7.6 shows the overall energy consumption with PV electricity generation, lighting and heating and cooling electricity consumption in two room depth cases of 6 m (a) and 12 m (b).

For the 6 m room depth (short-room) cases, when the WWR increases from 0.2 to 0.7, the heating and cooling electricity consumption increases to 6.4 kWh/m^2, whereas the lighting electricity consumption decreases to 8.7 kWh/m^2. PV electricity generation increases 1.4 kWh/m^2. In addition, when the WWR is below 0.4, the heating and cooling electricity consumption is larger than that of lighting. When the WWR is above 0.4, this situation reverses. The overall energy consumption decreases with the increase in WWR at first and subsequently increases. A 0.5 WWR achieves the lowest electricity consumption at a yearly overall energy consumption of 50.6 kWh/m^2.

In the 12 m room depth (deep-room) cases, when the WWR increases from 0.2 to 0.7, the heating and cooling electricity consumption increases to 2.8 kWh/m^2, whereas that of lighting decreases to 10.7 kWh/m^2. The PV electricity generation increases to 0.7 kWh/m^2. The PV electricity generation becomes notably insignificant compared to the entire energy consumption and contributes notably little to the energy saving. When the WWR is small, the lighting electricity consumption is much larger than that of heating and cooling. This gap narrows with the increase in WWR. The overall energy consumption decreases with the increase in WWR for all cases. Thus, a WWR of 0.7 has the lowest overall electricity consumption.
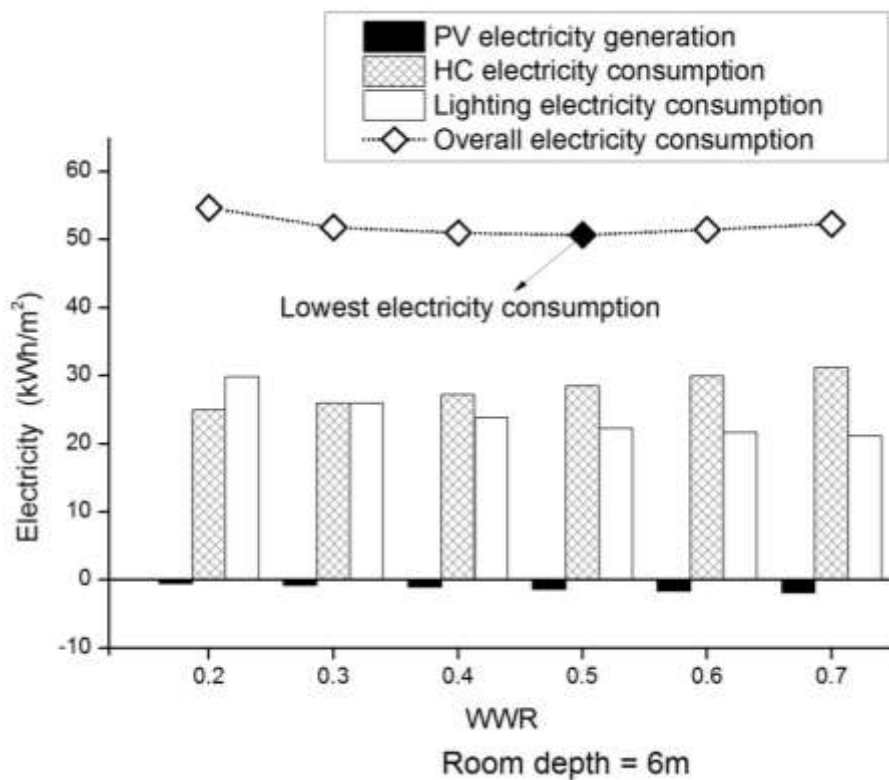
Room depth = 6m

(a)
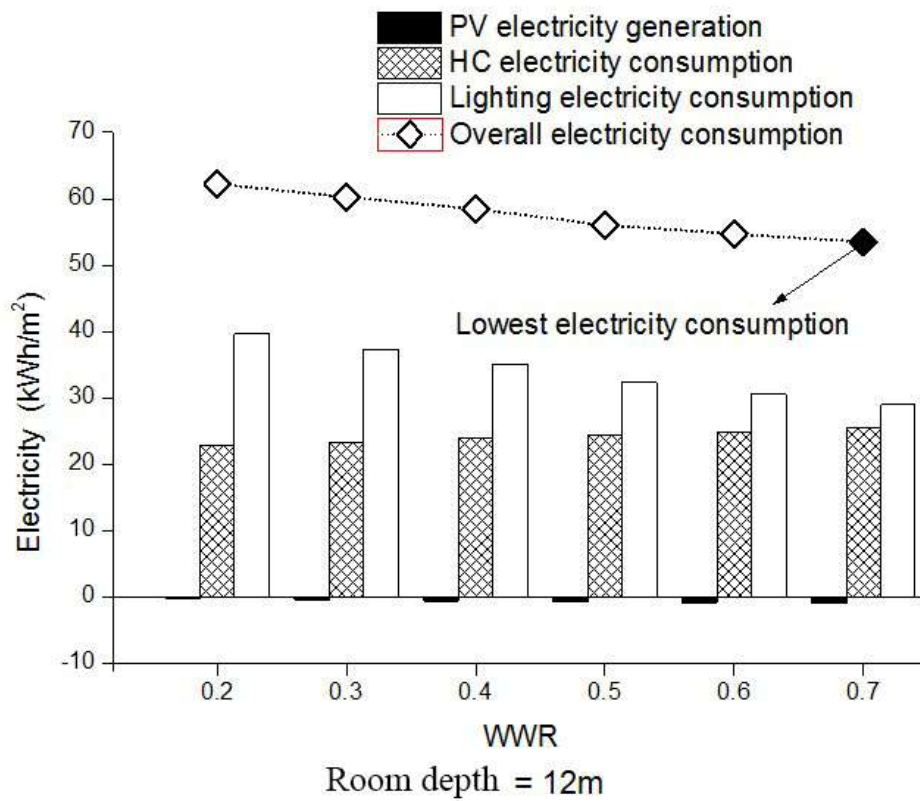
(b)

Figure 7.6 Overall energy consumption of different WWR in cases of

room depth (a) 6 m and (b) 12 m

7.3. Optimal WWR according to the overall energy performance

From the parametric analysis above, it seems there is a certain value of WWR would achieve the lowest overall electricity consumption. This particular value is defined as optimal WWR, which is chosen by comparing the overall energy consumption results of all WWR cases in different Room depth in the southern orientation. Variations in room depth can lead to considerable variation in optimal WWR (Table 7.1).

In short rooms (<8m), optimal WWR increases when Room depth increases. In deep room (>8m), optimal WWR remains 0.7 (large window) for all cases. Since a lager window area could provide more area for semi-transparent PV installation, this results indicate that amorphous-silicon semi-transparent PV is more preferable and practical in rooms with larger windows.

To show the benefits of optimal WWR, electricity saving in percentage figure by optimal WWR compared to most disadvantaged WWR is showed in Table 7.2. There is at least 8%, up to 15%, with an average of 12% of deviation is seen by comparison. The impact of optimal WWR is most significant in cases at Room depth between 8m to 11m, with maximum figure seen in case at 9m Room depth.

Table 7.1 Optimal WWR in different room depth in south orientation

	Room depth (m)									
	4	5	6	7	8	9	10	11	12	13
Optimal WWR	0.25	0.35	0.5	0.55	0.7	0.7	0.7	0.7	0.7	0.7

Table 7.2 Deviation by optimal WWR compared to most disadvantaged WWR

	Room depth (m)									
	4	5	6	7	8	9	10	11	12	13
Deviation (%)	8.6	4.3	8.9	12.5	14.7	15.8	15.7	15.0	14.0	13.0

7.4. Energy saving of amorphous-silicon semi-transparent PV glazing compared to three traditional glazings

In this section, the overall energy performance of the amorphous-silicon semi-transparent PV façades layouts of each optimal WWR is compared with that of three traditional glazings: (1) single glazing, (2) Low-E double glazing and (3) normal double glazing.

Figure 7.7 (a) shows the sections of amorphous-silicon semi-transparent PV, whose calculation methods were discussed and presented in Chapter 5. Figures 7.7 (b), (c) and (d) show the sections of the three traditional glazings, whose properties and simulation methods were discussed in Section 6.4.
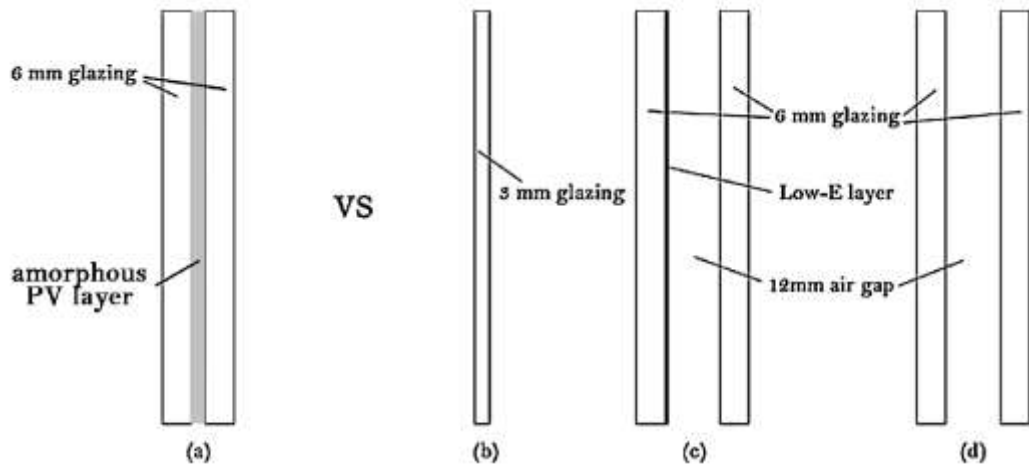
Figure 7.7 Amorphous-silicon PV glazing and three traditional glazings

(a) Amorphous-silicon PV glazing, (b) 3 mm single glazing, (c) 6 mm Low-E double glazing with a 12 mm air gap, (d) 6 mm double glazing with a 12 mm air gap

Two types of architectural models are used in this section and are illustrated in Figure 6.18 in Chapter 6. The first type is generic rooms with relatively small windows at a WWR of 0.3. The other type is generic rooms with larger windows at a WWR of 0.6. The details of the architectural models are discussed and provided in Section 5.3. Amorphous-silicon semi-transparent PV and the three traditional glazings are first compared in the small WWR cases and subsequently in the large WWR cases to investigate the performance of lighting, heating and cooling energy performance. The PV electricity generation of PV glazing is automatically included in all comparisons. The results are presented in annual value with different room depths.

7.4.1   Energy savings in small WWR cases

Figure 7.8 shows the Daylight illuminance of different glazing at 0.3 WWR cases. Compared to the three traditional glazings, daylight illuminance of amorphous-silicon semi-transparent PV glazing is very low. Traditional glazings are roughly 6-7 times higher than amorphous-silicon semi-transparent PV.
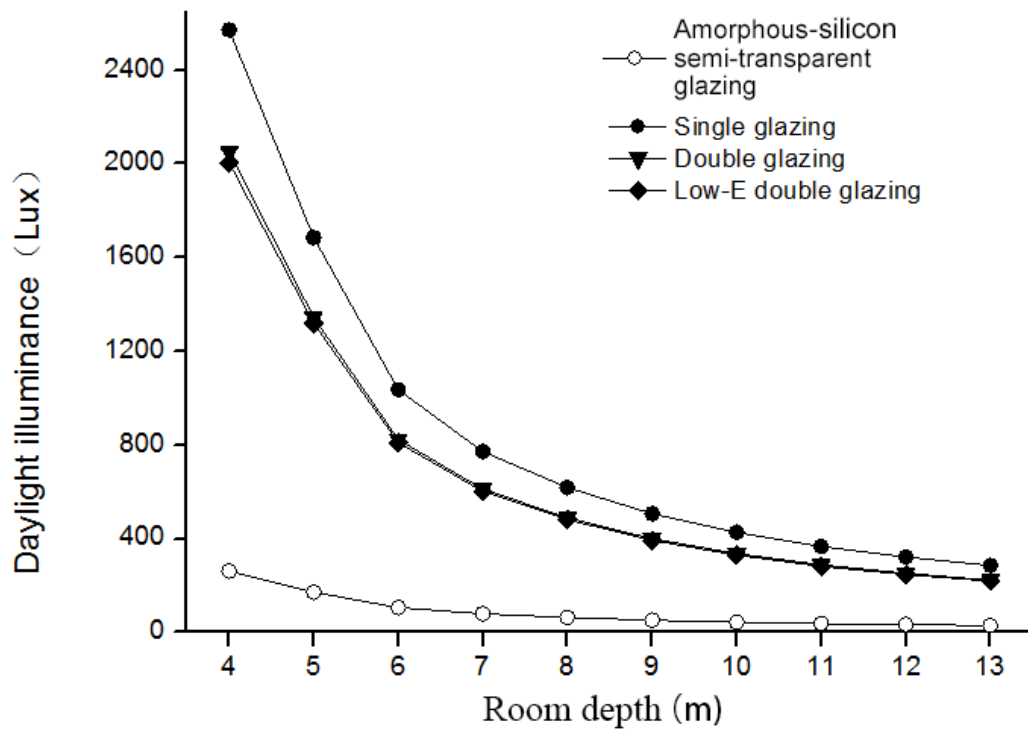
Figure 7.8 Daylight illuminance of different glazings at WWR of 0.3
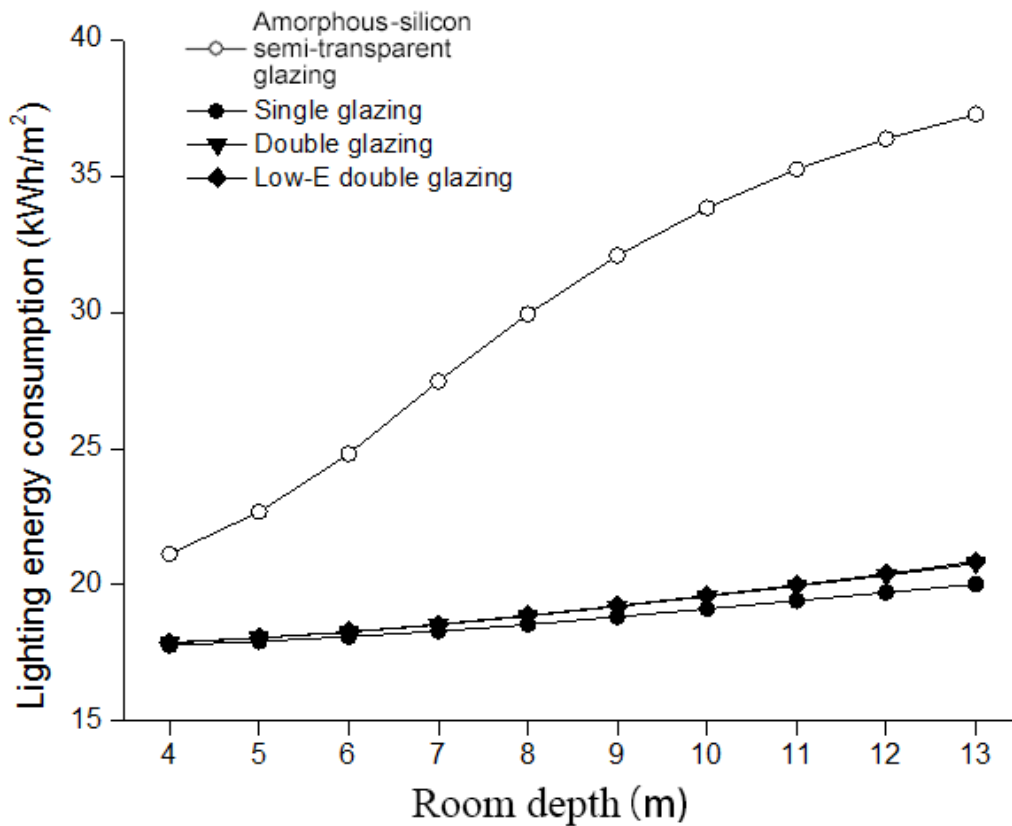
Figure 7.9 Lighting electricity consumption of different glazings at WWR of 0.3

Because of the huge disadvantage of the indoor illuminance level, the artificial-lighting electricity consumption of the amorphous-silicon semi-transparent PV is also significantly higher than that of traditional glazings, as Figure 7.9 shows. In the 4-m-deep room case, 26% more electricity was consumed by the amorphous-silicon semi-transparent PV glazing compared to the traditional glazings. In the 13-m-deep room, 95% more electricity is consumed by amorphous-silicon semi-transparent PV glazing.

These results clearly show that amorphous-silicon semi-transparent PV is significantly inferior to transitional glazings in terms of lighting energy performance, which is particularly true for deep-room cases.
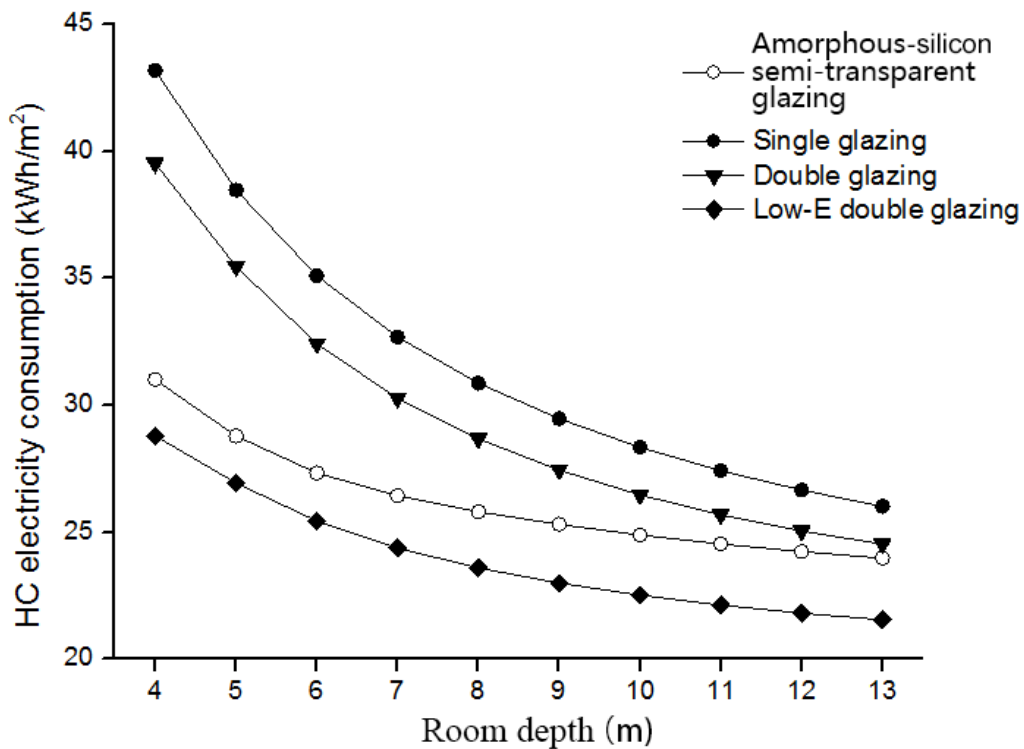
Figure 7.10 Heating and cooling electricity consumption of different glazings at WWR of 0.3

Figure 7.10 shows the heating and cooling electricity consumption of different glazings at 0.3 WWR. Low-E double glazing has the lowest electricity consumption, followed by amorphous-silicon semi-transparent PV glazing. Single glazing has the highest electricity consumption among all types. In the 4-m-deep

room, the amorphous-silicon semi-transparent PV glazing saves 20% and 18% electricity compared to double glazing and single glazing, respectively. However, this advantage decreases when the room depth increases. In the 13-m-deep room, the difference between amorphous-silicon semi-transparent PV glazing and double glazing becomes insignificant.

Figure 7.11 shows the overall energy consumption of different glazings at 0.3 WWR. In the rooms with room depth below 6 m, the amorphous-silicon semi-transparent PV glazing has a better energy performance than single glazing and double glazing. However, in the rooms with room depth above 6 m, the amorphous-silicon semi-transparent PV has the worst overall energy performance mainly because the lighting electricity consumption of the amorphous-silicon semi-transparent PV increases. In a 13-m-deep room, the overall electricity consumption is 26-39% higher for amorphous semi-transparent PV glazing than for the three traditional glazings.
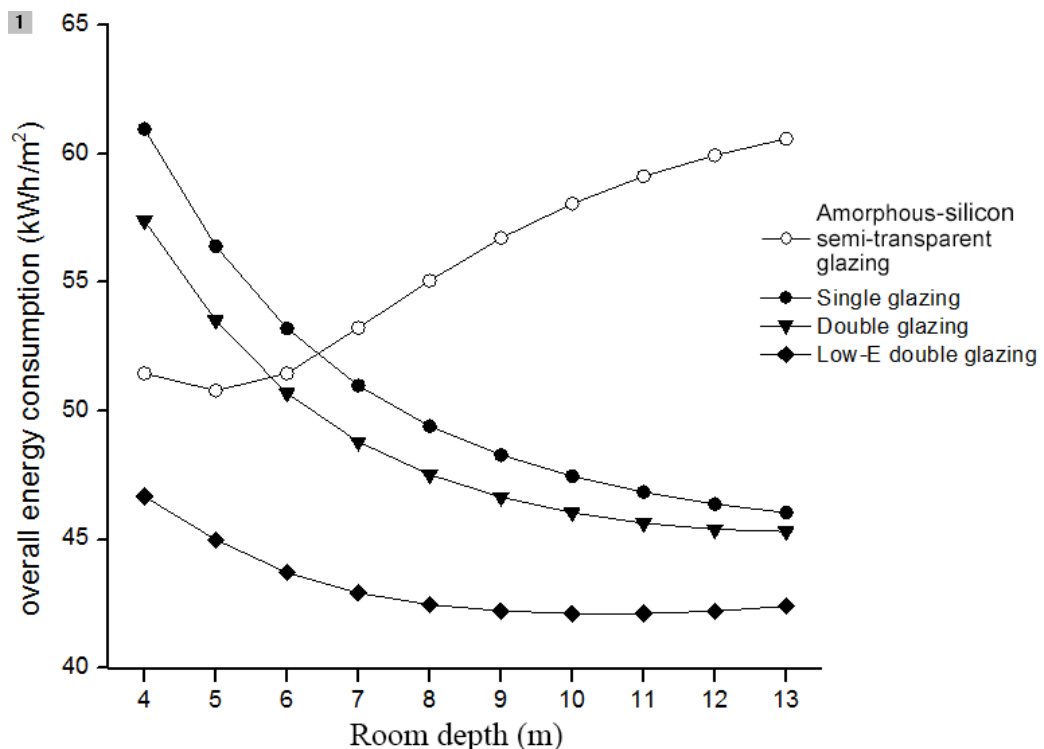
Figure 7.11 Overall energy consumption of different glazings at WWR of 0.3

By comparing the overall energy performance of different glazings the in small WWR (small-window) cases, we conclude that:

(1) Amorphous-silicon semi-transparent PV is significantly inferior to traditional glazings in terms of daylighting and lighting energy performance.

(2) In rooms that are less than 6 m deep, the amorphous-silicon semi-transparent PV glazing has a better overall energy performance than single glazing and double glazing.

(3) In rooms that are deeper than 6 m, all three traditional glazings are better than amorphous-silicon semi-transparent PV glazing in terms of the overall energy performance.

7.4.2   Energy savings in large WWR cases

Figure 7.12 shows the daylight illuminance of different glazings at 0.6 WWR. Compared to the small WWR cases in 7.3.1, a larger window provides better daylight illuminance, which is notably limited. The amorphous-silicon semi-transparent PV remains having a notably lower illuminance than the traditional glazings. Thus, the artificial-lighting electricity consumption of amorphous-silicon semi-transparent PV in large WWR cases remains significantly higher than that of traditional glazings, as Figure 7.13 shows. In the 4-m-deep room, 11% more electricity was consumed by amorphous-silicon semi-transparent PV glazing compared to traditional glazings. In the 13-m-deep room, 72% more electricity is consumed by amorphous-silicon semi-transparent PV glazing.

Figure 7.14 shows the heating and cooling electricity consumption of different glazings at 0.6 WWR. The difference between Low-E double glazing and amorphous-silicon semi-transparent PV glazing is small, and both types save a significant amount of energy compared to single and double glazing. In the 4-m-deep room, amorphous-silicon semi-transparent PV glazing saves 33% and 38% electricity compared to double glazing and single glazing, respectively. However, the saving becomes less significant in large room depth cases.
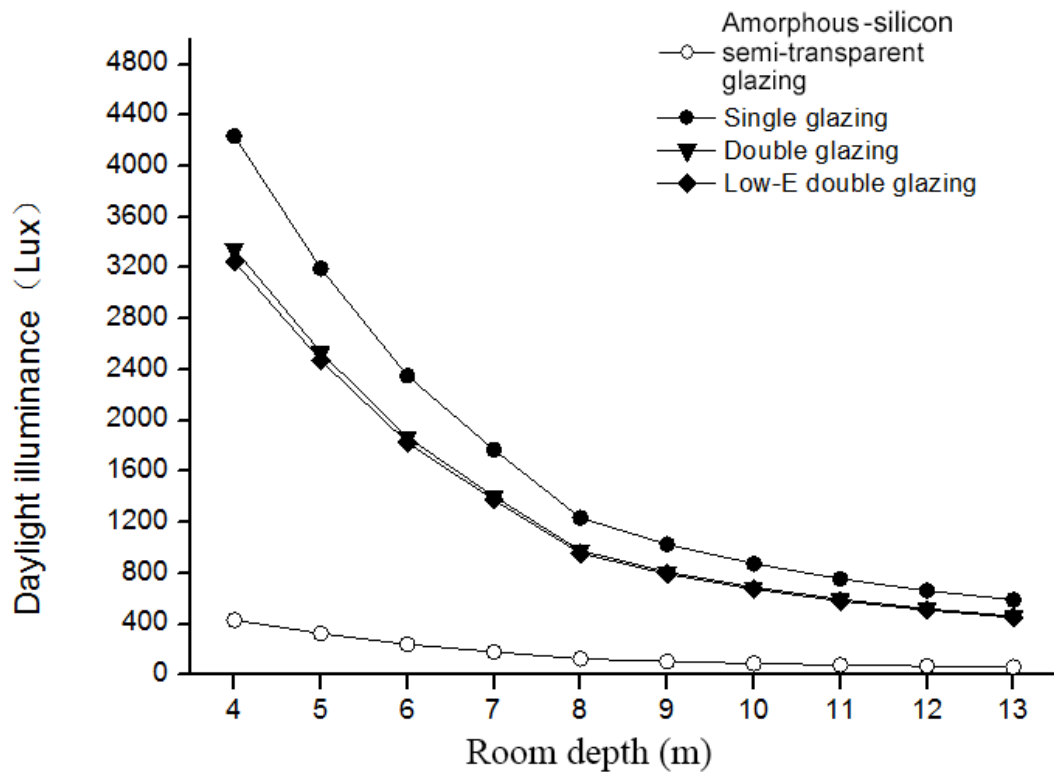
Figure 7.12 Daylight illuminance of different glazings at WWR of 0.6
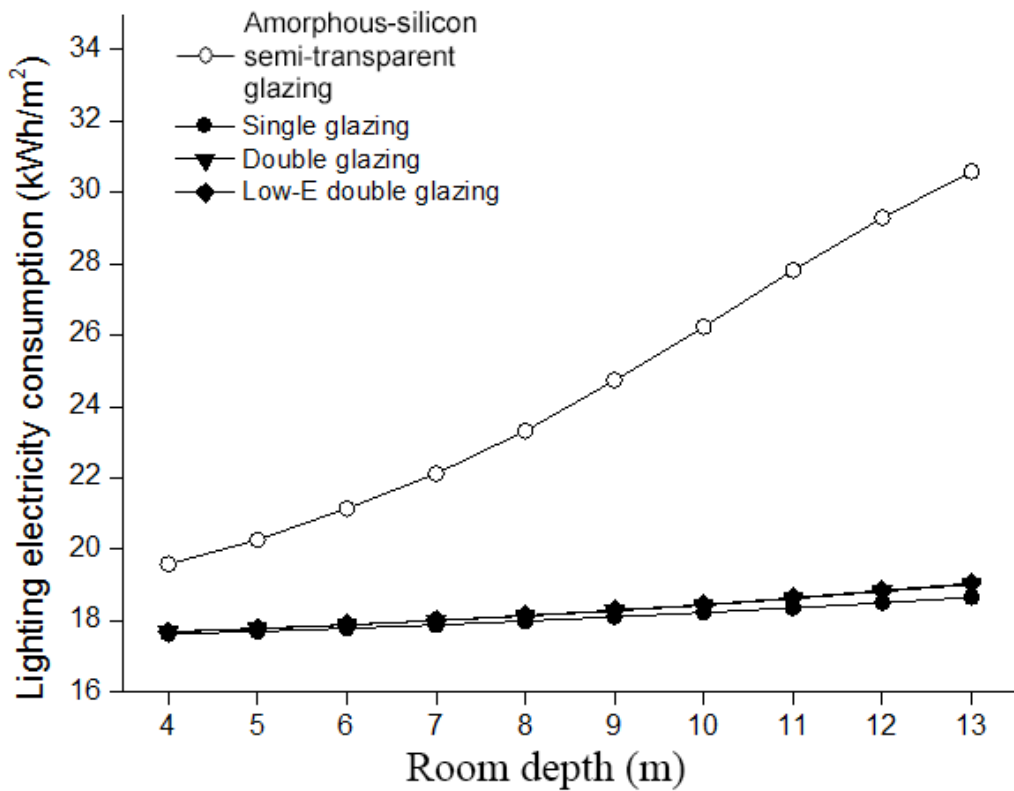
Figure 7.13 Lighting electricity consumption of different glazings at WWR of 0.6
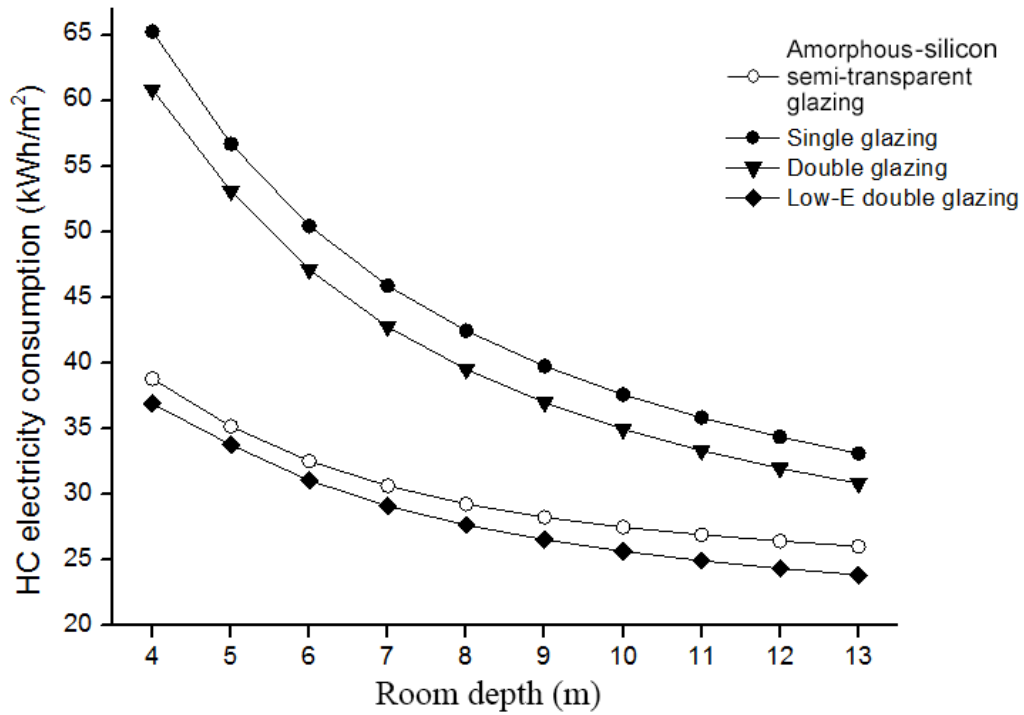
Figure 7.14 Heating and cooling electricity consumption of different glazings at WWR of 0.6
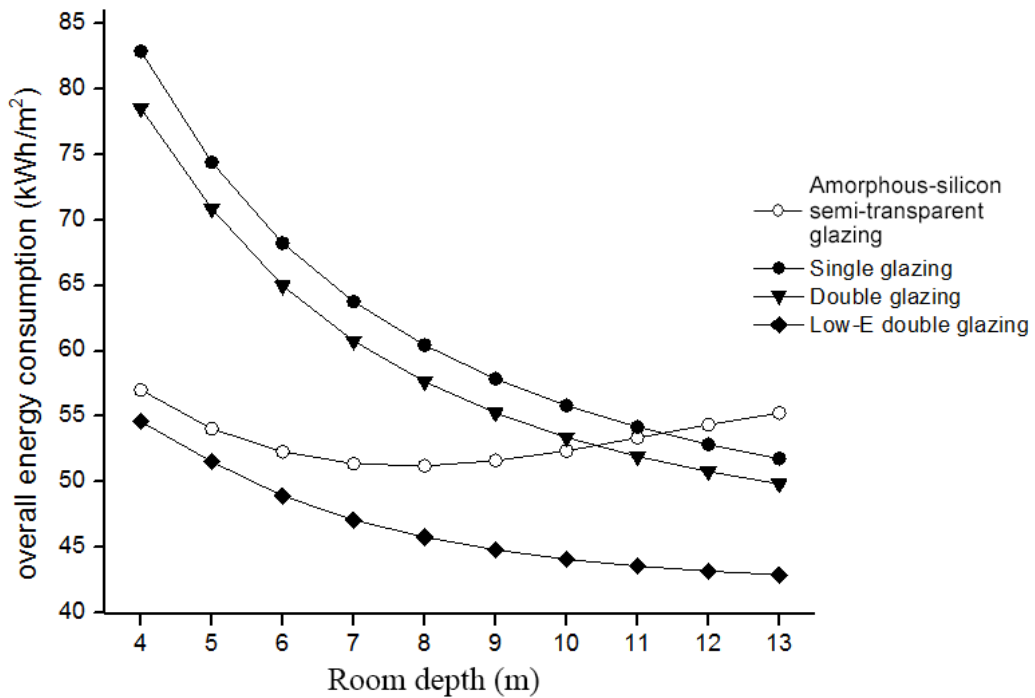
Figure 7.15 Overall energy consumption of different glazings at WWR of 0.6

Figure 7.15 shows the overall energy consumption of different glazings at 0.6 WWR. In rooms with room depth below 10 m, the amorphous-silicon semi-transparent PV glazing has a better energy performance than single glazing and double glazing. The overall energy performance of all three traditional glazings decreases when the room depth increases, whereas the amorphous-silicon semi-transparent PV consumes the least energy when it is used in the 8-m-deep room. In the 8-m-deep room, the overall electricity consumption of amorphous-silicon semi-transparent PV glazing is 10% higher than that of Low-E double glazing, 8% lower than that of double glazing and 14% lower than that of single glazing. For amorphous-silicon semi-transparent PV, a proper room depth appears to give the best overall energy performance.

By comparing the overall energy performance of different glazings in the large WWR (large-window) cases, we conclude that:

(1) Amorphous-silicon semi-transparent PV is significantly inferior to traditional glazings in terms of daylighting and lighting energy performance even in rooms with large windows.

(2) In rooms that are less than 10 m deep, the amorphous-silicon semi-transparent PV glazing has a better overall energy performance than single glazing and double glazing.

(3) Amorphous-silicon semi-transparent PV glazing is inferior to Low-E double glazing in all room cases.

7.5. Conclusions

This chapter discusses the parametric analysis of the overall energy performance of amorphous-crystalline semi-transparent PV glazing. A comparison analysis between amorphous-silicon semi-transparent PV and traditional glazings is conducted. Optimal WWR is investigated in different room depth cases. The main discoveries are listed as following.

In the parametric analysis of the overall energy performance, the PV electricity generation and the electricity consumption of lighting, heating and cooling of amorphous-silicon semi-transparent PV are analysed, with the following discoveries:

(1) The results show that there is no tangible relation between the WWR and the PV conversion efficiency. The total amount of PV electricity output is also less significant than that of mono-crystalline semi-transparent PV.

(2) When the WWR increases, the indoor daylight illuminance linearly increases, and the electricity consumption decreases. However, because of the low visible and solar transmittance value of the amorphous-silicon layer in the PV glazing, the amorphous-silicon semi-transparent PV does not perform well in terms of indoor daylighting and lighting energy performance.

(3) Amorphous-silicon semi-transparent PV glazing is beneficial in terms of saving the overall heating and cooling energy. Its heating and cooling electricity consumption is relatively less than that of mono-crystalline semi-transparent PV glazing.

(4) An optimal WWR (i.e., one that achieves the lowest overall electricity consumption) can be obtained for a particular combination of room depth and orientation. When the overall energy performance is considered, adopting the optimal WWR can result in electricity savings of up to 15.8% compared to the least favourable WWR, although the achieved savings vary depending on the combination of room depth, at least in the south orientation. This result demonstrates the importance of selecting the optimal WWR based on the architectural conditions.

(5) The results of the optimal WWR indicate that amorphous-silicon semi-transparent PV is preferable and more practical in rooms with large windows.

The main results of the comparison analysis among three traditional glazings (single glazing, double glazing and Low-E double glazing) are as follows.

(1) Amorphous-silicon semi-transparent PV is significantly inferior to traditional glazings in terms of daylighting and lighting energy performance in all situations.

(2) In short rooms, amorphous-silicon semi-transparent PV glazing generally has a better overall energy performance than single glazing and double glazing.

(3) Amorphous-silicon semi-transparent PV glazing is inferior to Low-E double glazing in all room cases.

Chapter 8 Other implications of semi-transparent PV façades in office buildings

In this chapter, other implications of semi-transparent PV façades in office buildings are discussed. With the effects of other architectural factors, the overall energy performance of semi-transparent PV façades is discussed in Section 8.2. Suitability of optimal PVR/WWR strategies in different architectural conditions is investigated in Section 8.3. In addition, Environmental performance of semi-transparent PV façades is investigated in Section 8.4.

8.1 Introduction

The effects of other architectural factors on the overall energy performance when semi-transparent PV façades are used are discussed. These architectural factors are considered less important than the architectural factors such as WWR and room depth, but they should be discussed to further understand different architectural contributions to the effects on the overall energy performance when semi-transparent PV façades are used.

The suitability of optimal PVR/WWR strategies in different architectural conditions is investigated. We aimed to discover the performance of each optimal PVR/WWR under different architectural conditions compared to the baseline buildings (A and B) in terms of energy saving. If the optimal PVR/WWR strategy achieves a lower overall energy consumption than the baseline buildings (energy saving) in an architectural condition, this optimal PVR/WWR strategy can be refer as "suitable" in this architectural condition. In addition, the energy saving of each optimal PVR/WWR is presented. Energy saving from office buildings becomes increasingly more economically significant because the energy cost continues to increase in China. This statement is particularly true when office buildings has relatively higher electricity price than resident buildings in China, which indicates that the economic savings from PV façades of office buildings will be even more profitable.

The environmental performance of semi-transparent PV façades based on the carbon reduction by the amount of CO_2 and polluted emission such as SO_2, NO and carbonaceous dust is presented in this chapter. These polluted gases are produced during the electricity production using thermal power generation. They can be

reduced by using PV façades and replacing the power demand with solar energy, which is notably clean and produces no harmful material to the environment.

8.2 Effects of other architectural factors on overall energy performance of semi-transparent PV

In this section, other architectural factors such as room height, window height and room width are developed and incorporated into the architectural models. A room of 8 m room depth and 0.3 WWR is chosen as the study sample; its room setups were discussed in Section 5.3. A mono-crystalline semi-transparent PV of 40% PVR is chosen as the sample of semi-transparent PV. The overall energy consumption, which includes the PV electricity generation, heating and cooling electricity consumption and lighting electricity consumption, is simulated and presented to discover the effects of other architectural factors on the energy performance. All figures show the annual values.

8.2.1. Effects of different room height

Figure 8.1 shows the overall energy consumption for different room heights. The room height is set at 3.0 m, 3.5 m, 4.0 m and 4.5 m, which are the most common heights for office buildings. When the room height increases, the PV electricity generation slightly increases by 0.6 kWh/m^2 because the wall area increases when the room height increases, which increases the window area because all cases have identical WWR. When the room height increases, the lighting energy consumption decreases because the window area increases. However, with a great increase in heating and cooling electricity consumption, the overall energy consumption increases by 14.6% when the room height increases from 3 m to 4.5 m.
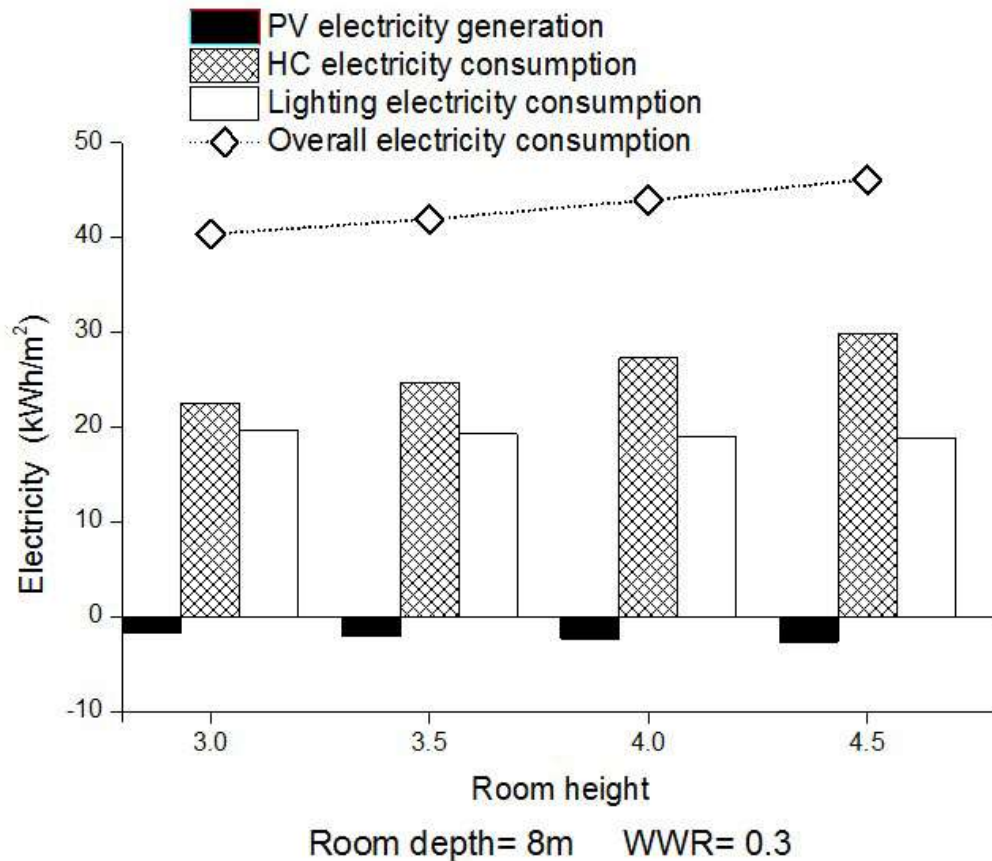
Figure 8.1 Overall energy consumption for different room heights

8.2.2. Effects of different window height

Figure 8.2 shows the overall energy consumption for different window heights. The window height is defined as the window-sill height, which is set at 0.6 m, 0.9 m and 1.2 m. The height of 0.9 m is most common in office buildings, and 0.6 m is usually used for better views in large WWR situations. When the window height increases, the PV electricity remains unchanged because the wall area does not change. The lighting energy slightly decreases with insignificant change. The heating and cooling electricity consumption remains unchanged for all cases. The overall energy consumption decreases by 3.3% when the window height increases from 0.6 m to 1.2 m. The window height appears to not significantly affect the overall energy performance in terms of the semi-transparent PV façades application.
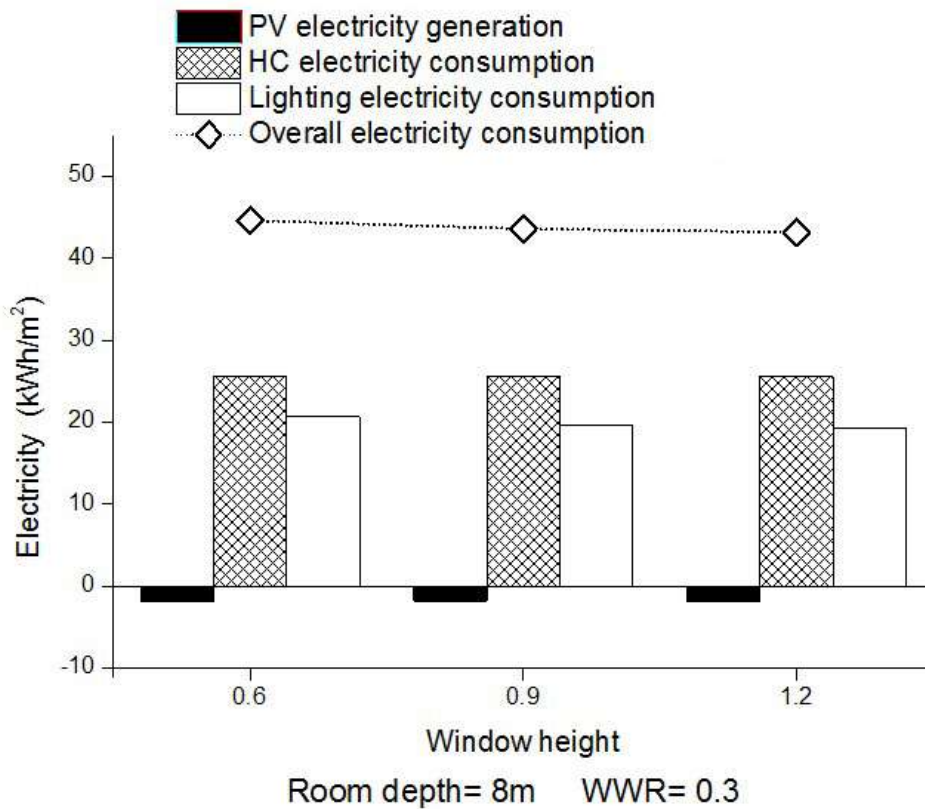
Figure 8.2 Overall energy consumption for different window heights

8.2.3. Effects of different room width

Figure 8.3 shows the overall energy consumption for different room widths, which are set at 4 m, 5 m and 6 m. It should be noticed that with the increase in room width, the window area and the floor area of the room also increase and remain at a constant proportion. In that case, the PV electricity per floor area remains constant. The lighting energy decreases by 4.1% when the room width increases from 4 m to 6 m. The heating and cooling electricity consumption decreases by 5.2%. In this case, the overall energy consumption decreases by 4.8% when the room width increases from 4 m to 6 m.
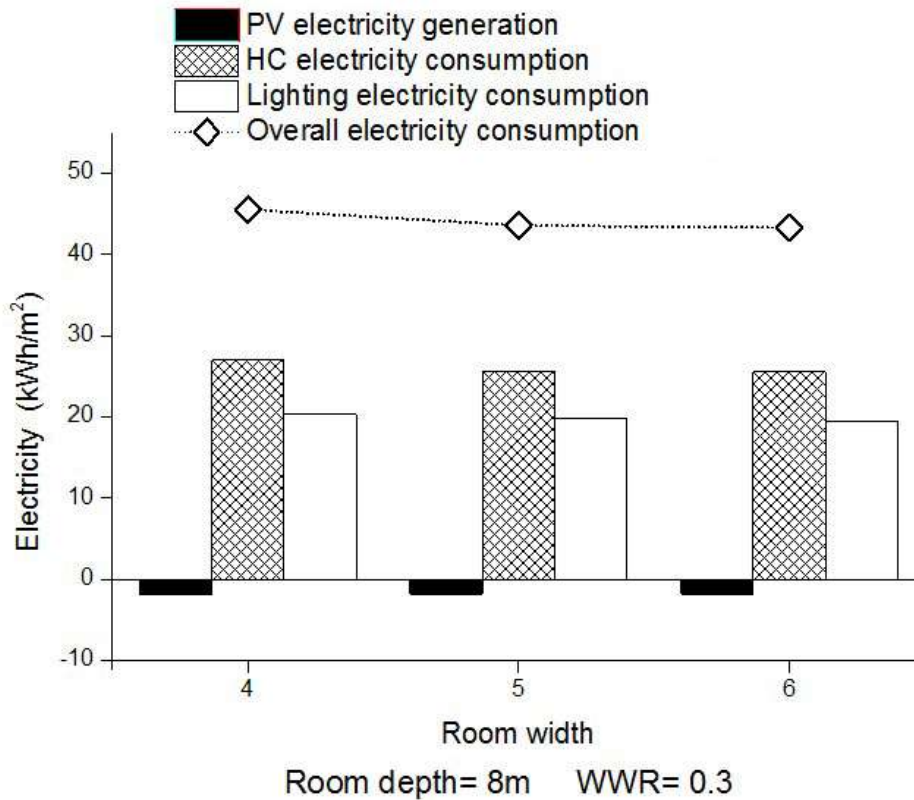
Figure 8.3 Overall energy consumption for different room widths

Among the three architectural factors, the room height has the most significant effect on the overall energy consumption with a 14.6% change, followed by the room width with a 4.8% change and the window height with a 3.3% change. However, compared to PVR and WWR, these three factors have a less significant effect on the energy performance in terms of semi-transparent PV façade applications in office buildings.

8.3. Suitability of optimal PVR/WWR for semi-transparent PV on office building façades

8.3.1 Introduction

In this section, the suitability of optimal PVR/WWR strategies in different architectural conditions is investigated by comparing the energy saving to the baseline buildings (A and B) of each optimal PVR/WWR under different architectural conditions.

The suitability is defined as follows: when the optimal PVR/WWR is adopted in certain architectural conditions, the overall energy consumption is lower than that of the baseline buildings (energy saving). In other words, if the optimal PVR/WWR strategy achieves a lower overall energy consumption than the baseline buildings (energy saving) in an architectural condition, this optimal PVR/WWR strategy can be referred to as "suitable" in this architectural condition.

8.3.2 Mono-crystalline semi-transparent PV façades

Table 8.1 Overall electricity consumption of office rooms with mono-crystalline semi-transparent PV for each optimal PVR

WWR	Electricity consumption (kWh/m2)									
	Room depth(m)									
	4	**5**	**6**	**7**	**8**	**9**	**10**	**11**	**12**	**13**
0.2	45.8	44.9	44.4	44.2	44.3	44.4	44.5	44.8	45.1	45.4
0.25	46.2	45.4	44.7	44.5	44.3	44.4	44.6	44.7	44.8	45.0
0.3	46.6	45.8	45.2	44.8	44.6	44.5	44.6	44.8	44.9	45.0
0.35	47.1	46.2	45.7	45.2	44.8	44.7	44.7	44.7	44.9	45.0
0.4	47.7	46.5	45.9	45.6	45.1	44.9	44.9	44.8	44.9	45.0
0.45	48.1	46.8	46.1	45.7	45.3	45.0	44.9	44.8	44.8	44.8
0.5	48.6	47.1	46.2	45.8	45.6	45.2	44.9	44.8	44.8	44.8
0.55	49.2	47.5	46.5	46.0	45.7	45.5	45.2	45.0	44.9	44.9
0.6	49.7	48.0	46.8	46.2	45.9	45.8	45.4	45.2	45.1	45.0
0.65	50.2	48.4	47.1	46.4	46.1	45.9	45.7	45.4	45.2	45.1
0.7	50.7	48.8	47.4	46.6	46.2	46.0	45.9	45.6	45.4	45.2

With the optimal PVR provided in Section 6.3, the energy saving of the optimal PVR of mono-crystalline semi-transparent PV is presented in this section by comparing the energy consumption of each PVR in different architectural conditions to the baseline buildings, which were discussed in Section 5.4. The economic saving is also presented based on energy saving. This analysis shows us the maximum benefits of mono-crystalline semi-transparent PV glazing as façades for office buildings and its suitability under different architectural conditions.

Table 8.1 shows the overall electricity consumption (kWh/m^2) of office rooms with mono-crystalline semi-transparent PV for each optimal PVR according to each combination of room depth and WWR. Tables 8.2 and 8.3 show the overall electricity consumption (kWh/m^2) of office rooms of baseline buildings A and B, respectively.

Table 8.2 Overall electricity consumption of office rooms of baseline building A for each combination of room depth and WWR

	Electricity consumption (kWh/m2)									
WWR	Room depth(m)									
	4	**5**	**6**	**7**	**8**	**9**	**10**	**11**	**12**	**13**
0.2	109.0	103.3	99.7	97.8	97.0	97.0	97.6	98.7	100.2	101.9
0.25	95.3	92.2	90.3	89.4	89.3	89.8	90.5	91.7	93.2	94.9
0.3	98.1	94.2	91.8	90.4	89.7	89.7	90.1	90.7	91.6	92.7
0.35	97.4	93.6	91.1	89.6	88.8	88.5	88.7	89.1	89.7	90.5
0.4	99.1	94.7	91.3	89.0	87.5	86.6	85.9	85.5	85.3	85.2
0.45	98.5	94.1	90.8	88.5	86.9	85.9	85.2	84.7	84.4	84.3
0.5	100.9	96.4	93.0	90.7	89.3	88.4	87.8	87.5	87.5	87.8
0.55	99.7	95.5	92.1	89.9	88.5	87.6	87.0	86.7	86.6	86.7
0.6	101.5	96.9	93.3	90.8	89.2	88.2	87.4	87.0	86.8	86.7
0.65	103.2	98.4	94.5	91.8	90.0	88.8	87.9	87.4	87.0	86.9
0.7	104.9	99.8	95.6	92.8	90.8	89.4	88.5	87.8	87.3	87.1

Table 8.3 Overall electricity consumption of office rooms of baseline building B

for each combination of room depth and WWR

WWR	Electricity consumption (kWh/m2)									
	Room depth(m)									
	4	**5**	**6**	**7**	**8**	**9**	**10**	**11**	**12**	**13**
0.2	54.5	51.7	49.9	48.9	48.5	48.5	48.8	49.4	50.1	50.9
0.25	47.7	46.1	45.2	44.7	44.6	44.9	45.3	45.8	46.6	47.4
0.3	49.0	47.1	45.9	45.2	44.9	44.8	45.0	45.4	45.8	46.4
0.35	48.7	46.8	45.5	44.8	44.4	44.2	44.3	44.6	44.9	45.3
0.4	49.6	47.3	45.7	44.5	43.8	43.3	43.0	42.8	42.6	42.6
0.45	49.2	47.1	45.4	44.2	43.5	42.9	42.6	42.4	42.2	42.1
0.5	50.5	48.2	46.5	45.4	44.7	44.2	43.9	43.8	43.8	43.9
0.55	49.9	47.7	46.1	44.9	44.2	43.8	43.5	43.3	43.3	43.4
0.6	50.7	48.5	46.6	45.4	44.6	44.1	43.7	43.5	43.4	43.4
0.65	51.6	49.2	47.2	45.9	45.0	44.4	44.0	43.7	43.5	43.4
0.7	52.4	49.9	47.8	46.4	45.4	44.7	44.2	43.9	43.7	43.5

According to these results, the energy saving is calculated by comparing the overall energy of mono-crystalline with that of baseline buildings A and B. Table 8.4 shows the energy saving of mono-crystalline semi-transparent PV compared to baseline building A in different architectural combinations. Table 8.5 shows the energy saving of mono-crystalline semi-transparent PV compared to baseline building B in different architectural combinations. The green area shows the part where mono-crystalline semi-transparent PV performs better than the baseline buildings. With an optimal PVR, mono-crystalline semi-transparent PV can save 48-58% of the energy on average compared to baseline building A. However, compared to baseline building B, mono-crystalline semi-transparent PV can only save energy in relatively short rooms with small windows. In a 4-m-deep room

with WWR 0.2, mono-crystalline semi-transparent PV glazing can save 16.0% energy. In a 13-m-deep room with WWR 0.7, mono-crystalline semi-transparent PV consumes 3.9% more energy than baseline building B.

Table 8.4 Energy saving with mono-crystalline semi-transparent PV compared to baseline building A for each combination of room depth and WWR

	Electricity saving(%)									
WWR	Room depth(m)									
	4	5	6	7	8	9	10	11	12	13
0.2	58.0	56.6	55.5	54.8	54.4	54.2	54.3	54.7	55.0	55.4
0.25	51.5	50.7	50.5	50.3	50.3	50.5	50.7	51.2	51.9	52.5
0.3	52.5	51.4	50.7	50.5	50.3	50.4	50.5	50.6	51.0	51.5
0.35	51.6	50.6	49.8	49.6	49.5	49.5	49.6	49.8	50.0	50.3
0.4	51.9	50.8	49.7	48.8	48.4	48.1	47.8	47.6	47.4	47.2
0.45	51.1	50.3	49.3	48.4	47.8	47.6	47.3	47.1	47.0	46.8
0.5	51.9	51.2	50.3	49.6	49.0	48.9	48.8	48.8	48.9	49.0
0.55	50.7	50.2	49.5	48.8	48.3	48.1	48.0	48.1	48.1	48.2
0.6	51.0	50.5	49.8	49.1	48.6	48.1	48.0	48.0	48.0	48.1
0.65	51.3	50.8	50.1	49.4	48.8	48.3	48.0	48.0	48.0	48.0
0.7	51.7	51.1	50.4	49.7	49.1	48.6	48.1	48.0	48.0	48.0

Note: The green area shows the part where mono-crystalline semi-transparent PV performs better than building A

From these results, based on the comparison with baseline building B, **it can be concluded that PV façades are more suitable in short rooms or rooms with small windows.** However, this conclusion is based on baseline building B, which is consistent with the Chinese Design Standard for Energy Efficiency of Public Buildings (GB-50189-2005). **If the setting and conditions of the baseline buildings change, the suitability situation will change accordingly. The key factor is the standard that we use for the baseline buildings.**

Table 8.5 Energy saving with mono-crystalline semi-transparent PV compared to baseline building B for each combination of room depth and WWR

WWR	Electricity saving(%)									
	Room depth(m)									
	4	5	6	7	8	9	10	11	12	13
0.2	16.0	13.2	11.0	9.6	8.7	8.4	8.7	9.3	10.0	10.8
0.25	3.1	1.5	0.9	0.6	0.7	1.0	1.4	2.4	3.7	5.1
0.3	5.0	2.8	1.5	1.0	0.7	0.8	1.0	1.3	1.9	3.0
0.35	3.2	1.3	-0.3	-0.8	-1.0	-1.1	-0.7	-0.4	-0.1	0.5
0.4	3.8	1.7	-0.7	-2.4	-3.2	-3.8	-4.4	-4.8	-5.3	-5.7
0.45	2.3	0.6	-1.5	-3.3	-4.3	-4.9	-5.4	-5.8	-6.1	-6.4
0.5	3.7	2.4	0.6	-0.9	-2.0	-2.3	-2.3	-2.4	-2.3	-2.0
0.55	1.4	0.4	-1.0	-2.4	-3.3	-3.9	-3.9	-3.9	-3.7	-3.5
0.6	2.0	1.0	-0.4	-1.7	-2.9	-3.8	-4.0	-4.0	-3.9	-3.8
0.65	2.7	1.6	0.2	-1.1	-2.5	-3.3	-3.9	-4.0	-3.9	-3.9
0.7	3.4	2.2	0.8	-0.5	-1.8	-2.9	-3.8	-3.9	-4.0	-3.9

Note: The green area shows the part where mono-crystalline semi-transparent PV performs better than building B

With the energy saving of the mono-crystalline semi-transparent PV for each optimal PVR, which was discussed in Section 8.3.1, the economic saving is calculated using the electricity cost in Wuhan (0.93 RMB/kWh). Table 8.6 and 8.7 show the economical saving with mono-crystalline semi-transparent PV compared to baseline buildings A and B in different architectural combinations.

Compared to baseline building A, mono-crystalline semi-transparent PV could save 38.9-58.8 RMB/m^2 and an average of 42.8 RMB/m^2 each year. This result indicates that approximately 428,000 RMB of electricity cost was saved for an office building of 10000 m^2 floor area.

Compared to baseline building B, mono-crystalline semi-transparent PV could save 0.3-8.1 RMB/m^2 with an average of 1.8 RMB/m^2 in office rooms with less than 0.3 WWR and less than 6 m room depth. For a building of 10000 m^2 floor area, this result indicates that approximately 18,000 RMB electricity cost was saved. However, in rooms with WWR over 0.35 and room depth over 6 m, mono-crystalline semi-transparent PV consumes more energy than baseline building B with a maximum of 2.5 RMB/m^2.

Table 8.6 Economic saving with mono-crystalline semi-transparent PV compared to baseline building A for each combination of room depth and WWR

	Economic saving(RMB/m^2)									
WWR	Room depth(m)									
	4	5	6	7	8	9	10	11	12	13
0.2	58.8	54.4	51.5	49.9	49.0	48.9	49.3	50.2	51.3	52.5
0.25	45.7	43.5	42.4	41.8	41.8	42.1	42.7	43.7	44.9	46.4
0.3	47.9	45.0	43.3	42.4	42.0	42.0	42.3	42.7	43.4	44.4
0.35	46.7	44.1	42.2	41.3	40.8	40.7	40.9	41.3	41.7	42.3
0.4	47.8	44.8	42.2	40.4	39.4	38.7	38.2	37.8	37.6	37.4
0.45	46.8	44.0	41.6	39.8	38.7	38.0	37.5	37.1	36.9	36.7
0.5	48.7	45.9	43.5	41.8	40.7	40.2	39.9	39.7	39.8	40.0
0.55	47.0	44.6	42.4	40.8	39.8	39.1	38.9	38.7	38.8	38.9
0.6	48.1	45.5	43.2	41.5	40.3	39.4	39.0	38.9	38.8	38.8
0.65	49.3	46.5	44.0	42.2	40.8	39.9	39.3	39.0	38.9	38.8
0.7	50.4	47.4	44.8	42.9	41.4	40.4	39.6	39.2	39.0	38.9

Note: The green area shows the part where mono-crystalline semi-transparent PV performs better than building A

Table 8.7 Economic saving from mono-crystalline semi-transparent PV compared to baseline buildings B for each combination of room depth and WWR

	Economic saving(RMB/m^2)									
WWR	Room depth(m)									
	4	**5**	**6**	**7**	**8**	**9**	**10**	**11**	**12**	**13**
0.2	8.1	6.3	5.1	4.4	3.9	3.8	3.9	4.3	4.7	5.1
0.25	1.4	0.6	0.4	0.2	0.3	0.4	0.6	1.0	1.6	2.2
0.3	2.3	1.2	0.6	0.4	0.3	0.3	0.4	0.5	0.8	1.3
0.35	1.5	0.6	-0.1	-0.3	-0.4	-0.4	-0.3	-0.2	0.0	0.2
0.4	1.8	0.7	-0.3	-1.0	-1.3	-1.5	-1.8	-1.9	-2.1	-2.2
0.45	1.0	0.3	-0.6	-1.3	-1.7	-1.9	-2.1	-2.3	-2.4	-2.5
0.5	1.8	1.1	0.3	-0.4	-0.8	-0.9	-1.0	-1.0	-0.9	-0.8
0.55	0.7	0.2	-0.4	-1.0	-1.4	-1.6	-1.6	-1.6	-1.5	-1.4
0.6	0.9	0.4	-0.2	-0.7	-1.2	-1.6	-1.6	-1.6	-1.6	-1.5
0.65	1.3	0.7	0.1	-0.5	-1.0	-1.4	-1.6	-1.6	-1.6	-1.6
0.7	1.6	1.0	0.4	-0.2	-0.8	-1.2	-1.6	-1.6	-1.6	-1.6

Note: The green area shows the part where mono-crystalline semi-transparent PV performs better than building B

8.3.3 Amorphous-silicon semi-transparent PV façades

With the optimal WWR provided in Section 7.3, the energy saving by the optimal use of amorphous-silicon semi-transparent PV is presented in this section and compared with the baseline buildings, which were discussed in 5.4. The economic saving is also presented based on the energy saving. This result shows us the maximum benefits of amorphous-silicon semi-transparent PV glazing as office buildings' façades and its suitability under different architectural conditions.

In Table 8.8, the optimal WWR for different room depths is presented with its overall electricity consumption. The overall energy consumption of 44.2-45.8 kWh/m^2 is achieved by different optimal WWR. These figures are compared with

the overall energy consumption of baseline buildings A and B as shown in Table 8.9. A maximum saving of 47.9 kWh/m^2 is compared to baseline building A. With the increase in room depth, this value decreases to 38.2 kWh/m^2. However, compared to baseline building B, all optimal WWR fail to achieve a better performance. Amorphous-silicon semi-transparent PV consumes 4.2-23.5% more electricity than baseline building B.

Table 8.8 Overall electricity consumption of office rooms with amorphous-silicon semi-transparent PV with optimal WWR for each room depth cases

	Room depth(m)									
	4	5	6	7	8	9	10	11	12	13
Optimal WWR	0.25	0.35	0.5	0.55	0.7	0.7	0.7	0.7	0.7	0.7
Electricity consumption (kWh/m2)	45.8	44.9	44.4	44.2	44.3	44.4	44.5	44.8	45.1	45.4

Table 8.9 Energy saving with amorphous-silicon semi-transparent PV compared to baseline buildings A and B in different room depth cases

	Room depth(m)									
	4	5	6	7	8	9	10	11	12	13
Electricity saving(%) from baseline building A	47.9	46.8	46.6	44.8	45.1	43.9	42.4	40.9	39.5	38.2
Electricity saving(%) from baseline building B	-4.2	-6.4	-6.7	-10.5	-9.7	-12.2	-15.1	-18.2	-21.0	-23.5

Note: The green area shows the part where mono-crystalline semi-transparent PV performs better than the baseline buildings

Amorphous-silicon semi-transparent PV glazings appear to achieve better energy performance than traditional office buildings (baseline building A) but fail to perform better than baseline building B. **In general, amorphous-silicon semi-transparent PV façades are more suitable in short rooms (small room depth).** Again, it must be noted that if the setting and conditions of baseline buildings change, the suitability situation will change accordingly. The key factor is the standard that we use for the baseline buildings.

With the energy saving of the amorphous-silicon semi-transparent PV for each optimal WWR, the economic savings of baseline buildings A and B are calculated and presented in Table 8.10.

Table 8.10 Economic saving of mono-crystalline semi-transparent PV compared to baseline buildings A and B of rooms with optimal WWR for different room depth

	Room depth(m)									
	4	**5**	**6**	**7**	**8**	**9**	**10**	**11**	**12**	**13**
Optimal WWR	0.25	0.35	0.5	0.55	0.7	0.7	0.7	0.7	0.7	0.7
Economic saving(%) from baseline building A	54.5	47.6	41.8	39.3	37.7	36.1	34.5	34.2	35.1	36.3
Economic saving(%) from baseline building B	4.3	0.1	-2.7	-3.3	-4.1	-5.0	-6.2	-7.4	-8.5	-9.4

Compared to baseline building A, amorphous-silicon semi-transparent PV could save 36.3-54.5 RMB/m^2 with an average of 39.7 RMB/m^2 per year. This result indicates that approximately 397,000 RMB of electricity cost was saved for an office building of 10000 m^2 floor area. Compared to baseline building B, amorphous-silicon semi-transparent PV could save 4.3 RMB/m^2 and 0.1 RMB/m^2 in office rooms with room depth of 4 m and 5 m, respectively. However, for rooms over 6 m, amorphous-silicon semi-transparent PV consumes 2.7-9.4% more energy than baseline building B.

8.4. Environmental benefit of the semi-transparent PV façades

To evaluate the environmental performance of semi-transparent PV façades, two aspects are examined:

- Carbon reduction by the amount of CO_2.
- Polluted emission including SO_2, NO and carbonaceous dust.

CO_2 has major effects on global warming, which causes serious problems including meteorological disasters, sea level rising, species extinction,. SO_2, NO and carbonaceous dust are currently parts of the major air pollutions in cities and can cause health problems to humanity, particularly in China, where air pollution has become a serious problem for every major city. It has been well recgnized of the seriousness of such problem and the importance of reducing the air pollution emission from thermal power gernation plants (Yang, 2008). In another study carried out in 2012 (Zhang et al., 2012), the characteristics and sources of trace elements in PM2.5 (main air pollution factor in China) in Wuhan city is investigated. Concentrations of eleven typical trace elements in PM2.5 are analyzed by inductively coupled plasma mass spectrum-try. The results show that in Wuhan the pollution of trace elements in PM2.5 in autumn is less serious than that of summer, but more serious than that of winter. Compared with other cities of China, in Wuhan the concentrations of Zn, Mn, Cu, Pb are much higher, which are strong correlated with the steel industry in Wuhan. However, human activities also play an important part in emission of air pollutants including Ti, Se, Cd and Ni from the electricity power consumption. Gases that are produced during the electricity production by thermal power generation takes a great part of the total emission. They can be reduced by using PV façades and replacing the power demand with solar energy, which is notably clean and produces no harmful material to the environment.

In China, every produced kWh yields 0.814 kg of CO_2, 0.272 kg of carbonaceous dust, 0.03 kg of SO_2 and 0.015 kg of NO. The electricity benefit of semi-transparent PV will be translated into the reduction of each of these emissions(Yang, 2008).

Table 8.11 Emission reduction each year using mono-crystalline semi-transparent PV compared to baseline building A

	CO_2	SO_2	NO	Carbonaceous dust
Reduction Kg/m^2	36.06	1.33	0.66	12.04

The energy saving from mono-crystalline semi-transparent PV with optimal PVR is discussed and presented in 8.4.1. An average of 44.3 kWh/m^2 of electricity is saved per year compared to baseline building A. Thus, CO_2 and each polluted emission is translated from electricity saving and presented in Table 8.11. For a building with 10000 m^2 floor area, this result indicates a reduction of 360 tons of CO_2, 13.3 tons of SO_2, 6.6 tons of NO and 120 tons of carbonaceous dust.The energy saving from amorphous-silicon semi-transparent PV with optimal WWR is discussed and presented in 8.4.2. An average of 37.8 kWh/m^2 of electricity is saved per year compared to baseline building A. CO_2 emission and each polluted emission are translated from electricity saving and presented in Table 8.12.

Table 8.12 Emission reduction each year using amorphous-silicon semi-transparent PV compared to baseline building A

	CO_2	SO_2	NO	Carbonaceous dust
Reduction Kg/m^2	30.76	1.13	0.57	10.28

PBT (payback time) analysis is often used in economic and environmental assessments during the early design stages of PV roof systems (Hyoungseok et al., 2014; Sergio et al., 2007; A. et al., 2010; Masakazu et al., 2010.). This analysis is also an important method according to the Guidelines for the Economic Evaluation of BIPV of the National Renewable Energy Laboratory (NREL) (Eiffert et al., 2003). A detailed economic and environmental assessment of a PV system is very complex and involves accounting for PV panel and inverter costs, PV structures, the replacement of PV panels and inverters, maintenance costs, assurance costs,

inflation, incentives, and other factors. These products can displace traditional construction materials. As such, the added costs and embodied energy for a BIPV system (rather than the full costs) should be considered in economic assessments, including those that would be incurred regardless of the inclusion of a BIPV system, as specifically noted in the guidelines established by NREL. In a study with such method carried out in countries of Gulf cooperation council (Steve and Hassan, 2013), a range of estimated payback time between 42 to 266 years is presented, which indicates its great dependence on the energy cost price level from its location. Unfortunately, in our study, the resources available are not enough to carry out a detailed economic or environmental assessment of studied PV glazings in Wuhan.

8.5. Conclusions

In this chapter, other implications of semi-transparent PV façades in office buildings are discussed.

Other architectural factors such as room height, window height and room width are developed and incorporated into the architectural models. The overall energy consumption, which includes the PV electricity generation, heating and cooling electricity consumption and lighting electricity consumption, is simulated and presented to discover the effects of other architectural factors on the energy performance. Among the three architectural factors, the room height has the most significant effect on the overall energy consumption with a 14.6% change, followed by the room width with a 4.8% change and the window height with a 3.3% change. However, compared to PVR and WWR, these three factors have a less significant effect on the energy performance in terms of semi-transparent PV façade applications in office buildings.

The suitability of optimal PVR/WWR strategies in different architectural conditions is investigated by comparing the energy saving to baseline buildings (A and B) for each optimal PVR/WWR under different architectural conditions. The results show that mono-crystalline semi-transparent PV façades are more suitable in short rooms or rooms with small windows. Amorphous-silicon semi-transparent

PV faç ades are more suitable in short room (small room depth). However, this conclusion is based on baseline building B, which is consistent with the Chinese Design Standard for Energy Efficiency of Public Buildings (GB-50189-2005). If the setting and conditions of baseline buildings change, the suitability situation will change accordingly. The energy saving of semi-transparent PV compared to the baseline buildings is discussed and presented. Office rooms with both mono-crystalline semi-transparent PV and amorphous-silicon semi-transparent PV have much better energy performance than baseline building A. However, compare to baseline building B, mono-crystalline semi-transparent PV could only achieve a better energy performance in small WWR and room depth office rooms, and amorphous-silicon fail to perform better in all cases.

The environmental benefit of semi-transparent PV faç ades based on the carbon reduction by the amount of CO_2 and polluted emission, which includes SO_2, NO and carbonaceous dust, is presented in this chapter. The environmental benefit is also evaluated and presented using the emission reduction amount of CO_2, SO_2, NO and carbonaceous dust. The results show that the use of semi-transparent PV faç ades is notably beneficial for the air environment and may aid in reducing the air pollution problem in china.

Chapter 9 Main contributions and

Future work

In this study, with the establishment of the experimental room, the calculation models of solar irradiance on inclined surface and PV generation power based on operating temperature are developed and presented. Energy evaluation including PV generation, lighting, heating and cooling performance of semi-transparent PV façades for office buildings is provided and presented. Related calculation methods and models for semi-transparent PV façades are developed and provided in different architectural conditions. An optimizing design approach for semi-transparent PV façade by the use of optimal PVR/WWR is developed and presented.

9.1. Main contributions

The main contributions of this study can be listed as following five aspects.

(1) Establishment of the experimental room to evaluate the PV façade performance in the local climate

To evaluate the energy performance of PV façades in the realistic local climate, the experimental room with two inner and separate chambers was set up on the flat rooftop of a building in Wuhan. With smart design, skillful construction, durable measurement and careful calibration in the experimental room, the systemically measured and recorded data of environmental parameters and the parameters that are related to PV façades was verified to be effective and valid. The PV façades parameters achieved from the field experiment in this study agree reasonably well with the results of previous works of other researchers. In particularly, the establishment of the experimental room can be considered an achievement in this study because not only it provided high-quality data in the realistic local climate but also the experimental procedures and measurement techniques were developed and gained in the process.

(2) Estimation of annual power generation of PV façade in China

The calculation models of solar irradiance on an inclined surface and PV generation power based on the operating temperature are developed and validated with the measured data. The good agreements between measured results and calculated results demonstrate that the calculation models can predict annual power generation of PV façades with good accuracy. In addition, the developed and

validated calculation method in this study can be used as an easy-to-use tool in the pre-design of BIPV.

With the validated calculation methods and the typical yearly weather data of CSWD, the annual power generation of PV façades in China is calculated in parametric studies. The results show that with various cities, building orientations, building forms, materials and arrangements of PV modules, there is a distinct difference in the electrical output energy of PV façades. PV façades have maximum electrical generation in the south and minimum in the north. However, although the gap between the most favourable orientation (south) and the most unfavourable direction (north) in Beijing is relatively large, the difference of the photovoltaic power generation in Wuhan and Guangzhou is relatively small. In addition, the difference of PV electrical energy generated in rectangular, rhombus and circular building forms was slightly higher in Beijing and relatively small in the other cities. The parametric study results can serve as reference for architects, engineers and installers in the BIPV project in China.

(3) Evaluation of overall energy performance of two type of semi-transparent PV façade for office buildings in Wuhan, China

The energy evaluation based on the overall energy consumption is performed in study for two types of semi-transparent PV façades with the following main findings.

● Mono-crystalline semi-transparent PV

By evaluating the overall energy performance of mono-crystalline semi-transparent PV, we conclude that increasing PVR under the climatic conditions of central China typically decreases the PV electricity conversion efficiency and heating and cooling electricity consumption but increases the lighting electricity consumption. Temperature significantly affects the conversion efficiency. When the PVR increases, the PV electricity conversion efficiency decreases.

When the PVR increases, the indoor daylight illuminance linearly decreases, and the electricity consumption increases. Mono-crystalline semi-transparent PV façades are more suitable and can provide better lighting energy performance in

relatively short rooms, or in relatively larger-window rooms. Under the climatic conditions of central China, increasing the PVR appears to decrease the heating and cooling electricity consumption.

Compared with traditional glazings, in small WWR rooms, low PVR (below 50%) mono-crystalline semi-transparent PV glazing has a better overall energy performance than single glazing and double glazing in all room depth cases. In small WWR rooms, high PVR (above 50%) mono-crystalline semi-transparent PV glazing has a better overall energy performance than single glazing and double glazing in short rooms; however, in deep-room cases, it is worse than all traditional glazings. In small WWR rooms, the mono-crystalline semi-transparent PV glazing has a worse overall energy performance than Low-E double glazing in all cases, particularly in deep rooms. In large WWR rooms, high PVR mono-crystalline semi-transparent PV glazing was the most efficient energy performance (even better than Low-E double glazing) in certain conditions.

● Amorphous-silicon semi-transparent PV

In the parametric analysis of the overall energy performance of amorphous-silicon semi-transparent PV, the results show that there is no tangible relation between the WWR and the PV conversion efficiency. Its total amount of PV electricity output is also less significant than that of mono-crystalline semi-transparent PV. When the WWR increases, the indoor daylight illuminance linearly increases, and the electricity consumption decreases. However, because of the low visible and solar transmittance value of the amorphous-silicon layer in the PV glazing, the amorphous-silicon semi-transparent PV does not perform well in terms of indoor daylighting and lighting energy performance. Amorphous-silicon semi-transparent PV glazing is beneficial in terms of saving overall heating and cooling energy. Amorphous-silicon semi-transparent PV glazing is beneficial in terms of saving the overall heating and cooling energy. Its heating and cooling electricity consumption is relatively less than that of mono-crystalline semi-transparent PV glazing.

Compared with three traditional glazings(single glazing, double glazing and Low-E double glazing), discoveries are as follows. Amorphous-silicon

semi-transparent PV is significantly inferior to traditional glazings in terms of daylighting and lighting energy performance in all situations. In short rooms, amorphous-silicon semi-transparent PV glazing generally has a better overall energy performance than single glazing and double glazing.

(4) The development of an optimizing design approach for semi-transparent PV façade by the use of optimal PVR/WWR.

In the study, improved design approaches considering the optimal PVR (for mono-crystalline semi-transparent PV façade) and WWR (for amorphous-silicon semi-transparent PV façade) are developed.

For mono-crystalline semi-transparent PV façade, an optimal PVR can be obtained with a particular combination of WWR, room depth, and orientation. When the overall energy performance is considered, adopting the optimal PVR can result in electricity savings of up to 30% (average savings: 13%) compared to the least favourable PVR. This result demonstrates the importance of selecting optimal PVR based the on architectural conditions.

The rooms with small room depth have relatively smaller optimal PVR than rooms with lager room depth. Large WWR rooms have relatively larger optimal PVR than small WWR rooms. This result indicates that high PVR PV façades are more suitable for deep rooms with larger window and small PVR PV façades are more suitable for short rooms with small window. The building orientation can also affect the optimal ratio with changes of 5–10% according to the specific orientation, and the optimal PVR is higher in the western orientation; however, these changes are much less pronounced than those induced by the variations in WWR and room depth.

For amorphous-silicon semi-transparent PV façade, an optimal WWR (i.e., one that achieves the lowest overall electricity consumption) can be obtained for a particular combination of room depth and orientation. When the overall energy performance is considered, adopting the optimal WWR can result in electricity savings of up to 15.8% compared to the least favourable WWR, although the achieved savings vary depending on the combination of room depth at least in the south orientation. This result demonstrates the importance of selecting the optimal

WWR based on the architectural conditions. The results of optimal WWR indicate that amorphous-silicon semi-transparent PV is preferable and more practical in rooms with large windows.

(5) The suitability of optimal PVR/WWR strategies of semi-transparent PV façades

The suitability of optimal PVR/WWR strategies in different architectural conditions is investigated by comparing the energy saving to baseline buildings (A and B) for each optimal PVR/WWR under different architectural conditions. The results show that mono-crystalline semi-transparent PV façades are more suitable in short rooms or rooms with small windows. Amorphous-silicon semi-transparent PV façades are more suitable for short room (small room depth). However, this conclusion is based on baseline building B, which is consistent with the Chinese Design Standard for Energy Efficiency of Public Buildings (GB-50189-2005). If the setting and conditions of baseline buildings change, the suitability situation will change accordingly. The key factor is the standard that we use for the baseline buildings. The energy saving of semi-transparent PV compared to the baseline buildings is discussed and presented. Office rooms with both mono-crystalline semi-transparent PV and amorphous-silicon semi-transparent PV have a much better energy performance than baseline building A. However, compare to baseline building B, mono-crystalline semi-transparent PV only achieves a better energy performance in small WWR and small room depth office rooms, and amorphous-silicon fail to perform better in all cases.

9.2. Limitations and future work

Some of the assumptions made earlier in the study would lead to some technical limitations. The construction of the façades is simplified without detailed consideration of air leakage, heat bridge and other possible impacts from façades components. In a real situation, especially in a poorly built and maintained building, this could lead to a significant impact on energy performance. All the energy units relevant to the overall energy consumption are unified by electricity unit (kWh), or (kWh/m^2). The impact of better usage of passive applications without the use of electricity in buildings could have an impact on the results.

However, with the same configurations (which are also represent the most common cases of office buildings in Central China) for the study cases, the results still give a fair and consistent outcome and conclusions of how different semi-transparent PV façadess impact on general office building cases. The indoor shading methods of curtain or other shading devices are assumed not existed as semi-transparent provides a certain level of shading. However, if indoor shading is used in some particular circumstances, these shading devices could lead to significant impact on energy performance. The operation schedule of the building is a fixed assumption with same daily routines, in which people behave equally by the fractions of percentage of different activities. However, in a real case people could behave differently, for example, if there's a party planned on weekend, the activity could lead a significant change to the energy consumption.

The study of semi-transparent PV façades is mainly based on office buildings, but the application of PV façades to other types of buildings such as hotel and residential buildings are also important. Buildings of different functions have different energy consumption demands and different times when the consumption occurs. For example, residential buildings mainly function at night time, which is completely different from office buildings. Thus, other types of buildings should be included in the future study.

Semi-transparent PV façades with single glazing were thoroughly studied. However, other types of glazing such as double-glazing PV were not included in this study. Double glazing is currently commonly used in buildings, and the potential of semi-transparent PV double-glazing façades is notably promising because they provide better thermal performance than single glazing. To demonstrate a sense of the difference of energy performance between single glazing, double glazing and Low-E double glazing, three typical models of which are established with Energy Plus (same settings as described in chapter 5) operated on a CSWD weather data of Wuhan (whole year); properties of each glazing is shown in table 9.1, scheme diagram of which is shown in figure 9.1. By doing so , overall energy consumption of each glazing is calculated and shown in table 9.2. The energy performance of double glazing is approximately 5% better than that of single glazing, of which the Low-E double glazing is 21% better. A further study of

double PV glazing can proceed based on the existing experiment rooms with the developed calculation models and methods, in which we expect a better energy performance on cooling and heating energy consumption, however how much better is the question and needs to be further studied; The advantage of PV glazing could be even more prominent in semi-transparent double glazing PV façades.

Table 9. 1 Properties of the studied glazings

Glazing	U-value(W/m^{2}K)	Visible transmittance	SHGC
Single glazing	5.8	0.87	0.87
Double glazing	2.8	0.71	0.75
Low-E double glazing	1.9	0.62	0.45

Note: Data obtained from "Calculation specification for thermal performance of windows, doors and glass curtain-walls" (JGJ/T 151-2008) (MHUDC, 2008)
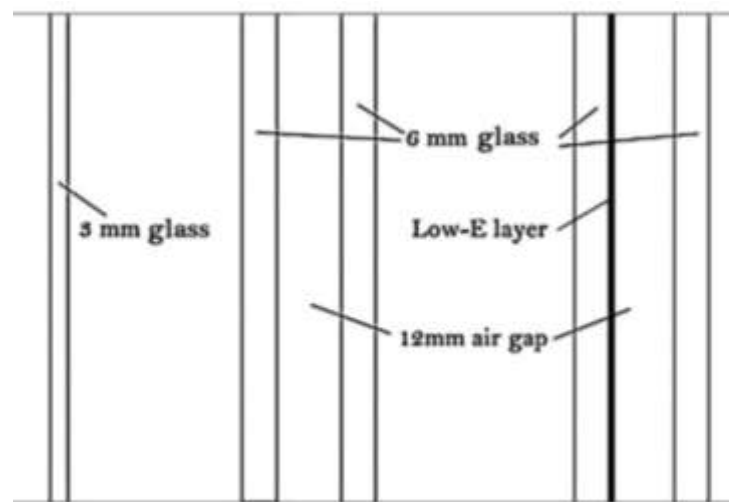
Figure 9.1 Scheme of the glazing; single glazing(left), double glazing(middle), Low-E double glazing(right).

Table 9.2 Average energy consumption of each glazing

Glazing	Energy consumption			Overall energy performance
	Lighting	Heating	Cooling	
Single glazing (with shading slab)	18.3	4.3	68.5	91.1
Double glazing (with shading slab)	18.5	2.2	66.2	86.8
Low-E double glazing (with shading slab)	18.6	4.3	48.7	71.6

kWh/m^2

In urban environment, shadows from other buildings will have a major effect on the solar irradiation distribution on building façades. The effect of urban environment should be included in the future study. This speculation is particularly true in China because most cities in the country, including minor cities, have high population densities and many high-rise buildings, which create complex shadow. The use of solar energy technology on building façades in these urban areas is challenging and should be included in future work.

Papers Arising from This Thesis

1. **Xu, S.**, Liao W., Huang J. and Kang J. (2014). Optimal PV cell coverage ratio for semi-transparent photovoltaics on office building façades in central China. *Energy and Buildings* 77 (0): 130-138. (SCI journal paper, published)

2. **Xu S.**, Hu Z.M., Kang J. and Liao W. Estimation on annual power generation of PV façades in China. Submit to *Journal of Harbin Institute of Technology (New Series)*. (EI journal paper, accepted)

3. **Xu S.**, Kang J. Liao W. and Huang J. Suitability of semi-transparent PV façades for energy efficient office buildings in central China. Submit to *Architectural Journal*. [in Chinese] (in preparation)

References

Alonso-Abella, M., Chenlo, F., Nofuentes, G., and Torres-Ramírez, M. (2014). Analysis of spectral effects on the energy yield of different PV (photovoltaic) technologies: The case of four specific sites. *Energy*, 67(0), 435-443.

Andolsun, S., Culp, C. H., Haberl, J., and Witte, M. J. (2011). EnergyPlus vs. DOE-2.1e: The effect of ground-coupling on energy use of a code house with basement in a hot-humid climate. Energy and Buildings, 43(7), 1663-1675.

A. S., J. U., Varun. (2010) Life cycle assessment of solar PV based electricity generation systems: A review. Renewable and Sustainable Energy Reviews, 14(1), 540-544.

Balenzategui, J. L. (1999). SRADLIB: AC Library for Solar Radiation Modelling. Informes técnicos Ciemat, Madrid, 904.

Becker, C., Amkreutz, D., Sontheimer, T., Preidel, V., Lockau, D., Haschke, J., Jogschies, L., Klimm, C., Merkel, J. J., Plocica, P., Steffens, S., and Rech, B. (2013). Polycrystalline silicon thin-film solar cells: Status and perspectives. Solar Energy Materials and Solar Cells, 119(0), 112-123.

Birol, F. (2010). World energy outlook 2010. International Energy Agency. <http://www.worldenergyoutlook.org> [accessed 07 June 2011]

Boyano, A., Hernandez, P., and Wolf, O. (2013). Energy demands and potential savings in European office buildings: Case studies based on EnergyPlus simulations. Energy and Buildings, 65(0), 19-28.

Brennan, J. (2014). Sustainability Hub. U-values: definition and calculation< http://www.architecture.com/SustainabilityHub/Designstrategies/Earth/1-1-1-10-Uvalues(INCOMPLETE).aspx >[accessed 11 March 2014]

Carmody, J., Selkowitz, S., Lee, E., Arasteh, D., Willmert, T. (2004). Window systems for high-performance buildings. W.W. Norton & Company, New York.

Chao, S. C. (1986). Physical geography of China. Science Press, New York.

Charron, R., and Athienitis, A. K. (2006). Optimization of the performance of double-façades with integrated photovoltaic panels and motorized blinds. Solar Energy, 80(5), 482-491.

Chen, B. (2012). Energy and Resources .China's PV industry urges for commercialization < http://www.china.org.cn/business/2012-04/13/content_25137463.htm > [Accessed 07 Oct 2012]

China Academic of Building Research. (2008). Standard for Lighting Design of Buildings. China Architectural & Building Press, Beijing.

China Academic of Building. (2004). Research Design Standard for Energy Efficiency of Public Buildings. China Architectural & Building Press, Beijing.

China Meteorological Bureau, Climate Information Center, Climate Data Office and Tsinghua University, Department of Building Science and Technology. (2005). China Standard Weather Data for Analyzing Building Thermal Conditions. China Architecture and Building Press, Beijing. [in Chinese]

China State Bureau of Technical Supervision, and Ministry of Construction of China. (1993). National Standard of China: Thermal design code for civil building GB 50176-93. China Planning Press, Beijing. [in Chinese]

Ciulla, G., Lo Brano, V., Di Dio, V., and Cipriani, G. (2014). A comparison of different one-diode models for the representation of I–V characteristic of a PV cell. Renewable and Sustainable Energy Reviews, 32(0), 684-696.

Crawley, D. B., Lawrie, L. K., Winkelmann, F. C., Buhl, W. F., Huang, Y. J., Pedersen, C. O., Strand, R. K., Liesen, R. J., Fisher, D. E., Witte, M. J., and Glazer, J. (2001). EnergyPlus: creating a new-generation building energy simulation program. Energy and Buildings, 33(4), 319-331.

DOE. (2014). EnergyPlus Energy Simulation Software. Weather Data: All regions: Asia WMO Region 2: China<http://apps1.eere.energy.gov/buildings/energyplus/cfm/weather_data3.cfm/region=2_asia_wmo_region_2/country=CHN/cname=China>[accessed 12 March 2014]

Duffie, J. A. and Beckman W. A. (1980). Solar Engineering of Thermal Processes. John Wiley & Sons, New York.

Eiffert P. (2003). Guidelines for the economic evaluation of building-integrated photovoltaic power systems. In: International energy agency PVPS task 7: photovoltaic power systems in the built environment. National Renewable Energy Laboratory.

Evans, D. L. (1981). Simplified method for predicting photovoltaic array output. Solar energy, 27(6), 555-560.

Fung, T. Y., and Yang, H. (2008). Study on thermal performance of semi-transparent building-integrated photovoltaic glazings. Energy and Buildings, 40(3), 341-350.

Garcia, A., and Balenzategui, J. L. (2004). Estimation of photovoltaic module yearly temperature and performance based on nominal operation cell temperature calculations. Renewable Energy, 29(12), 1997-2010.

Gevorkian, P. (2007). Solar Power in Building Design (Green Source): The Engineer's Complete Project Resource. McGraw-Hill Professional, New York.

Ghadimi, M., Ghadamian, H., Hamidi, A. A., Shakouri, M., and Ghahremanian, S. (2013). Numerical analysis and parametric study of the thermal behavior in multiple-skin façades. Energy and Buildings, 67(0), 44-55.

Goetzberger, A., and Hebling, C. (2000). Photovoltaic materials, past, present, future. Solar Energy Materials and Solar Cells, 62(1–2), 1-19.

Goia, F., Bianco, L., Perino, M., and Serra, V. (2014). Energy Performance Assessment of and Advanced Integrated Façade through Experimental Data Analysis. Energy Procedia, 48(0), 1262-1271.

Gracin, D., Siketić, Z., Juraić, K., and Čeh, M. (2013). Analysis of amorphous-nanocrystalline silicon thin films by time-of-flight elastic recoil detection analysis and high-resolution electron microscopy. Applied Surface Science, 275(0), 19-22.

Hall, I. J., Prairie, R. R., Anderson, H. E. and Boes, E. C. (1978). Generation of a typical meteorological year. Proc. of the 1978 Annual Meeting of the American Section of the International Solar Energy Society. Denver, 669-671.

Han, J., Lu, L., Peng, J., and Yang, H. (2013). Performance of ventilated double-sided PV façade compared with conventional clear glass façade. Energy and Buildings, 56(0), 204-209.

Hart, G. W., and Raghuraman, P. (1982). Simulation of thermal aspects of residential photovoltaic systems. NASA STI/Recon Technical Report N, 83, 12555.

Hausladen, G., de Saldanha, M., and Liedl, P. (2008). ClimateSkin: Building-skin Concepts that Can Do More with Less Energy. Birkhäuser, Basel.

Hay, J. E. (1979). Calculation of monthly mean solar radiation for horizontal and inclined surfaces. Solar Energy, 23(4), 301-307.

Hay, J. E., and Davies, J. A. (1980). Calculation of the solar radiation incident on an inclined surface. In Proc. of First Canadian Solar Radiation Data Workshop, Ministry of Supply and Services Canada, 59(0), 59-72.

Hindrichs, D. U., and Daniels, K. (2007). Plusminus 20/40 latitude: sustainable building design in tropical and subtropical regions. Axel Menges, Stuttgart .

Hoang, P., Bourdin, V., Liu, Q., Caruso, G., and Archambault, V. (2014). Coupling optical and thermal models to accurately predict PV panel electricity production. Solar Energy Materials and Solar Cells, 125(0), 325-338.

Hong, T. (2009). A close look at the China Design Standard for Energy Efficiency of Public Buildings. Energy and Buildings, 41(4), 426-435.

Hong, T., Chou, S. K., and Bong, T. Y. (2000). Building simulation: an overview of developments and information sources. Building and environment, 35(4), 347-361.

Hoover, E. R. (1980). SOLCEL-II: An improved photovoltaic system analysis program (No. SAND-79-1785). Sandia Labs., Albuquerque, NM.

Hua, C., and Shen, C. (1998). Comparative study of peak power tracking techniques for solar storage system. Applied Power Electronics Conference and Exposition, 2, 679-685.

Hui, S. C., and Lam, J. C. (1992). Test reference year (TRY) for comparative energy study. Hong Kong Engineer, 20(2), 13-16.

Huld, T., Friesen, G., Skoczek, A., Kenny, R. P., Sample, T., Field, M., and Dunlop, E. D. (2011). A power-rating model for crystalline silicon PV modules. Solar Energy Materials and Solar Cells, 95(12), 3359-3369.

Hussein, K. H., Muta, I., Hoshino, T., and Osakada, M. (1995). Maximum photovoltaic power tracking: an algorithm for rapidly changing atmospheric conditions. IEE Proceedings-Generation, Transmission and Distribution, 142(1), 59-64.

Hyoungseok K., Kyounghoon C., Vasilis F., Parikhit S., Tak H. (2014). Life cycle assessment of cadmium telluride photovoltaic (CdTe PV) systems. Solar Energy, 103, 78-88.

IEC. (2006). Standard IEC 60904-1: Photovoltaic Devices. Part 1: Measurement of Photovoltaic Current–Voltage Characteristics. International Electrotechnical Commission, Geneva, Switzerland.

IEC. (2007). Standard IEC 60904-9: Photovoltaic Devices. Part 9: Solar Simulator Performance Requirements. International Electrotechnical Commission, Geneva, Switzerland.

IEC. (2008a). Standar IEC 61646: Thin-film photovoltaic (PV) modules – Desing qualification and typ approbal. International Electrotechnical Commission, Geneva, Switzerland.

IEC. (2008b). Standard IEC 60904-3.: Photovoltaic devices. Part 3: Measurement Principles for Terrestrial Photovoltaic (PV) Solar Devices With Reference Spectral Irradiance Data. International Electrotechnical Commission, Geneva, Switzerland.

Infield, D., Eicker, U., Fux, V., Mei, L., and Schumacher, J. (2006). A simplified approach to thermal performance calculation for building integrated mechanically ventilated PV façades. Building and Environment, 41(7), 893-901.

Iqbal, M. (1983). An introduction to solar radiation. Academic Press, New York.

Ishaque, K., Salam, Z., and Taheri, H. (2011). Modeling and simulation of photovoltaic (PV) system during partial shading based on a two-diode model. Simulation Modelling Practice and Theory, 19(7), 1613-1626.

Jaber, S., and Ajib, S. (2011). Thermal and economic windows design for different climate zones. Energy and Buildings, 43(11), 3208-3215.

Jiang, B., Ji, J., and Yi, H. (2008). The influence of PV coverage ratio on thermal and electrical performance of photovoltaic-Trombe wall. Renewable Energy, 33(11), 2491-2498.

Jin, Q., and Overend, M. (2014). Sensitivity of façade performance on early-stage design variables. Energy and Buildings, 77(0), 457-466.

Kamthania, D., and Tiwari, G. N. (2014). Energy metrics analysis of semi-transparent hybrid PVT double pass façade considering various silicon and non-silicon based PV module Hyphen is accepted. Solar Energy, 100, 124-140.

Klein, S. A. and Beckman W.A. (1993). PV F-Chart User's Manual: Windows Version. F-Chart Software, 4406 Fox Bluff Road, Middleton, Wisc. 53562, Accessed on March 4, 2014，from www.fchart.com.

Klein, S. A., University of Wisconsin—Madison. Solar Energy Laboratory. (1979). TRNSYS, a transient system simulation program. Solar Energy Laboratory, University of Wisconsin—Madison.

Klems, J. H. (1988). Measurement of fenestration net energy performance: considerations leading to development of the Mobile Window Thermal Test (MoWitt) facility. Journal of solar energy engineering, 110(3), 208-216.

Klems, J. H. (1988b). U-values, solar heat gain, and thermal performance: Recent studies using the MoWiTT. Lawrence Berkeley Laboratory.

Klems, J., and Keller, H. (1987). Measurement of Single and Double Glazing Thermal Performance Under Realistic Conditions Using the Mobile Window Thermal Test (MOWITT) Facility. Solar Engineering, 1, 424-430.

Kottas, T. L., Boutalis, Y. S., and Karlis, A. D. (2006). New maximum power point tracker for PV arrays using fuzzy controller in close cooperation with fuzzy cognitive networks. Energy Conversion, 21(3), 793-803.

Lam, J. C., Hui, S. C. M. and Yuen, R. K. K. (1992). Typical weather year for building energy simulation in Hong Kong. Hong Kong Meteorological Society Bulletin, 2 (1): 36-44.

Lam, J. C., Li, D. H. W., and Cheung, S. O. (2003). An analysis of electricity end-use in air-conditioned office buildings in Hong Kong. Building and Environment, 38(3), 493-498.

Leal, V., and Maldonado, E. (2008). The role of the PASLINK test cell in the modelling and integrated simulation of an innovative window. Building and Environment, 43(2), 217-227.

Leite Didoné, E., and Wagner, A. (2013). Semi-transparent PV windows: A study for office buildings in Brazil. Energy and Buildings, 67(0), 136-142.

Li, D. H. W., Cheung, G. H. W., Cheung, K. L., and Lam, T. N. T. (2010). Determination of vertical daylight illuminance under non-overcast sky conditions. Building and Environment, 45(2), 498-508.

Li, D. H. W., Lam, T. N. T., Chan, W. W. H., and Mak, A. H. L. (2009). Energy and cost analysis of semi-transparent photovoltaic in office buildings. Applied Energy, 86(5), 722-729.

Li, H., Lian, Y., Wang, X., Ma, W., and Zhao, L. (2011). Solar constant values for estimating solar radiation. Energy, 36(3), 1785-1789.

Li, J., Dou, W., Xu, Z., Peng, Y., and Xu, H. (2007). Research on MPPT methods of photovoltaic power generation system. Acta Energiae Solaris Sinica, 28(3), 268-273.[in Chinese]

Li, J., Wang, S., Zhang, M. J., and Ma, L. J. (2007). China solar PV report-2007.China Environmental Science Press, Beijing.

Lim, J. W., Lee, S. H., Lee, D. J., Lee, Y. J., and Yun, S. J. (2013). Performances of amorphous silicon and silicon germanium semi-transparent solar cells. Thin Solid Films, 547(0), 212-215.

Liu, B., and Jordan, R. (1962). Daily insolation on surfaces tilted towards equator. Trans ASHRAE, 67.

Lu, L., and Law, K. M. (2013). Overall energy performance of semi-transparent single-glazed photovoltaic (PV) window for a typical office in Hong Kong. Renewable Energy, 49(0), 250-254.

Lukač, N., and Žalik, B. (2013). GPU-based roofs' solar potential estimation using LiDAR data. Computers & Geosciences, 52, 34-41.

Lv, F. (2012). Workshop Presentations. Perspectives for a post-FiT regulatory framework in China < http://iea-pvps.org/index.php?id=15&no_cache=1&tx_damfrontend_pi1%5B showUid%5D=1257&tx_damfrontend_pi1%5BbackPid%5D=15&tx_damfro ntend_pi1%5Bpointer%5D=5 >[accessed 21 May 2014]

Marion, B., and Anderberg, M. (2000). PVWATTS-an online performance calculator for grid-connected PV systems. In Proceedings of the solar conference,119-124. Lakewood, U.S. October 14-17, 2001.

Masakazu I., Keiichi K., Kosuke K. (2010). Life-cycle analyses of very-large scale PV systems using six types of PV modules. Current Applied Physics, 10(2), 271-273.

Mateus, N. M., Pinto, A., and Graça, G. C. D. (2014). Validation of EnergyPlus thermal simulation of a double skin naturally and mechanically ventilated test cell. Energy and Buildings, 75(0), 511-522.

Mei, L., Infield, D., Eicker, U., and Fux, V. (2003). Thermal modelling of a building with an integrated ventilated PV façade. Energy and buildings, 35(6), 605-617.

Menicucci, D. F., and Fernandez, J. P. (1989). User's manual for PVFORM: A photovoltaic system simulation program for stand-alone and grid-interactive applications (No. SAND-85-0376). Sandia National Labs., Albuquerque, NM.

Mermoud, A. (1995). Use and validation of PVSYST, a user-friendly software for PV-system design. In 13th European photovoltaic solar energy conference, Nice, 736-739.

Ministry of Housing and Urban-rural Development of China. (2008). Calculation Specification for Thermal Performance of Windows, Doors and Glass Curtain-walls. China Architectural & Building Press, Beijing.

Miyazaki, T., Akisawa, A., and Kashiwagi, T. (2005). Energy savings of office buildings by the use of semi-transparent solar cells for windows. Renewable Energy, 30(3), 281-304.

Motuziene, V., and Juodis, E. S. (2010). Simulation based complex energy assessment of office building fenestration. Journal of civil Engineering and management, 16(3), 345-351.

Nalanie, M. (2014). Academia.edu. Semi-Transparent Building-Integrated Photovoltaic Windows: Potential Energy Savings of Office Buildings in Tropical Singapore <http://www.academia.edu/3146904/Semi-transparent_building_integrated_Photovoltaic_Windows_Potential_energy_savings_of_office_buildings_in_tropical_Singapore> [accessed 03 April 2014]

NCC. (1976). Test Reference Year (TRY) Tape Reference Manual. TD-9706. National Climatic Center, Asheville.

NCC. (1981). Typical Meteorological Year User Manual. TD-9734. Hourly Solar Radiation—Surface Meteorological Observations. National Climatic Center, Asheville.

NDRC (National Development and Reform Commission). (2011). Notice on Improving the Policy Regarding Feed-in Tariff for Solar PV Generation. <http://www.ndrc.gov.cn/zcfb/zcfbtz/2011tz/t20110801_426501.htm> [accessed 12 October 2011][in Chinese]

NDRC (National Development and Reform Commission). (2013). Notice on Promoting the Healthy Development of Solar PV Industry through Price Leverage <http://www.sdpc.gov.cn/zfdj/jggg/dian/t20130830_56127.htm>[accessed 12 September 2013] [in Chinese]

NEA. (2012a). The 12th Five-Year Plan for Solar Energy Development <http://zfxxgk.nea.gov.cn/auto87/ 201209/P020120912536329466033.pdf> [accessed 13 October 2013] [in Chinese]

NEA. (2012b). Notice on Application for Scaling Up Demonstration Zones for Distributed Solar Power <http://zfxxgk.nea.gov.cn/auto87/201209/t20120928_1513.htm> [accessed 14 October 2013] [in Chinese]

NEA. (2013). Notice on the Construction of Scaling Up Demonstration Zones for Distributed Solar Power

<http://www.cnre.info/zcfg/gnzc/tyn/2013-08-22-2915.html>[accessed   04 September 2013] [in Chinese]

Ng, P. K., Mithraratne, N., and Kua, H. W. (2013). Energy analysis of semi-transparent BIPV in Singapore buildings. Energy and Buildings, 66(0), 274-281.

Noorian, A. M., Moradi, I., and Kamali, G. A. (2008). Evaluation of 12 models to estimate hourly diffuse irradiation on inclined surfaces. Renewable Energy, 33(6), 1406-1412.

Norton, B., Eames, P. C., Mallick, T. K., Huang, M. J., McCormack, S. J., Mondol, J. D., and Yohanis, Y. G. (2011). Enhancing the performance of building integrated photovoltaics. Solar Energy, 85(8), 1629-1664.

OFweek Research. (2012). Global solar PV industries on road <http://www.doc88.com/ p-680406267386.html> [accessed 07 October 2012]

Olivieri, L., Caamaño-Martin, E., Olivieri, F., and Neila, J. (2014). Integral energy performance characterization of semi-transparent photovoltaic elements for building integration under real operation conditions. Energy and Buildings, 68, Part A(0), 280-291.

Olivieri, L., Caamaño-Martin, E., Olivieri, F., and Neila, J. (2014). Integral energy performance characterization of semi-transparent photovoltaic elements for building integration under real operation conditions. Energy and Buildings, 68, Part A(0), 280-291.

Parida, B., Iniyan, S., and Goic, R. (2011). A review of solar photovoltaic technologies. Renewable and Sustainable Energy Reviews, 15(3), 1625-1636.

Peng, C., Huang, Y., and Wu, Z. (2011). Building-integrated photovoltaics (BIPV) in architectural design in China. Energy and Buildings, 43(12), 3592-3598.

Petter Jelle, B., Breivik, C., and Drolsum Røkenes, H. (2012). Building integrated photovoltaic products: A state-of-the-art review and future research opportunities. Solar Energy Materials and Solar Cells, 100(0), 69-96.

Pissimanis, D., Karras, G., Notaridou, V., and Gavra, K. (1988). The generation of a "typical meteorological year" for the city of Athens. Solar Energy, 40(5), 405-411.

Poirazis, H., Blomsterberg, Å., and Wall, M. (2008). Energy simulations for glazed office buildings in Sweden. Energy and Buildings, 40(7), 1161-1170.

Posadillo, R., and López Luque, R. (2009). Evaluation of the performance of three diffuse hourly irradiation models on tilted surfaces according to the utilizability concept. Energy Conversion and Management, 50(9), 2324-2330.

Reindl, D. T., Beckman, W. A., and Duffie, J. A. (1990). Evaluation of hourly tilted surface radiation models. Solar Energy, 45(1), 9-17.

Rempel, A. R., Rempel, A. W., Cashman, K. V., Gates, K. N., Page, C. J., and Shaw, B. (2013). Interpretation of passive solar field data with EnergyPlus models: Un-conventional wisdom from four sunspaces in Eugene, Oregon. Building and Environment, 60(0), 158-172.

RIBA. (2014). Efficient windows. Measuring Performance: Solar Heat Gain Coefficient (SHGC) <http://efficientwindows.org/shgc.php > [accessed 11 March 2014]

Roberts, S., and Guariento, N. (2009). Building Integrated Photovoltaics: A Handbook. Birkhäuser Verlag AG, Berlin.

Roberts, S., and Guariento, N. (2009). Building Integrated Photovoltaics: A Handbook. Birkhäuser Verlag AG, Berlin.

Rozario, J., Vora, A. H., Debnath, S. K., Pathak, M. J. M., and Pearce, J. M. (2014). The effects of dispatch strategy on electrical performance of amorphous silicon-based solar photovoltaic-thermal systems. Renewable Energy, 68(0), 459-465.

Saridar, S., and Elkadi, H. (2002). The impact of applying recent façade technology on daylighting performance in buildings in eastern Mediterranean. Building and Environment, 37(11), 1205-1212.

Sastry, O. S., Saurabh, S., Shil, S. K., Pant, P. C., Kumar, R., Kumar, A., and Bandopadhyay, B. (2010). Performance analysis of field exposed single crystalline silicon modules. Solar Energy Materials and Solar Cells, 94(9), 1463-1468.

Sergio P., Deepak S., Gregory K. (2007). Parameters affecting the life cycle performance of PV technologies and systems. Energy Policy, 35(6), 3316-3326.

Serra, V., Zanghirella, F., and Perino, M. (2010). Experimental evaluation of a climate façade: Energy efficiency and thermal comfort performance. Energy and Buildings, 42(1), 50-62.

Shen, H., and Zeng, Z. (2005). Photovoltaic Technology. Chemical Industry Press, Beijing.

Siurna, D. L., D'Andrea, L. J., and Hollands, K. G. T. (1984). A Canadian representative meteorological year for solar system simulation. In Processdings 10th annual conference of the Solar Energy Society of Canada. Alberta, 85-88, August 2-6, 1984.

Skoplaki, E., and Palyvos, J. A. (2009). On the temperature dependence of photovoltaic module electrical performance: A review of efficiency/power correlations. Solar energy, 83(5), 614-624.

Smart, M. G., and Ballinger, J. A. (1984). Fourier-synthesized weather data for building energy use estimation. Building and Environment, 19(1), 41-48.

Solomon, S., Qin, D., Manning, M., Chen, Z., Marquis, M., Averyt, K.B., Tignor, M., and Miller, H.L. (2007). Climate Change 2007 - the Physical Science Basis: Working Group I Contribution to the Fourth Assessment Report of the IPCC. Cambridge University Press, Cambridge.

Sonnenenergie, D. G. (2008). Planning and Installing Photovoltaic Systems: A Guide for Installers, Architects and Engineers. James & James/Earthscan, London.

Steve S, Hassan R. (2013). Assessing the technical and economic performance of building integrated photovoltaics and their value to the GCC society. Renewable Energy, 55, 150-159.

Strachan, P. A. (2008). Simulation support for performance assessment of building components. Building and Environment, 43(2), 228-236.

Strachan, P. A., and Vandaele, L. (2008). Case studies of outdoor testing and analysis of building components. Building and Environment, 43(2), 129-142.

Sun, X., Wu, W., Li, X., and Zhao, Q. (2002). A research on photovoltaic energy controlling system with maximum power point tracking. Power Conversion Conference, 2, 822-826.

Susorova, I., Tabibzadeh, M., Rahman, A., Clack, H. L., and Elnimeiri, M. (2013). The effect of geometry factors on fenestration energy performance and energy savings in office buildings. Energy and Buildings, 57, 6-13.

Tabares-Velasco, P. C., Christensen, C., and Bianchi, M. (2012). Verification and validation of EnergyPlus phase change material model for opaque wall assemblies. Building and Environment, 54(0), 186-196.

Taleb, H. M., and Pitts, A. C. (2009). The potential to exploit use of building-integrated photovoltaics in countries of the Gulf Cooperation Council. Renewable Energy, 34(4), 1092-1099.

Temps, R. C., and Coulson, K. L. (1977). Solar radiation incident upon slopes of different orientations. Solar Energy, 19(2), 179-184.

Torres Lobera, D., and Valkealahti, S. (2013). Dynamic thermal model of solar PV systems under varying climatic conditions. Solar Energy, 93(0), 183-194.

Vartiainen, E. (2000). A new approach to estimating the diffuse irradiance on inclined surfaces. Renewable Energy, 20(1), 45-64.

Vartiainen, E. (2001). Electricity benefits of daylighting and photovoltaics for various solar façade layouts in office buildings. Energy and Buildings, 33(2), 113-120.

Wawer, P., Müller, J., Fischer, M., Engelhart, P., Mohr, A., and Petter, K. (2011). Latest Trends in Development and Manufacturing of Industrial, Crystalline Silicon Solar-Cells. Energy Procedia, 8(0), 2-8.

Weller, B., Hemmerle, C., Jakubetz, S., and Unnewehr, S. (2010). Detail Practice: Photovoltaics: Technology, Architecture, Installation, Birkhäuser Verlag AG, Basel.

Wong, P. W., Shimoda, Y., Nonaka, M., Inoue, M., and Mizuno, M. (2005). Field Study and Modeling of Semi-Transparent PV in Power, Thermal and Optical Aspects. Journal of Asian Architecture and Building Engineering 4 (2), 549-556.

Wong, P. W., Shimoda, Y., Nonaka, M., Inoue, M., and Mizuno, M. (2008). Semi-transparent PV: Thermal performance, power generation, daylight modelling and energy saving potential in a residential application. Renewable Energy, 33(5), 1024-1036.

Xie, H., Yu, Z., and Wu, J. (2011). The Current Situation and Problems in China's Building Energy Efficiency. Procedia Engineering, 21(0), 1145-1151.

Xu, H. (2012). Status and trends of PV industry and technology in China <http://apps1.eere.energy.gov/solar/newsletter/pdfs/01_statusandtrendsofpvinchina_xuhonghua_s.pdf> [accessed 07 October 2012]

Xu, H., Dou, C., Wang, S., and Lv, F. (2011). National survey report on PV power application in China < http://iea-pvps.org/index.php?id=93&tx_damfrontend_pi1=&tx_damfrontend_pi1[catPlus]=&tx_damfrontend_pi1[catEquals]=&tx_damfrontend_pi1[catMinus]=&tx_damfrontend_pi1[catPlus_Rec]=87&tx_damfrontend_pi1[catMinus_Rec]=&tx_damfrontend_pi1[treeID]=201&tx_damfrontend_pi1[id]=93 >[accessed 05 May 2011]

Yang, L., Lam, J. C., and Liu, J. (2007). Analysis of typical meteorological years in different climates of China. Energy Conversion and Management, 48(2), 654-668.

Yang. (2008). Analysis of potential for CO_2 mitigation by photovoltaic systems. Collection Theses of the 10th Solar Conference of China, 05, 845-849.

Yao, R., Li, B., and Steemers, K. (2005). Energy policy and standard for built environment in China. Renewable Energy, 30(13), 1973-1988.

Ye, Z., Nobre, A., Reindl, T., Luther, J., and Reise, C. (2013). On PV module temperatures in tropical regions. Solar Energy, 88, 80-87.

Yu, G. J., Jung, Y. S., Choi, J. Y., and Kim, G. S. (2004). A novel two-mode MPPT control algorithm based on comparative study of existing algorithms. Solar Energy, 76(4), 455-463.

Yu, J., Yang, C., Tian, L., and Liao, D. (2009). Evaluation on energy and thermal performance for residential envelopes in hot summer and cold winter zone of China. Applied Energy, 86(10), 1970-1985.

Yun, G. Y., McEvoy, M., and Steemers, K. (2007). Design and overall energy performance of a ventilated photovoltaic façade. Solar Energy, 81(3), 383-394.

Zhang, J., and Lin, Z. (1992). Climate of China. John Wiley & Sons, New York.

Zhang, Z. X. (1995). Energy conservation in China: an international perspective. *Energy Policy*, 23(2), 159-166.

Zhang, X., Zhao, X., Smith, S., Xu, J., and Yu, X. (2012). Review of R&D progress and practical application of the solar photovoltaic/thermal (PV/T) technologies. Renewable and Sustainable Energy Reviews, 16(1), 599-617.

Zhang F., Cheng H., Wang Z., Chen H. and Liu J.(2012). Pollution characteristics and sources analysis of trace elements in PM2.5 in Wuhan City. Engineering Journal of Wuhan University, 45(06), 755-761.

Appendix A: The images of experimental room set-up and experimental process

A1-A5: The construction process of the experimental room

B1-B8: Various types of the semi-transparent PV glazings on the façades

C1-C7: The equipment and measurement process in the field experiment

No.	Image	Description
A1		The bottom frame of the experimental room
A2		The steel frame of the experimental room

A3   The construction process (I)

A4   The construction process (II)

A5   The construction process (III)

B1

The outside view of mono-crystalline semi-transparent PV glazing

B2

The inside view of mono-crystalline semi-transparent PV glazing

B3

The installation of mono-crystalline semi-transparent PV glazing

B4

The outside view of the experimental façades (I)

B5

The outside view of the experimental façades (II)

B6

The installation of amorphous-silicon semi-transparent PV glazing

B7

The outside view of amorphous-silicon opaque PV glazing

B8

The inside view of amorphous-silicon opaque PV glazing

C1

The pyranometer with shading ring on the roof

C2 — The group of pyranometers on the roof

C3 — The outside luxmeter on the roof and and the pyranometer on the east façade

C4 — The luxmeter inside the experimental room

C5

The power recorder and data logger inside the experimental room

C6

Fixing the thermocouple on outside surface of PV glazing

C7

The measurement of the transmittance of the amorphous-silicon semi-transparent PV glazing

Appendix B: Optimal PV cell coverage ratio for semi-transparent photovoltaics on office building façades in central China

Optimal PV cell coverage ratio for semi-transparent photovoltaics on office building façades in central China

CrossMark

Shen Xu [a,b], Wei Liao [b], Jing Huang [b], Jian Kang [a,*]

[a] School of Architecture, University of Sheffield, Arts Tower, Western Bank, Sheffield S10 2TN, UK
[b] School of Architecture and Urban Planning, Huazhong University of Science and Technology, 1037 Luoyu Road, Wuhan, China

ARTICLE INFO

ABSTRACT

The present study investigates the optimal PV cell coverage ratio in terms of the overall energy consumption of office buildings in central China for which semi-transparent photovoltaic façades have been implemented, with various combinations of architectural variables including room depth, window-to-wall ratio (WWR), and orientation. Here, models and methods are established for the calculation of PV cell coverage ratio for a single-glazed semi-transparent PV façade and these models and methods are validated through field experiments. The established techniques are then incorporated into Energy Plus to perform a parametric analysis of the effects of different PV cell coverage ratios on overall energy consumption. The results show that PV cell coverage ratio has a pronounced effect on electricity consumption and that its impact is influenced by different combinations of room depth, WWR, and orientation. Moreover, the selection of an optimal PV cell coverage ratio is found to be an important element of the design approach in building-integrated PV (BIPV) systems: use of the optimal PV cell coverage ratio can achieve overall energy consumption savings of 13% (on average) compared to the least favourable PV cell coverage ratio.

© 2014 Elsevier B.V. All rights reserved.

1. Introduction

In recent years, interest in low-carbon development and renewable energy applications in buildings has increased considerably [1]. In particular, building-integrated photovoltaic (BIPV) technology is becoming widely used in parts of the façades of modern buildings [2–5]. Office buildings are particularly suitable for BIPV as they consume energy primarily in daytime, which is when the PV system collects and converts solar energy into electricity; thus, the effort and cost associated with energy storage can be avoided [6]. Such PV façades are being used increasingly in office building designs in China [7]. Accordingly, the development of an optimal PV façade design for architects, constructors, and installers is becoming increasingly urgent.

Semi-transparent PV technology is known to be beneficial for office buildings in terms of overall energy savings. For example, semi-transparent photovoltaics not only generate electricity, but also introduce daylight that can reduce artificial lighting energy consumption in daytime [8]. Conversely, semi-transparent photovoltaics reduce heat gain by blocking incoming solar radiation with PV cells [9], which increases heating demand indoors in winter but reduces the cooling demand in summer.

The transmittance of PV panels or glass for PV façades, which is determined by the PV cell coverage ratio, has been shown to have a profound impact on the overall energy consumption of buildings, particularly through its effects on PV electricity generation, lighting, cooling, and heating [10–12]. For example, Jiang et al. [10] conducted a study to investigate the influence of PV cell coverage ratio on the thermal and electrical performance of photovoltaic Trombe walls and discovered that a higher PV cell coverage ratio does not necessarily result in better thermal performance. In terms of overall energy consumption, Wong et al. [11] described the minimisation of energy consumption based on combinations of semi-transparent PV transmittance and window-to-wall ratios (WWRs). Conversely, Miyazaki et al. [12] found lighting control to be an important element in maximising the usage of daylight and demonstrated that the impact of solar cell transmittance on energy performance varied with WWR. In general, PV cell coverage ratio controls the transmittance of semi-transparent PV façades and the studies described above suggest the existence of an optimal PV cell coverage ratio that can achieve the minimum overall energy consumption. However, Yun et al. [13] found that adopting a certain range of WWR and room depth could maximise the benefits of a ventilated PV façade; this suggests that the optimal PV cell

* Corresponding author. Tel.: +44 0114 222 0325.
E-mail address: j.kang@sheffield.ac.uk (J. Kang).

coverage ratio must be determined under different combinations of architectural factors to ensure that the best energy performance is achieved.

The overall energy-saving effects of semi-transparent PV windows appear to vary with climate. In Brazil, the use of a semi-transparent PV window has been shown to save up to 43% of energy [14]. Conversely, in Japan, 55% energy savings were achieved (compared to a single-glazed window) with a solar cell transmittance of 40% and WWR of 50% [12], whereas energy savings of 16.7–41.3% were achieved in Singapore for a WWR range of 70–100% [15]. Other previous studies [16,17] have also demonstrated the importance of considering climatic conditions in the investigation of semi-transparent PV window applications. However, few studies to date have attempted a comprehensive determination of optimal PV cell coverage ratio for semi-transparent PV technology using different combinations of architectural factors such as room depth, WWR, and orientation. Accordingly, no general trends have been defined regarding variations in optimal PV cell coverage ratio. Such knowledge will play a crucial role in future optimal design approaches for semi-transparent PV façades, and improvements in the understanding of the variation in PV cell coverage ratio are required urgently. In particular, previous studies providing accurate assessments of the overall energy performance of semi-transparent PV façades in China are extremely limited, and few relevant experiments have been conducted under climatic conditions such as those in central China. Studies conducted under real climatic conditions are necessary because several studies investigating semi-transparent PV in different climate zones have produced different results.

The present study aims primarily to improve the determination of optimal PV cell coverage ratio, to understand trends in the variation of optimal PV cell coverage ratio with different architectural conditions, and to investigate the impact of architectural conditions on overall energy consumption. Additionally, it is hoped that the results presented here will provide a general reference point for the incorporation of optimal PV cell coverage ratio into the design approach as an important element necessary for the implementation of semi-transparent PV technology in office buildings. This should help to maximise the benefits of semi-transparent PV usage in office buildings, particularly in central China. In this paper, the methodology adopted for the present study (including field experiments, architectural models, and calculation models and methods) is first described. Then, the results are presented in terms of the different effects of PV cell coverage ratio on lighting, cooling, and heating energy consumption. Finally, the determination of optimal PV cell coverage ratio is described and the variation in optimal PV cell coverage ratio with variations in room depth, WWR, and orientation is discussed.

2. Methodology

In the present study, models and methods for the calculation of PV cell coverage ratio in relation to semi-transparent PV technology were established and validated based on field experiments in Wuhan, which can be considered representative of the climatic conditions of central China. The field experiments also provided more accurate data regarding the properties of semi-transparent PV glasses. An architectural model was developed with a series of generic office rooms. In these rooms, architectural characteristics including room depth, WWR, and orientation were incorporated in different combinations to allow evaluation of the effects of PV cell coverage ratio under different architectural conditions. Finally, the architectural model and validated models and methods were used in computational simulations with Energy Plus. In this manner, a parametric analysis was conducted to evaluate the effects of

Fig. 1. Photo of the experimental room.

PV cell coverage ratio on electricity consumption under different architectural conditions.

2.1. Experimental set up

The experiments were conducted in an experimental room built on the roof of a building in Wuhan (29°58′ N, 113°53′ E). The experimental room had length, width, and height of 4.65 m, 3.4 m, and 3.6 m, respectively, and was constructed using mineral wool board with a thickness of 12 mm as thermal insulation wall. The experimental room contained two inner chambers sharing a guarded room, each of which included a window that was 1.1 m long and 1.3 m high on the southern façade. A photo of the experiment room is shown in Fig. 1.

The field experiment was conducted 24 h a day from June 2012 to August 2013. The temperature on both sides of the PV glass was recorded with several T-type thermocouples at the surface of the glass. These thermocouples have been calibrated by placing them, together with a standard mercury thermometer (with precision of 0.1 °C), into a thermostatic water bath with temperature ranging from 0 °C to 100 °C. Through this calibration, the accuracy of the thermocouples was improved to ±0.1 °C, which meets the test requirements. The vertical solar irradiance of the southern orientation was recorded with a pyranometer device of Jinzhou Sunshine TBQ-2 set at the southern wall. The pyranometer device was calibrated by the manufacturer before the experiments. The PV electricity generation of each PV glass was recorded every minute throughout the test period. Because the maximum power varied according to the solar irradiance and the maximum power point changed constantly, MPPT (maximum power point tracking) systems were used to detect the maximum power point of PV electricity generation. General data describing weather conditions were recorded at hourly intervals with the Davis Vantage Pro 2 weather station. Solar irradiance, temperature, and PV electricity generation data were collected using the Agilent 34972A data logger and sent to a central computer for storage.

2.2. Calculation models and methods for semi-transparent PV

2.2.1. Power generation

PV power generation efficiency is affected by the temperature of solar cells, such that PV efficiency decreases with increasing
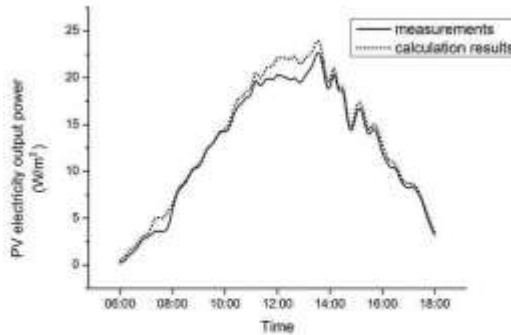
Fig. 2. Comparison of measured and calculated PV electricity output power.

temperature [18]. Moreover, a PV panel with high PV cell coverage ratio will absorb more solar radiation (and thus achieve a higher temperature) than a panel with low PV cell coverage ratio; this produces inconsistent results in terms of PV power generation efficiency, even under the same climatic conditions [10]. To address this, a temperature coefficient power generation model [19] must be included.

$$P = G\eta_0[1 - \beta_C(T_c - 25°C)] \tag{1}$$

where P is the instant power of the PV panel, G is solar radiation on the PV plane (W/m^2), η_0 is PV efficiency under standard conditions, β_C is the temperature coefficient, and T_c is the solar cell temperature (°C), which will be affected by PV cell coverage ratio. In this model, the solar cell temperature T_c is unknown and must be provided using heat balance models (as described in Section 2.2.2). In the present study, the temperature coefficient β_C was determined to be $-0.72\%/°C$ based on field experiments.

The results obtained using the power generation model were compared with measurements obtained during field experiments. It was demonstrated that the power generation model can predict PV electricity output with satisfactory accuracy. For example, Fig. 2 compares the measured and calculated PV electricity output results for a semi-transparent PV panel with PV cell coverage ratio of 40% using the climate data obtained for August 1 2013 and clearly indicates good agreement, with an average deviation of 7.5%. Other comparisons in all four seasons were also made; the results show good agreement, with less than 9.2% deviation in all cases.

2.2.2. Heat balance model

The temperature of the solar cell layers of semi-transparent PV panels must be calculated using a heat balance model. Single-glazing semi-transparent PV glass consists of multiple layers of materials, including internal and external layers of clear glass (each 6 mm thick) with a central layer of EVA that contains a silicon cell of different PV cell coverage ratio. In the heat balance model adopted here, the semi-transparent PV glass is divided into 3 layers with 4 boundaries. The properties of each layer are provided by the manufacturer and are presented in Table 1. The temperature of each boundary was calculated based on heat balance equations. The temperature of the solar cell layer T_c was assumed to be the average

of T_2 and T_3 because the difference between these two values was negligible in the context of the model outcome. Heat storage in the single glazing was not considered and heat transfer was assumed to be in quasi-steady state. Thus, the heat balance equations for the first, second, third, and fourth boundaries were established as in Eqs. (2)–(5), respectively.

$$G\alpha_1 = (T_1 - T_{out})h_{out,c} + \xi\sigma[(T_1 + 273.15)^4$$
$$- (T_{out} + 273.15)^4] + \frac{\lambda_1}{d_1}(T_1 - T_2) \tag{2}$$

$$G\tau_1[(1 - PVR)\alpha_{EVA} + PVR\alpha_{sc}] + \frac{\lambda_1}{d_1}(T_1 - T_2)$$
$$= \frac{\lambda_2}{d_2}(T_2 - T_3) + P \tag{3}$$

$$G\tau_1(1 - PVR)\tau_{EVA}\alpha_3 + \frac{\lambda_2}{d_2}(T_2 - T_3) = \frac{\lambda_3}{d_3}(T_3 - T_4) \tag{4}$$

$$\frac{\lambda_3}{d_3}(T_3 - T_4) = h_{in,c}(T_4 - T_{in}) + \xi\sigma[(T_4 + 273.15)^4$$
$$- (T_{in} + 273.15)^4] \tag{5}$$

where G is solar radiation on the PV plane (W/m^2), α_i is the solar absorptance of layer i, and T_i is the temperature of boundary i. Additionally, T_{out} and T_{in} are the outdoor and indoor temperatures, respectively; $h_{out,c}$ and $h_{in,c}$ are the convective heat transfer coefficients for the outside and inside surfaces, respectively, of the semi-transparent PV panel; ξ is the emissivity of the front glass; σ is the Stefan–Boltzmann constant (W/m^{2}K^4); τ_i is the solar transmittance of layer i; PV cell coverage ratio is the solar cell coverage ratio; λ_i is the heat conductivity of layer i (W/m K); λ_{sc} and λ_{EVA} are the heat conductivity of the solar cell and EVA, respectively (W/m K); P is the PV power generation (W/m^2); and d_i is the thickness of layer i (m). The external and internal surface convection heat transfer coefficients were set to 16 W/m^{2}K and 3.6 W/m^{2}K, respectively, based on data obtained from the standard entitled 'Calculation specification for thermal performance of windows, doors and glass curtain-walls' (JGJ/T 151-2008) [20].

The results calculated from the heat balance model were compared with the measurements collected during field experiments. Fig. 3 illustrates variations in the inside surface temperature of a semi-transparent PV panel with PV cell coverage ratio of 40% throughout the course of a day (March 1 2013) and demonstrates clearly that the calculated results agree well with the measurements, with less than 0.61 °C deviation. Other comparisons in all four seasons were also made; the results show good agreement, with an average deviation of less than 1.1 °C in all cases.

To calculate the heat and solar radiation transfer, which affects the heating and cooling loads of the indoor space, it is necessary to obtain the U-factors and solar heat gain coefficients (SHGCs) for the different PV cell coverage ratio glasses studied [20]. SHGCs can be calculated according to Eq. (6):

$$SHGC = \tau + N\alpha \tag{6}$$

where τ is total solar transmittance of semi-transparent photovoltaics, N is the inward-flowing fraction of the absorbed radiation,

Table 1
Properties of individual layers of PV cells.

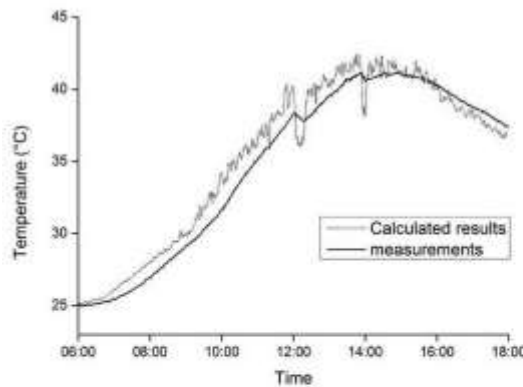| Layer	Thickness (mm)	Thermal conductivity (W/m K)	Absorptance	Transmittance	Reflectance
Glass	6	0.760	0.108	0.810	0.082
EVA	1.8	0.116	0.060	0.900	0.040
Silicon cell	0.3	168.0	0.970	0	0.030

Fig. 3. Comparison of observed and simulated inside surface temperatures for single-glazed semi-transparent PV panels.

and α is the total solar absorptance of semi-transparent photovoltaics with different PV cell coverage ratio and can be obtained from WINDOW 6.3 using the properties presented in Table 1. Furthermore, τ and N can be defined as in Eqs. (7) and (8), respectively.

$$\tau = \tau_1 \tau_2 \tau_3 (1 - PVR) \tag{7}$$

$$N = \frac{h_{in}}{h_{in} + h_{out}} \tag{8}$$

where h_{out} and h_{in} are outside and inside heat transfer coefficients, respectively, for the surfaces of semi-transparent PV panels. Similarly, U-factors can be calculated for different PV cell coverage ratio as follows:

$$U = \frac{1}{(1/h_{out}) + (d_1/\lambda_1) + (d_2/\lambda_2) + (d_3/\lambda_3) + (1/h_{in})} \tag{10}$$

In the present study, the outside and inside surface heat transfer coefficients were set to 20.2 W/m²K and 8.3 W/m²K, respectively,

based on data obtained from the standard entitled 'Calculation specification for thermal performance of windows, doors and glass curtain-walls' (JGJ/T 151-2008) [20]. After calculation of SHGCs and U-factors, heating and cooling loads were simulated in Energy Plus.

2.2.3. Daylight and lighting control

According to the Standard for Lighting Design of Buildings for China (GB50034-2004) [21], indoor illuminance should reach 300 lx in general office rooms. To simulate such conditions and incorporate the energy savings achieved during daylight, daylight detection and lighting control were introduced into the simulation with the help of Energy Plus. When the daylight illuminance level fell below 300 lx, artificial lighting was initiated to achieve the required illuminance level; however, this resulted in extra electricity consumption. Therefore, to obtain an accurate simulation outcome, visible transmittance was obtained from WINDOW 6.3 for each semi-transparent PV panel with different PV cell coverage ratio and was incorporated into Energy Plus as part of the daylight simulation. Thus, daylight illuminance was calculated and recorded in Energy Plus, allowing the simulation and calculation of lighting energy consumption [11].

2.3. Architectural model

An architectural model is a crucial part of the investigation of the energy performance of semi-transparent photovoltaics in office façades. To develop such a model, information was obtained by conducting a survey of 60 office building cases in the Wuhan area. Two typical types of office building were identified in the survey: buildings with core tubes and slab-type buildings. The division of large rooms into separate smaller rooms was found to be common in both types of office building; in fact, the majority of cases investigated exhibited such division. Thus, these separate rooms were incorporated into the models described here and used to represent the generic office rooms of the present study.

These generic office rooms were set to allow control of three main variables: (1) room depth, as shown in Fig. 4(a); (2) WWR, as shown as Fig. 4(b); and (3) orientation. By adopting various combinations of these variables, different PV cell coverage ratio could
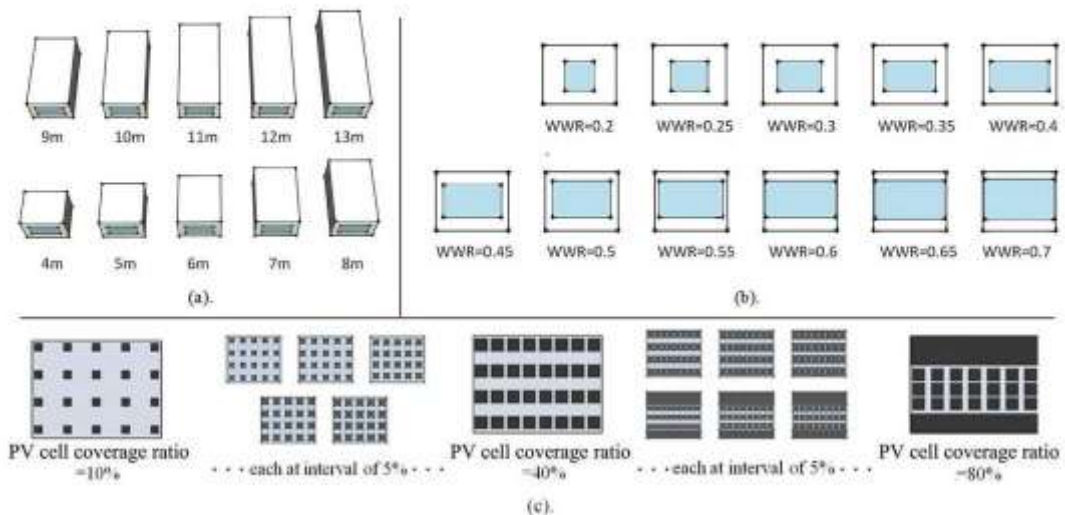

Fig. 4. Illustrations of variations in (a) room depth, (b) WWR, and (c) PV cell coverage ratio.

134   S. Xu et al. / Energy and Buildings 77 (2014) 130–138

Table 2
Thermal and optical properties of building layers.

Layer	Thickness (mm)	Thermal conductivity (W/m K)	Density (kg/m³)	Specific heat (J/kg K)
Exterior wall				
Brick	200	0.89	1920	790
Insulation board	40	0.03	50	1210
Surface finish*2	20	0.16	800	1100
Interior wall				
Brick	100	0.89	1920	790
Surface finish*2	20	0.16	800	1100
Ceiling/floor				
Standard wood board	8	0.12	540	1210
Cast concrete	120	1.60	2200	860
Surface finish	20	0.16	800	1100

be examined under different architectural conditions, as shown in Fig. 4(c). Room depth was varied from 4 m to 13 m at intervals of 1 m; this range can be considered representative of common office room sizes in the Wuhan area. WWR was restricted to the range 0.2–0.7 based on guidelines presented in the Design Standard for Energy Efficiency of Public Buildings proposed by the Ministry of Housing and Urban–Rural Development of the PRC [22], which forbids office buildings with a WWR over 0.7 in the hot summer/cold winter climate zone [22]. PV cell coverage ratio was varied from 10% to 80% at intervals of 5%. PV cell coverage ratio lower than 10% would make PV applications uneconomical; conversely, PV cell coverage ratio higher than 80% would block the entire window area, making it difficult for daylight to enter the room and for occupants to see out. The adopted PV cell coverage ratio interval of 5% should allow a distinction to be made between the different impacts of PV cell coverage ratio while still remaining sufficiently practical for the simulation parametric analysis to be conducted.

Other simulation features required were assumed to be fixed and were based on the Design Standard for Energy Efficiency of Public Buildings for China [22], as follows. (1) A rectangular office room on an intermediate floor was assumed to have width and height of 5 m and 4 m, respectively. (2) The thermal properties of exterior and interior walls and ceilings and floors were as detailed in Table 2. (3) A single window area with no sun blinds was assumed, since the semi-transparent PV model serves as a shading device. (4) Room lights were assigned a design value of 11 W/m² in all instances. The daylight control sensor was located in the geometric centre of the room at a height of 0.75 m. Daylight control initiated artificial lighting when the indoor illuminance level fell below 300 lx. (5) The daily heating and cooling schedules assigned for the air conditioning are presented in Table 3. COP was set to 4.5 and the ventilation system was set to ensure 1.5 air changes/h. (6) Office occupancy was set to 0.25 people/m² and the electricity consumption of the equipment was assumed to be 20 W/m². (7) Lighting and office equipment operation schedules were set according to the office occupancy conditions presented in Table 3.

3. Results and discussion

This section provides a discussion of the parametric analysis conducted. The validated calculation models and methods were incorporated into the architectural model defined above to investigate the effects of different PV cell coverage ratio on energy performance using Energy Plus. The overall energy performance, including PV electricity generation and lighting and heating and cooling electricity consumption, was examined under different architectural conditions. Different combinations of room depth and WWR were examined carefully for a southern orientation while PV cell coverage ratio was varied from 10% to 80% at 5% intervals. The criterion of electricity consumption per floor area (kWh/m²) was used to account for differences in floor area for different values of room depth, thus providing normalised results. Other orientations are discussed in Section 3.4. All figures were evaluated based on annual or average annual values to ensure a holistic view of overall energy consumption with the consideration of all four seasons.

3.1. Effects on PV electricity generation

Solar cells convert solar energy into electricity and typically operate with a specific conversion efficiency, which is affected primarily by the material characteristics and operating temperature of the cells. Compared to transparent glass, silicon solar cells typically have higher solar absorbance. Thus, the amount of solar heat gained can be increased by adopting a denser solar cell array and, therefore, a higher PV cell coverage ratio. Accordingly, this should also increase the temperature and reduce the conversion efficiency of the solar cells. In the present study, the temperature and conversion efficiency of solar cells were investigated throughout March 1 2013 (Fig. 5). The results demonstrate that conversion efficiency decreases with increasing temperature. At noon, the temperature for the 80% PV cell coverage ratio case was 7 °C higher than that for the 10% PV cell coverage ratio case; this temperature difference corresponded to a 0.007 decrease in conversion efficiency, which was 5.5% lower than the 10% PV cell coverage ratio case. Thus, the
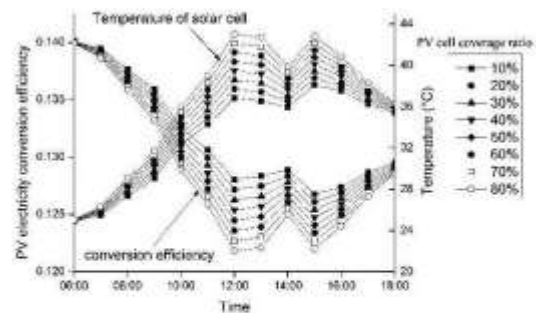
Fig. 5. Solar cell temperature and conversion efficiency for different PV cell coverage ratio.

Table 3
Hourly heating and cooling schedules.

	Time				
	00:00–07:00	07:00–08:00	08:00–17:00	17:00–19:00	19:00–24:00
Cooling system (°C)	37	28	26	26	37
Heating system (°C)	12	18	20	20	12
Lighting, equipment, operation schedules (fraction of full operation)	0	0.5	0.95	0.3	0

135

Fig. 6. Lighting electricity consumption for different PV cell coverage ratio for various room depth cases.

results demonstrate the importance of considering PV cell coverage ratio in PV electricity generation.

3.2. Effects on lighting electricity consumption

The amount of daylight blocked by solar cells can vary considerably in response to differences in PV cell coverage ratio between semi-transparent PV panels, which can have a vital impact on indoor illuminance. If the indoor illuminance drops below a given threshold, artificial lighting is required to achieve a comfortable lighting environment and electricity must be consumed to achieve this. However, room depth and WWR may also affect the performance of semi-transparent PV panels at different PV cell coverage ratio. Thus, it is important to understand the relationship between PV cell coverage ratio and indoor illuminance for different combinations of room depth and WWR.

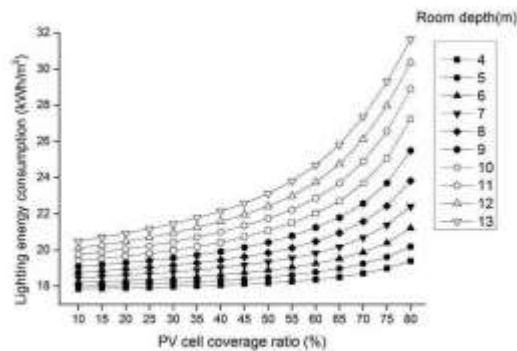For larger room depth (i.e. deeper rooms), it is more difficult for daylight to reach deep inside the room. Thus, even for the same PV cell coverage ratio, daylight illuminance will tend to vary depending on room depth conditions. The results show that indoor illuminance decreases rapidly with increasing PV cell coverage ratio, with more pronounced decreases for smaller room depths. In general, shorter rooms (i.e. smaller room depth) experience much higher daylight illuminance than deep rooms (i.e. larger room depth). Moreover, indoor illuminance remains below 400 lx for all cases in which room depth exceeds 9 m. These results demonstrate that the effects of PV cell coverage ratio on daylight illuminance are strongly dependent on room depth.

Fig. 6 illustrates the lighting electricity consumed for artificial lighting (which compensates for natural daylight) for different PV cell coverage ratio in different room depth cases. It is clear that this electricity consumption increases when daylight illuminance decreases in response to high PV cell coverage ratio. However, the relationship between consumption and PV cell coverage ratio is not linear. For small room depth, lighting electricity consumption increases much more rapidly when PV cell coverage ratio exceeds 50%; conversely, for larger room depth cases, the overall trend is much closer to a linear relationship. Cases in which room depth is small typically consume less lighting electricity (15 kWh/m² less at most) owing to their high indoor illuminance.

A greater WWR allows more daylight to penetrate into the room and presents a greater window area upon which semi-transparent PV panels can be installed. However, the results show that the impact of WWR on daylight illuminance is less pronounced than that of room depth. A similar pattern is apparent in the results demonstrating the relationship between lighting electricity
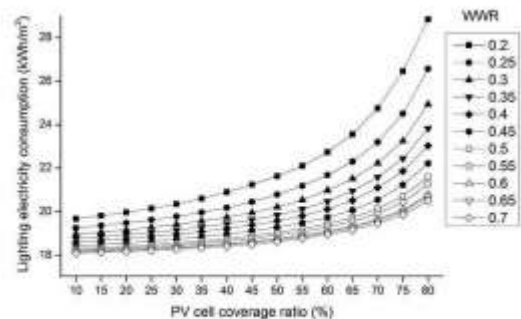

Fig. 7. Lighting electricity consumption for different PV cell coverage ratio for various WWR cases.

consumption and PV cell coverage ratio for variable WWR (Fig. 7): lighting electricity consumption increases with increasing PV cell coverage ratio, although the differences between different WWR cases are relatively small, with electricity savings of 9 kWh/m² at most (at 80% PV cell coverage ratio).

3.3. Effects on heating and cooling electricity consumption

Heating and cooling loads of office buildings are more easily affected by solar radiation, as office buildings typically function primarily during daytime. Varying the amount of solar radiation entering a building by installing semi-transparent PV panels with different PV cell coverage ratio can have an impact on heating and cooling loads. Increasing the influx of solar radiation can reduce heating demand in winter; however, it also increases cooling demand in summer. Fig. 8 illustrates the heating and cooling electricity consumption for different PV cell coverage ratio for several room depth cases with a fixed WWR of 0.35. Heating and cooling electricity consumption first decreases with increasing PV cell coverage ratio, although the rate of decrease slows when PV cell coverage ratio exceeds 50%. The cases with higher PV cell coverage ratio appear to perform better in terms of heating and cooling energy savings based on annual data. This can be attributed primarily to the climatic conditions in central China, where the cooling load in summer is typically greater than the heating load in winter. However, the benefits of high PV cell coverage ratio become less pronounced as room depth increases: the shortest room has the highest heating and cooling electricity consumption, although
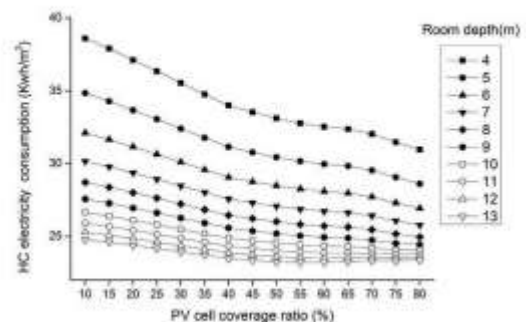

Fig. 8. Heating and cooling electricity consumption for different PV cell coverage ratio for various room depth cases.
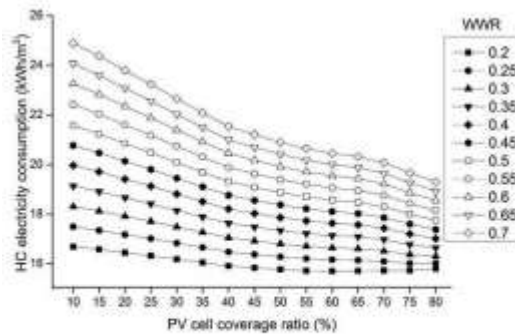
136   S. Xu et al. / Energy and Buildings 77 (2014) 130–138

Fig. 9. Heating and cooling electricity consumption for different PV cell coverage ratio for various WWR cases.

variations in consumption with changes in room depth become less pronounced when room depth exceeds 9 m. These results highlight the importance of considering PV cell coverage ratio, particularly in cases with small room depth.

Fig. 9 illustrates the heating and cooling electricity consumption for different PV cell coverage ratio in cases with different WWR. As for the cases with variable room depth, heating and cooling electricity consumption first decreases with increasing PV cell coverage ratio, with the rate of decrease slowing when PV cell coverage ratio exceeds 60%. Cases with small WWR typically perform better in terms of heating and cooling energy saving, and the effects of varying PV cell coverage ratio are typically less pronounced when WWR is small. However, in such cases, the effects of WWR remain relatively constant between cases, meaning that heating and cooling electricity consumption will continue to increase with increasing WWR, with no signs of slowing down or stabilising.

3.4. Effects on overall energy performance

Based on the analysis presented above, it can be concluded that increasing PV cell coverage ratio under the climatic conditions in central China typically leads to decreases in PV electricity conversion efficiency and heating and cooling electricity consumption, but increases in lighting electricity consumption. However,

the effects of room depth and WWR on these relationships are pronounced, demonstrating that these factors must be considered carefully when designing semi-transparent PV technology for buildings. Therefore, it is necessary to evaluate overall energy consumption considering all of these factors to allow determination of an optimal PV cell coverage ratio. In such case, overall energy consumption is defined as following.

Overall energy consumption = lighting energy consumption + cooling and heating energy consumption − PV electricity generation. Fig. 10(a) and (b) illustrates the overall energy consumption for cases with large WWR (0.6) for two different values of room depth (6 m and 12 m, respectively). For a room depth of 6 m, PV cell coverage ratio of 80% achieves the lowest overall electricity consumption, allowing electricity savings of 18.9% compared to the case with PV cell coverage ratio of 10%. This can be attributed primarily to the influence of heating and cooling electricity consumption: high PV cell coverage ratio can reduce the enormous cooling demands for short rooms. Conversely, for a room depth of 12 m, the greatest electricity savings are achieved for PV cell coverage ratio of 50%. This can be attributed primarily to decreases in lighting electricity consumption during daytime owing to the smaller PV cell coverage ratio; these savings overwhelm the effects of heating and cooling electricity consumption.

Fig. 11(a) and (b) illustrates the overall energy consumption for cases with small WWR (0.3) for two different values of room depth (6 m and 12 m, respectively). In such cases, PV electricity generation is typically very small compared to lighting and heating and cooling electricity consumption owing to the limited area available for the installation of semi-transparent PV panels. However, the influence of PV cell coverage ratio remains pronounced, particularly in terms of its effects on daylight and heating and cooling demand. For the 6 m room, PV cell coverage ratio of 60% achieves the lowest electricity consumption, with electricity savings of 6.8% compared to PV cell coverage ratio of 10%. Conversely, in the 12 m room, PV cell coverage ratio of 20% achieves the lowest electricity consumption, with electricity savings of 17.3% compared to PV cell coverage ratio of 80%.

3.5. Optimal PV cell coverage ratio

Based on the parametric analysis above, it is clear that an optimal PV cell coverage ratio (i.e. that which will achieve the lowest overall electricity consumption) can be obtained based on a particular
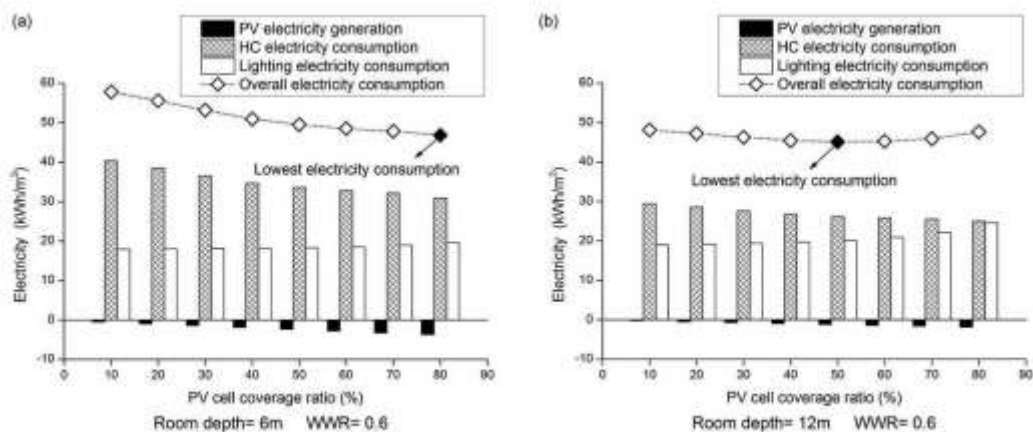

Fig. 10. Changes in overall energy consumption in response to variations in WWR and room depth: (a) room depth = 6 m, WWR = 0.3; (b) room depth = 12 m, WWR = 0.3.
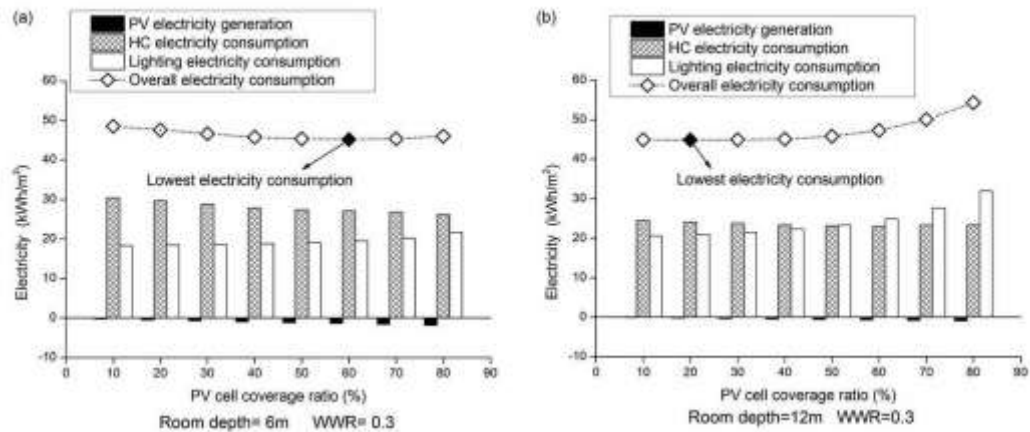
Fig. 11. Changes in overall energy consumption in response to variations in WWR and room depth: (a) room depth = 6 m, WWR = 0.6; (b) room depth = 12 m, WWR = 0.6.

combination of WWR, room depth, and orientation. Thus, optimal PV cell coverage ratio should be selected by comparing the overall energy consumption results for all PV cell coverage ratio cases under different architectural conditions (i.e. WWR, room depth, and orientation). The southern orientation is typically affected more extensively by solar energy than other orientations; accordingly, it is often the preferred orientation for the installation of photovoltaic applications. Variations in WWR and room depth can lead to considerable variation in optimal PV cell coverage ratio (Table 4).

Differences in electricity consumption between the most and least favourable PV cell coverage ratio were calculated; in particular, electricity savings for different combinations of room depth and WWR were calculated. The results demonstrate electricity savings ranging from 5% to 30%, with an average saving of 13% for the optimal PV cell coverage ratio. Moreover, optimal PV cell coverage ratio

was found to be particularly important in short rooms with large WWR, where electricity savings of over 20% were achieved.

Variations in optimal PV cell coverage ratio were also investigated. Optimal PV cell coverage ratio was found to decrease with increasing room depth (i.e. from 4 m to 13 m). This can be attributed primarily to the fact that the electricity demand during daytime increases faster than the compensation achieved through savings in heating and cooling. This also explains why rooms with greater depths typically have smaller optimal PV cell coverage ratio. Furthermore, optimal PV cell coverage ratio increases when WWR increases from 0.2 to 0.7, primarily because the electricity savings achieved by adopting a larger WWR (combined with the greater PV electricity generation and lower cooling load) result in higher optimal PV cell coverage ratio.

To demonstrate the effects of different orientations on optimal PV cell coverage ratio, different combinations of orientation and room depth (WWR) were investigated with WWR (room depth) fixed at 0.35 (8 m); orientation was varied between east, southeast, south, southwest, and west (Tables 5 and 6). The northern orientation was not included in this investigation because it is known to be particularly unfavourable for PV applications. The results demonstrate that the optimal PV cell coverage ratio is highest in the west orientation. Under the climatic conditions prevalent in central China, cooling demands in summer typically exceed heating demands in winter. Thus, in summer, high PV cell coverage ratio

Table 4
Optimal PV cell coverage ratio for different combinations of room depth and WWR in southern orientation.

WWR	optimal PV cell coverage ratio (%) room depth (m)									
	4	5	6	7	8	9	10	11	12	13
0.2	75	55	50	40	35	20	10	10	10	10
0.25	80	60	55	50	40	40	30	10	10	10
0.3	80	75	60	55	50	40	40	30	20	10
0.35	80	80	75	55	55	45	40	40	35	30
0.4	80	80	75	60	55	50	45	40	40	40
0.45	80	80	80	75	60	55	50	45	40	40
0.5	80	80	80	75	70	60	55	50	45	40
0.55	80	80	80	80	75	60	55	55	50	45
0.6	80	80	80	80	75	75	60	55	55	50
0.65	80	80	80	80	75	75	60	60	55	50
0.7	80	80	80	80	80	75	75	60	55	55

Table 5
Optimal PV cell coverage ratio for different combinations of orientation and room depth.

orientation	optimal PV cell coverage ratio (%) room depth (m)									
	4	5	6	7	8	9	10	11	12	13
E	75	60	50	45	35	25	20	20	20	15
SE	75	60	50	45	40	35	30	30	25	20
S	80	80	75	55	55	45	40	40	35	30
SW	80	80	75	65	55	50	50	45	40	35
W	80	80	80	75	65	55	55	50	45	40

138   S. Xu et al. / Energy and Buildings 77 (2014) 130–138

Table 6
Optimal PV cell coverage ratio for different combinations of orientation and WWR.

orientation	optimal PV cell coverage ratio (%)										
	WWR										
	0.2	0.25	0.3	0.35	0.4	0.45	0.5	0.6	0.6	0.65	0.7
E	25	40	40	45	50	60	60	60	70	70	70
SE	25	40	40	45	50	60	60	65	70	70	75
S	35	40	50	55	55	60	70	75	75	75	80
SW	35	50	50	60	65	65	70	75	75	75	80
W	35	50	50	60	65	65	70	75	75	75	80

can reduce the cooling load associated with the heat accumulated indoors during daytime.

4. Conclusions

In the present study, calculation models were established to investigate the properties of semi-transparent PV installations in relation to PV cell coverage ratio and the models were validated using data obtained in field experiments. In particular, an architectural model was developed to incorporate a series of generic office rooms. The validated calculation methods and properties were incorporated into Energy Plus to perform a parametric analysis of the effects of different PV cell coverage ratio on electricity consumption under different architectural conditions (room depth, WWR, and orientation). The results of the study can be summarised as follows.

(1) PV electricity conversion efficiency decreases as PV cell coverage ratio increases. Conversion efficiency decreases by 5.5% as PV cell coverage ratio is increased from 10% to 80%. (2) With increasing PV cell coverage ratio, indoor daylight illuminance decreases linearly and electricity consumption increases. Room depth appears to have a greater effect than WWR on both daylight illuminance and lighting electricity consumption. (3) Under the climatic conditions of central China, increasing PV cell coverage ratio appears to result in decreases in heating and cooling electricity consumption. (4) When overall energy performance is considered, adopting optimal PV cell coverage ratio can result in electricity savings of up to 30% (average savings: 13%) compared to the least favourable PV cell coverage ratio, although the savings achieved vary depending on the combination of room depth and WWR adopted, at least in the south orientation. This demonstrates the importance of selecting optimal PV cell coverage ratio based on architectural conditions. (5) In rooms with small room depth, optimal PV cell coverage ratios are relatively small compared to rooms with larger room depths. In rooms with large WWR, optimal PV cell coverage ratios are relatively large compared to rooms with small WWR. This means that PV façades with high PV cell coverage ratios are more suitable for deep rooms with larger windows, whereas the PV façades of small PV cell coverage ratio are more suitable for short rooms with small windows. (5) Building orientation can also affect the optimal ratio, with changes of 5–10% depending on specific orientation and optimal PV cell coverage ratio. Changes are typically highest in the western orientation; however, these changes induced by orientation are much less pronounced than those induced by variation in WWR and room depth.

It is hoped that the results presented here will act as a general reference point for the selection of optimal PV cell coverage

ratio in the semi-transparent PV design approach. In particular, the present study should provide assistance in maximising the benefits of semi-transparent PV application with reference to the overall energy performance of buildings, including electricity generation, lighting, and cooling and heating. Thus, these results represent a solid foundation for the optimisation of the architectural design of office buildings with semi-transparent PV façades.

References

[1] S. Natarajan, G.J. Levermore, Domestic futures – which way to a low-carbon housing stock? Energy Policy 35 (11) (2007) 5728–5736.
[2] S. Roberts, Building Integrated Photovoltaics, first ed., Birkhäuser Architecture, Berlin, 2009.
[3] B. Weller, Detail Practice: Photovoltaics: Technology, Architecture, Installation, Basel, 2010.
[4] X. Zhang, X. Zhao, S. Smith, J. Xu, X. Yu, Review of R&D progress and practical application of the solar photovoltaic/thermal (PV/T) technologies, Renewable and Sustainable Energy Reviews 16 (1) (2012) 599–617.
[5] H.M. Taleb, A.C. Pitts, The potential to exploit use of building-integrated photovoltaics in countries of the Gulf Cooperation Council, Renewable Energy 34 (4) (2009) 1092–1099.
[6] J.C. Lam, D.H.W. Li, S.O. Cheung, An analysis of electricity end-use in air-conditioned office buildings in Hong Kong, Building and Environment 38 (3) (2003) 493–498.
[7] C. Peng, Y. Huang, Z. Wu, Building-integrated photovoltaics (BIPV) in architectural design in China, Energy and Buildings 43 (12) (2011) 3592–3598.
[8] D.H.W. Li, T.N.T. Lam, W.W.H. Chan, A.H.L. Mak, Energy and cost analysis of semi-transparent photovoltaic in office buildings, Applied Energy 86 (5) (2009) 722–729.
[9] T.Y.Y. Fung, H. Yang, Study on thermal performance of semi-transparent building-integrated photovoltaic glazings, Energy and Buildings 40 (3) (2008) 341–350.
[10] R. Jiang, J. Ji, H. Yi, The influence of PV coverage ratio on thermal and electrical performance of photovoltaic-Trombe wall, Renewable Energy 33 (11) (2008) 2491–2498.
[11] F.W. Wong, Y. Shimoda, M. Nonaka, M. Inoue, M. Mizuno, P.V. Semi-transparent, Thermal performance, power generation, daylight modelling and energy saving potential in a residential application, Renewable Energy 33 (5) (2008) 1024–1036.
[12] T. Miyazaki, A. Akisawa, T. Kashiwagi, Energy savings of office buildings by the use of semi-transparent solar cells for windows, Renewable Energy 30 (3) (2005) 281–304.
[13] G.Y. Yun, M. McEvoy, K. Steemers, Design and overall energy performance of a ventilated photovoltaic façade, Solar Energy 81 (3) (2007) 383–394.
[14] E.L. Didoné, A. Wagner, Semi-transparent PV windows: a study for office buildings in Brazil, Energy and Buildings 67 (2013) 136–142.
[15] P.K. Ng, N. Mithraratne, H.W. Kua, Energy analysis of semi-transparent BIPV in Singapore buildings, Energy and Buildings 66 (2013) 274–281.
[16] L. Lu, K.M. Law, Overall energy performance of semi-transparent single-glazed photovoltaic (PV) window for a typical office in Hong Kong, Renewable Energy 49 (2013) 250–354.
[17] L. Olivieri, E. Caamaño-Martín, F. Olivieri, J. Neila, Integral energy performance characterization of semi-transparent photovoltaic elements for building integration under real operation conditions, Energy and Buildings 68 (Part A) (2014) 280–291.
[18] Z. Ye, A. Nobre, T. Reindl, J. Luther, C. Reise, On PV module temperatures in tropical regions, Solar Energy 88 (2013) 80–87.
[19] E. Skoplaki, J.A. Palyvos, On the temperature dependence of photovoltaic module electrical performance: a review of efficiency/power correlations, Solar Energy 83 (5) (2009) 614–624.
[20] Ministry of Housing and Urban-Rural Development of the People's Republic of China, Calculation Specification for Thermal Performance of Windows, Doors and Glass Curtain-walls, China Architectural & Building Press, Beijing, 2008.
[21] China Academy of Building Research, Standard for Lighting Design of Buildings, China Architectural & Building Press, Beijing, 2008.
[22] China Academy of Building Research, Design Standard for Energy Efficiency of Public Buildings, China Architectural & Building Press, Beijing, 2004.